



Universiteit
Leiden
The Netherlands

Activity-based protein profiling of diacylglycerol lipases

Baggelaar, M.P.

Citation

Baggelaar, M. P. (2017, April 6). *Activity-based protein profiling of diacylglycerol lipases*. Retrieved from <https://hdl.handle.net/1887/48284>

Version: Not Applicable (or Unknown)

License: [Licence agreement concerning inclusion of doctoral thesis in the Institutional Repository of the University of Leiden](#)

Downloaded from: <https://hdl.handle.net/1887/48284>

Note: To cite this publication please use the final published version (if applicable).

Cover Page



Universiteit Leiden



The handle <http://hdl.handle.net/1887/48284> holds various files of this Leiden University dissertation

Author: Baggelaar, M.P.

Title: Activity-based protein profiling of diacylglycerol lipases

Issue Date: 2017-04-06

Activity-based Protein Profiling of Diacylglycerol Lipases

PROEFSCHRIFT

ter verkrijging van
de graad van Doctor aan de Universiteit Leiden,
op gezag van Rector Magnificus prof. mr. C.J.J.M. Stolker,
volgens het besluit van het College voor Promoties
te verdedigen op 6 April 2016
klokke 15:00 uur

door

Marc Pieter Baggelaar

Geboren te Harlingen in 1984

Promotiecommissie

Promotor Prof. dr. H. S. Overkleeft

Co-promotor Dr. M. van der Stelt

Overige leden : Prof. dr. B. F. Cravatt
 Prof. dr. H. Ovaa
 Prof. dr. C. A. A. van Boeckel
 Prof. dr. G. A. van der Marel
 Prof. dr J. Brouwer
 Dr. K. Bonger

Printed by Ridderprint

Cover picture: Robert van Sluis

ISBN 978-94-6299-551-2

Table of contents

Chapter 1

Activity-based Protein Profiling Drives Inhibitor Discovery	7
---	---

Chapter 2

2-Arachidonoylglycerol: a Signaling Lipid	15
---	----

Chapter 3

Development of an Activity-Based Probe and Focused Library Screening Reveal Highly Selective Inhibitors for DAG-lipase- α in Brain	49
---	----

Chapter 4

A highly Selective, Reversible Inhibitor Identified by Comparative Chemoproteomics Modulates Diacylglycerol Lipase Activity in Neurons	81
--	----

Chapter 5

Structure Activity Relationship of LEI105	113
---	-----

Chapter 6

Chemical Proteomics Maps Brain Region Dependent Activity of Endocannabinoid Hydrolases	139
--	-----

Chapter 7

Focused Library Screening Using Activity-based Probes Reveals Novel Inhibitors of the α,β -hydrolase Fold Family	159
--	------------

Chapter 8

Summary and Future Prospects	177
------------------------------	------------

Samenvatting	191
---------------------	------------

List of publications	195
-----------------------------	------------

Curriculum Vitae	198
-------------------------	------------

CHAPTER 1

Activity-based Protein Profiling Drives Inhibitor Discovery

1. Activity-based protein profiling

Over the years extensive enzyme expression databases have been generated by *in-situ* hybridization and global proteomics.^{1,2} However, the activity of enzymes in complex proteomes does not always correlate directly with their expression, due to multiple factors, including post-translational modifications, allosteric control, and the presence of endogenous small molecule inhibitors that can regulate enzyme activity.^{3,4} Activity-based protein profiling (ABPP) has emerged as a powerful technique to analyze the functional states of enzymes in complex biological systems.

ABPP relies on active site directed small molecules, termed “activity-based probes” (ABPs) that inhibit a specific enzyme or an entire enzyme family.⁵ They react in a mechanism-based fashion, thereby establishing a covalent interaction with the catalytic residue of only the active form of its target enzyme(s). ABPs generally consist of three fundamental features with distinct functions (Figure 1). 1) A reactive group, the so-called “warhead” that establishes a covalent and irreversible interaction with the catalytic residue of the target enzyme; 2) a recognition element that directs the ABP towards its specific target 3) and a reporter tag that enables visualization, identification and/or quantification of labeled proteins. A biotin reporter group is commonly used for enrichment and subsequent mass spectrometric analysis. Fluorescent reporter groups are often used for visualization by microscopy or in-gel fluorescence detection after the proteome is resolved on SDS-PAGE. These reporter groups can be directly incorporated in the ABP (direct ABP), or a detection

element can be introduced in a later stage via ligation chemistry (two-step ABP).⁶ Two-step ABPs contain a latent affinity handle, which can be coupled to a reporter group via biorthogonal ligation chemistry. Multiple ligation strategies have been employed for ABPP, including Staudinger ligation, copper(I) catalyzed alkyne-azide [3+2] cycloaddition (click) reaction and reverse electron demand Diels Alder ligation.⁷ The advantage of using two-step probes is that the bioorthogonal ligation handles are generally very small and, therefore, they may not interfere with protein binding and cellular penetration, which contrasts bulky fluorophores and biotin reporter groups.

One of the advantages of ABPP is that it can assess enzyme activity in diverse biological systems, including cell and tissue lysates, cell cultures and even living organisms. ABPP can be employed for a wide variety of

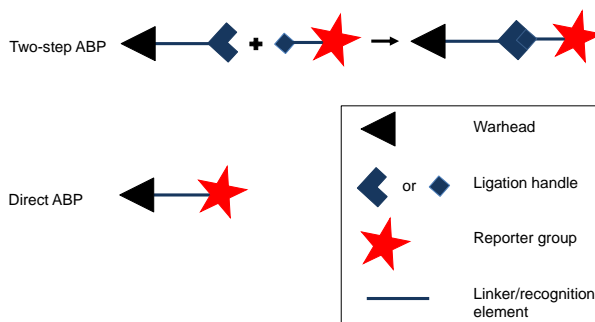


Figure 1. Schematic representation of a direct and a 2-step ABP.

purposes, such as the discovery of new enzyme inhibitors, identification of down-regulated enzyme activities in disease states, enzyme activity assays, target elucidation, and localization of enzyme activity in cells and *in vivo*.^{5, 8-10}

2. Competitive ABPP

Competitive ABPP involves treatment of a proteome with a small molecule inhibitor before labeling with an ABP. Reduction of probe labeling provides information on the affinity of the small molecule inhibitor for the targeted enzyme(s). A schematic representation of a competitive ABPP workflow is given in Figure 2.¹¹ This methodology to monitor enzyme inhibition has several advantages compared to conventional substrate assays. First, the inhibitor activity measurement can be conducted directly in native proteomes. Therefore, recombinant expression and purification are not required. Second, when broad spectrum ABPs are used, evaluation of selectivity and potency against many enzymes can be performed in parallel. Finally, probe labeling acts as a surrogate for substrates, thus inhibitors can also be developed for enzymes with unknown substrates.

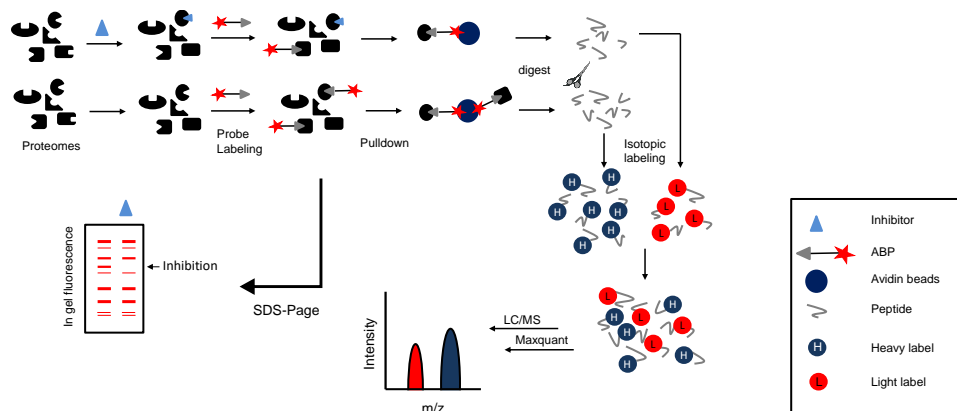


Figure 2. Schematic representation of competitive ABPP. Proteomes are treated with inhibitor or vehicle and subsequently labeled with ABP. At this stage, the proteome can be resolved on SDS-PAGE and the in gel fluorescence can be analyzed when the ABP is equipped with a fluorescent reporter group. Reduction of the intensity of fluorescence of specific bands in inhibitor treated samples compared to control samples indicates inhibition of that specific protein. Alternatively, for biotinylated ABPs, the labeled proteome can be analyzed by mass-spectrometry. Therefore, labeled proteomes are enriched using avidin beads and subsequently digested by trypsin. Peptides are labeled with different isotopic labels for comparison between inhibitor treated and untreated proteomes. The differentially labeled peptides are mixed and analyzed by mass spectrometry. The identity of the proteins can be determined by correlating measured tryptic peptides with predicted tryptic peptides. Information on inhibition can be retrieved from the isotopic ratio between the inhibitor treated and untreated proteome.

3. Small molecule inhibitors to study enzyme function

In the postgenomic era, the identification and characterization of the biological functions of proteins that coordinate and control biological processes in health and disease has become one of the most important challenges in the field of chemical biology. Although predicted gene products can be divided in sequence related protein families such as receptors, enzymes or transport channels, their exact biological function remains often obscure. Understanding the role and importance of a given gene product in (patho)physiological processes, requires knowledge of its substrates, ligands and other interacting biomolecules.¹² Congenital deletion and targeted gene disruption by siRNA and CRISPR-Cas9 are regularly used tools to investigate the biochemical function of enzymes in cells and animals. However, they may produce outcomes that are difficult to interpret. Congenital deletion of genes may lead to developmental defects and cellular compensation by other proteins. Additionally, genetic techniques are not suitable for separating a scaffolding function from the catalytic activity of enzymes.

Small molecule inhibitors that inhibit enzyme activity in an acute fashion are a complementary approach and can address some of the above mentioned shortcomings of the genetic techniques. Perturbation of enzyme activity using selective small molecule inhibitors has several distinct advantages over genetic approaches. They allow control of

enzyme activity rapidly, reversibly and without compensation of enzyme expression. In addition, small molecule probes provide the possibility to tune the extent and timing of inhibition and can serve as starting points for the development of drugs for human diseases.

A complete understanding of the target profile of small molecule inhibitors in native biological systems is highly important to retrieve reliable information on the function of specific enzymes. ABPP is a powerful technique to evaluate the activity and selectivity of small molecule inhibitors over specific enzyme families. In contrast to genetic techniques, not all protein classes can be addressed by activity-based protein profiling. Enzymes require a nucleophilic amino acid in the active site that can covalently bind with the warhead of an ABP, which is in general an electrophilic trap. ABPs have been developed to covalently bind to aspartate, glutamate, cysteine, lysine, tyrosine, and serine residues across a mechanistically diverse set of enzymes, e.g. cysteine proteases,¹³ serine hydrolases,¹⁴ phosphatases,¹⁵ glycosidases¹⁶ and palmitoyl transferases.¹⁷

The main focus of the work described in this thesis is the development of ABPs and inhibitors for endocannabinoid hydrolases. Many of these enzymes belong to the serine hydrolase family and regulate the biosynthesis and degradation of endocannabinoids. The activated nature of the catalytic serine makes these enzymes susceptible for covalent modification by a wide array of electrophiles, such as lactones,¹⁴ triazole ureas,¹⁸ fluorophosphonates¹⁹ and carbamates.²⁰ Therefore, they are highly suitable to study by ABPP. Fluorophosphonates have proven to be exceptionally useful for the generation of broad-spectrum ABPs for this enzyme family.²¹ It has been shown that the large majority (>80%) of the mammalian serine hydrolases are targeted by a single fluorophosphonate based ABP.¹⁹ Tailor-made ABPs with different warheads, such as carbamates and triazole ureas, are employed to study the remaining enzymes.^{18,22}

In particular the diacylglycerol lipases were studied in depth. There are two diacylglycerol lipase isoforms, diacylglycerol lipase- α and - β (DAGL- α and DAGL- β). These enzymes play a key role in the biosynthesis of the major endocannabinoid 2-arachidonoylglycerol. This signalling lipid is involved in multiple (patho)physiological processes, including neuroinflammation, anxiety, metabolism and addiction. Tools to study and modulate the activity of these enzymes can be used to provide insight in the physiological role of 2-arachidonoylglycerol. In addition, these tools may lead to novel therapeutics for the treatment human disorders such as the metabolic syndrome, Parkinson's disease, Alzheimer's disease and Multiple Sclerosis.

5. Aim and outline of the Thesis:

The aim of the research described in this thesis is to identify, develop and apply novel chemical tools and methodologies to study the function of endocannabinoid hydrolases in complex proteomes.

2-Arachidonoylglycerol (2-AG) is one of the most extensively studied monoacylglycerols. It is an important signaling lipid as well as an intermediate in lipid metabolism in the brain. **Chapter 2** describes the physiological role of 2-AG, which is tightly regulated by enzymes responsible for its biosynthesis and catabolism. The function of each of these enzymes is described in detail.

Diacylglycerol lipase α (DAGL- α) is a key enzyme involved in the biosynthesis of 2-AG in the brain. To gain insight in the physiological role of 2-AG, selective inhibitors for DAGL- α are required. An ABP that detects diacylglycerol lipases in native biological systems is a highly valuable tool for the identification and characterization of inhibitors for DAGL- α . **Chapter 3** describes the synthesis and characterization of a tetrahydrolipstatin (THL)-derived ABP (MB064) for DAGL- α . This ABP is required, because the commonly used fluorophosphonate-based broad-spectrum serine hydrolase ABPs do not react well with DAGL- α .

MB064 was used to screen a targeted compound library against DAGL- α activity in the mouse brain membrane proteome. This screen revealed a new inhibitor for DAGL- α and DAGL- β . The inhibitor was termed “LEI104”. A gel-based assay in the mouse brain membrane proteome revealed that the inhibitor had an important off-target that could complicate analysis when using this inhibitor to study the physiological function of 2-AG.

The aim of the research described in **Chapter 4** was to optimize LEI104 towards a more selective DAGL- α/β inhibitor. This optimization requires an assay that can determine the target interaction profile of reversible serine hydrolase inhibitors in complex proteomes. To this end, a chemoproteomic assay using MB108, a biotinylated version of MB064, was developed and applied. MB108 was instrumental in the discovery of LEI105, the most selective inhibitor for DAGL- α and DAGL- β to date.

The aim of the research described in **Chapter 5** was to investigate the structure activity relationship of LEI105 on DAGL- α . This may provide insight in important enzyme-inhibitor interactions and lead to the discovery of potent inhibitors with improved physicochemical properties. Competitive and comparative ABPP assays enabled the determination of their selectivity profile across a large panel of serine hydrolases.

The aim of the research described in **Chapter 6** was to use the chemoproteomics assay to study the relative activity of different hydrolases involved in endocannabinoid biosynthesis and metabolism in various mouse brain regions, such as the hippocampus, cerebellum, striatum and frontal cortex. Comparison of specific serine hydrolase activities between the brain regions provided insight in which endocannabinoid metabolic pathway is important in specific brain regions. Subsequently the regulatory function of the CB₁ receptor on

endocannabinoid hydrolase activities was investigated by comparing serine hydrolase activity in brain regions from CB₁ knockout and wild type mice.

The aim of the research described in **Chapter 7** was to investigate the interaction landscape of MB064 and MB108. In this Chapter a chemoproteomic mouse tissue screen was performed to identify all targets of MB064 and MB108. This revealed that these ABPs react with multiple members of the α,β -hydrolase family. Several members of this class were recombinantly expressed and screened against a focused library of lipase inhibitors. This led to the identification of new inhibitors for ABHD2 and ABHD3.

Chapter 8 summarizes the work described in this thesis and presents some future challenges.

References

1. Sharma, K.; Schmitt, S.; Bergner, C. G.; Tyanova, S.; Kannaiyan, N.; Manrique-Hoyos, N.; Kongi, K.; Cantuti, L.; Hanisch, U. K.; Philips, M. A.; Rossner, M. J.; Mann, M.; Simons, M. *Nat. Neurosci.* **2015**, *18*, 1819.
2. Uhlen, M.; Fagerberg, L.; Hallstrom, B. M.; Lindskog, C.; Oksvold, P.; Mardinoglu, A.; Sivertsson, A.; Kampf, C.; Sjostedt, E.; Asplund, A.; Olsson, I.; Edlund, K.; Lundberg, E.; Navani, S.; Szigartyo, C. A.; Odeberg, J.; Djureinovic, D.; Takanen, J. O.; Hober, S.; Alm, T.; Edqvist, P. H.; Berling, H.; Tegel, H.; Mulder, J.; Rockberg, J.; Nilsson, P.; Schwenk, J. M.; Hamsten, M.; von Feilitzen, K.; Forsberg, M.; Persson, L.; Johansson, F.; Zwahlen, M.; von Heijne, G.; Nielsen, J.; Ponten, F. *Science* **2015**, *347*, 1260419.
3. Otlewski, J.; Jelen, F.; Zakrzewska, M.; Oleksy, A. **2005**, *24*, 1303.
4. Lindsley, J. E.; Rutter, J. *Proc. Natl. Acad. Sci. U. S. A.* **2006**, *103*, 10533.
5. Moellering, R. E.; Cravatt, B. F. *Chem. Biol.* **2012**, *19*, 11.
6. Willems, L. I.; Overkleeft, H. S.; van Kasteren, S. I. *Bioconjugate Chem.* **2014**, *25*, 1181.
7. Debets, M. F.; van Hest, J. C.; Rutjes, F. P. *Org. Biomol. Chem.* **2013**, *11*, 6439.
8. Niphakis, M. J.; Cravatt, B. F. *Annu. Rev. Biochem.* **2014**, *83*, 341.
9. Hoover, H. S.; Blankman, J. L.; Niessen, S.; Cravatt, B. F. *Bioorg. Med. Chem. Lett.* **2008**, *18*, 5838.
10. de Bruin, G.; Xin, B. T.; Kraus, M.; van der Stelt, M.; van der Marel, G. A.; Kisselev, A. F.; Driessen, C.; Florea, B. I.; Overkleeft, H. S. *Angew. Chem. Int. Ed.* **2016**, *55*, 4199.
11. Niphakis, M. J.; Cravatt, B. F. *Annu. Rev. Biochem.* **2014**, *83*, 341.
12. Saghatelian, A.; Cravatt, B. F. *Nat. Chem. Biol.* **2005**, *1*, 130.
13. Fonovic, M.; Bogyo, M. *Expert Rev. Proteomics* **2008**, *5*, 721.
14. Baggelaar, M. P.; Janssen, F. J.; van Esbroeck, A. C.; den Dulk, H.; Allara, M.; Hoogendoorn, S.; McGuire, R.; Florea, B. I.; Meeuwenoord, N.; van den Elst, H.; van der Marel, G. A.; Brouwer, J.; Di Marzo, V.; Overkleeft, H. S.; van der Stelt, M. *Angew. Chem. Int. Ed.* **2013**, *52*, 12081.
15. Kumar, S.; Zhou, B.; Liang, F.; Wang, W. Q.; Huang, Z.; Zhang, Z. Y. *Proc. Natl. Acad. Sci. U. S. A.* **2004**, *101*, 7943.
16. Willems, L. I.; Jiang, J.; Li, K. Y.; Witte, M. D.; Kallemeyjn, W. W.; Beenakker, T. J.; Schroder, S. P.; Aerts, J. M.; van der Marel, G. A.; Codee, J. D.; Overkleeft, H. S. *Chem. Eur. J.* **2014**, *20*, 10864.
17. Zheng, B.; DeRan, M.; Li, X.; Liao, X.; Fukata, M.; Wu, X. *J. Am. Chem. Soc.* **2013**, *135*, 7082.

18. Ogasawara, D.; Deng, H.; Viader, A.; Baggelaar, M. P.; Breman, A.; den Dulk, H.; van den Nieuwendijk, A. M.; Soethoudt, M.; van der Wel, T.; Zhou, J.; Overkleeft, H. S.; Sanchez-Alavez, M.; Mori, S.; Nguyen, W.; Conti, B.; Liu, X.; Chen, Y.; Liu, Q. S.; Cravatt, B. F.; van der Stelt, M. *Proc. Natl. Acad. Sci. U. S. A.* **2016**, *113*, 26.
19. Bachovchin, D. A.; Ji, T.; Li, W.; Simon, G. M.; Blankman, J. L.; Adibekian, A.; Hoover, H.; Niessen, S.; Cravatt, B. F. *Proc. Natl. Acad. Sci. U. S. A.* **2010**, *107*, 20941.
20. Hsu, K. L.; Tsuboi, K.; Adibekian, A.; Pugh, H.; Masuda, K.; Cravatt, B. F. *Nat. Chem. Biol.* **2012**, *8*, 999.
21. Liu, Y.; Patricelli, M. P.; Cravatt, B. F. *Proc. Natl. Acad. Sci. U. S. A.* **1999**, *96*, 14694.
22. Chang, J. W.; Cognetta, A. B., 3rd; Niphakis, M. J.; Cravatt, B. F. *ACS Chem. Biol.* **2013**, *8*, 1590.

CHAPTER 2

2-Arachidonoylglycerol: a Signaling Lipid

1. Introduction

2-Arachidonoylglycerol (2-AG) is one of the most extensively studied monoacylglycerols. It is an important signaling lipid as well as an intermediate in lipid metabolism.^{1,2} It was isolated from canine gut and identified as an endogenous ligand for the cannabinoid receptors in 1995.^{3,4} 2-AG behaves as a full agonist for the cannabinoid CB₁ and CB₂ receptors,⁵⁻⁸ which are the main receptors through which 2-AG exerts its physiological effects. 2-AG and the cannabinoid receptors are part of an endogenous signaling system termed “the endocannabinoid system”, which is also modulated by Δ^9 -tetrahydrocannabinol (Δ^9 -THC), the main psychoactive constituent of the plant *cannabis sativa*.⁹ Both CB receptors are associated with the regulation of many physiological processes, including inflammation,¹⁰ food intake,¹¹⁻¹³ locomotor activity,^{14,15} pain sensation,¹⁶ mood,^{17,18} addiction and reward.¹⁹ The cannabinoid receptors share ~44% sequence homology, and show different expression profiles.²⁰ The CB₁ receptor is expressed throughout the body, but it is most extensively studied in the central nervous system where it is one of the highest expressed GPCRs in the brain.^{21,22} While there is a strong debate about CB₂ receptor expression in the brain, its predominant localization on immune cells is well established, which is in line with its role in modulating immune responses.²³⁻²⁵ While several other endogenous biomolecules interact with the CB₁ and CB₂ receptors, including *N*-arachidonylethanolamine (anandamide; AEA)²⁶, virodhamine, *N*-arachidonoyldopamine (NADA) and noladin ether (see Table 1 for a complete list, and Pertwee *et al.*²⁷ for their in vitro binding affinities), 2-AG, together with AEA, is considered to be one of the most important endocannabinoids. Of note, brain 2-AG levels are ~170 times higher than those of AEA.²⁸ 2-AG is involved in neurogenesis, synapse formation and synaptic transmission, thereby mediating various forms of long- and short-term plasticity.²⁹ 2-AG is synthesized

“on demand” and acts as a retrograde messenger that inhibits neurotransmitter release at both inhibitory and excitatory synapses.³⁰⁻³²

Several reports indicate that 2-AG produces physiological effects independent of the CB₁ and CB₂ receptors. 2-AG has been shown to interact with a number of other receptors, including GABA_A,³³ TRPV1,³⁴ Adenosine A₃,³⁵ GPR55,³⁶ and PPAR γ .³⁷ Interactions with these proteins are important to consider when studying the physiological role of 2-AG. The levels of 2-AG, and thereby the interaction with its target receptors, are tightly regulated by its biosynthetic and catabolic enzymes (Figure 1). Multiple enzymes in different pathways contribute to the biosynthesis and catabolism of 2-AG. Notably, multiple precursors and metabolites of 2-AG have signaling functions as well. This chapter describes the physiological role of 2-AG in the brain, and how disrupting 2-AG biosynthesis and catabolism facilitates insight in these physiological functions.

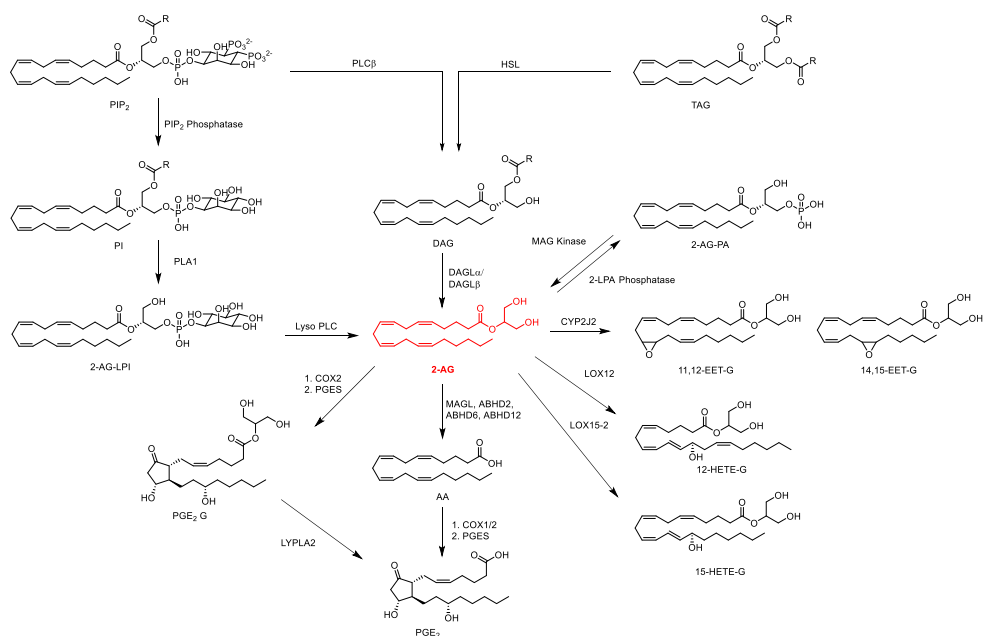


Figure 1. Overview of the major biosynthetic and metabolic pathways for 2-AG. PLC β : phospholipase C β , HSL: hormone sensitive lipase, PIP₂: phosphatidylinositol-4,5-bisphosphate, PI: phosphatidylinositol, TAG: triacylglycerol, DAG: diacylglycerol, PLA1: phospholipase A1, 2-AG-LPI: 2-arachidonoyl lyso-phosphatidylinositol, Lyso-PLC: lyso-phospholipase C, MAG kinase: monoacylglycerol kinase, 2-LPA phosphatase: 2-lysophosphatidic acid phosphatase, 2-AG: 2-arachidonoylglycerol, 2-AG-PA: 2-arachidonoylglycerol phosphatidic acid, CYP2J2: cytochrome P2J2, LOX-12: lipoxygenase 12, LOX-15-2: lipoxygenase 15-2, MAGL: monoacylglycerol lipase, ABHD2, 6, 12: alpha/beta hydrolase domain containing 2, 6, 12, COX1/2: cyclooxygenase 1/2, LYPLA2: lysophospholipase 2, 11, 12-EET-G: 11, 12-epoxyeicosatrienoic acid glycerol ester, 14, 15-EET-G: 14, 15-epoxyeicosatrienoic acid glycerol ester, PGE₂-G: prostaglandin E₂ glycerol ester, PGE₂: prostaglandin E₂, 12-HETE-G: 12-hydroxyeicosatetraenoic glyceryl ester, 15-HETE-G: 15-hydroxyeicosatetraenoic glyceryl ester.

2. 2-AG biosynthesis

The biosynthesis of 2-AG can be divided in two main pathways with different functionalities (Figure 1). A signaling pathway, starting from phosphatidylinositol-4,5-bisphosphate (PIP₂), and a metabolic pathway using *sn*-2-arachidonate containing triglycerides. PIP₂ is converted into two important second messengers by phospholipase C β (PLC β): diacylglycerol (DAG) and inositol-1,4,5-triphosphate.^{28,38} PLC β uses Ca²⁺ as a cofactor and acts as a coincidence detector by integrating the signals coming from G_q-coupled receptor activation and the influx of extracellular Ca²⁺ via ionotropic receptors and voltage gated calcium channels.^{28,39-42} The metabolic pathway involves the hydrolysis of triglycerides by hormone-sensitive lipase, carboxyl esterase and other lipases to *sn*-2-arachidonoylglycerol containing diglycerides.²⁸ At this point the two pathways converge and the diglycerides are further processed by two isoforms of a *sn*-1-specific diacylglycerol lipase, diacylglycerol lipase- α and - β (DAGL- α and - β).⁴³ The DAG lipases hydrolyze diacylglycerols at the *sn*-1 position, generating 2-AG and a fatty acid. DDHD domain-containing protein 2 (DDHD2) has recently been reported to possess also the ability to hydrolyze DAG.⁴⁴ Partially purified DDHD2 from rat brain, and rat DDHD2 expressed in Chinese hamster ovary cells (CHO cells) exhibited diacylglycerol lipase activity in vitro. However, Inloes *et al.* generated a DDHD2 KO mouse, which revealed that DDHD2 was a principal triglyceride lipase *in vivo*.⁴⁵ Thus, further research is required to establish the physiological relevance of this pathway with regard to 2-AG biosynthesis in the brain.

2-AG can also be generated from PIP₂ by PIP₂ phosphatase towards phosphatidyl inositol (PI), followed by hydrolysis of the *sn*-1-ester by phospholipase A1 to generate 2-arachidonoyl-LPI. In a final step the phosphate is removed by lysophospholipase C (LysoPLC) to form 2-AG.⁴⁶ In 2002, lysophosphatidic acid was found in rat brain. This lipid could be quickly converted to 2-AG by 2-LPA phosphatase.⁴⁷ Although these alternative pathways may provide 2-AG, diacylglycerol lipases are considered to be the most important enzymes. These proteins are the main contributors to 2-AG biosynthesis as identified by selective DAGL inhibitor studies, as well as by DAGL- α and DAGL- β KO studies.⁴⁸⁻⁵⁰

2.1 Diacylglycerol lipase alpha and beta

The enzymatic activity that hydrolyses the *sn*-1-acyl chain from 1,2-diglycerides yielding 2-AG in human platelets was first detected by Prescott and Majerus in 1983.⁵¹ Substrates containing *sn*-1-palmitate and stearate showed the same rate of hydrolysis. After the identification of this transformation, considerable efforts were undertaken to characterize and isolate the enzyme from bovine brain.^{52,53} It was not until 2003 that two enzymes were identified and cloned, and designated as diacylglycerol lipase- α and - β .⁴³ The human genes show a high homology compared with those of mouse, 97% for DAGL- α and 79% for

DAGL- β . DAGL- α and DAGL- β structurally differ by the absence of a large C-terminal tail in DAGL- β compared to DAGL- α . Transfection of the DAGL- α and DAGL- β genes in COS cells resulted in enzymes with a molecular weight of ~120 kD for DAGL- α and ~70 kD for DAGL- β . Molecular characterization of these two enzymes revealed that they are plasma membrane bound serine hydrolases that show specificity for hydrolysis at the *sn*-1-position of diacylglycerols.⁴³

The C-terminal tail of DAGL- α plays an important regulatory function. The activity of DAGL- α is modulated by calcium/calmodulin dependent protein kinase II (CaMKII) which phosphorylates Ser⁷⁸² and Ser⁸⁰⁸ on the C-terminal tail of DAGL- α .⁵⁴ DAGL- α phosphorylation significantly reduced its activity. The C-terminal tail of DAGL- α contains also a consensus motif (PPxxF) for binding with the coiled coil domain of homer proteins. Homers are adaptor proteins that interact with many different proteins, including the metabotropic glutamate receptor. An interaction between homer-1b and homer-2 with DAGL- α was shown to be important for DAGL- α localization at the plasma membrane, but is not required for its catalytic activity.⁵⁵ Moreover, the surface expression of DAGL- α is dynamic, undergoing endocytosis and recycling back to the postsynaptic membrane.⁵⁶ DAGL- α cycling between the cell surface and intracellular endosomal compartments is regulated by protein kinase C (PKC). Rapid degradation and replenishment of DAGL- α upon inhibition with covalent inhibitor DH376 indicates a short protein half-life.⁵⁷ These observations indicate that the activity, expression and localization of DAGL- α have a tight spatiotemporal control on 2-AG synthesis and release.

Two landmark studies have shown the importance of the contribution of DAGL- α and DAGL- β to the *in vivo* biosynthesis of 2-AG. Congenital deletion of DAGL- α or - β reduced 2-AG levels in the brain with 80% and 50%, respectively.^{48,49} These studies also revealed a tissue specific contribution of the DAG-lipases to the biosynthesis of 2-AG. In the liver, the roles were reversed with a 50% reduction of 2-AG in DAGL- α KO mice compared to a 90% reduction in DAGL- β KO mice. DAGL- α is highly expressed in neurons and is found at (peri)post-synaptic sites. 2-AG acts as a retrograde neurotransmitter, suppressing synaptic transmission at central synapses. Stimulation of 2-AG release by depolarization of postsynaptic neurons, activation of G_{q/11}-coupled receptors and a combination of G_{q/11}-coupled receptor activation and Ca²⁺ elevation resulted in suppression of synaptic transmission at both excitatory and inhibitory synapses (DSE and DSI respectively). This suppression was absent in DAGL- α KO brain slices, but DAGL- β knockout brain slices maintained retrograde suppression of synaptic transmission.^{58,59} This is in line with the higher activity of DAGL- α in the brain and the cellular distribution of both isoforms. DAGL- α displays higher activity in neurons, while DAGL- β is relatively more active in microglia.⁶⁰

Over the years multiple pharmacological tools have been developed to modulate DAGL activity, see Kohnz *et al.*⁶¹ and Janssen *et al.*⁶² for recent reviews on DAGL inhibitors. Subtype selective inhibitors for the diacylglycerol lipases have not been identified to date.

Dual DAGL- α and DAGL- β inhibitors in combination with DAGL- α and DAGL- β knockout mice have greatly facilitated the study of the physiological role 2-AG in health and disease models. Recently, Ogasawara *et al.* reported the first CNS active dual DAGL- α/β inhibitors.⁵⁷ Lipid analysis in the brain revealed an extensive rewiring of lipid metabolic pathways in the brain upon inactivation of DAGL- α and DAGL- β . Not only levels of *sn*-1-stearyl-2-arachidonoyl-glycerol, but also levels of *sn*1-palmitoyl-2-arachidonoyl-glycerol, *sn*-1-palmitoyl-2-stearyl-glycerol, *sn*-1-oleyl-2-stearyl-glycerol were elevated in DAGL- α KO, and DAGL inhibitor treated mouse brains. Downstream, not only levels of 2-AG were reduced, but also levels of palmitoyl-glycerol, oleoyl glycerol and docosahexaenoyl-glycerol. These lipids are important signaling lipids in their own right, which could complicate interpretation of physiological effects observed upon DAGL blockade to 2-AG.

3. 2-AG Catabolism

2-AG is catabolized by multiple different pathways and enzymes (Figure 1). All of these lead to a decrease in the 2-AG levels and signaling. The predominant pathway for 2-AG catabolism is the hydrolysis of the ester bond into arachidonic acid (AA) and glycerol. Blankman *et al.* showed that MAGL was responsible for ~85%, ABHD12 (~9%) and ABHD6 (~4%) of 2-AG hydrolysis in mouse brain.⁶³ Together they are responsible for more than 98% of the 2-AG hydrolysis in the brain. Cyclooxygenases (COX), lipoxygenases (LOX), and cytochrome P450s (CytP450) have been reported use 2-AG also as a substrate. Recently ABHD2 has been reported to hydrolyze 2-AG in spermatozoa. This enzyme has a relatively high expression in the brain compared to other tissues. Therefore this enzyme could be an important player to consider in this context. In the next section the enzymes responsible for the metabolism of 2-AG will be discussed in more detail.

3.1 Monoacylglycerol Lipase (MAGL)

In the early sixties, it was demonstrated that two proteins distinct from lipoprotein lipase, were involved in the hydrolysis of triacylglycerol towards fatty acids in adipose tissue of both rats and rabbits. Hormone sensitive lipase (HSL) was believed to hydrolyze triacylglycerol to monoacylglycerols, and a dedicated lipase subsequently hydrolysed monoacylglycerols towards free fatty acids and glycerol.⁶⁴ Partial purification of the monoacylglycerol lipase activity convincingly showed its preference towards monoacylglycerols over diacylglycerols and triacylglycerols.⁶⁵ It took until 1997 before a specific monoacylglycerol lipase (MAGL) was cloned for the first time.⁶⁶ The enzyme consists of 302 amino acids and has a molecular weight of 33 kD.⁶⁶ It is an ubiquitously expressed serine hydrolase containing the typical GX SXG motif with Ser-122, Asp-239 and His-269 forming the catalytic triad.^{61,64} The active site of the enzyme resides in the cytosol, but the enzyme also associates with membranes. MAGL exists in several splice forms in the

brain and testes.⁶⁷⁻⁶⁹ MAGL has a broad substrate specificity and hydrolyses multiple monoacylglycerols with different chain lengths and degrees of unsaturation, including 2-palmitoylglycerol, 2-stearoylglycerol and 2-oleoylglycerol.⁷⁰⁻⁷²

The interest in MAGL boosted when, next to its original role in mobilizing free fatty acids in adipose tissue, the enzyme was linked to the endocannabinoid system.²⁷ This was demonstrated by overexpression of the enzyme in HeLa cells, which significantly increased 2-AG hydrolysis. In line with this observation, RNA interference in the same cell line elevated 2-AG levels.²⁷ Immunodepletion of MAGL reduced 2-AG hydrolyzing activity in rat brain with ~50%.^{27,33}

The development of mouse models with congenital deletion of MAGL has significantly advanced our understanding of the role of MAGL *in vivo*.⁷³⁻⁷⁶ Chronic disruption of MAGL activity severely decreased the mouse brain ability to hydrolyse 2-AG. This leads to a >10 fold increase of 2-AG in the brain and less pronounced but significant reduction of 2-AG in the thymus, spleen and liver.⁷⁶ Noteworthy, levels of other monoacylglycerols were also increased *in vivo*. Tonic elevation of 2-AG levels by MAGL knockout in the brain causes CB₁ receptor adaptations. MAGL knockout mice exhibited impaired endocannabinoid-dependent synaptic plasticity, physical dependence and desensitization of brain CB₁ receptors.⁷⁴ Opposite to the increase in 2-AG levels, AA abundance in the brain dropped significantly in the absence of MAGL.^{74,76} This indicates that a large extent of the metabolic route towards AA travels through MAGL. Therefore, the activity of MAGL affected levels of pro-inflammatory oxidative metabolites of AA, and designated MAGL as a key enzyme in regulating neuro-inflammatory responses.⁷⁷

Several selective and *in vivo* active MAGL inhibitors have been developed to study the role of MAGL in 2-AG metabolism and signaling.^{69,78-81} MAGL is relatively abundant in neurons compared to astrocytes and microglia. In contrast to the major 2-AG biosynthetic enzyme DAGL- α , MAGL is positioned presynaptically along with the cannabinoid CB₁ receptor. Evidence for the role of MAGL in retrograde 2-AG signaling was shown in electrophysiology experiments in cultured neurons and brain slices, where both MAGL inhibitors and genetic deletion of MAGL enhanced DSI/DSE.⁸²⁻⁸⁸ Hydrogen peroxide mediated MAGL sulfonylation of C-201 and C-208 reduces MAGL activity and thereby increases endocannabinoid signaling in neurons.⁸⁹ However, the effect of this posttranslational modification on DSI and DSE remains to be investigated.

The tissue specific role of MAGL was further investigated using the MAGL inhibitor JZL184. The levels of 2-AG were 8-fold increased in the brain, whereas in peripheral tissues, such as liver, kidney, spleen, BAT and heart, the change was less pronounced. No significant changes were observed in the testis, lung and white adipose tissue.⁶⁹ Interestingly, C16:0 and 18:1 MAGs were more increased in peripheral tissues compared to the brain. This suggests that MAGL has a more general metabolic function in peripheral tissues.^{69,76}

Repeated administration of the selective MAGL inhibitor JZL184 mirrored the observations in the knockout mice and caused CB₁ receptor desensitization, tolerance to

CB₁ receptor agonists and downregulation of CB₁ receptors.⁷⁴ This points towards a major role for MAGL in regulating bulk 2-AG levels and raises the question whether a therapeutic window to elevate 2-AG levels can be achieved without causing desensitization of CB₁ signaling. Several studies have addressed this question and investigated the effect of partial blockade of MAGL using low doses of JZL184.⁹⁰⁻⁹³ Chronic JZL184 dosing for ~7 days up to 8 mg/kg per day did not lead to CB₁ receptor desensitization or behavioral tolerance, while chronically treated animals with 16 mg/kg JZL184 per day did show tolerance.^{92,93} Thus, it appears to be possible to elevate 2-AG levels without desensitization of the CB₁ receptor.

3.2 Alpha/beta hydrolase domain containing 6 (ABHD6)

The α,β -hydrolase domain-containing protein 6 (ABHD6) is part of a superfamily of proteins having an α,β -hydrolase fold.⁹⁴ It is a membrane bound protein consisting of 337 amino acids and has a mass of 38 kD.⁶³ It is a serine hydrolase that contains a catalytic triad with the typical GX SXG motif surrounding the catalytic Ser-148; the other two members of the catalytic triad are Asp-278 and His-306.⁹⁵ mRNA expression analysis in mice showed that ABHD6 is ubiquitously expressed throughout the body with relatively high expression in brown adipose tissue and the brain.⁹⁶ In the human cortex mRNA expression of ABHD6 steadily increased from neonatal age until adulthood.⁹⁷ It is postulated that ABHD6 is membrane bound, with its active site facing the cytosol. ABHD6 is responsible for ~4% of the total 2-AG hydrolysis in mouse brain homogenate.⁶³ Several selective inhibitors have been developed to study ABHD6 function.⁹⁸⁻¹⁰¹ In microglial (BV-2) cells ~50% of 2-AG degradation is mediated by ABHD6. In Neuro2A cells, 2-AG levels are increased after inhibition with the selective ABHD6 inhibitor KT195.⁵⁰ Both Neuro2A and BV-2 cells lack MAGL activity, therefore ABHD6 can be an important player in 2-AG hydrolysis in specific cell types. Many studies have focused on the role of ABHD6 in 2-AG metabolism and endocannabinoid signaling in the brain. Electron microscopy and immunofluorescence experiments revealed localization of ABHD6 in postsynaptic dendrites in adult mouse brain, whereas MAGL is predominantly expressed pre-synaptically.¹⁰² Positioning ABHD6 at the site of 2-AG production. Inhibition of ABHD6 in prefrontal cortical brain slices by the selective inhibitor WWL70 could reduce CB₁ receptor mediated long term depression (LTD).¹⁰² Depolarization induced suppression of inhibition (DSI) or excitation (DSE) in autaptic hippocampal neurons were not reduced by inhibition of ABHD6.^{87,103,104} ABHD6 is considered an interesting drug target for moderate elevation of 2-AG levels. Inhibition of ABHD6 had anti-inflammatory and neuroprotective effects in a mouse model of traumatic brain injury, exerted antiepileptic activity and reduced neuro-inflammation and neurodegeneration in a mouse model of multiple sclerosis.¹⁰⁵⁻¹⁰⁷ Interestingly, ABHD6 has recently been reported to negatively regulate surface delivery and synaptic function of the

AMPA receptors, ionotropic glutamate receptors that mediate synaptic transmission. ABHD6 overexpression in neurons could drastically reduce excitatory neurotransmission mediated by the AMPA receptor independent of its hydrolytic activity.¹⁰⁸

Several studies have assessed the role of ABHD6 in peripheral tissues. ABHD6 inhibition raises 2-AG levels in macrophages and is subsequently converted by COX2 to PGD₂-G, which demonstrated an anti-inflammatory effect.¹⁰⁹ Targeted antisense oligonucleotides (ASOs) to knockdown ABHD6 *in vivo* in peripheral tissues (liver, white adipose tissue and kidney) did not affect monoacylglycerol levels, however, lysophospholipid levels were strongly elevated. Knocking down ABHD6 in the liver exerted a protective effect against high-fat diet induced obesity in mice.⁴⁷ Studies with ABHD6 knockout and inhibitor treatment showed a role of ABHD6 in insulin secretion by pancreatic β -cells and identified Munc13-1 as the intracellular receptor for MAG-induced exocytosis.^{110,111} Recently, it was demonstrated that genetic deletion of ABHD6 elevates 1-MAG concentrations and plays a role in fuel homeostasis, BAT-function and WAT browning via PPAR α/γ activation.¹¹² Furthermore, ABHD6 has been shown to degrade bis(monoacylglycerol)phosphate (BMP).¹¹³ ABHD6 is responsible for 90% and 50% of the BMP hydrolysis in the liver and brain, respectively. ABHD6 co-localizes with the late endosomes/lysosomes. It would be interesting to see whether changes in lipid sorting or cargo recycling by inhibition of ABHD6 can affect cannabinoid signalling or steatosis. The role of 2-AG in these metabolic effects might be small, since ABHD6 has been shown to have a broad substrate specificity.^{95,112}

3.3 Alpha/beta hydrolase domain containing 12 (ABHD12)

The α,β -hydrolase domain-containing protein 12 (ABHD12) belongs to the same α, β -hydrolase fold containing superfamily as ABHD6.⁹⁴ ABHD12 is a membrane bound protein with an extracellular orientation of its active site.^{63,114} It is a 398 amino acid containing enzyme with a molecular weight of 45 kD. It is a serine hydrolase having a lipase motif (GTSMG) and the catalytic triad is formed by Ser-246, Asp-333 and His-372.⁹⁵ ABHD12 contributes approximately ~9% of the total 2-AG metabolism in mouse brain homogenates.⁶³ Null mutations in ABHD12 cause the human neurodegenerative disorder PHARC (polyneuropathy, hearing loss, ataxia, retinosis pigmentosa, and cataract).¹¹⁵ ABHD12 transcripts are highly expressed in the brain, with a significant enrichment in microglia.¹¹⁶ No selective inhibitors of ABHD12 are available, but the generation and analysis of the metabolic and behavioral phenotype of a mouse model with congenital deletion of ABHD12 has greatly facilitated the understanding of its biological role.¹¹⁷ ABHD12 knockout mice showed PHARC like symptoms such as hearing disruptions, muscle weakness and ataxia. Importantly, these mice showed high elevations in lysophosphatidylserines (LPS), whereas the 2-AG hydrolyzing capacity of ABHD12 knockout brain homogenate did not significantly differ compared to wild type brain

homogenate. Interestingly, after incubation with a MAGL inhibitor, a significant reduction in 2-AG hydrolyzing capacity was observed compared to wild type brain homogenate. A possible explanation for this observation could be that ABHD12 plays a more specialized role and is recruited when there is insufficient 2-AG hydrolyzing capacity. This is in line with the observation that ABHD12 overexpression did not affect DSE.⁸⁷ No data supporting endogenous ABHD12 hydrolysis of 2-AG in *in situ* or *in vivo* have been generated so far. Identification of selective inhibitors that allow spatiotemporal control over ABHD12 activity will be a crucial tool to elucidate the role of ABHD12 in 2-AG metabolism.

3.4 ABHD2

The α,β -hydrolase domain-containing protein 2 (ABHD2) is another member of α,β -hydrolase fold containing superfamily. The enzyme is a serine hydrolase with a classical Ser-207, His-376, Asp-345 catalytic triad. ABHD2 is predicted to be a single pass type-II membrane protein. The expression of the enzyme is highest in the lung, brain and adrenal glands.⁹⁶ Knockdown of ABHD2 using antisense oligonucleotides and gene trapping techniques demonstrated an essential role of 2-AG in Hepatitis B virus propagation.¹¹⁸ ABHD2 appears to play an important role in chronic diseases involved in monocyte/macrophage recruitment, such as atherosclerosis and emphysema.^{119,120} It was not until recently that ABHD2 was linked to 2-AG metabolism.¹²¹ The enzyme is highly expressed in spermatozoa and acts as a progesterone-dependent hydrolase. Activation of ABHD2 reduces inhibition of sperm calcium channel CatSper by 2-AG, which leads to calcium influx and stimulates sperm activation. No inhibitors for ABHD2 have been reported to date, and the contribution of ABHD2 in 2-AG metabolism in the brain requires further investigation.

3.4 Cyclooxygenase-2 (COX-2)

Cyclooxygenases exist in two isoforms cyclooxygenase-1 and -2 (COX-1 and COX-2). Both enzymes play an important role in inflammation. The expression of COX-2 is increased in inflammatory processes and is essential for the oxidation of AA as part of its transformation into prostaglandins.¹⁰⁹ In contrast to the constitutively expressed COX-1, which has a strong preference for substrates with a free carboxylate group, COX-2 metabolizes both AA and 2-AG with similar K_{cat} and K_m .^{122,123} Several papers suggest that COX-2 plays a role in terminating 2-AG signaling in the CNS. Kim and Alger showed that inhibition of COX-2 prolonged DSI in hippocampal slice preparation.¹²⁴ A later study in cultured hippocampal neurons showed that the duration of DSI in a subpopulation of interneurons was influenced by both MAGL and COX-2.¹⁰³ Substrate selective inhibitors for COX-2 have been developed, which selectively block the oxidation of 2-AG but not

AA.^{125,126} The substrate selective inhibitor LM-4131 could increase 2-AG levels in RAW264.7 cells and intraperitoneal (IP) injection of this inhibitor led to an *in vivo* increase of 2-AG levels in the brain.¹²⁶

COX-2 mediated oxidation of 2-AG produces the prostaglandin glyceryl ester PGE₂-G (Figure 2). Most of the effects of substrate selective blockade of COX-2 appear to be caused by changes in PGE₂-G concentrations rather than minor alterations in 2-AG levels.¹²⁶ PGE₂-G is a multifunctional signaling molecule that plays a role in pain, immunomodulation, and synaptic plasticity.¹²⁷⁻¹²⁹ The receptor for PGE₂-G has not been identified, but the actions of PGE₂-G are mediated through ERK, p38 mitogen-activated protein kinase (MAPK), IP(3), and NF-κβ.¹²⁹ In contrast to the anti-nociceptive and anti-inflammatory role of 2-AG, the COX-2 metabolite PGE₂-G produces hyperalgesia and enhances inflammation induced neurodegeneration.^{127,129,130} Important to note is that 2-AG suppresses elevation of COX-2 expression via a CB₁ receptor mediated mechanism involving PPARγ and the MAPK/NFκ-B signaling pathway.^{131,132} PGE₂-G can be further processed by lysophospholipase A2 (LYPLA2) towards PGE₂.¹³³

3.5 Lipoxygenase

Lipoxygenases are a family of non-heme iron containing dioxygenases that catalyze the oxidation of polyunsaturated fatty acids that contain one or more (1Z,4Z)-pentadiene moieties.¹³⁴ This oxidation yields the corresponding (1S,2E,4Z)-hydroperoxides. Moody *et al.* showed that lipoxygenase-12 (LOX-12) oxygenates glycerol esters towards 12-hydroxyeicosatetraenoic (12-HETE) glyceryl ester.¹³⁵ Kozak *et al.* screened a panel of 6 lipoxygenases for their 2-AG oxygenating properties. They found that LOX-15-1 and LOX-15-2 also catalyse the oxygenation of 2-AG towards 15-HETE-glycerol ester.¹³⁶ Moreover, among a series of structural related arachidonoyl esters, 2-AG was the most optimal substrate for LOX-15 oxygenation. 2-AG treatment of COS-7 cell transfected with 15-LOX led to the biosynthesis and excretion of 15-HETE-G. Van der Stelt *et al.* investigated the affinity of LOX metabolites of 2-AG for the cannabinoid receptors. It was found that 15-HETE-1-AG showed moderate affinity for the CB₂ receptor, but not for the CB₁ receptor.¹³⁷ No data on *in vivo* conversion of 2-AG by LOX-15 or LOX-12 has been reported. Therefore, the physiological role of this pathway has yet to be established.

3.6 Cytochrome P450

Cytochrome P450 (CYP450) are heme-containing oxidative enzymes involved in drug metabolism, but they can also use endogenous lipids, such as 2-AG, as substrates.^{138,139} Two epoxide regioisomers (2-11, 12- and 2-14, 15-epoxyeicosatrienoic acid glycerol ester (EET-EG)) of CYP metabolites of 2-AG have been isolated from rat kidney and spleen,

whereas 2-14, 15-EET-EG was also detected in the brain.¹⁴⁰ These metabolites had a higher binding affinity for the CB₁ and CB₂ receptors compared to 2-AG, whereas the corresponding oxidized metabolites from AA (11,12-EET and 14,15-EET) did not display any CB receptor affinity. Incubation of 2-AG with the predominant CYP450 in the heart, CYP2J2 epoxigenase produces 2-11, 12- and 2-14, 15-EET-EG in vitro.¹⁴¹ In addition, heart microsomes derived from bovine and porcine tissues also produced 2-11, 12- and 2-14, 15-EET-EG. The physiological role of these CYP450 metabolites remains to be elucidated.

4. 2-AG storage and transport

2-AG is a retrograde messenger. It is produced in the postsynaptic cell, and travels across the synapse to the presynaptic nerve terminal where it inhibits neurotransmitter release by activation of the CB receptors. There has been an outstanding question whether 2-AG is synthesized “on demand” or stored and released from preformed pools. DSI was robustly absent in DAGL- α , but not DAGL- β knockout models.^{48,58} However, pharmacological inhibition gave inconsistent results.¹⁴² Several studies found a reduction in DSI,^{84,143-146} where others did not.^{147,148} Recently new chemotypes were identified as DAGL inhibitors that could reduce DSI,^{57,149} supporting the hypothesis of on demand synthesis. A possible explanation for the discrepancies between the earlier studies is poor penetration of lipophilic inhibitors in brain slices. The localization, expression and activity of DAGL- α is highly regulated, and the site of 2-AG synthesis in combination with transport might be a pivotal determinant for its fate. Therefore, understanding whether and how 2-AG is stored and transported is crucial for understanding the physiological role of 2-AG.

In contrast to polar neurotransmitters that are stored in vesicles, AEA and 2-AG are neutral lipids that have the intrinsic tendency to associate with membranes. It is poorly understood how 2-AG and AEA move across the synapse, traverse within the cellular interior and how cellular uptake of 2-AG and AEA is regulated. Possible routes for 2-AG and AEA transmembrane transport are passive diffusion, endocytosis, transporter proteins, or a combination of these mechanisms. The transport of AEA has been subject of intensive research, but the mechanisms of AEA uptake and transport are still under debate (for reviews see Niculussi & Gertsch¹⁵⁰, and Fowler^{151,152}). Fewer studies have addressed the transport process of 2-AG, because its metabolism complicates the analysis of the transport processes.

Ben Shabat *et al.* found the first indication of cellular 2-AG uptake.¹⁵³ Co-incubation of 2-AG with 2-lineoyl-glycerol reduced 2-AG depletion from media, while 2-palmitoyl-glycerol had no effect.¹⁵³ 2-AG accumulation in rat basophilic RBL-2H3 and mouse neuroblastoma N18TG2 cells was also observed by Di Marzo *et al.*¹⁵⁴ Saturable 2-AG uptake by human astrocytoma cells with a Michaelis-Menten constant (K_M) of 0.7 ± 0.1

μM and a V_{max} of 28 ± 6 pmol/min/mg, indicated the existence of a specific transporter protein.¹⁵⁵ In addition, 2-AG uptake could be inhibited by AEA and the putative AEA transport inhibitor AM404.^{156,157} Recently, it was found that UCM707 and OMDM-2 could also inhibit 2-AG and AEA uptake with equal potency. A common carrier mechanism was proposed for both AEA and 2-AG.¹⁵⁸ Importantly, not only the uptake could be blocked, but also 2-AG release. Suggesting that the putative transporter is responsible for bidirectional trafficking of 2-AG. Identification and functional characterization of the putative transporter protein(s) will be highly important for a better understanding of 2-AG storage, release and transport.

In addition to transport across the membrane, it is also unclear how intracellular transport of 2-AG is regulated. Recently, the first evidence for intracellular 2-AG transport was demonstrated.¹⁵⁹ A fluorescence polarization assay with a 12-N-methyl-(7-nitrobenz-2-oxa-1,3-diazo) aminostearic acid (NBD-stearate) probe showed that both 2-AG and AEA bind to cytosolic carrier protein FABP5. Further evidence for this binding was provided in a co-crystallization study of FAB5 and 2-AG.¹⁶⁰ It would be interesting to see to what degree FABP5 regulates the physiological role of 2-AG.

5. Non CB₁/CB₂ receptors targeted by 2-AG

The CB₁ and CB₂ receptors are not the only receptors that have been shown to interact with 2-AG. Interactions with non-classical cannabinoid receptors may be responsible for some of the physiological functions of 2-AG. 2-AG potentiates GABA_A receptor function at low GABA concentrations.³³ The GABA_A receptor is a ligand-gated ion channel that is activated by GABA, the most widely distributed inhibitory neurotransmitter in the CNS. Activation of the GABA_A receptor allows conductance of Cl⁻ ions, causing an inhibitory effect on neurotransmission. The GABA_A receptor is involved in many physiological functions, including amnesia, motility, sedation, anxiety and insomnia.¹⁶¹ Potentiation of the GABA_A receptor by 2-AG inhibits motility. It was shown that 2-AG binds at the M4 transmembrane region of the $\beta 2$ subunit, and the observed effect was still present in CB₁/CB₂ double knockout mice.³³ The interaction of 2-AG can have important implications on studies involving 2-AG on sedation and locomotion.³³ In addition, an interaction between 2-AG and the peroxisome proliferator-activated receptor- γ (PPAR- γ) has been

Table 1. 2-AG interacting proteins.

	Receptor	Ligand	K _i , IC ₅₀ or EC ₅₀	Additional ligands	physiological effect	Reference ^a
Receptor interaction	CB1	2-AG	K _i = 34.6 -472 nM ^a	AEA, Virodhamine, Noladin ether ¹⁷⁰ , NADA ¹⁷¹ , oleamide ¹⁷² , DTEA ¹⁷³ , DLEA ¹⁷³ , EPEA ¹⁷⁴ , DHEA ¹⁷⁴ , Hemopressin ¹⁷⁵	Anxiety, pain, metabolism, addiction, inflammation	176, 153
	CB2	2-AG	K _i =1400 nM ^a	AEA, Noladin ether ¹⁷⁰ , NADA ¹⁷¹ , DLEA ¹⁷³ , EPEA ¹⁷⁴ , DHEA ¹⁷⁴	Inflammation	176
	TRPV1	2-AG	EC ₅₀ = 2.5 μM ^b	AEA, NADA ¹⁷⁷	Pain	34
	GABA _A	2-AG	EC ₅₀ = 2.1 μM ^c	GABA		33
	A ₃	2-AG	IC ₅₀ = 12.6 μM ^d	Adenosine		35
	GPR55	2-AG	EC ₅₀ = 3 nM ^e	Lyso-PI, AEA, Noladin ether, virodhamine		36
	PPAR _γ	2-AG	EC ₅₀ = 10 μM ^f	Prostaglandins	Inflammation	37
	Enzyme	substrate	K _m	Additional substrates	physiological effect	Reference
Biosynthesis	DAGL-α	DG (18:0/20:4)	155 μM ^g	DG(18:1/18:1), DG(18:1/18:0), DG (16:0/18:0), DG(16:0/20:4), DG(18:1/20:4).	metabolism, anxiety, inflammation	178
	DAGL-β	DG (18:0/20:4)	74 μM ^g	DG(18:1/18:1), DG(18:1/18:0)	Inflammation	178
	DDHD2	DG (18:0/20:4)	248 μM ^h	TAG species with combinations of C16:0, C18:0, C18:1, C20:4, C22:5, C22:6 fatty acyl chains. ⁴⁵ (DG 18:0/18:2), DG (18/22:6).	-	44,179
	2-LPA Phosphatase	2-AG-LPA	-	Oleoyl-LPA	-	180
	Lyso PI-PLC	2-AG-LPI	-	LysoPC, LysoPS ¹⁸¹	-	4,46
	Enzyme	Metabolite	K _m	Additional substrates	physiological effect	Reference
Metabolism	MAGL	AA	110 μM ⁱ	MG (18:1), MG(18:2) ⁷⁶ MAG (16:0), MAG (18:1), MG (18:2), MG (22:6) ⁷⁴	Anxiety, pain, addiction, metabolism	95
	ABHD6	AA	159 μM ⁱ	MG(14:0), MG(16:0) , MG(18:0) ,MG(18:1) ¹¹⁰ in vivo in BAT ABHD6 KO.	Inflammation, metabolism	95
	ABHD12	AA	117 μM ⁱ	LPS(16:0), (18:0), (20:4), (22:4), (22:1), (22:0), (18:0), (18:0) and PS(16:0/18:1), (18:1/18:1), (16:1/20:4), (18:1/20:4), (18:0/20:4), (20:1/20:4), (20:0/20:4), (22:1/20:4), (22:0/20:4) , (24:1/20:4) ¹¹⁷	Inflammation	95
	COX2	PGE ₂ -G	4.4 ±μM ^j	AA, AEA ¹²⁶	Inflammation	122
	LOX12	12-HpETE-G	6 μM ^k	AA, AEA, linoleic acid, docohexanoic acid	Inflammation	135
	LOX15-2	15-HpETE-G	9 μM ^l	AA, AEA	Inflammation	136
	CYP2J2	11,12-EET-G 14,15-EET-G	13.6 μM ^m 32.6 μM ^m	AA, AEA	Inflammation	138,141

^aRange of K_i's measured by ligand displacement assay with [³H]HU-243 in membrane fractions of COS cells transfected with the corresponding receptor.^{153,176} ^bEffect on intracellular calcium concentration in TRPV1 expressing HK293 cells, maximum responses were normalized to the 10 μM CAP induced response. ^cDose dependent potentiation of currents elicited by 1 μM GABA. ^dLigand displacement assay with [¹²⁵I] AB MECA in CHO membranes expressing the hA₃ receptor. ^eGTPγS binding assay. ^fIC50 competition for fluorescent ligand

occupancy the purified PPAR γ ligand binding domain. ⁸Membrane of COS cells overexpressing DAGL- α or DAGL- β respectively. ^hRecombinant rDDHD2. ⁱFluorescent glycerol assay for 2-AG hydrolase activity in HEK293 cells transiently transfected with the corresponding hydrolase. ^jOxygenation by purified human COX2.¹²² ^kUV assay for the conjugated diene (leukocyte LOX12).¹³⁵ ^lHexahistidine-tagged human 15 LOX-2 expressed in Sf-9 cells and purified on Ni-NTA agarose. ^mFormation kinetics for CYP2J2 nanodisc incubations with 2-arachidonoyl glycerol. ⁿReference regarding the K_i, K_m, IC₅₀ or EC₅₀.

reported. However it is not completely clear if this interaction is mediated by 2-AG itself, via the CB₁/CB₂ receptors or through COX-2 metabolites of 2-AG.¹⁶²

Adenosine is an orthosteric endogenous ligand for the adenosine A₃ receptor. This GPCR plays an important role in modulation of inflammation.¹⁶³ 2-AG acts as a negative allosteric modulator of human adenosine A₃ receptor ligand binding. Therefore, the adenosine A₃ receptor can be a potential alternative pathway for 2-AG to mediate inflammatory responses.¹⁶⁴ In addition, 2-AG has also been reported to act as a ligand for the TRPV1 receptor, which is an outwardly rectifying Ca²⁺ permeable nonselective cation channel. The receptor is activated by stimuli such as heat (T > 42 °C) and low extracellular pH, and also by endogenous ligands including lysophosphatidic acid and AEA. TRPV1 plays an important role in the regulation of core body temperature and inflammatory pain.¹⁶⁵ Therefore, TRPV1 is an important target to consider when studying the relation between 2-AG and pain sensation.^{34,166-168} GPR55 has been called the type 3 cannabinoid receptor, because of its affinity for multiple cannabinoids. Rydberg *et al.* showed that 2-AG has a ~150 fold higher affinity for the GPR55 receptor compared to the CB₁ and CB₂ receptor.³⁶ In addition to 2-AG, also other endogenous endocannabinoids showed affinity for GPR55, including virodhamine, AEA, oleamide and noladin ether. GPR55 has been linked to energy balance and is a potential drug target for various cancer types.¹⁶⁹ Together, these studies indicate that 2-AG has a wide variety of targets distinct from the classical cannabinoid receptors. To a large extent, the physiological relevance of these non-CB₁/CB₂ receptors has yet to be established *in vivo*. Further research will reveal the extent of physiological effects governed by interactions between 2-AG and the other proteins.

6. *In vivo* physiological effects of 2-AG

This section aims to map the physiological role of 2-AG, and whether an effect can be directly or indirectly ascribed to 2-AG. To gain insight in the role of 2-AG, multiple tools and techniques have been developed and applied during the past decades. These include pharmacological blockade and genetic disruption of its target receptor(s), catabolic and metabolic enzymes, modulation of 2-AG localization, and administration of exogenous 2-AG. A single approach is often not sufficient to gain information on the role of 2-AG. A combination of these approaches is often required because:

1) 2-AG biosynthetic and metabolic enzymes have multiple substrates and roles. Thus, disruption of these enzymes results in decreased 2-AG levels, but levels of other substrates or metabolites of targeted enzymes will also be altered.

2) 2-AG precursors and metabolites have important signaling functions and are intermediates for multiple lipid metabolic pathways.

3) Receptors targeted by 2-AG recognize multiple ligands. Additionally, 2-AG is a promiscuous ligand that interacts with multiple receptors, resulting in a considerable increase of possible interactions through which 2-AG can mediate its physiological effects. Intensive research has provided insight in the physiological role of 2-AG, which will be discussed below.

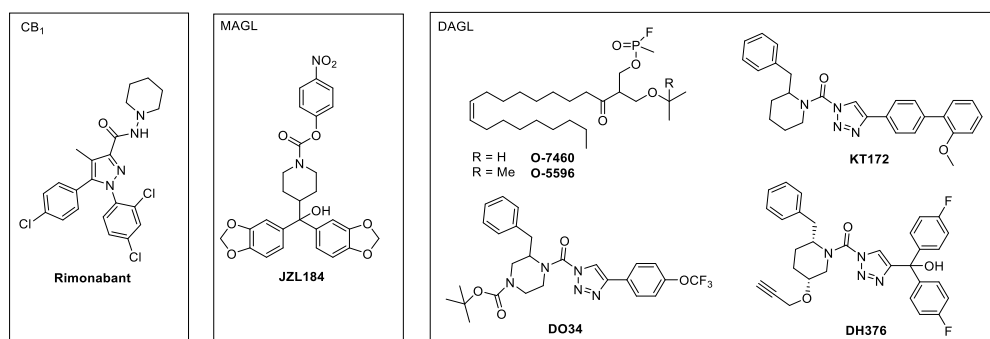


Figure 2. Tool compounds used to study the physiological role of 2-AG.

6.1 Food intake and metabolism

The intimate link between the endocannabinoid system and energy balance is well established.¹⁸² CB₁ knockout mice display a lean phenotype, reduced adiposity and feeding efficiency. When fed a high fat diet, they display decreased triglyceride, plasma insulin, cholesterol, and leptin levels, while having increased adiponectin levels compared to their wild type littermates.^{183,184} This phenotype can be mirrored by treatment with the CB₁ inverse agonist rimonabant.¹⁸⁵ Importantly, rimonabant was approved on the European market in 2006 as a drug for the treatment of obesity. However, rimonabant was withdrawn from the European market in 2008 due to serious psychiatric side effects, in particular depression.

Several lines of evidence indicate that 2-AG is, to a large extent, responsible for CB₁ mediated regulation of food intake and energy metabolism. Fasting increases levels of 2-AG in the limbic forebrain and the hypothalamus. Additionally, bilateral injection of 2-AG into the nucleus accumbens stimulated increased feeding, and pretreatment with rimonabant could reduce the effect elicited by 2-AG infusion.¹⁸⁶ DAGL- α knockout mice showed a similar phenotype with decreased body weight, low triglyceride, cholesterol, and insulin levels as observed in the CB₁ knockout mice.¹⁸⁷ This phenotype was absent in

DAGL- β knockout mice, indicating that 2-AG biosynthesized by DAGL- α is responsible for the observed effects. Acute disruption of DAGL activity by (i.p.) administration of O-7460, a fluorophosphonate-based DAGL inhibitor, dose dependently inhibited intake of high fat diet in mice.¹⁸⁸ This is in line with a previous report where the DAGL inhibitor O-5596 reduced the intake of palatable food in mice.¹⁸⁹

Jung *et al.* provided further evidence for the involvement of 2-AG in metabolism.¹⁹⁰ Upregulation of 2-AG hydrolysis by overexpression of MAGL in the mouse forebrain led to a 50% decrease of 2-AG levels in this brain region, but did not affect AEA nor AA levels. These mice were lean, hyperphagic, resistant to diet induced obesity, hyperthermic and hypersensitive to β_3 -adrenergic-stimulated thermogenesis. Inhibition with the MAGL inhibitor JZL184 showed that recovering 2-AG signaling at the CB₁ receptors normalized β_3 -adrenergic-dependent thermogenesis. This indicated that 2-AG mediated CB₁ signaling helps to conserve body energy by moderating heat production.

6.2 Neuro-inflammation

2-AG plays a central role in multiple neuro-inflammatory processes. In 2001, Panikashvili *et al.* reported a neuroprotective role of 2-AG in a traumatic brain injury model.¹⁹¹ After infliction of closed head injury, a strong elevation, reaching a ten-fold increase after 4h, of mouse brain 2-AG levels was observed. Injection of exogenous 2-AG after closed head injury elicited a neuroprotective effect. This effect was reduced in CB₁ knockout models and after pretreatment with rimonabant. Neuro-inflammation is one of the early neurochemical responses after closed head injury.¹⁹² Elevations of pro-inflammatory mediators, such as TNF- α and IL-1 β , at early stages after injury are observed. 2-AG inhibited NF- κ B transactivation and reduced acute expression of the pro-inflammatory cytokines TNF- α , IL1 β and IL-6 via a CB₁ dependent mechanism.¹⁹³

Of note, metabolites of 2-AG are also involved in the modulation of neuro-inflammatory processes. Previously, phospholipase A₂ (PLA₂) was considered to be the primary source of AA for COX-mediated biosynthesis of prostaglandins, but this model has significantly changed in recent years. Nomura *et al.* showed that MAGL hydrolysis of 2-AG provides the major pool of AA for the generation of neuro-inflammatory eicosanoids in specific tissues, such as the brain, liver and lungs.⁷⁷ Chemical inhibition or genetic disruption of MAGL activity lowered lipopolysaccharide (LPS)-induced pro-inflammatory eicosanoid production in the brain, such as prostaglandin E₂ (PGE₂), PGD₂, PGF₂, and thromboxane B₂ (TXB₂), via a CB₁ and CB₂ receptor independent mechanism. In addition, abolishment of MAGL activity did not affect basal cytokine levels, but almost completely blocked LPS-induced elevation of interleukin-1 α (IL-1 α), IL-1 β , IL-6 and TNF- α . Specific knockdown of MAGL in astrocytes moderately elevated 2-AG levels and did not cause CB₁ receptor desensitization nor any behavioral effect, but decreased cytokine and prostaglandin levels via a CB₁/CB₂ independent mechanism.¹⁹⁴ This is in line with the anti-inflammatory

effects observed with blocking 2-AG biosynthesis. DAGL- α/β inhibitors DO34 and DH376 reduced brain levels of 2-AG, AA and AEA.⁵⁷ The pro-inflammatory prostaglandins PGE₂ and PGD₂ and cytokine IL-1 β were also reduced in LPS-treated animals. In line, Viader *et al.* showed that DAGL- β is important for regulation of 2-AG levels in microglia without change in global 2-AG and prostaglandin levels in the brain.⁶⁰ Finally, LPS-induced anapyrexia, i.e. lowering of core body temperature, was substantially reduced in DAGL- α and DAGL- β KO and inhibitor-treated mice,⁶⁰ which is consistent with increased anapyrexia observed in MAGL inhibitor treated mice.¹⁹⁵ This implies an important role for 2-AG in the regulation of body temperature.

Multiple neurological disorders, including multiple sclerosis (MS), Parkinson's and Alzheimer's disease, have a neuro-inflammatory component. Consequently, modulation of MAGL activity has been tested in various animal models of neurodegenerative diseases. Nomura *et al.* used a 1-methyl-4-phenyl-1,2,3,6-tetrahydropyridine (MPTP) mouse model for Parkinson's disease.⁷⁷ JZL184 provided neuroprotective effects, which were not reversed by the CB receptor antagonists, but were recapitulated by COX inhibition. This indicated that the neuroprotective effects were not mediated via the CB receptors, but due to reductions in AA and pro-inflammatory prostaglandins. Mounsey *et al.* confirmed these findings.¹⁹⁶

Perturbation of MAGL activity has been investigated in animal models of Alzheimer's disease, such as 5XFAD and PS1/APP⁺ models. Genetic and pharmacological inactivation of MAGL suppresses proinflammatory responses and amyloidosis in a PS1/APP⁺ mouse model.¹⁹⁷ In the 5XFAD mouse model, inhibition of MAGL reduces production and accumulation of β -amyloid (A β) and improves cognitive function.¹⁹⁸ In mice suffering from experimental autoimmune encephalitis (EAE), a mouse model for MS, inhibition of MAGL activity reduced the severity of the clinical symptoms.^{199,200} Inhibition of DAGL with the fluorophosphonate-based inhibitor O-3841 was neuroprotective in a malonate model of Huntington's disease in rat brain.²⁰¹ In contrast, inhibition of MAGL activity and administration of PGE₂-G worsened malonate-induced injury. Therefore oxidative metabolites of 2-AG have been suggested to play a role in the toxic effects.

6.3 Anxiety

Endocannabinoid signaling via the CB₁ receptor has a primary role in modulating anxiety and depressive behaviors.^{202,203} The effects of CB₁ receptor agonists on anxiety are complex and show biphasic effects. Low agonist doses lead to anxiolytic effects,^{204,205} while high doses lead to anxiogenic effects.²⁰⁶ Pharmacological blockade and genetic deletion of the CB₁ receptor has been shown to increase anxiety.^{204,207-210}

2-AG plays an important role in stress and anxiety. Studies have generally shown a bidirectional effect of stress on endocannabinoid levels, AEA levels decrease, while 2-AG

levels increase.^{211,212} Shonesy *et al.* investigated the role of DAGL- α in anxiety.²¹³ An increase in anxiety and depressive behavior in DAGL- α KO mice was observed. This effect was reversed by normalization of deficient 2-AG by pharmacological inhibition of MAGL. This normalization experiment provides extra confidence that the observed effects are 2-AG mediated and not caused by reduction downstream metabolites. Jenniches *et al.* observed a similar anxiogenic phenotype in DAGL- α knockout mice.²¹⁴ Currently, it is unknown whether acute blockade of DAGL- α also results in anxiogenic behavior. In line with anxiogenic effects when 2-AG levels are lowered by disruption of 2-AG biosynthesis, anxiolytic effects are observed when 2-AG levels are increased.

Elevation of 2-AG levels by inhibition of MAGL with JZL184 at relatively low doses did not affect motility, induced anxiolytic like effects in a marble burying test,⁷⁸ and in elevated plus mazes.^{90,215-217} Sumislawski *et al.* showed that chronic administration of JZL184 prevented chronic stress induced anxiety like behavior, but that acute MAGL inhibition has little effect on anxiety like behaviors. This could indicate that long term synaptic adaptations play an important role. Additionally, it was shown that elevated 2-AG tone prevents behavioral and synaptic adaptations to chronic stress.⁹² The anxiolytic effect in most studies could be blocked by rimonabant, indicating it is likely CB₁ mediated.

6.4 Addiction

The endocannabinoid system has been implicated in multiple aspects of addiction.²¹⁸⁻²²⁰ CB₁ receptor agonists have been shown to alleviate withdrawal symptoms,^{221,222} while the inverse agonist and antagonists reduce nicotine self-administration.²²⁰ Several lines of evidence indicate an important role of 2-AG in addictive behavior and withdrawal symptoms. Injection of exogenous 2-AG was moderately effective in reducing the intensity of precipitated withdrawal signs in morphine-dependent mice.²²² Ramesh *et al.* investigated the effect of MAGL inhibition by JZL184 on naloxone-precipitated morphine withdrawal symptoms.²²³ Selective elevation of 2-AG levels over AEA levels completely blocks behavioral effects of spontaneous and precipitated withdrawal, including paw flutters, diarrhea, jumps, and weight loss. Reduction of precipitated withdrawal effects by 2-AG elevation is blunted by rimonabant, suggesting a CB₁ receptor mediated effect. The role of 2-AG in relation to nicotine addiction was also studied.²²⁴ Somatic and aversive withdrawal signs in nicotine-dependent mice were reduced by both genetic and pharmacological inactivation of MAGL via a CB₁ receptor mediated mechanism.²²⁴

In agreement with experiments with CB₁ receptor antagonists,²²⁵ reduction of 2-AG levels by inhibition of its biosynthetic enzymes DAGL- α and DAGL- β reduced nicotine self-administration of mice. Release of the inhibitory neurotransmitter GABA is diminished upon chronic nicotine exposure.^{220,226} To gain insight in the underlying mechanism, the authors studied the effect of DAGL inhibition on GABA signaling. Inhibition of DAGL by the 1,2,3-triazole urea KT172 rescues GABAergic signaling at

dopaminergic neurons in the ventral tegmental area (VTA).²²⁶ Conversely, increasing 2-AG signaling by blocking the 2-AG metabolizing enzyme MAGL recapitulates the loss of nicotine-induced GABA signaling following chronic nicotine exposure.

6.5 Pain

Cannabinoids have been used for their ability to reduce pain for many centuries.²²⁷ In addition, various studies have demonstrated the analgesic efficacy of local administration of 2-AG.^{228,229} Elevation of 2-AG has also been observed in preclinical models of inflammatory pain, indicating a role of endogenous 2-AG in pain perception.^{230,231} Anti-nociceptive effects by elevation of 2-AG via MAGL inhibition has been well established. Robust analgesic effects by MAGL inactivation are demonstrated in neuropathic pain,²³² peripheral inflammatory pain,⁹³ gastrointestinal pain²³³ and chemotherapy-induced neuropathy.^{234,235} For a comprehensive review on the endocannabinoid system in pain see S. G. Woodhams *et al.*²³⁶ Anti-nociceptive effects in thermal, noxious chemical, and neuropathic pain sensation by MAGL inhibition were blocked by the CB₁ receptor inverse agonist rimonabant.^{78,234} Intracerebroventricular injection of JZL184 produced TRPV1-dependent anti-nociception in the mouse formalin test, which indicates that anti-nociceptive effects are not only mediated by CB receptors, but that TRPV1 can also contribute to anti-nociceptive effects.¹⁶⁸ Recently, inhibition of DAGL was reported to reduce nociception in preclinical models of inflammatory and neuropathic pain.²³⁷ A likely explanation for this effect is a decrease in AA levels. Lower AA levels result in decreased levels of prostaglandins and subsequent modulation of inflammation and pain.

Taken together, these data demonstrate an important role for 2-AG in pain sensation via multiple mechanisms, including TRPV1, CB₁, and CB₂ signaling and as a precursor for prostaglandins that modulate inflammation and pain.

7. Conclusions

A major mechanism through which 2-AG exerts its physiological effects in the brain are the CB₁ receptors. Activation of the CB₁ receptor by 2-AG regulates multiple physiological processes. This chapter described important roles of 2-AG signaling in food intake, neuroprotection, neuro-inflammation, addiction, anxiety and pain. In addition to classical CB receptors, 2-AG has shown remarkable affinity for multiple other receptors, including GABA_A, adenosine A₃, TRPV1, PPAR γ , and GPR55 receptor. To date it is, however, unknown whether these proteins are involved in physiological effects of 2-AG *in vivo*. Next to its function as a signaling lipid, 2-AG is also a key intermediate many lipid metabolic pathways. A number of 2-AG metabolites have important signaling functions in their own right. 2-AG is a key precursor for the biosynthesis of eicosanoids in the brain, which in

turn, act on several G-protein coupled receptors to propagate inflammation.¹²³ Its involvement in multiple important (patho)physiological processes makes modulation of 2-AG levels an interesting strategy from a therapeutic perspective.

Modulation of 2-AG levels *in vivo*, in particular by blocking MAGL or DAGL activity, triggers multidirectional effects in various (patho)physiological processes (Figure 3). Reduction of 2-AG levels by blocking its major, DAGL- α/β biosynthetic pathway can be beneficial for treatment of the metabolic syndrome, addiction, and neuro-inflammatory disorders, while elevation of 2-AG levels by blocking MAGL, the major hydrolytic pathway towards AA, reduces neuro-inflammation, anxiety related behavior, withdrawal symptoms and nociception. However, its prime role in many important physiological pathways makes modulation of 2-AG levels sensitive to untoward effects (Figure 3). The essential role of cannabinoid signaling in the brain was emphasized by the retraction of the CB₁ inverse agonist and anti-obesity drug rimonabant from the European market because of severe neuropsychiatric side effects.

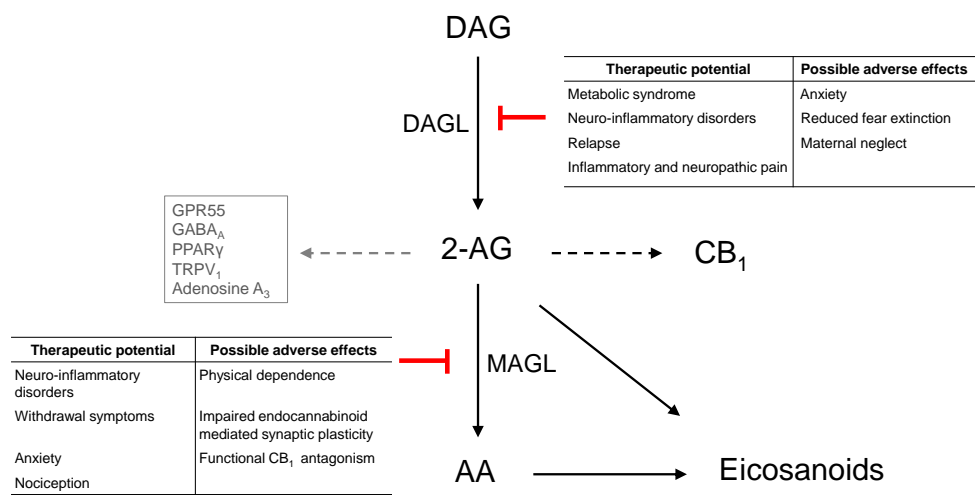


Figure 3. 2-AG plays a central role in multiple pathophysiological processes. Both elevation and reduction of 2-AG has therapeutic potential. However, untoward neurological effects could pose a serious threat for the use 2-AG modulation for the treatment of human disorders.

It is important to note that not all behavioral phenotypes of CB₁ KO mice were mirrored in DAGL- α KO mice, for example, they showed less anxiogenic behavior compared to CB₁ KO mice in open field test and platform tests.¹⁸⁷ These differences can partly be explained by considering some CB₁ signaling pathways (e.g. AEA) remain intact when modulating 2-AG levels. Therefore, selective modulation of 2-AG metabolism can help to dissect the signaling roles of 2-AG and AEA, and potentially circumvent adverse effects observed by direct blockade of the CB₁ receptor. In addition, elevation of 2-AG

levels by blockade of MAGL did not cause the full spectrum of cannabinoid-behavioral effects such as hypothermia and catalepsy as observed with direct cannabinoid agonists.^{69,238}

Although modulation 2-AG levels does not reproduce all untoward effects observed with direct CB₁ interference, several adverse effects have been observed upon pharmacological or genetic disruption of the major biosynthetic and metabolic pathways of 2-AG. Chronic blockade of MAGL causes desensitization and down regulation of the CB₁ receptor, while disruption of DAGL increases anxiety, maternal neglect and reduced fear extinction. Therefore fine-tuning rather than complete disruption of 2-AG metabolism and biosynthesis could be a promising approach to establish a therapeutic window. This therapeutic window can be achieved via several strategies: 1) Partial blockade of major biosynthetic (DAGL) or metabolic (MAGL) pathways. 2) Targeting 2-AG metabolizing enzymes that have a smaller contribution to bulk 2-AG regulation compared to DAGL and MAGL.

Lowering of 2-AG levels by partial blockade of the DAGL pathway can be achieved by subtype selective DAGL inhibitors. DAGL- β has been shown to reduce inflammatory responses *in vivo* without affecting synaptic transmission.⁶⁰ In addition, incomplete inhibition of the DAGL enzymes can be used to tweak endocannabinoid tone. In opposite direction, moderate increase of 2-AG could be achieved by partial inhibition of MAGL. For partial inhibition of both MAGL and DAGL reversible inhibitors would be highly valuable tools. The *in vivo* role with respect to 2-AG of enzymes with a less defined contribution to 2-AG metabolism (ABHD2, 6 and 12, COX2, LOX and Cyp450), transport (FABP5) and signaling (GABA_A, adenosine A₃, TRPV1, PPAR γ , and GPR55) requires further investigation. Future research on these enzymes might uncover new physiological roles of 2-AG and novel approaches to modulate 2-AG in health and disease.

References

1. Ahn, K.; McKinney, M. K.; Cravatt, B. F. *Chem. Rev.* **2008**, *108*, 1687.
2. Murataeva, N.; Straiker, A.; Mackie, K. *Br. J. Pharmacol.* **2014**, *171*, 1379.
3. Mechoulam, R.; Benshabat, S.; Hanus, L.; Ligumsky, M.; Kaminski, N. E.; Schatz, A. R.; Gopher, A.; Almog, S.; Martin, B. R.; Compton, D. R.; Pertwee, R. G.; Griffin, G.; Bayewitch, M.; Barg, J.; Vogel, Z. *Biochem. Pharmacol.* **1995**, *50*, 83.
4. Sugiura, T.; Kondo, S.; Sukagawa, A.; Nakane, S.; Shinoda, A.; Itoh, K.; Yamashita, A.; Waku, K. *Biochem. Biophys. Res. Commun.* **1995**, *215*, 89.
5. Sugiura, T.; Kodaka, T.; Nakane, S.; Miyashita, T.; Kondo, S.; Suhara, Y.; Takayama, H.; Waku, K.; Seki, C.; Baba, N.; Ishima, Y. *J. Biol. Chem.* **1999**, *274*, 2794.
6. Savinainen, J. R.; Jarvinen, T.; Laine, K.; Laitinen, J. T. *Br. J. Pharmacol.* **2001**, *134*, 664.
7. Sugiura, T.; Kondo, S.; Kishimoto, S.; Miyashita, T.; Nakane, S.; Kodaka, T.; Suhara, Y.; Takayama, H.; Waku, K. *J. Biol. Chem.* **2000**, *275*, 605.
8. Gonsiorek, W.; Lunn, C.; Fan, X.; Narula, S.; Lundell, D.; Hipkin, R. W. *Mol. Pharmacol.* **2000**, *57*, 1045.
9. Gaoni, Y.; Mechoulam, R. *J. Am. Chem. Soc.* **1964**, *86*, 1646.
10. Rajesh, M.; Pan, H.; Mukhopadhyay, P.; Batkai, S.; Osei-Hyiaman, D.; Hasko, G.; Liaudet, L.; Gao, B.; Pacher, P. *J. Leukoc. Biol.* **2007**, *82*, 1382.
11. Colombo, G.; Agabio, R.; Diaz, G.; Lobina, C.; Reali, R.; Gessa, G. L. *Life sciences* **1998**, *63*, PL113.
12. Di Marzo, V.; Goparaju, S. K.; Wang, L.; Liu, J.; Batkai, S.; Jarai, Z.; Fezza, F.; Miura, G. I.; Palmiter, R. D.; Sugiura, T.; Kunos, G. *Nature* **2001**, *410*, 822.
13. Koch, M.; Varela, L.; Kim, J. G.; Kim, J. D.; Hernandez-Nuno, F.; Simonds, S. E.; Castorena, C. M.; Vianna, C. R.; Elmquist, J. K.; Morozov, Y. M.; Rakic, P.; Bechmann, I.; Cowley, M. A.; Szigeti-Buck, K.; Dietrich, M. O.; Gao, X. B.; Diano, S.; Horvath, T. L. *Nature* **2015**, *519*, 45.
14. Dewey, W. L. *Pharmacol. Rev.* **1986**, *38*, 151.
15. Zimmer, A.; Zimmer, A. M.; Hohmann, A. G.; Herkenham, M.; Bonner, T. I. *Proc. Natl. Acad. Sci. U. S. A.* **1999**, *96*, 5780.
16. Calignano, A.; La Rana, G.; Giuffrida, A.; Piomelli, D. *Nature* **1998**, *394*, 277.
17. Navarro, M.; Hernandez, E.; Munoz, R. M.; del Arco, I.; Villanua, M. A.; Carrera, M. R.; Rodriguez de Fonseca, F. *Neuroreport* **1997**, *8*, 491.
18. Haller, J.; Bakos, N.; Szirmay, M.; Ledent, C.; Freund, T. F. *Eur. J. Neurosci.* **2002**, *16*, 1395.
19. Ledent, C.; Valverde, O.; Cossu, G.; Petitet, F.; Aubert, J. F.; Beslot, F.; Bohme, G. A.; Imperato, A.; Pedrazzini, T.; Roques, B. P.; Vassart, G.; Fratta, W.; Parmentier, M. *Science* **1999**, *283*, 401.

20. Munro, S.; Thomas, K. L.; Abu-Shaar, M. *Nature* **1993**, *365*, 61.
21. Herkenham, M.; Lynn, A. B.; Little, M. D.; Johnson, M. R.; Melvin, L. S.; de Costa, B. R.; Rice, K. C. *Proc. Natl. Acad. Sci. U. S. A.* **1990**, *87*, 1932.
22. Devane, W. A.; Dysarz, F. A., 3rd; Johnson, M. R.; Melvin, L. S.; Howlett, A. C. *Mol. Pharmacol.* **1988**, *34*, 605.
23. Onaivi, E. S. *Curr Neuropsychopharmacol.* **2011**, *9*, 205.
24. Atwood, B. K.; Straiker, A.; Mackie, K. *Neuropharmacol.* **2012**, *63*, 514.
25. Cabral, G. A.; Griffin-Thomas, L. *Expert. Rev. Mol. Med.* **2009**, *11*, e3.
26. Devane, W. A.; Hanus, L.; Breuer, A.; Pertwee, R. G.; Stevenson, L. A.; Griffin, G.; Gibson, D.; Mandelbaum, A.; Etinger, A.; Mechoulam, R. *Science* **1992**, *258*, 1946.
27. Pertwee, R. G. *Handb. Exp. Pharmacol.* **2015**, *231*, 1.
28. Stella, N.; Schweitzer, P.; Piomelli, D. *Nature* **1997**, *388*, 773.
29. Alger, B. E. *J. Physiol.* **2012**, *590*, 2203.
30. Di Marzo, V.; Melck, D.; Bisogno, T.; De Petrocellis, L. *Trends Neurosci.* **1998**, *21*, 521.
31. Muccioli, G. G. *Drug. Discov. Today* **2010**, *15*, 474.
32. Mackie, K. *Int. J. Obes. (Lond).* **2006**, *30 Suppl 1*, S19.
33. Sigel, E.; Baur, R.; Racz, I.; Marazzi, J.; Smart, T. G.; Zimmer, A.; Gertsch, J. *Proc. Natl. Acad. Sci. U. S. A.* **2011**, *108*, 18150.
34. Iwasaki, Y.; Saito, O.; Tanabe, M.; Inayoshi, K.; Kobata, K.; Uno, S.; Morita, A.; Watanabe, T. *Lipids* **2008**, *43*, 471.
35. Lane, J. R.; Beukers, M. W.; Mulder-Krieger, T.; Ijzerman, A. P. *Biochem. Pharmacol.* **2010**, *79*, 48.
36. Ryberg, E.; Larsson, N.; Sjogren, S.; Hjorth, S.; Hermansson, N. O.; Leonova, J.; Elebring, T.; Nilsson, K.; Drmota, T.; Greasley, P. J. *Br. J. Pharmacol.* **2007**, *152*, 1092.
37. Bouaboula, M.; Hilairet, S.; Marchand, J.; Fajas, L.; Le Fur, G.; Casellas, P. *Eur. J. Pharmacol.* **2005**, *517*, 174.
38. Farooqui, A. A.; Rammohan, K. W.; Horrocks, L. A. *Ann. N.Y. Acad. Sci.* **1989**, *559*, 25.
39. Brose, N.; Betz, A.; Wegmeyer, H. *Curr. Opin. Neurobiol.* **2004**, *14*, 328.
40. Ohno-Shosaku, T.; Shosaku, J.; Tsubokawa, H.; Kano, M. *Eur. J. Neurosci.* **2002**, *15*, 953.
41. Fukudome, Y.; Ohno-Shosaku, T.; Matsui, M.; Omori, Y.; Fukaya, M.; Tsubokawa, H.; Taketo, M. M.; Watanabe, M.; Manabe, T.; Kano, M. *Eur. J. Neurosci.* **2004**, *19*, 2682.
42. Hashimotodani, Y.; Ohno-Shosaku, T.; Tsubokawa, H.; Ogata, H.; Emoto, K.; Maejima, T.; Araishi, K.; Shin, H. S.; Kano, M. *Neuron* **2005**, *45*, 257.

43. Bisogno, T.; Howell, F.; Williams, G.; Minassi, A.; Cascio, M. G.; Ligresti, A.; Matias, I.; Schiano-Moriello, A.; Paul, P.; Williams, E. J.; Gangadharan, U.; Hobbs, C.; Di Marzo, V.; Doherty, P. *J. Cell Biol.* **2003**, *163*, 463.
44. Aso, C.; Araki, M.; Ohshima, N.; Tatei, K.; Hirano, T.; Obinata, H.; Kishi, M.; Kishimoto, K.; Konishi, A.; Goto, F.; Sugimoto, H.; Izumi, T. *J. Biochem.* **2016**, *159*, 585.
45. Inloes, J. M.; Hsu, K. L.; Dix, M. M.; Viader, A.; Masuda, K.; Takei, T.; Wood, M. R.; Cravatt, B. F. *Proc. Natl. Acad. Sci. U. S. A.* **2014**, *111*, 14924.
46. Ueda, H.; Kobayashi, T.; Kishimoto, M.; Tsutsumi, T.; Okuyama, H. *J. Neurochem.* **1993**, *61*, 1874.
47. Nakane, S.; Oka, S.; Arai, S.; Waku, K.; Ishima, Y.; Tokumura, A.; Sugiura, T. *Arch. Biochem. Biophys.* **2002**, *402*, 51.
48. Gao, Y.; Vasilyev, D. V.; Goncalves, M. B.; Howell, F. V.; Hobbs, C.; Reisenberg, M.; Shen, R.; Zhang, M. Y.; Strassle, B. W.; Lu, P. M.; Mark, L.; Piesla, M. J.; Deng, K. W.; Kouranova, E. V.; Ring, R. H.; Whiteside, G. T.; Bates, B.; Walsh, F. S.; Williams, G.; Pangalos, M. N.; Samad, T. A.; Doherty, P. *J. Neurosci.* **2010**, *30*, 2017.
49. Tanimura, A.; Yamazaki, M.; Hashimoto, Y.; Uchigashima, M.; Kawata, S.; Abe, M.; Kita, Y.; Hashimoto, K.; Shimizu, T.; Watanabe, M.; Sakimura, K.; Kano, M. *Neuron* **2010**, *65*, 320.
50. Hsu, K. L.; Tsuboi, K.; Adibekian, A.; Pugh, H.; Masuda, K.; Cravatt, B. F. *Nat. Chem. Biol.* **2012**, *8*, 999.
51. Prescott, S. M.; Majerus, P. W. *J. Biol. Chem.* **1983**, *258*, 764.
52. Farooqui, A. A.; Taylor, W. A.; Horrocks, L. A. *Biochem. Biophys. Res. Commun.* **1984**, *122*, 1241.
53. Farooqui, A. A.; Taylor, W. A.; Horrocks, L. A. *International J. Biochem.* **1986**, *18*, 991.
54. Shonesy, B. C.; Wang, X.; Rose, K. L.; Ramikie, T. S.; Cavener, V. S.; Rentz, T.; Baucum, A. J., 2nd; Jalan-Sakrikar, N.; Mackie, K.; Winder, D. G.; Patel, S.; Colbran, R. J. *Nat. Neurosci.* **2013**, *16*, 456.
55. Reisenberg, M.; Singh, P. K.; Williams, G.; Doherty, P. *Philos. Trans. R. Soc. Lond., B, Biol. Sci.* **2012**, *367*, 3264.
56. Zhou, Y.; Howell, F. V.; Glebov, O. O.; Albrecht, D.; Williams, G.; Doherty, P. *Mol. Cell. Neurosci.* **2016**, *76*, 76.
57. Ogasawara, D.; Deng, H.; Viader, A.; Baggelaar, M. P.; Breman, A.; den Dulk, H.; van den Nieuwendijk, A. M.; Soethoudt, M.; van der Wel, T.; Zhou, J.; Overkleeft, H. S.; Sanchez-Alavez, M.; Mori, S.; Nguyen, W.; Conti, B.; Liu, X.; Chen, Y.; Liu, Q. S.; Cravatt, B. F.; van der Stelt, M. *Proc. Natl. Acad. Sci. U. S. A.* **2016**, *113*, 26.

58. Tanimura, A.; Yamazaki, M.; Hashimoto, Y.; Uchigashima, M.; Kawata, S.; Abe, M.; Kita, Y.; Hashimoto, K.; Shimizu, T.; Watanabe, M.; Sakimura, K.; Kano, M. *Neuron* **2010**, *65*, 320.
59. Gao, Y.; Vasilyev, D. V.; Goncalves, M. B.; Howell, F. V.; Hobbs, C.; Reisenberg, M.; Shen, R.; Zhang, M. Y.; Strassle, B. W.; Lu, P.; Mark, L.; Piesla, M. J.; Deng, K.; Kouranova, E. V.; Ring, R. H.; Whiteside, G. T.; Bates, B.; Walsh, F. S.; Williams, G.; Pangalos, M. N.; Samad, T. A.; Doherty, P. J. *J. Neurosci.* **2010**, *30*, 2017.
60. Viader, A.; Ogasawara, D.; Joslyn, C. M.; Sanchez-Alavez, M.; Mori, S.; Nguyen, W.; Conti, B.; Cravatt, B. F. *eLife* **2016**, *5*, e12345.
61. Kohnz, R. A.; Nomura, D. K. *Chem. Soc. Rev.* **2014**, *43*, 6859.
62. Janssen, F. J.; van der Stelt, M. *Bioorg. Med. Chem. Lett.* , **2016**.
63. Blankman, J. L.; Simon, G. M.; Cravatt, B. F. *Chem. Biol.* **2007**, *14*, 1347.
64. Vaughan, M.; Berger, J. E.; Steinberg, D. *The J. Biol. Chem.* **1964**, *239*, 401.
65. Kupiecki, F. P. *J. Lipid Res.* **1966**, *7*, 230.
66. Karlsson, M.; Contreras, J. A.; Hellman, U.; Tornqvist, H.; Holm, C. *The J. Biol. Chem.* **1997**, *272*, 27218.
67. Karlsson, M.; Reue, K.; Xia, Y. R.; Lusi, A. J.; Langin, D.; Tornqvist, H.; Holm, C. *Gene* **2001**, *272*, 11.
68. Dinh, T. P.; Freund, T. F.; Piomelli, D. *Chem. Phys. Lipids* **2002**, *121*, 149.
69. Long, J. Z.; Nomura, D. K.; Cravatt, B. F. *Chem. Biol.* **2009**, *16*, 744.
70. Vandevoorde, S.; Saha, B.; Mahadevan, A.; Razdan, R. K.; Pertwee, R. G.; Martin, B. R.; Fowler, C. J. *Biochem. Biophys. Res. Commun.* **2005**, *337*, 104.
71. Tornqvist, H.; Krabisch, L.; Belfrage, P. *J. Lipid Res.* **1974**, *15*, 291.
72. Nomura, D. K.; Long, J. Z.; Niessen, S.; Hoover, H. S.; Ng, S. W.; Cravatt, B. F. *Cell* **2010**, *140*, 49.
73. Chanda, P. K.; Gao, Y.; Mark, L.; Btesh, J.; Strassle, B. W.; Lu, P.; Piesla, M. J.; Zhang, M. Y.; Bingham, B.; Uveges, A.; Kowal, D.; Garbe, D.; Kouranova, E. V.; Ring, R. H.; Bates, B.; Pangalos, M. N.; Kennedy, J. D.; Whiteside, G. T.; Samad, T. A. *Mol. Pharmacol.* **2010**, *78*, 996.
74. Schlosburg, J. E.; Blankman, J. L.; Long, J. Z.; Nomura, D. K.; Pan, B.; Kinsey, S. G.; Nguyen, P. T.; Ramesh, D.; Booker, L.; Burston, J. J.; Thomas, E. A.; Selley, D. E.; Sim-Selley, L. J.; Liu, Q. S.; Lichtman, A. H.; Cravatt, B. F. *Nat. Neurosci.* **2010**, *13*, 1113.
75. Long, J. Z.; Li, W.; Booker, L.; Burston, J. J.; Kinsey, S. G.; Schlosburg, J. E.; Pavon, F. J.; Serrano, A. M.; Selley, D. E.; Parsons, L. H.; Lichtman, A. H.; Cravatt, B. F. *Nat. Chem. Biol.* **2009**, *5*, 37.
76. Taschler, U.; Radner, F. P.; Heier, C.; Schreiber, R.; Schweiger, M.; Schoiswohl, G.; Preiss-Landl, K.; Jaeger, D.; Reiter, B.; Koefeler, H. C.; Wojciechowski, J.; Theussl, C.; Penninger, J. M.; Lass, A.; Haemmerle, G.; Zechner, R.; Zimmermann, R. *The J. Biol. Chem.* **2011**, *286*, 17467.

77. Nomura, D. K.; Morrison, B. E.; Blankman, J. L.; Long, J. Z.; Kinsey, S. G.; Marcondes, M. C.; Ward, A. M.; Hahn, Y. K.; Lichtman, A. H.; Conti, B.; Cravatt, B. F. *Science* **2011**, *334*, 809.
78. Long, J. Z.; Li, W. W.; Booker, L.; Burston, J. J.; Kinsey, S. G.; Schlosburg, J. E.; Pavon, F. J.; Serrano, A. M.; Selley, D. E.; Parsons, L. H.; Lichtman, A. H.; Cravatt, B. F. *Nat. Chem. Biol.* **2009**, *5*, 37.
79. Chang, J. W.; Niphakis, M. J.; Lum, K. M.; Cognetta, A. B., 3rd; Wang, C.; Matthews, M. L.; Niessen, S.; Buczynski, M. W.; Parsons, L. H.; Cravatt, B. F. *Chem. Biol.* **2012**, *19*, 579.
80. Niphakis, M. J.; Cognetta, A. B., 3rd; Chang, J. W.; Buczynski, M. W.; Parsons, L. H.; Byrne, F.; Burston, J. J.; Chapman, V.; Cravatt, B. F. *ACS Chem. Neurosci.* **2013**, *4*, 1322.
81. Kohnz, R. A.; Nomura, D. K. *Chem. Soc. Rev.* **2014**, *43*, 6859.
82. Makara, J. K.; Mor, M.; Fegley, D.; Szabo, S. I.; Kathuria, S.; Astarita, G.; Duranti, A.; Tontini, A.; Tarzia, G.; Rivara, S.; Freund, T. F.; Piomelli, D. *Nat. Neurosci.* **2005**, *8*, 1139.
83. Straiker, A.; Mackie, K. *J. Physiol.* **2005**, *569*, 501.
84. Szabo, B.; Urbanski, M. J.; Bisogno, T.; Di Marzo, V.; Mendiguren, A.; Baer, W. U.; Freiman, I. *J. Physiol.* **2006**, *577*, 263.
85. Hashimotodani, Y.; Ohno-Shosaku, T.; Kano, M. *J. Neurosci.* **2007**, *27*, 1211.
86. Pan, B.; Wang, W.; Long, J. Z.; Sun, D.; Hillard, C. J.; Cravatt, B. F.; Liu, Q. S. *J. Pharm. Exp. Ther.* **2009**, *331*, 591.
87. Straiker, A.; Wager-Miller, J.; Hu, S. S.; Blankman, J. L.; Cravatt, B. F.; Mackie, K. *Br. J. Pharmacol.* **2011**, *164*, 1672.
88. Pan, B.; Wang, W.; Zhong, P.; Blankman, J. L.; Cravatt, B. F.; Liu, Q. S. *J. Neurosci.* **2011**, *31*, 13420.
89. Dotsey, E. Y.; Jung, K. M.; Basit, A.; Wei, D.; Daglian, J.; Vacondio, F.; Armirotti, A.; Mor, M.; Piomelli, D. *Chem. Biol.* **2015**, *22*, 619.
90. Busquets-Garcia, A.; Puighermanal, E.; Pastor, A.; de la Torre, R.; Maldonado, R.; Ozaita, A. *Biol. Psychiatry* **2011**, *70*, 479.
91. Kinsey, S. G.; O'Neal, S. T.; Long, J. Z.; Cravatt, B. F.; Lichtman, A. H. *Pharmacol. Biochem. Behav.* **2011**, *98*, 21.
92. Sumislawski, J. J.; Ramikie, T. S.; Patel, S. *Neuropsychopharmacology* **2011**, *36*, 2750.
93. Ghosh, S.; Wise, L. E.; Chen, Y.; Gujjar, R.; Mahadevan, A.; Cravatt, B. F.; Lichtman, A. H. *Life sciences* **2013**, *92*, 498.
94. Ollis, D. L.; Cheah, E.; Cygler, M.; Dijkstra, B.; Frolow, F.; Franken, S. M.; Harel, M.; Remington, S. J.; Silman, I.; Schrag, J.; et al. *Protein Eng.* **1992**, *5*, 197.
95. Navia-Paldanius, D.; Savinainen, J. R.; Laitinen, J. T. *J. Lipid Res.* **2012**, *53*, 2413.
96. Lord, C. C.; Thomas, G.; Brown, J. M. *Biochim. Biophys. Acta* **2013**, *1831*, 792.
97. Long, L. E.; Lind, J.; Webster, M.; Weickert, C. S. *BMC Neurosci.* **2012**, *13*, 87.

98. Li, W.; Blankman, J. L.; Cravatt, B. F. *J. Am. Chem. Soc.* **2007**, *129*, 9594.
99. Hsu, K. L.; Tsuboi, K.; Chang, J. W.; Whitby, L. R.; Speers, A. E.; Pugh, H.; Cravatt, B. F. *J. Med. Chem.* **2013**, *56*, 8270.
100. Janssen, F. J.; Deng, H.; Baggelaar, M. P.; Allara, M.; van der Wel, T.; den Dulk, H.; Ligresti, A.; an Esbroeck, A. C.; McGuire, R.; Di Marzo, V.; Overkleeft, H. S.; van der Stelt, M. *J. Med. Chem.* **2014**, *57*, 6610.
101. Patel, J. Z.; Nevalainen, T. J.; Savinainen, J. R.; Adams, Y.; Laitinen, T.; Runyon, R. S.; Vaara, M.; Ahenkorah, S.; Kaczor, A. A.; Navia-Paldanius, D.; Gynther, M.; Aaltonen, N.; Joharapurkar, A. A.; Jain, M. R.; Haka, A. S.; Maxfield, F. R.; Laitinen, J. T.; Parkkari, T. *ChemMedChem* **2015**, *10*, 253.
102. Marrs, W. R.; Blankman, J. L.; Horne, E. A.; Thomazeau, A.; Lin, Y. H.; Coy, J.; Bodor, A. L.; Muccioli, G. G.; Hu, S. S.; Woodruff, G.; Fung, S.; Lafourcade, M.; Alexander, J. P.; Long, J. Z.; Li, W.; Xu, C.; Moller, T.; Mackie, K.; Manzoni, O. J.; Cravatt, B. F.; Stella, N. *Nat. Neurosci.* **2010**, *13*, 951.
103. Straiker, A.; Mackie, K. *Neuroscience* **2009**, *163*, 190.
104. Straiker, A.; Hu, S. S.; Long, J. Z.; Arnold, A.; Wager-Miller, J.; Cravatt, B. F.; Mackie, K. *Mol. Pharmacol.* **2009**, *76*, 1220.
105. Wen, J.; Ribeiro, R.; Tanaka, M.; Zhang, Y. *Neuropharmacol.* **2015**, *99*, 196.
106. Naydenov, A. V.; Horne, E. A.; Cheah, C. S.; Swinney, K.; Hsu, K. L.; Cao, J. K.; Marrs, W. R.; Blankman, J. L.; Tu, S.; Cherry, A. E.; Fung, S.; Wen, A.; Li, W.; Saporito, M. S.; Selley, D. E.; Cravatt, B. F.; Oakley, J. C.; Stella, N. *Neuron* **2014**, *83*, 361.
107. Tchantchou, F.; Zhang, Y. *J. Neurotrauma* **2013**, *30*, 565.
108. Wei, M.; Zhang, J.; Jia, M.; Yang, C.; Pan, Y.; Li, S.; Luo, Y.; Zheng, J.; Ji, J.; Chen, J.; Hu, X.; Xiong, J.; Shi, Y.; Zhang, C. *Proc. Natl. Acad. Sci. U. S. A.* **2016**, *113*, E2695.
109. Alhouayek, M.; Masquelier, J.; Cani, P. D.; Lambert, D. M.; Muccioli, G. G. *Proc. Natl. Acad. Sci. U. S. A.* **2013**, *110*, 17558.
110. Zhao, S.; Mugabo, Y.; Iglesias, J.; Xie, L.; Delghingaro-Augusto, V.; Lussier, R.; Peyot, M. L.; Joly, E.; Taib, B.; Davis, M. A.; Brown, J. M.; Abousalham, A.; Gaisano, H.; Madiraju, S. R.; Prentki, M. *Cell Metab.* **2014**, *19*, 993.
111. Zhao, S.; Poursharifi, P.; Mugabo, Y.; Levens, E. J.; Vivot, K.; Attane, C.; Iglesias, J.; Peyot, M. L.; Joly, E.; Madiraju, S. R.; Prentki, M. *Mol. Metab.* **2015**, *4*, 940.
112. Zhao, S.; Mugabo, Y.; Ballentine, G.; Attane, C.; Iglesias, J.; Poursharifi, P.; Zhang, D.; Nguyen, T. A.; Erb, H.; Prentki, R.; Peyot, M. L.; Joly, E.; Tobin, S.; Fulton, S.; Brown, J. M.; Madiraju, S. R.; Prentki, M. *Cell Rep.* **2016**, *14*, 2872.
113. Pribasnig, M. A.; Mrak, I.; Grabner, G. F.; Taschler, U.; Knittelfelder, O.; Scherz, B.; Eichmann, T. O.; Heier, C.; Grumet, L.; Kowaliuk, J.; Romauch, M.; Holler, S.; Anderl, F.; Wolinski, H.; Lass, A.; Breinbauer, R.; Marsche, G.; Brown, J. M.; Zimmermann, R. *J. Biol. Chem.* **2015**, *290*, 29869.

114. Kamat, S. S.; Camara, K.; Parsons, W. H.; Chen, D. H.; Dix, M. M.; Bird, T. D.; Howell, A. R.; Cravatt, B. F. *Nat. Chem. Biol.* **2015**, *11*, 164.
115. Chen, D. H.; Naydenov, A.; Blankman, J. L.; Mefford, H. C.; Davis, M.; Sul, Y.; Barloon, A. S.; Bonkowski, E.; Wolff, J.; Matsushita, M.; Smith, C.; Cravatt, B. F.; Mackie, K.; Raskind, W. H.; Stella, N.; Bird, T. D. *Hum. Mutat.* **2013**, *34*, 1672.
116. Fiskerstrand, T.; H'Mida-Ben Brahim, D.; Johansson, S.; M'Zahem, A.; Haukanes, B. I.; Drouot, N.; Zimmermann, J.; Cole, A. J.; Vedeler, C.; Bredrup, C.; Assoum, M.; Tazir, M.; Klockgether, T.; Hamri, A.; Steen, V. M.; Boman, H.; Bindoff, L. A.; Koenig, M.; Knappskog, P. M. *Am. J. Hum. Genet.* **2010**, *87*, 410.
117. Blankman, J. L.; Long, J. Z.; Trauger, S. A.; Siuzdak, G.; Cravatt, B. F. *Proc. Natl. Acad. Sci. U. S. A.* **2013**, *110*, 1500.
118. Ding, X.; Yang, J.; Wang, S. *Oligonucleotides* **2011**, *21*, 77.
119. Miyata, K.; Nakayama, M.; Mizuta, S.; Hokimoto, S.; Sugamura, K.; Oshima, S.; Oike, Y.; Sugiyama, S.; Ogawa, H.; Yamamura, K. *Biochem. Biophys. Res. Commun.* **2008**, *365*, 207.
120. Jin, S.; Zhao, G.; Li, Z.; Nishimoto, Y.; Isohama, Y.; Shen, J.; Ito, T.; Takeya, M.; Araki, K.; He, P.; Yamamura, K. *Biochem. Biophys. Res. Commun.* **2009**, *380*, 419.
121. Miller, M. R.; Mannowetz, N.; Iavarone, A. T.; Safavi, R.; Gracheva, E. O.; Smith, J. F.; Hill, R. Z.; Bautista, D. M.; Kirichok, Y.; Lishko, P. V. *Science* **2016**, *352*, 555.
122. Kozak, K. R.; Rowlinson, S. W.; Marnett, L. J. *J. Biol. Chem.* **2000**, *275*, 33744.
123. Rouzer, C. A.; Marnett, L. J. *Chem. Rev.* **2011**, *111*, 5899.
124. Kim, J.; Alger, B. E. *Nat. Neurosci.* **2004**, *7*, 697.
125. Duggan, K. C.; Hermanson, D. J.; Musee, J.; Prusakiewicz, J. J.; Scheib, J. L.; Carter, B. D.; Banerjee, S.; Oates, J. A.; Marnett, L. J. *Nat. Chem. Biol.* **2011**, *7*, 803.
126. Hermanson, D. J.; Hartley, N. D.; Gamble-George, J.; Brown, N.; Shonesy, B. C.; Kingsley, P. J.; Colbran, R. J.; Reese, J.; Marnett, L. J.; Patel, S. *Nat. Neurosci.* **2013**, *16*, 1291.
127. Hu, S. S.; Bradshaw, H. B.; Chen, J. S.; Tan, B.; Walker, J. M. *Br. J. Pharmacol.* **2008**, *153*, 1538.
128. Sang, N.; Chen, C. *Neuroscientist* **2006**, *12*, 425.
129. Sang, N.; Zhang, J.; Chen, C. *J. Neurochem.* **2007**, *102*, 1966.
130. Guindon, J.; Hohmann, A. G. *Br. J. Pharmacol.* **2008**, *153*, 1341.
131. Du, H.; Chen, X.; Zhang, J.; Chen, C. *Br. J. Pharmacol.* **2011**, *163*, 1533.
132. Zhang, J.; Chen, C. *J. Biol. Chem.* **2008**, *283*, 22601.
133. Manna, J. D.; Wepy, J. A.; Hsu, K. L.; Chang, J. W.; Cravatt, B. F.; Marnett, L. J. *The J. Biol. Chem.* **2014**, *289*, 33741.
134. Andreou, A.; Feussner, I. *Phytochemistry* **2009**, *70*, 1504.

135. Moody, J. S.; Kozak, K. R.; Ji, C.; Marnett, L. J. *Biochemistry* **2001**, *40*, 861.
136. Kozak, K. R.; Gupta, R. A.; Moody, J. S.; Ji, C.; Boeglin, W. E.; DuBois, R. N.; Brash, A. R.; Marnett, L. J. *The J. Biol. Chem.* **2002**, *277*, 23278.
137. van der Stelt, M.; van Kuik, J. A.; Bari, M.; van Zadelhoff, G.; Leeftang, B. R.; Veldink, G. A.; Finazzi-Agro, A.; Vliegthart, J. F.; Maccarrone, M. *J. Med. Chem.* **2002**, *45*, 3709.
138. Zelasko, S.; Arnold, W. R.; Das, A. *Prostaglandins Other Lipid Mediat.* **2015**, *116-117*, 112.
139. Urquhart, P.; Nicolaou, A.; Woodward, D. F. *Biochim. Biophys. Acta* **2015**, *1851*, 366.
140. Chen, J. K.; Chen, J.; Imig, J. D.; Wei, S.; Hachey, D. L.; Guthi, J. S.; Falck, J. R.; Capdevila, J. H.; Harris, R. C. *The J. Biol. Chem.* **2008**, *283*, 24514.
141. McDougale, D. R.; Kambalyal, A.; Meling, D. D.; Das, A. *J. Pharm. Exp. Ther.* **2014**, *351*, 616.
142. Alger, B. E.; Kim, J. *Trends Neurosci.* **2011**, *34*, 304.
143. Hashimoto, Y.; Ohno-Shosaku, T.; Maejima, T.; Fukami, K.; Kano, M. *Neuropharmacol.* **2008**, *54*, 58.
144. Hashimoto, Y.; Ohno-Shosaku, T.; Tanimura, A.; Kita, Y.; Sano, Y.; Shimizu, T.; Di Marzo, V.; Kano, M. *J. Physiol.* **2013**, *591*, 4765.
145. Edwards, D. A.; Zhang, L. H.; Alger, B. E. *Proc. Natl. Acad. Sci. U. S. A.* **2008**, *105*, 8142.
146. Zhang, L. H.; Wang, M. N.; Bisogno, T.; Di Marzo, V.; Alger, B. E. *Plos One* **2011**, *6*.
147. Edwards, D. A.; Kim, J.; Alger, B. E. *J. Neurophysiol.* **2006**, *95*, 67.
148. Min, R.; Testa-Silva, G.; Heistek, T. S.; Canto, C. B.; Lodder, J. C.; Bisogno, T.; Di Marzo, V.; Brussaard, A. B.; Burnashev, N.; Mansvelder, H. D. *J. Neurosci.* **2010**, *30*, 2710.
149. Baggelaar, M. P.; Chameau, P. J.; Kantae, V.; Hummel, J.; Hsu, K. L.; Janssen, F.; van der Wel, T.; Soethoudt, M.; Deng, H.; den Dulk, H.; Allara, M.; Florea, B. I.; Di Marzo, V.; Wadman, W. J.; Kruse, C. G.; Overkleeft, H. S.; Hankemeier, T.; Werkman, T. R.; Cravatt, B. F.; van der Stelt, M. *J. Am. Chem. Soc.* **2015**, *137*, 8851.
150. Nicolussi, S.; Gertsch, J. *Vitam. Horm.* **2015**, *98*, 441.
151. Fowler, C. J. *Trends Pharmacol. Sci.* **2012**, *33*, 181.
152. Fowler, C. J. *FEBS J.* **2013**, *280*, 1895.
153. Ben-Shabat, S.; Frider, E.; Sheskin, T.; Tamiri, T.; Rhee, M. H.; Vogel, Z.; Bisogno, T.; De Petrocellis, L.; Di Marzo, V.; Mechoulam, R. *Eur. J. Pharmacol.* **1998**, *353*, 23.
154. Di Marzo, V.; Bisogno, T.; Sugiura, T.; Melck, D.; De Petrocellis, L. *Biochem. J.* **1998**, *331*, 15.

155. Piomelli, D.; Beltramo, M.; Glasnapp, S.; Lin, S. Y.; Goutopoulos, A.; Xie, X. Q.; Makriyannis, A. *Proc. Natl. Acad. Sci. U. S. A.* **1999**, *96*, 5802.
156. Beltramo, M.; Piomelli, D. *Neuroreport* **2000**, *11*, 1231.
157. Bisogno, T.; MacCarrone, M.; De Petrocellis, L.; Jarrahian, A.; Finazzi-Agro, A.; Hillard, C.; Di Marzo, V. *Eur. J. Biochem.* **2001**, *268*, 1982.
158. Chicca, A.; Marazzi, J.; Nicolussi, S.; Gertsch, J. *The J. Biol. Chem.* **2012**, *287*, 34660.
159. Nicolussi, S.; Viveros-Paredes, J. M.; Gachet, M. S.; Rau, M.; Flores-Soto, M. E.; Blunder, M.; Gertsch, J. *Pharmacol. Res.* **2014**, *80*, 52.
160. Sanson, B.; Wang, T.; Sun, J.; Wang, L.; Kaczocha, M.; Ojima, I.; Deutsch, D.; Li, H. *Acta Crystallogr. D Biol. Crystallogr.* **2014**, *70*, 290.
161. Macdonald, R. L.; Olsen, R. W. *Annu. Rev. Neurosci.* **1994**, *17*, 569.
162. Rockwell, C. E.; Snider, N. T.; Thompson, J. T.; Vanden Heuvel, J. P.; Kaminski, N. E. *Mol. Pharmacol.* **2006**, *70*, 101.
163. Gessi, S.; Merighi, S.; Varani, K.; Leung, E.; Mac Lennan, S.; Borea, P. A. *Pharmacol. Ther.* **2008**, *117*, 123.
164. Kurabayashi, M.; Takeyoshi, I.; Yoshinari, D.; Matsumoto, K.; Maruyama, I.; Morishita, Y. *J. Invest. Surg.* **2005**, *18*, 25.
165. Carnevale, V.; Rohacs, T. *Pharmaceuticals (Basel)* **2016**, *9*.
166. McVey, D. C.; Schmid, P. C.; Schmid, H. H.; Vigna, S. R. *J. Pharm. Exp. Ther.* **2003**, *304*, 713.
167. Golech, S. A.; McCarron, R. M.; Chen, Y.; Bembry, J.; Lenz, F.; Mechoulam, R.; Shohami, E.; Spatz, M. *Brain Res. Mol. Brain Res.* **2004**, *132*, 87.
168. Zygmunt, P. M.; Ermund, A.; Movahed, P.; Andersson, D. A.; Simonsen, C.; Jonsson, B. A.; Blomgren, A.; Birnir, B.; Bevan, S.; Eschaliier, A.; Mallet, C.; Gomis, A.; Hogestatt, E. D. *Plos One* **2013**, *8*, e81618.
169. Shore, D. M.; Reggio, P. H. *Front. Pharmacol.* **2015**, *6*, 69.
170. Hanus, L.; Abu-Lafi, S.; Frider, E.; Breuer, A.; Vogel, Z.; Shalev, D. E.; Kustanovich, I.; Mechoulam, R. *Proc. Natl. Acad. Sci. U. S. A.* **2001**, *98*, 3662.
171. Bisogno, T.; Melck, D.; Bobrov, M.; Gretskeya, N. M.; Bezuglov, V. V.; De Petrocellis, L.; Di Marzo, V. *Biochem. J.* **2000**, *351 Pt 3*, 817.
172. Leggett, J. D.; Aspley, S.; Beckett, S. R.; D'Antona, A. M.; Kendall, D. A. *Br. J. Pharmacol.* **2004**, *141*, 253.
173. Barg, J.; Frider, E.; Hanus, L.; Levy, R.; Matus-Leibovitch, N.; Heldman, E.; Bayewitch, M.; Mechoulam, R.; Vogel, Z. *Eur. J. Pharmacol.* **1995**, *287*, 145.
174. Brown, I.; Cascio, M. G.; Wahle, K. W.; Smoum, R.; Mechoulam, R.; Ross, R. A.; Pertwee, R. G.; Heys, S. D. *Carcinogenesis* **2010**, *31*, 1584.
175. Heimann, A. S.; Gomes, I.; Dale, C. S.; Pagano, R. L.; Gupta, A.; de Souza, L. L.; Luchessi, A. D.; Castro, L. M.; Giorgi, R.; Rioli, V.; Ferro, E. S.; Devi, L. A. *Proc. Natl. Acad. Sci. U. S. A.* **2007**, *104*, 20588.

176. Mechoulam, R.; Ben-Shabat, S.; Hanus, L.; Ligumsky, M.; Kaminski, N. E.; Schatz, A. R.; Gopher, A.; Almog, S.; Martin, B. R.; Compton, D. R.; et al. *Biochem. Pharmacol.* **1995**, *50*, 83.
177. Huang, S. M.; Bisogno, T.; Trevisani, M.; Al-Hayani, A.; De Petrocellis, L.; Fezza, F.; Tognetto, M.; Petros, T. J.; Krey, J. F.; Chu, C. J.; Miller, J. D.; Davies, S. N.; Geppetti, P.; Walker, J. M.; Di Marzo, V. *Proc. Natl. Acad. Sci. U. S. A.* **2002**, *99*, 8400.
178. Bisogno, T.; Howell, F.; Williams, G.; Minassi, A.; Cascio, M. G.; Ligresti, A.; Matias, I.; Schiano-Moriello, A.; Paul, P.; Williams, E. J.; Gangadharan, U.; Hobbs, C.; Di Marzo, V.; Doherty, P. *J. Cell Biol.* **2003**, *163*, 463.
179. Araki, M.; Ohshima, N.; Aso, C.; Konishi, A.; Obinata, H.; Tatei, K.; Izumi, T. *J. Biochem.* **2016**.
180. Nakane, S.; Oka, S.; Arai, S.; Waku, K.; Ishima, Y.; Tokumura, A.; Sugiura, T. *Arch. Biochem. Biophys.* **2002**, *402*, 51.
181. Tsutsumi, T.; Kobayashi, T.; Ueda, H.; Yamauchi, E.; Watanabe, S.; Okuyama, H. *Neurochem. Res.* **1994**, *19*, 399.
182. Silvestri, C.; Di Marzo, V. *Cell Metab.* **2013**, *17*, 475.
183. Ravinet Trillou, C.; Delgorge, C.; Menet, C.; Arnone, M.; Soubrie, P. *Int. J. Obes. Relat. Metab. Disord.* **2004**, *28*, 640.
184. Pang, Z.; Wu, N. N.; Zhao, W.; Chain, D. C.; Schaffer, E.; Zhang, X.; Yamdagni, P.; Palejwala, V. A.; Fan, C.; Favara, S. G.; Dressler, H. M.; Economides, K. D.; Weinstock, D.; Cavallo, J. S.; Naimi, S.; Galzin, A. M.; Guillot, E.; Pruniaux, M. P.; Tocci, M. J.; Polites, H. G. *Obesity Silver Spring.* **2011**, *19*, 1923.
185. Simiand, J.; Keane, M.; Keane, P. E.; Soubrie, P. *Behav. Pharmacol.* **1998**, *9*, 179.
186. Kirkham, T. C.; Williams, C. M.; Fezza, F.; Di Marzo, V. *Br. J. Pharmacol.* **2002**, *136*, 550.
187. Powell, D. R.; Gay, J. P.; Wilganowski, N.; Doree, D.; Savelieva, K. V.; Lanthorn, T. H.; Read, R.; Vogel, P.; Hansen, G. M.; Brommage, R.; Ding, Z. M.; Desai, U.; Zambrowicz, B. *Front. Endocrinol.* **2015**, *6*, 86.
188. Bisogno, T.; Mahadevan, A.; Coccurello, R.; Chang, J. W.; Allara, M.; Chen, Y.; Giacobuzzo, G.; Lichtman, A.; Cravatt, B.; Moles, A.; Di Marzo, V. *Br. J. Pharmacol.* **2013**, *169*, 784.
189. Bisogno, T.; Burston, J. J.; Rai, R.; Allara, M.; Saha, B.; Mahadevan, A.; Razdan, R. K.; Wiley, J. L.; Di Marzo, V. *ChemMedChem* **2009**, *4*, 946.
190. Jung, K. M.; Clapper, J. R.; Fu, J.; D'Agostino, G.; Guijarro, A.; Thongkham, D.; Avanesian, A.; Astarita, G.; DiPatrizio, N. V.; Frontini, A.; Cinti, S.; Diano, S.; Piomelli, D. *Cell Metab.* **2012**, *15*, 299.
191. Panikashvili, D.; Simeonidou, C.; Ben-Shabat, S.; Hanus, L.; Breuer, A.; Mechoulam, R.; Shohami, E. *Nature* **2001**, *413*, 527.
192. Mechoulam, R.; Shohami, E. *Mol. Neurobiol.* **2007**, *36*, 68.

193. Panikashvili, D.; Shein, N. A.; Mechoulam, R.; Trembovler, V.; Kohen, R.; Alexandrovich, A.; Shohami, E. *Neurobiol. Dis.* **2006**, 22, 257.
194. Grabner, G. F.; Eichmann, T. O.; Wagner, B.; Gao, Y.; Farzi, A.; Taschler, U.; Radner, F. P.; Schweiger, M.; Lass, A.; Holzer, P.; Zinser, E.; Tschop, M. H.; Yi, C. X.; Zimmermann, R. *The J. Biol. Chem.* **2016**, 291, 913.
195. Nass, S. R.; Long, J. Z.; Schlosburg, J. E.; Cravatt, B. F.; Lichtman, A. H.; Kinsey, S. G. *J. Neuroimmune Pharmacol.* **2015**, 10, 364.
196. Mounsey, R. B.; Mustafa, S.; Robinson, L.; Ross, R. A.; Riedel, G.; Pertwee, R. G.; Teismann, P. *Exp. Neurol.* **2015**, 273, 36.
197. Piro, J. R.; Benjamin, D. I.; Duerr, J. M.; Pi, Y.; Gonzales, C.; Wood, K. M.; Schwartz, J. W.; Nomura, D. K.; Samad, T. A. *Cell Rep.* **2012**, 1, 617.
198. Chen, R. Q.; Zhang, J.; Wu, Y.; Wang, D. Q.; Feng, G. P.; Tang, Y. P.; Teng, Z. Q.; Chen, C. *Cell Rep.* **2012**, 2, 1329.
199. Hernandez-Torres, G.; Cipriano, M.; Heden, E.; Bjorklund, E.; Canales, A.; Zian, D.; Feliu, A.; Mecha, M.; Guaza, C.; Fowler, C. J.; Ortega-Gutierrez, S.; Lopez-Rodriguez, M. L. *Angew. Chem. Int. Ed.* **2014**, 53, 13765.
200. Brindisi, M.; Maramai, S.; Gemma, S.; Brogi, S.; Grillo, A.; Mannelli, L. D.; Gabellieri, E.; Lamponi, S.; Saponara, S.; Gorelli, B.; Tedesco, D.; Bonfiglio, T.; Landry, C.; Jung, K. M.; Armirotti, A.; Luongo, L.; Ligresti, A.; Piscitelli, F.; Bertucci, C.; Dehouck, M. P.; Campiani, G.; Malone, S.; Ghelardini, C.; Pittaluga, A.; Piomelli, D.; Di Marzo, V.; Butini, S. *J. Med. Chem.* **2016**, 59, 2612.
201. Valdeolivas, S.; Pazos, M. R.; Bisogno, T.; Piscitelli, F.; Iannotti, F. A.; Allara, M.; Sagredo, O.; Di Marzo, V.; Fernandez-Ruiz, J. *Cell Death Dis.* **2013**, 4, e862.
202. Hill, M. N.; Patel, S. *Biol. Mood Anxiety Disord.* **2013**, 3, 19.
203. Lutz, B. *Curr. Opin. Pharmacol.* **2009**, 9, 46.
204. Patel, S.; Hillard, C. J. *J. Pharm. Exp. Ther.* **2006**, 318, 304.
205. Rey, A. A.; Purrio, M.; Viveros, M. P.; Lutz, B. *Neuropsychopharmacology* **2012**, 37, 2624.
206. Zanettini, C.; Panlilio, L. V.; Alicki, M.; Goldberg, S. R.; Haller, J.; Yasar, S. *Front. Behav. Neurosci.* **2011**, 5, 57.
207. Gamble-George, J. C.; Conger, J. R.; Hartley, N. D.; Gupta, P.; Sumislowski, J. J.; Patel, S. *Psychopharmacology* **2013**, 228, 401.
208. Hill, M. N.; Gorzalka, B. B. *Eur. J. Pharmacol.* **2004**, 499, 291.
209. Moreira, F. A.; Grieb, M.; Lutz, B. *Best Pract. Res. Clin. Endocrinol. Metab.* **2009**, 23, 133.
210. Valverde, O.; Torrens, M. *Neuroscience* **2012**, 204, 193.
211. Morena, M.; Patel, S.; Bains, J. S.; Hill, M. N. *Neuropsychopharmacology* **2016**, 41, 80.
212. Patel, S.; Hillard, C. J. *Eur. J. Neurosci.* **2008**, 27, 2821.

213. Shonesy, B. C.; Bluett, R. J.; Ramikie, T. S.; Baldi, R.; Hermanson, D. J.; Kingsley, P. J.; Marnett, L. J.; Winder, D. G.; Colbran, R. J.; Patel, S. *Cell Rep.* **2014**, *9*, 1644.
214. Jenniches, I.; Ternes, S.; Albayram, O.; Otte, D. M.; Bach, K.; Bindila, L.; Michel, K.; Lutz, B.; Bilkei-Gorzo, A.; Zimmer, A. *Biol. Psychiatry* **2016**, *79*, 858.
215. Sciolino, N. R.; Zhou, W.; Hohmann, A. G. *Pharmacol. Res.* **2011**, *64*, 226.
216. Aliczki, M.; Balogh, Z.; Tulogdi, A.; Haller, J. *Behav. Pharmacol.* **2012**, *23*, 348.
217. Aliczki, M.; Zelena, D.; Mikics, E.; Varga, Z. K.; Pinter, O.; Bakos, N. V.; Varga, J.; Haller, J. *Horm. Behav.* **2013**, *63*, 752.
218. De Vries, T. J.; Shaham, Y.; Homberg, J. R.; Crombag, H.; Schuurman, K.; Dieben, J.; Vanderschuren, L. J.; Schoffelmeer, A. N. *Nat. Med.* **2001**, *7*, 1151.
219. Maldonado, R.; Valverde, O.; Berrendero, F. *Trends Neurosci.* **2006**, *29*, 225.
220. Le Foll, B.; Forget, B.; Aubin, H. J.; Goldberg, S. R. *Addict. Biol.* **2008**, *13*, 239.
221. Balerio, G. N.; Aso, E.; Berrendero, F.; Murtra, P.; Maldonado, R. *Eur. J. Neurosci.* **2004**, *20*, 2737.
222. Yamaguchi, T.; Hagiwara, Y.; Tanaka, H.; Sugiura, T.; Waku, K.; Shoyama, Y.; Watanabe, S.; Yamamoto, T. *Brain Res.* **2001**, *909*, 121.
223. Ramesh, D.; Ross, G. R.; Schlosburg, J. E.; Owens, R. A.; Abdullah, R. A.; Kinsey, S. G.; Long, J. *Pharmacol. Exp. Ther.* **2011**, *339*, 173.
224. Muldoon, P. P.; Chen, J.; Harenza, J. L.; Abdullah, R. A.; Sim-Selley, L. J.; Cravatt, B. F.; Miles, M. F.; Chen, X.; Lichtman, A. H.; Damaj, M. I. *Br. J. Pharmacol.* **2015**, *172*, 869.
225. Le Foll, B.; Goldberg, S. R. *J. Pharm. Exp. Ther.* **2005**, *312*, 875.
226. Buczynski, M. W.; Herman, M. A.; Hsu, K. L.; Natividad, L. A.; Irimia, C.; Polis, I. Y.; Pugh, H.; Chang, J. W.; Niphakis, M. J.; Cravatt, B. F.; Roberto, M.; Parsons, L. H. *Proc. Natl. Acad. Sci. U. S. A.* **2016**, *113*, 1086.
227. Walker, J. M.; Huang, S. M. *Pharmacol. Ther.* **2002**, *95*, 127.
228. Guindon, J.; Desroches, J.; Beaulieu, P. *Br. J. Pharmacol.* **2007**, *150*, 693.
229. Desroches, J.; Guindon, J.; Lambert, C.; Beaulieu, P. *Br. J. Pharmacol.* **2008**, *155*, 913.
230. Beaulieu, P.; Bisogno, T.; Punwar, S.; Farquhar-Smith, W. P.; Ambrosino, G.; Di Marzo, V.; Rice, A. S. *Eur. J. Pharmacol.* **2000**, *396*, 85.
231. Maione, S.; De Petrocellis, L.; de Novellis, V.; Moriello, A. S.; Petrosino, S.; Palazzo, E.; Rossi, F. S.; Woodward, D. F.; Di Marzo, V. *Br. J. Pharmacol.* **2007**, *150*, 766.
232. Guindon, J.; Lai, Y.; Takacs, S. M.; Bradshaw, H. B.; Hohmann, A. G. *Pharmacol. Res.* **2013**, *67*, 94.
233. Kinsey, S. G.; Nomura, D. K.; O'Neal, S. T.; Long, J. Z.; Mahadevan, A.; Cravatt, B. F.; Grider, J. R.; Lichtman, A. H. *J. Pharm. Exp. Ther.* **2011**, *338*, 795.
234. Kinsey, S. G.; Long, J. Z.; O'Neal, S. T.; Abdullah, R. A.; Poklis, J. L.; Boger, D. L.; Cravatt, B. F.; Lichtman, A. H. *J. Pharm. Exp. Ther.* **2009**, *330*, 902.

235. Kinsey, S. G.; Long, J. Z.; Cravatt, B. F.; Lichtman, A. H. *J. Pain* **2010**, *11*, 1420.
236. Woodhams, S. G.; Sagar, D. R.; Burston, J. J.; Chapman, V. *Handb. Exp. Pharmacol.* **2015**, 227, 119.
237. Wilkerson, J. L.; Ghosh, S.; Bagdas, D.; Mason, B. L.; Crowe, M. S.; Hsu, K. L.; Wise, L. E.; Kinsey, S. G.; Damaj, M. I.; Cravatt, B. F.; Lichtman, A. H. *Br. J. Pharmacol.* **2016**, *173*, 1678.
238. Long, J. Z.; Nomura, D. K.; Vann, R. E.; Walentiny, D. M.; Booker, L.; Jin, X.; Burston, J. J.; Sim-Selley, L. J.; Lichtman, A. H.; Wiley, J. L.; Cravatt, B. F. *Proc. Natl. Acad. Sci. U. S. A.* **2009**, *106*, 20270.

CHAPTER 3

Development of an Activity-Based Probe and Focused Library Screening Reveal Highly Selective Inhibitors for DAG-lipase- α in Brain^{*}

Introduction

Diacylglycerol lipase- α (DAGL- α) is an intracellular, multi-domain protein responsible for the formation of the endocannabinoid 2-arachidonoylglycerol (2-AG) in the central nervous system.^{1,2} 2-AG is an endogenous signaling lipid that interacts with the cannabinoid CB₁ and CB₂ receptors.³ Little is known about the regulation of its biosynthetic pathway and it is largely unclear to what extent 2-AG is responsible for distinct cannabinoid CB₁ receptor mediated biological processes. Selective inhibitors of DAGL- α may contribute to a more fundamental understanding of the physiological role of 2-AG and may serve as potential drug candidates for the treatment of obesity and neurodegenerative diseases.^{4,5} Currently, there are no selective inhibitors and activity-based probes available for the study of DAGL- α .⁶⁻¹²

The identification of selective DAGL- α inhibitors is hampered by a lack of structural knowledge of the target, and lack of assays that make use of endogenous DAGL- α activity in proteomes. No crystal structures are available and no homology

^{*}Published as part of: Baggelaar, M. P.; Janssen, F. J.; van Esbroeck A. C. M; den Dulk H.; Allarà M.; Hoogendoorn S.; McGuire R.; Florea B. I.; Meeuwenoord N.; van den Elst H.; van der Marel G. A.; Brouwer J.; Di Marzo V.; Overkleeft H. S.; van der Stelt M.; Development of an activity-based probe and in silico design reveal highly selective inhibitors for diacylglycerol lipase- α in brain. *Angew. Chem. Int. Ed.* **2013**, 52, 12081-12085.

models have been reported to aid hit identification and to guide optimization of the inhibitors. Determination of the selectivity of the inhibitors in native tissues is important, because DAGL- α belongs to the class of serine hydrolases, containing more than 200 members with various physiological functions.^{13,14}

Routinely, fluorophosphonate (FP)-based probes are employed in competitive activity-based protein profiling (ABPP) experiments to determine selectivity of serine hydrolase inhibitors in complex proteomes. Competitive ABPP is an attractive and powerful chemical biological technique. It integrates organic chemistry, pharmacology and chemical proteomics in the early stages of hit identification in the drug discovery process. It is unique in its ability to rapidly identify inhibitor activity and selectivity over large protein family classes in tissue samples.¹³ DAGL- α however does not react with the fluorophosphonate-based probes.¹⁵ Therefore a new probe that can label native DAGL- α would be of value to study the potency and selectivity of novel DAGL- α inhibitors in brain proteomes. This chapter describes the design, synthesis and application of MB064 as a novel activity-based probe (ABP) for DAGL- α . MB064 is based on the non-selective DAGL- α inhibitor tetrahydrolipstatin (THL; also known as Orlistat[®], a drug used for the treatment of obesity). MB064 was used to screen a focused library of lipase inhibitors, which resulted in the rapid identification of α -ketoheterocycles as a new chemotype of DAGL inhibitors which demonstrated high selectivity in brain proteome.

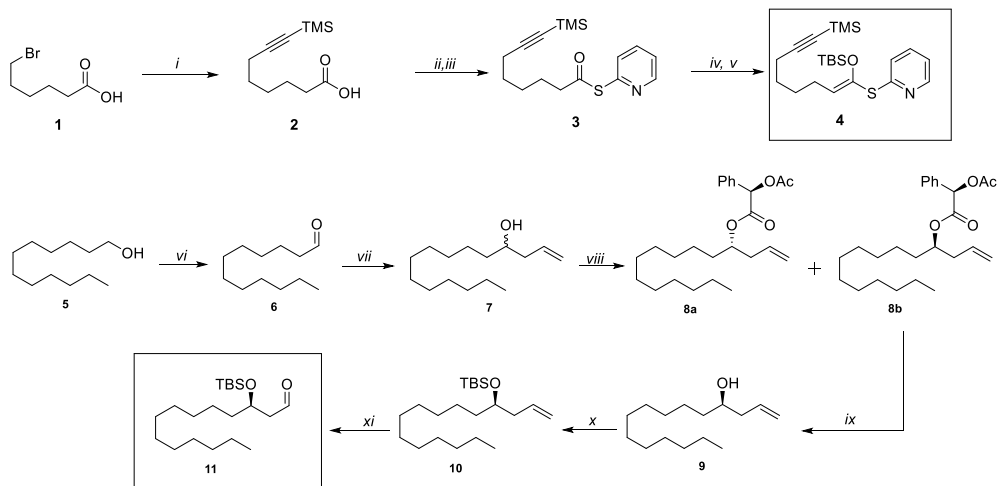
Results and discussion

Design & synthesis of MB064

It was envisioned that competitive activity-based protein profiling (ABPP) could be exploited to identify novel inhibitors for DAGL- α . For this purpose, MB064 (**15**) was synthesized as a novel activity-based probe (ABP) for DAGL- α . The probe is based on THL-analog **14**, which contains an alkyne for conjugation to a reporter group (e.g. fluorophore or biotin) and relies on a β -lactone warhead that forms a covalent bond with the catalytic nucleophilic serine. This principle has been used previously with bacterial, plant and mammalian enzymes that share an α,β -hydrolase fold motif.¹⁶⁻²⁰ MB064 was synthesized following an established strategy.²¹

The synthesis started with the preparation of two key building blocks: TMS-protected thiopyridyl ketene acetal **4** and chiral aldehyde **11** (Scheme 1). These building blocks were condensed via a Mukaiyama aldol lactonization to give the central β -lactone. The TMS-protected thiopyridyl ketene acetal was prepared in 5 steps from 6-bromohexanoic acid (Scheme 1). Substitution of the bromine for the TMS-alkyne and subsequent preparation of the thioester yielded **3** in 86%. The thiopyridyl ester was subjected to LiHMDS and TBSCl to obtain ketene acetal **4** in 60% yield over two steps. Chiral aldehyde **11** was prepared in 6

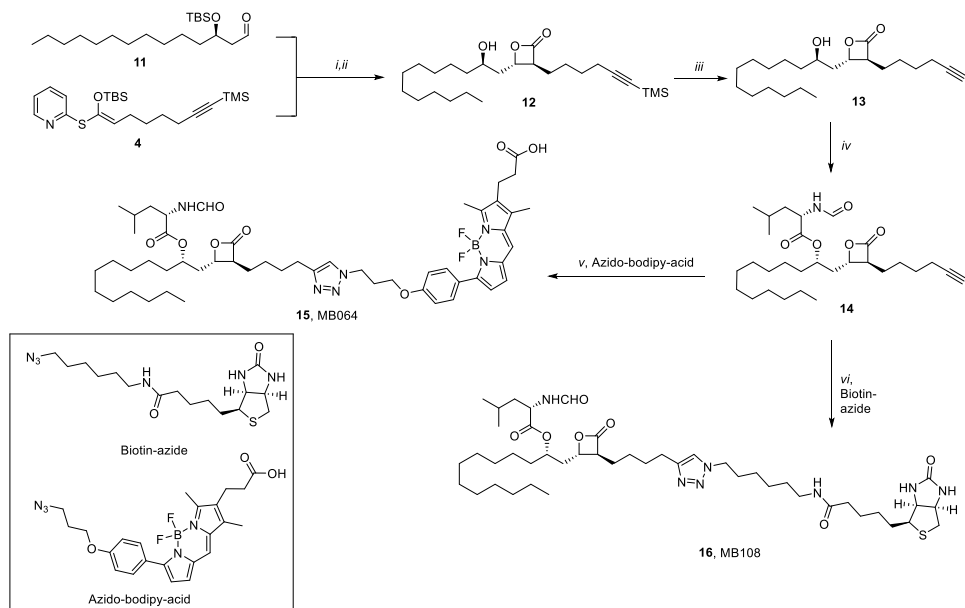
steps from dodecanol. The alcohol was oxidized using PCC, yielding lauraldehyde **6** in 80% yield. Allylation of **6** with allylmagnesiumbromide yielded the racemic homoallylic alcohol **7**. Esterification with commercially available (R)-(-)-*O*-acetylmandelic acid provided a mixture of diastereoisomers (**8a** and **8b**) which could be separated by silica gel column chromatography. Subsequent ester hydrolysis of **8b** under basic conditions provided enantiomerically pure homoallylic alcohol **9**. TBS protection of alcohol **9** followed by ozonolysis of the terminal double bond provided chiral aldehyde **11**.



Scheme 1: i) ethynyltrimethylsilane, n-BuLi, HMPA, THF, -78°C, 82%, ii) COCl₂, DMF, DCM, 0°C, iii) 2-thiopyridine, Et₃N, DCM, iv) LiHMDS, THF, -78°C, v) DMF, Et₃N, TBSCl, 60% (4 steps); vi) PCC, CH₂Cl₂, 0°C, 80% vii) allylmagnesium bromide, THF, -10 °C, 61%, viii) (R)-*O*-acetylmandelic acid, DCC, DMAP, ix) KOH, MeOH, 45% (two steps), x) TBSCl, imidazole, DMF, xi) O₃, MeOH/DCM, -78°C; Me₂S, Et₃N, 81% (two steps).

In the final stage of the synthesis, aldehyde **11** and TMS-protected thiopyridyl ketene acetal **4** were coupled to form the central lactone ring. The lactone ring was constructed using a tandem Mukayama aldol lactonization, yielding a (10:1 anti/syn) mixture of diastereomers, with a total selectivity for the *trans*- β -lactone. After removal of the TBS group, the diastereomers could be separated by column chromatography over silica gel. *N*-formyl-L-leucine was introduced by a Mitsunobu reaction inverting the δ -stereocenter towards the desired configuration. Coupling with a fluorophore (azido bodipy acid)²² by a copper catalyzed click reaction resulted in the first DAGL- α sensitive ABP MB064 (Scheme 2). To be able to perform pulldown experiments for target identification, **14** was also coupled to biotin-azide to obtain biotin probe **16** (MB108). To test whether MB064 was active against DAGL- α , an adapted version of a previously published biochemical DAGL- α assay was applied.²³ This assay is based on the hydrolysis of para-nitrophenylbutyrate by membrane preparations of HEK293T cells transiently

transfected with human DAGL- α (Figure 1; assay validation using the known DAGL- α inhibitor THL). MB064 was highly active with an IC_{50} of 6.0 ± 1.0 nM ($N=2$, $n=2$) in this colorimetric assay, indicating that the ABP maintains its activity when the bodipy-acid is attached.



Scheme 2: i) $ZnCl_2$, CH_2Cl_2 , dr 1:10, 50%, ii) HF, CH_3CN , $0^\circ C$, 91%, iii) 2,6-lutidine/acetone/ H_2O (0.1:1:1), $AgNO_3$, 79%, iv) *N*-formyl-L-leucine, PPh_3 , DIAD, THF v) sodium ascorbate, $CuSO_4$, H_2O , $CHCl_3$ azido-bodipy acid, vi) sodium ascorbate, $CuSO_4$, H_2O , $CHCl_3$, biotin-azide.

Characterization of MB064 as an activity-based probe for DAGL- α

To validate MB064 as a DAGL- α sensitive ABP, various hDAGL- α constructs were transiently transfected in HEK293T cells (Figure 2A). Incubation of hDAGL- α -FLAG transfected HEK293T cell membranes with MB064, followed by SDS-PAGE and fluorescence scanning revealed several fluorescent signals (Figure 2B). The signal at ~120 kDa, which corresponded to the molecular mass of hDAGL- α , overlapped with a band visualized by the FLAG-tag antibody and was absent in mock-transfected cells. Pre-incubation with 10 μM THL blocked enzymatic activity and prevented labeling of the proteins with MB064, thereby excluding non-specific labeling.

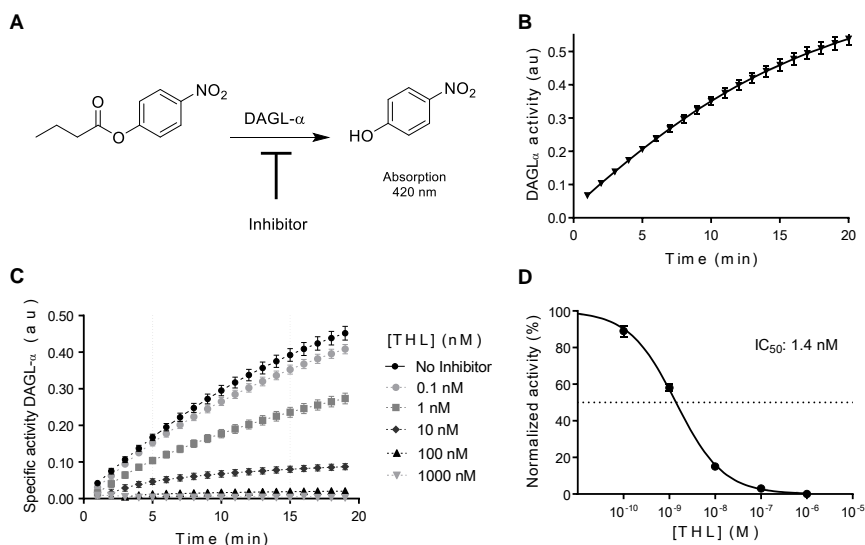


Figure 1. Biochemical hDAGL- α activity assay and dose response analysis (A) Enzymatic conversion, as performed by HEK293T cell membranes overexpressing hDAGL- α , in the colorimetric activity assay; the hydrolysis of para-nitrophenylbutyrate (PNPB) to para-nitrophenol, resulting in an increased absorption (\pm SEM) at 420 nm. Hydrolysis by an equal amount of protein from mock membranes was subtracted to correct for background. Measuring conditions: 0.05 μ g/ μ L hDAGL- α , 50mM Hepes pH 7.0, 300 μ M PNPB, 5% DMSO in a total volume of 200 μ L. N=2, n=2, Z' $>$ 0.6. (B) Time course of PNPB hydrolysis by hDAGL- α in absence of inhibitor. (C) Time course of PNPB hydrolysis by hDAGL- α in the presence of 0.1 to 1000 nM of known DAGL inhibitor THL. (D) IC_{50} analysis on normalized activity (\pm SEM) of hDAGL- α . Activities were determined from the slope of the linear region (5-15 minutes) in C.

Site-directed mutagenesis of the catalytic DAGL- α nucleophile Ser472 into an alanine abolished the enzymatic activity in the biochemical assay and no band at \sim 120 kD was observed. hDAGL- α protein expression was not altered by mutagenesis as determined with the FLAG-tag antibody (Figure 2A, B). Finally, a C-terminal deletion construct of hDAGL- α was made, this construct was lacking amino acids 688-1042. This mutant enzyme was still active as confirmed by our biochemical assay and was also labeled by MB064. Together, these data demonstrate that MB064 can efficiently label active hDAGL- α by forming a covalent bond with Ser472.

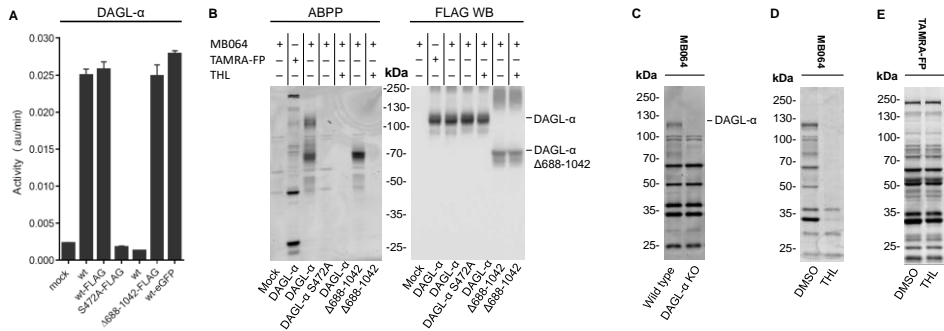


Figure 2. Validation of MB064 as a DAGL- α ABP. (A) Activity of different hDAGL- α constructs transiently transfected in HEK-293T cell membranes as measured with para-nitrophenylbutyrate as substrate. Mock membranes and different constructs measured at the same protein concentration (1 $\mu\text{g}/\mu\text{L}$), uncorrected activity ($\pm\text{SEM}$, $N=2$, $n=2$). (B) ABPP using MB064 (250 nM) in different hDAGL- α constructs at the same protein concentration (2 $\mu\text{g}/\mu\text{L}$), and Western Blot of the ABPP gel using an anti-FLAG antibody. (C) ABPP using MB064 (250 nM) in mouse brain membrane proteome of wild type and DAGL- α KO mice. (D) Competitive ABPP in mouse brain membrane proteome using MB064 (250 nM) and preincubation with THL (20 μM). (E) Competitive ABPP in mouse brain membrane proteome using TAMRA-FP (500 nM) and preincubation with THL (20 μM).

To determine whether the probe was able to react with native DAGL- α , MB064 was incubated in mouse brain membrane proteome. MB064 labeled at least eight different proteins in brain (Figure 2C), which was prevented (or reduced to a large extent) by preincubation with 20 μM THL (Figure 2). A distinct fluorescent band at ~120 kD was observed, this band could not be observed when the brain membrane proteome was incubated with TAMRA-FP (Figure 2E). Of note, MB064 showed a much more restricted labeling profile than TAMRA-FP. In DAGL- α KO mouse brain membrane proteomes no specific band at ~120 kD was found (Figure 2C). Incubation of mouse brain cytosolic proteomes with MB064 led to the labeling of several proteins, but no specific signal at ~120 kD was detected (Figure 3). This result is in line with the fact that DAGL- α resides in membranes.

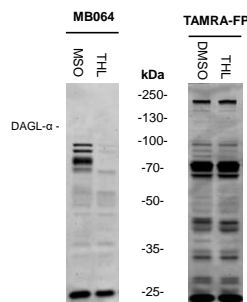


Figure 3. ABPP of mouse brain cytosolic proteome. (A) Mouse brain cytosolic proteome preincubated with vehicle (DMSO) or THL (20 μM), showing that DAGL- α is not present in the cytosolic fraction (B) Mouse brain cytosolic proteome preincubated with vehicle (DMSO) or THL (20 μM) and labeled with TAMRA-FP.

To investigate if DAGL- α could also be labeled in other tissues than brain, the membrane fractions of various mouse tissues of DAGL- α knockout and wild type were screened, including kidney, pancreas, liver, skeletal muscle, spinal cord, lung, spleen, heart, brown adipose tissue and white adipose tissue (Figure 4). A faint band at ~120 kDa was detected in the wild-type spinal cord and absent in its DAGL- α KO counterpart. This indicates that MB064 can detect DAGL- α activity in the spinal cord.

Finally, mouse DAGL- α protein and twelve other proteins (Table 1) were detected in a pull down experiment, using avidin-beads and a biotinylated THL derivative, MB108 (16), followed by tryptic digestion and mass spectrometric analysis of the isolated peptides. These proteins were not identified when the brain membrane proteome was heat denaturated. The proteomic experiments confirmed that THL reacted with multiple hydrolase enzymes (e.g. fatty acid synthase (FAS), ABHD16a and platelet-activating factor acetylhydrolase) as previously reported. To conclude, MB064 is able to visualize and detect DAGL- α in mouse brain membrane proteomes, and THL is a non-selective inhibitor of DAGL- α in mouse brain.

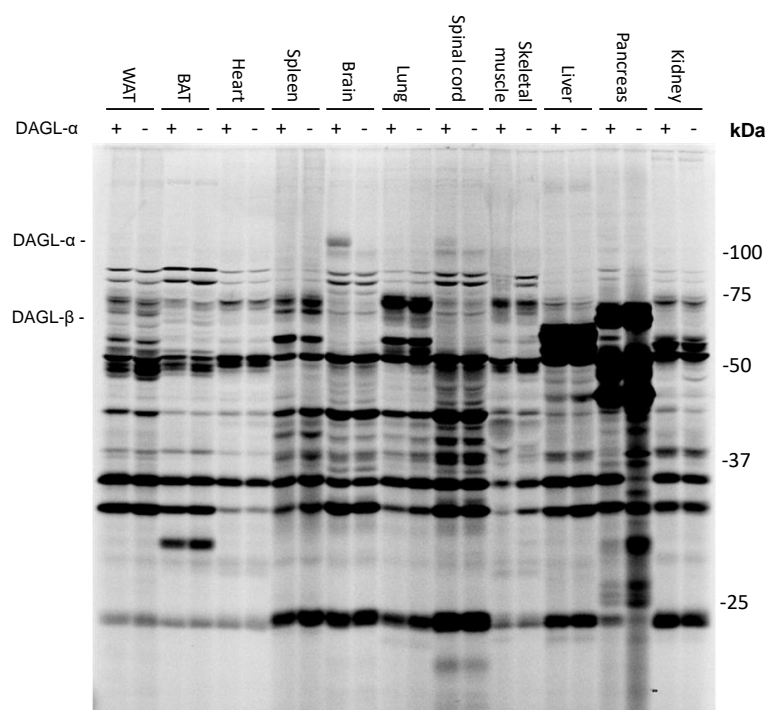


Figure 4. Screen of DAGL- α wild type (WT) and knockout (KO) tissues. DAGL- α WT and KO tissues were screened to obtain a tissue wide overview of DAGL- α activity. Mouse membrane proteome was incubated for 30 minutes with 1 μ M MB64 at rt. A fluorescent band at the molecular weight of DAGL- α (~120 kDa) was present in the WT brain and spinal cord membrane proteome but absent in their DAGL- α KO counterparts. This indicates that MB064 can visualize DAGL- α alpha activity in the brain and the spinal cord. (Abbreviations WAT: white adipose tissue; BAT: brown adipose tissue; (+) WT tissue and (-) DAGL- α KO tissue).

Table 1. Hydrolases detected by MB108 in a pull-down experiment.

Name	gene	Mw (kDa)
Palmitoyl-protein thioesterase 1	<i>Ppt1</i>	34,490
Fatty acid synthase	<i>Fasn</i>	272,428
Carboxylesterase 1C	<i>Ces1c</i>	61,056
Platelet-activating factor acetylhydrolase	<i>Pla2g7</i>	49,258
Sn1-specific diacylglycerol lipase alpha	<i>Dagla</i>	115,375
Phospholipase DDHD2	<i>Ddhd2</i>	79,577
Monoacylglycerol lipase ABHD6	<i>Abhd6</i>	38,205
Monoacylglycerol lipase ABHD12	<i>Abhd12</i>	45,270
Acyl-protein thioesterase 2	<i>Lypla2</i>	24,794
Abhydrolase domain-containing protein 16A	<i>Abhd16a</i>	63,086
Acyl-protein thioesterase 1	<i>Lypla1</i>	24,688
Alpha/beta hydrolase domain-containing protein 11	<i>Abhd11</i>	33,561
S-formylglutathione hydrolase	<i>Esd</i>	31,320

Next, a set of commercially available lipase inhibitors, which were mainly selected for their reactivity towards enzymes involved in endocannabinoid signaling (Table 2) was screened using the ABPP assay to investigate if library members showed DAGL- α inhibition and to map (off-targets of the focused library (Figure 5 and 6). It was found that compounds **17** and **21** demonstrated significant reductions in DAGL- α labeling. Other hits from the library screen did not inhibit DAGL- α (Figure 5).

Table 2: Structures and known targets of a set of commercially available lipase inhibitors, which were mainly selected for their reactivity towards enzymes involved in endocannabinoid signaling.

Name ^[a]	structure	Activity	Name ^[a]	structure	Activity
17 (LEI103) CAY10499		HSL inhibitor	25 NO-1886		lipoprotein lipase activator
18 CAY10590		PLA ₂ inhibitor	26 Chlorpromazine		Sphingomyelin- ase inhibitor
19 CAY10594		PLD ₂ inhibitor	27 URB597		FAAH inhibitor
20 CAY10566		SCD inhibitor	28 JZL 184		MAGL inhibitor
21 (LEI104) PHOP		FAAH inhibitor	29 URB602		MAGL inhibitor
22 JZL 195		FAAH and MAGL inhibitor	30 PF-3845		FAAH inhibitor
23 WWL70		ABHD6 inhibitor	31 TOFA		FAS inhibitor
24 FIPI		PLD inhibitor	32 RHC80267		Lipase inhibitor

^[a] Inhibitors were purchased at Cayman Chemicals, Sigma Aldrich or Thermo Fisher.

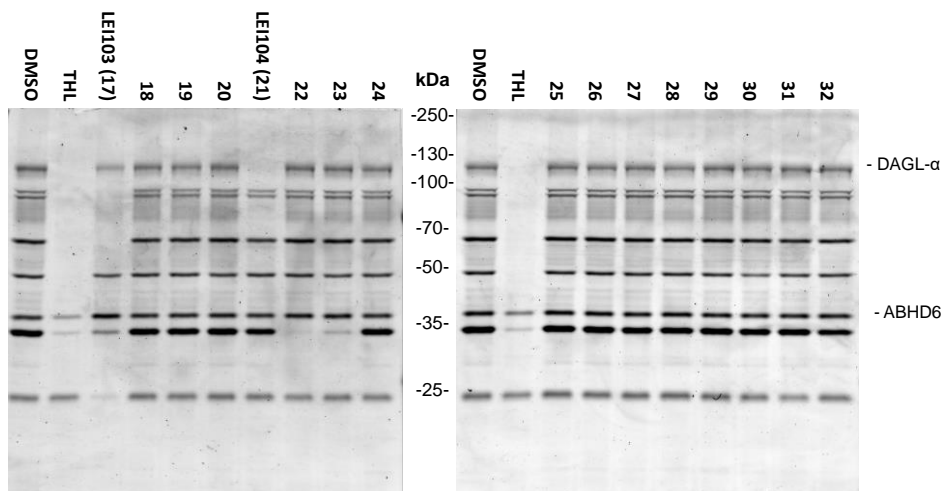


Figure 5. ABPP screen of mouse brain membrane proteome with ABP MB064. The mouse brain membrane proteome (total protein concentration 2.5 $\mu\text{g}/\mu\text{L}$; volume 20 μL) was preincubated with 20 μM (final concentration) of the indicated inhibitor, followed by 10 min labeling with 250 nM ABP MB064.

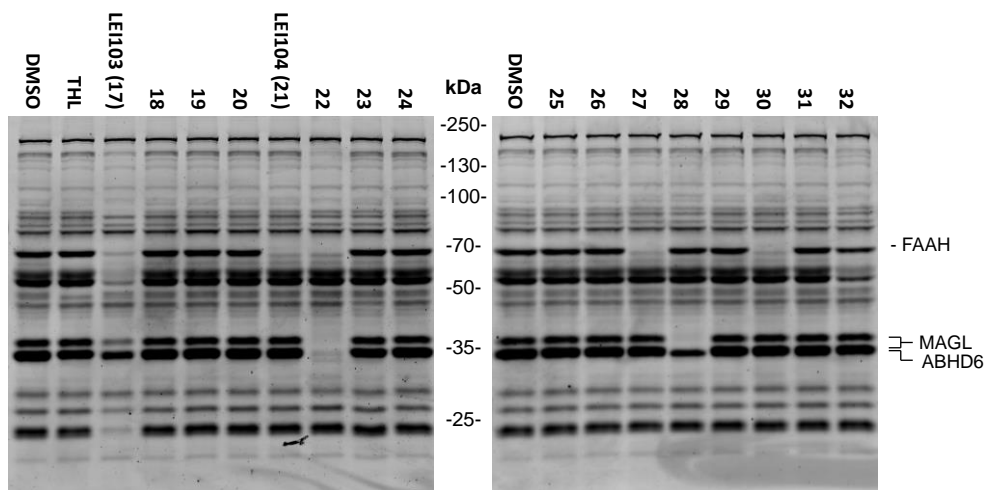


Figure 6. ABPP screen of mouse brain membrane proteome with TAMRA-FP. The mouse brain membrane proteome (total protein concentration 2.5 $\mu\text{g}/\mu\text{L}$; volume 20 μL) was preincubated with 20 μM (final concentration) of the indicated inhibitor, followed by 10 min labeling with 500 nM ABP TAMRA-FP.

To confirm the hits of the ABPP screen, the focused library was screened in an orthogonal colorimetric assay against hDAGL- α (Figure 7).²⁵ The orthogonal screen confirmed the results from the ABPP screen, LEI103 (17) and LEI104 (21) were the only compounds inhibiting hDAGL- α enzymatic activity to over 50% at 10 μM . Determination of the concentration response resulted in an IC_{50} of 37 ± 5 nM ($N=2$, $n=2$) for LEI104, making it a

hundred-fold more potent than LEI103 ($IC_{50} = 3.8 \pm 0.4 \mu M$; $N=2$, $n=2$) (Figure 7B). Of note, the reported DAGL- α inhibitor RHC80267¹ (compound **32**) showed no inhibitory activity.

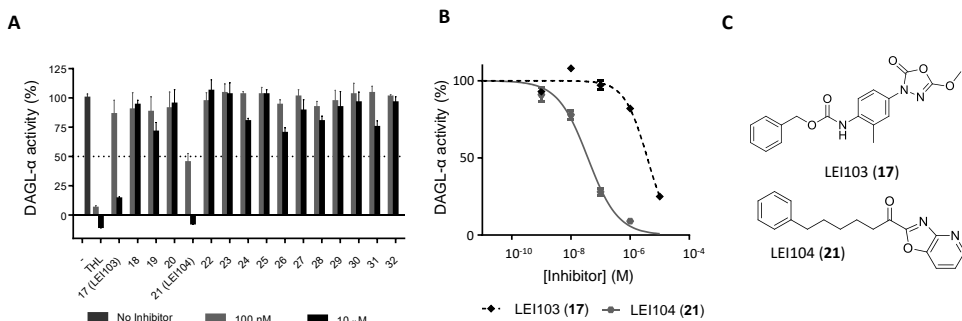


Figure 7. Screen of the targeted library using the colorimetric biochemical assay. (A) Normalized residual activity measured against hDAGL- α in HEK-293T cell membranes with para-nitrophenylbutyrate as substrate in the presence of 100 nM or 10 μM inhibitor. THL was used as a positive control for inhibition. (B) Dose-response curve of LEI103 and LEI104 as determined with the colorimetric assay. IC_{50} analysis on corrected and normalized activities (\pm SEM, $N=2$, $n=2$) against hDAGL- α . (C) Structures of LEI103 and LEI104.

Competitive ABPP with LEI103 and LEI104

To determine the activity and selectivity profiles in the brain, a competitive ABPP experiment with (**17**) and (**21**), which were termed LEI103 and LEI104, respectively, at 20 μM using mouse brain membrane proteome was performed (Figure 8A). LEI103 prevented labeling of six proteins by MB064, whereas LEI104 was much more selective and completely blocked the labeling of DAGL- α . A competitive concentration response experiment was performed to determine the activity of LEI103 and LEI104 against native DAGL- α in the mouse brain membrane proteome (Figure 8C, D). LEI104 inhibited DAGL- α labeling with an IC_{50} of 450 ± 203 nM ($n=3$), which is approximately 40-fold more potent than LEI103 ($IC_{50} = 18 \pm 9 \mu M$, $n=3$) (Figure 8C). In addition, a comparative ABPP experiment with TAMRA-FP was performed to obtain a selectivity profile of the hits on the serine hydrolase family (Figure 8A, B). LEI103 inhibited several proteins, whereas LEI104 abolished only one signal at ~ 64 kD, which corresponded to FAAH.²⁴ Quantification of integrated band intensities for the competition of THL, LEI103 and LEI104 (20 μM) with MB064 and TAMRA-FP is given in Table 3 and 4 respectively.

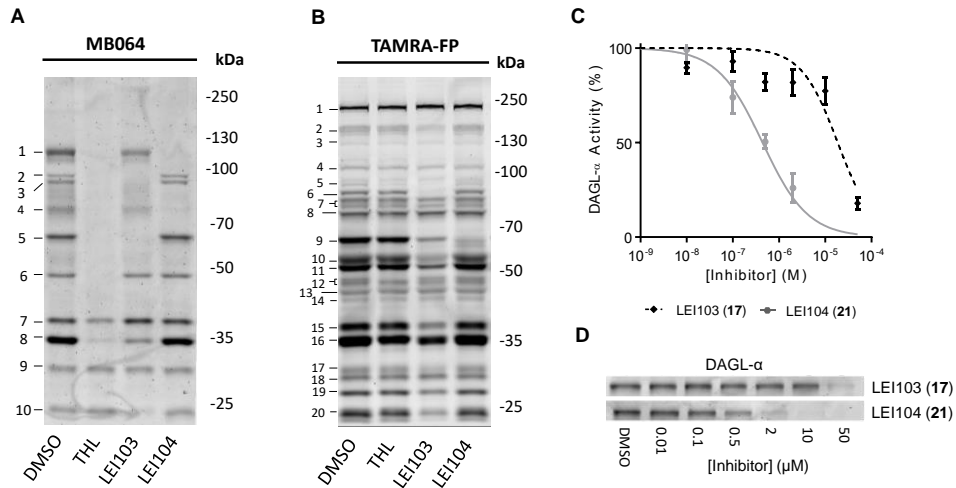


Figure 8. Selectivity profile and activity of LEI103 and LEI104 in the mouse brain membrane proteome. (A, B) Competitive ABPP with DAGL- α inhibitors THL, LEI103 and LEI104 (20 μ M) using ABPs MB064 (250 nM) and TAMRA-FP (500 nM) in mouse brain membrane proteome (enzyme concentration 2.5 μ g/ μ L). (C) Dose response curve for DAGL- α inhibition by LEI103 and LEI104 in the mouse brain membrane proteome as measured by competitive ABPP with ABP MB064 (\pm SEM, n=3). (D) Concentration dependent inhibition of DAGL- α in the mouse brain membrane proteome by LEI103 and LEI104 using ABP MB064.

Table 3. quantification of the protein bands in figure 8A.

Band	Vehicle (%)	THL (%)	LEI103 (%)	LEI104 (%)
1	100 \pm 4	1 \pm 3***	56 \pm 2***	1 \pm 3***
2	100 \pm 24	7 \pm 0***	7 \pm 6***	132 \pm 7
3	100 \pm 8	1 \pm 3***	4 \pm 4***	95 \pm 4
4 [#]	100 \pm 9	-5 \pm 3***	54 \pm 4***	4 \pm 4***
5	100 \pm 6	0 \pm 1***	2 \pm 5***	99 \pm 5
6	100 \pm 4	0 \pm 3***	85 \pm 7	109 \pm 7
7	100 \pm 2	40 \pm 6***	116 \pm 9	92 \pm 10
8	100 \pm 4	0 \pm 5***	17 \pm 8***	88 \pm 6
9	100 \pm 16	117 \pm 8	104 \pm 15	98 \pm 7
10	100 \pm 5	84 \pm 35	28 \pm 21***	103 \pm 9

Means \pm SD, N=3, normalized to the intensity of the protein bands from the samples treated with vehicle. Values are corrected for protein loading per lane as determined with coomassie staining.

[#]Labeling of protein band 4 by MB064 is completely inhibited by THL and LEI104, and partly by LEI103. This inhibitory profile together with the absence of this protein band in DAGL- α KO membrane proteome indicates that this is a DAGL- α breakdown product and not an additional off-target of these inhibitors. Statistical analysis: 2-way ANOVA with Bonferroni's posttest (*** = $p < 0.001$ vs vehicle).

Table 4. quantification of the protein bands in figure 8B

	Vehicle (%)	THL (%)	LEI103 (%)	LEI104 (%)
1	100 \pm 2	98 \pm 1	101 \pm 4	102 \pm 3
2	100 \pm 7	93 \pm 6	37 \pm 5***	97 \pm 5
3	100 \pm 19	99 \pm 15	61 \pm 38**	102 \pm 16
4	100 \pm 19	77 \pm 5	60 \pm 17**	82 \pm 13
5	100 \pm 16	18 \pm 20***	22 \pm 9***	73 \pm 24
6	100 \pm 5	94 \pm 10	-13 \pm 2***	99 \pm 4
7	100 \pm 6	97 \pm 2	68 \pm 11*	95 \pm 7
8	100 \pm 2	96 \pm 2	109 \pm 5	102 \pm 5
9	100 \pm 8	89 \pm 9	24 \pm 1***	12 \pm 1***
10	100 \pm 12	91 \pm 9	40 \pm 6***	99 \pm 5
11	100 \pm 7	92 \pm 11	44 \pm 2***	99 \pm 7
12	100 \pm 16	76 \pm 10	80 \pm 6	107 \pm 8
13	100 \pm 10	131 \pm 18	118 \pm 11	111 \pm 12
14	100 \pm 28	83 \pm 20	64 \pm 37**	83 \pm 37
15	100 \pm 12	90 \pm 5	42 \pm 2***	101 \pm 7
16	100 \pm 9	68 \pm 3*	52 \pm 2***	94 \pm 6
17	100 \pm 8	76 \pm 11	43 \pm 8***	85 \pm 10
18	100 \pm 3	91 \pm 5	94 \pm 4	90 \pm 1
19	100 \pm 7	96 \pm 4	58 \pm 5***	96 \pm 7
20	100 \pm 3	88 \pm 2	31 \pm 1***	94 \pm 2

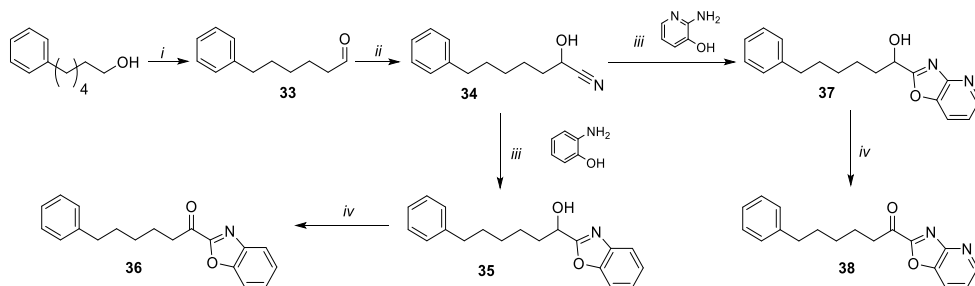
Means \pm SD, N=3, normalized to the intensity of the protein bands from the samples treated with vehicle. Values are corrected for protein loading per lane as determined with coomassie staining. Statistical analysis: 2-way ANOVA with Bonferroni's posttest (*** = $p < 0.001$; ** = $P < 0.01$; * = $p < 0.05$ vs vehicle).

Based on the activity and selectivity profile it was decided to test LEI104 in intact cells. LEI104 (20 μ M) or vehicle was incubated in intact SHSY5Y cells and stimulated with ionomycin (3 μ M), 2-AG levels were measured after 20 min.²⁶ The 2-AG levels were significantly lower (-46%) in treated cells versus control cells. This demonstrates that LEI104 is cell permeable and able to inhibit stimulus-induced 2-AG formation by DAGL- α in living cells. In conclusion, LEI104 represents a novel potent and selective chemotype for DAGL- α inhibition.

Preliminary structure-activity relationships of LEI104 with hDAGL- α were investigated using the colorimetric assay. Therefore we have synthesized a benzoxazole derivative of LEI104 and the reduced form of the α -keto-group following previously published synthetic procedures (Scheme 3).²⁷ 6-phenylhexan-1-ol was oxidized by a Swern oxidation to obtain aldehyde **33** in quantitative yield. Treatment of aldehyde **33** with potassium cyanide afforded 2-hydroxy-7-phenylheptanitrile. Treatment of **34** with acid in EtOH afforded the instable imide intermediate, which was directly coupled to 2-aminophenol or 2-amino-3-hydroxypyridine to obtain benzoxazole **35** or oxazolo-4N-pyridine **37** respectively. In the final step the alcohol was oxidized using Dess-Martin periodinane to obtain the final α -ketoheterocycles.

Replacement of the isoxazolepyridine heterocycle with a benzoxazole led to a 100-fold loss in activity, indicating that the pyridine nitrogen could form a potential important interaction

with the active site of the enzyme.²⁷ Reduction of the α -keto group to the alcohol abolished all activity, which was in line with the assumption that it functions as an electrophilic trap for the catalytic Ser472.



Scheme 4: i) DMSO, CH_2Cl_2 , oxalyl chloride, Et_3N , -78°C , 99% ii) $\text{THF}:\text{H}_2\text{O}$ (1:1), KCN, 64% iii) CHCl_3 , EtOH, acetyl chloride; EtOH, 2-amino-3-hydroxy-pyridine/2-aminophenol, reflux iv) Dess-Martin periodinane, CH_2Cl_2 .

A homology model of DAGL- α was developed to provide insight in the interaction of LEI104 with hDAGL- α at a molecular level (Figure 9). The model represented the typical α,β -hydrolase fold and had the catalytic triad (Ser472, His650 and Asp524) appropriately aligned in the binding cavity (Figure 9).

The tetrahedral transition state of LEI104, which is formed through the nucleophilic attack of Ser472 on the α -carbonyl was minimized and subjected to a short Molecular Dynamics refinement. According to the model, the oxyanion intermediate is stabilized by the backbone N-H of the residue adjacent to the catalytic serine, Leu473. In addition, both the side chain OH and backbone N-H of Thr400 are observed to make hydrogen bonds with the oxyanion. The oxazole nitrogen of LEI104 formed H-bond interactions with His650 and the pyridine nitrogen showed H-bond interactions with His471, which could further stabilize the transition state, while the hydrophobic pocket lined by aliphatic amino acids accommodated the flexible acyl chain of LEI104. This proposed binding mode is consistent with the observed structure-activity relationships. This model also provides a clear view on the opportunities to improve the potency and selectivity over FAAH. Since FAAH is the main enzyme responsible for degradation of the other endocannabinoid anandamide, its inhibition will lead to an upregulation of anandamide levels.

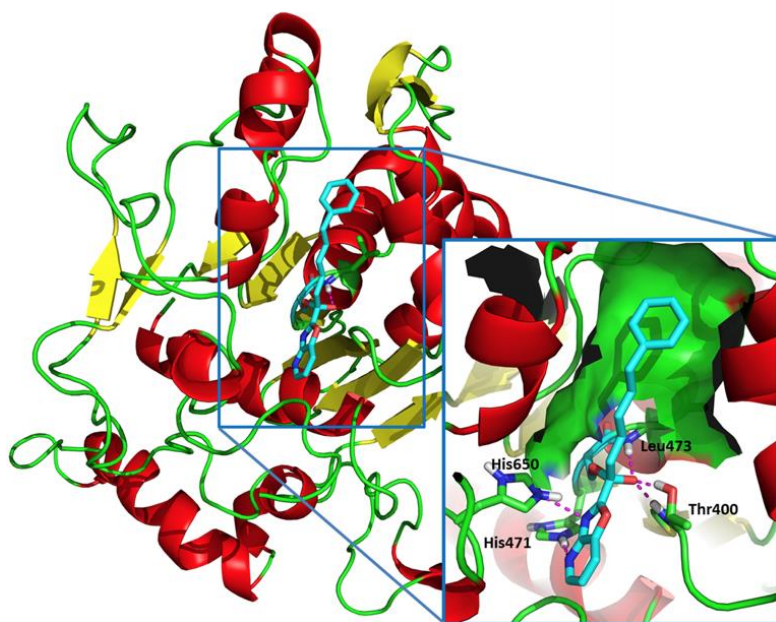


Figure 9. Binding pose of LEI-104 in a homology model of hDAGL- α .

Conclusions

The combination of a focused library screening approach with ABPP-based chemoproteomics led to the identification and profiling of a novel chemotype for DAGL- α inhibition. Using an existing drug (THL) for the generation of an activity-based probe, α -ketoheterocycle LEI104 was identified as a highly selective DAGL- α inhibitor. It is anticipated that the α -ketoheterocycle class provides an excellent lead series to dissect 2-AG and anandamide mediated cannabinoid CB1 signaling and for the development of *in vivo* active and selective DAGL- α inhibitors, because they a) have a clearly defined scaffold with excellent physico-chemical properties, b) are not based on the natural substrate and do not contain a known toxicophore (i.e. fluorophosphonate)²⁸; c) are plasma membrane permeable; d) are highly selective; e) are reversible inhibitors²⁹ that do not form covalent irreversible bonds, which could lead to problems with immunogenicity; and f) have shown to be bioavailable and active in animal models.^{15,24,30} Finally, MB064 and the α -ketoheterocycles, together with structural insights of the DAGL- α homology model, may serve as a basis for the development of new therapeutics, which can be used to study and treat diseases such as obesity and neurodegeneration. These studies are currently in progress.

Experimental Methods

Synthetic procedures

General remarks.

All reactions were performed using oven or flame-dried glassware and dry solvents. Reagents were purchased from Sigma Aldrich, Acros and Merck and used without further purification unless noted otherwise. All moisture sensitive reactions were performed under an argon atmosphere. Traces of water were removed from starting compounds by co-evaporation with toluene.

^1H - and ^{13}C -NMR spectra were recorded on a Bruker AV 400 MHz spectrometer at 400.2 (^1H) and 100.6 (^{13}C) MHz or a Bruker DMX-600 spectrometer 600 (^1H) and 150 (^{13}C) MHz using Chloroform- d or CD_3OD as solvent, unless stated otherwise. Chemical shift values are reported in ppm with tetramethylsilane or solvent resonance as the internal standard (Chloroform- d : δ 7.26 for ^1H , δ 77.0 for ^{13}C , CD_3OD : δ 3.31 for ^1H). Data are reported as follows: chemical shifts (δ), multiplicity (s = singlet, d = doublet, dd = double doublet, td = triple doublet, t = triplet, q = quartet, quint = quint, br = broad, m = multiplet), coupling constants J (Hz), and integration. HPLC purification was performed on a preparative LC-MS system (Agilent 1200 serie) with an Agilent 6130 Quadrupole MS detector. High-resolution mass spectra (HRMS) were recorded on a Thermo Scientific LTQ Orbitrap XL. IR spectra were recorded on a Shimadzu FTIR-8300 and are reported in cm^{-1} . Optical rotations were measured on a Propol automatic polarimeter (Sodium D-line, λ = 589 nm). Flash chromatography was performed using SiliCycle silica gel type SiliaFlash P60 (230 – 400 mesh). TLC analysis was performed on Merck silica gel 60/Kieselguhr F254, 0.25 mm. Compounds were visualized using either Seebach's reagent (a mixture of phosphomolybdic acid (25 g), cerium (IV) sulfate (7.5 g), H_2O (500 mL) and H_2SO_4 (25 mL)) or a KMnO_4 stain (K_2CO_3 (40 g), KMnO_4 (6 g), H_2O (600 mL) and 10% NaOH (5 mL)).

8-(trimethylsilyl)-oct-7-ynoic acid (2**):**³¹ Trimethylacetylene (6.5 mL, 46 mmol) was dissolved in THF (40 mL) and cooled to -78°C . $n\text{-BuLi}$ (1.6 M, 32 mL, 51 mmol) was added dropwise and the mixture was allowed to stir for 20 minutes. A solution of **1** (5.0 g, 25.6 mmol) in THF (150 mL) was slowly added before HMPA (50 mL) was introduced. After addition, stirring was continued for 3 h at -78°C for 3 h. The reaction was quenched with saturated NH_4Cl (aq.). Ether (300 mL) was added and the layers were separated, the organic layer was washed with brine and subsequently dried (Na_2SO_4). Volatiles were removed under reduced pressure and the residue was further purified by flash chromatography over silica gel using 4:1 n -pentane-EtOAc. This yielded **2** (6.6 g, 31.2 mmol, 82 %) as a colorless oil.

^1H NMR (400 MHz, Chloroform- d) δ 2.36 (t, J = 7.5 Hz, 2H), 2.23 (t, J = 7.0 Hz, 2H), 1.74 – 1.60 (m, 2H), 1.57 – 1.40 (m, 4H), 0.14 (s, 9H); ^{13}C NMR (101 MHz, Chloroform- d) δ

180.45, 107.26, 84.76, 34.08, 28.30, 28.26, 24.27, 19.78, 0.26. Spectroscopic data are in agreement with those reported in literature.³¹

S-pyridin-2-yl 8-(trimethylsilyl)-oct-7-ynethioate (3):³¹ Compound **2** (0.95 g, 4.5 mmol) was dissolved in DCM (12 mL) and cooled to 0 °C. Oxalyl chloride (0.85 g, 6.7 mmol) was added, and the mixture was stirred at rt for 2 h, before it was concentrated under reduced pressure. The residue was cooled to 0 °C and CH₂Cl₂ (12 mL) and Et₃N (1.25 mL, 9.0 mmol) were added, which resulted in an orange solution. Upon addition of mercaptopyridine (0.65 g, 5.8 mmol) the mixture turned deep blue. The reaction mixture was stirred for 2 h at rt before it was quenched with 1 M HCl (10 mL). The layers were separated, and the organic layer was washed with saturated NaHCO₃ (aq.) and dried (Na₂SO₄). The solvents were evaporated under reduced pressure and the residue was purified by flash chromatography over silica gel using 5:1 n-pentane-EtOAc. This yielded thiopyridyl ester **3** (1.17 g, 7.71 mmol, 86%) as a yellow oil. ¹H NMR (400 MHz, Chloroform-d) δ 8.61 (ddd, J = 4.8, 1.8, 0.8 Hz, 1H), 7.72 (td, J = 7.7, 1.9 Hz, 1H), 7.60 (dt, J = 7.9, 1.0 Hz, 1H), 7.27 (ddd, J = 7.5, 4.8, 1.1 Hz, 1H), 2.71 (t, J = 7.4 Hz, 2H), 2.22 (t, J = 6.9 Hz, 2H), 1.74 (p, J = 7.4 Hz, 2H), 1.61 – 1.41 (m, 4H), 0.14 (s, 9H); ¹³C NMR (101 MHz, CDCl₃) δ 196.14, 151.53, 150.29, 137.00, 130.01, 123.39, 107.00, 84.59, 43.95, 28.11, 27.96, 24.81, 19.58, 0.14. Spectroscopic data are in agreement with those reported in literature.³¹

(E)-2-(1-(tert-butyldimethylsilyloxy)-8-(trimethylsilyl)-oct-1-en-7-ynylthio)-pyridine (4):³¹ To a solution of thiopyridyl ester **3** (1.1 g, 3.7 mmol) in THF (10 mL) was added Et₃N (0.61 mL, 4.4 mmol) and DMF (0.34 mL, 4.4 mmol), the mixture was cooled to -78 °C. After 10 min, LiHMDS (1.0 M, 8.5 mL, 8.5 mmol) was added dropwise. The mixture was allowed to stir for 30 min before a dropwise addition of TBSCl (1.1 g, 7.35 mmol) in 5 mL THF. After stirring for 2 h at -78 °C the reaction was quenched with 4.5 mL pH 7.0 phosphate buffer (2x). The layers were separated and the aqueous layer was extracted with ether. The combined organic layers were dried (Na₂SO₄). Solvents were removed under reduced pressure and the residue was purified by flash chromatography over silica gel using 20:1 n-pentane-EtOAc. This yielded ketene acetal **4** (0.92 g, 2.2 mmol, 60%) as a yellow oil. ¹H NMR (400 MHz, Chloroform-d) δ 8.41 (ddd, J = 4.9, 1.8, 0.8 Hz, 1H), 7.60 – 7.50 (m, 1H), 7.32 (d, J = 8.1 Hz, 1H), 6.99 (ddd, J = 7.4, 4.9, 1.0 Hz, 1H), 5.40 (t, J = 7.3 Hz, 1H), 2.23 (dq, J = 14.4, 7.0 Hz, 4H), 1.64 – 1.48 (m, 4H), 0.88 (s, 9H), 0.15 (s, 9H), 0.08 (s, 6H); ¹³C NMR (101 MHz, CDCl₃) δ 160.40, 149.44, 139.76, 136.53, 123.41, 121.48, 119.68, 107.28, 84.54, 28.39, 28.35, 26.30, 25.73, 19.74, 18.14, 0.26, -4.32. Spectroscopic data are in agreement with those reported in literature.³¹

Dodecanal (6):³¹ 2 g of celite was added to a cooled (0 °C) a suspension of PCC (15 g, 70 mmol) in CH₂Cl₂ (100 mL). Dodecanol (8.7 g, 47 mmol) was added in one portion, and the

mixture was stirred at 0 °C for 2 h. The cooling was removed and the reaction was allowed to stir at rt overnight. Et₂O (100 mL) was added and the mixture was filtered over a pad of celite. The filtrate was concentrated under reduced pressure and the residue was purified by flash chromatography over silica gel using 30:1 n-pentane-EtOAc. This yielded **6** (7.0 g, 38 mmol, 81%) as a colorless oil. ¹H NMR (400 MHz, Chloroform-d) δ 9.76 (t, *J* = 1.9 Hz, 1H), 2.42 (td, *J* = 7.4, 1.9 Hz, 2H), 1.68 – 1.54 (m, 2H), 1.28 (br s, 16H), 0.96 – 0.80 (m, 3H); ¹³C NMR (101 MHz, CDCl₃) δ 203.13, 44.07, 32.05, 29.74 (2), 29.58, 29.51, 29.47, 29.32, 22.83, 22.25, 14.26. Spectroscopic data are in agreement with those reported in literature.³¹

4-Hydroxypentadec-1-ene (7):³¹ Dodecanal (**6**) was dissolved in THF (100 mL) and cooled to -25 °C. Allylmagnesiumbromide (1 M, 45.6 mL, 45.6 mmol) was added dropwise. The mixture was stirred for 2 h at -25 °C before it was quenched with saturated NH₄Cl (aq.). Et₂O (250 mL) and H₂O (50 mL) were added, and the layers were separated. The organic layer was washed with H₂O and brine, and dried (Na₂SO₄). Volatiles were removed under reduced pressure and the residue was purified by flash chromatography over silica gel using 30:1 n-pentane-EtOAc. This yielded allylic alcohol **7** (4.3 g, 18.84 mmol, 62 %) as a colorless oil. ¹H NMR (400 MHz, Chloroform-d) δ 5.90 – 5.75 (m, 1H), 5.15 (m, 1H), 5.11 (s, 1H), 3.67 – 3.60 (m, 1H), 2.34 – 2.25 (m, 1H), 2.14 (dt, *J* = 14.0, 7.8 Hz, 1H), 1.76 (s, 1H), 1.54 – 1.37 (m, 3H), 1.27 (d, *J* = 10.2 Hz, 17H), 0.88 (t, *J* = 6.7 Hz, 3H); ¹³C NMR (101 MHz, CDCl₃) δ 135.06, 118.03, 70.81, 42.06, 36.94, 32.04, 29.79 (3), 29.74 (2), 29.47, 25.80, 22.80, 14.22. Spectroscopic data are in agreement with those reported in literature.³¹

(4R)-4-[(2R)-Acetoxy-2-phenylacetoxy]pentadec-1-ene (8b):³¹ (R)-(-)-*O*-acetylmandelic acid (2.77 g, 14.3 mmol) and DMAP (0.83 g, 6.8 mmol) were dissolved in CH₂Cl₂ (40 mL) and cooled to 0 °C. A solution of allylic alcohol (**7**) (3.1 g, 13.6 mmol) dissolved in CH₂Cl₂ (20 mL) was added dropwise, followed by a solution of DCC (2.9 g, 14.3 mmol) in CH₂Cl₂ (30 mL). The mixture was stirred at 0 °C for 1 h, cooling was removed and the mixture was stirred at rt overnight. The white precipitate was removed by filtration, and the filtrate was concentrated under reduced pressure. The two diastereomers were separated by flash chromatography over silica gel using 1:10 n-pentane-toluene. This yielded 2.3 g, 5.6 mmol, 41% of (4*R*)-4-[(2*R*)-Acetoxy-2-phenylacetoxy]pentadec-1-ene (**8b**) and 2.4 g, 6.0 mmol, 44% as a mixture of two diastereomers as a colorless oil. ¹H NMR (400 MHz, Chloroform-d) δ 7.49 – 7.43 (m, 2H), 7.39 – 7.31 (m, 3H), 5.88 (s, 1H), 5.49 – 5.35 (m, 1H), 4.93 (ddd, *J* = 12.5, 7.0, 5.3 Hz, 1H), 4.84 – 4.71 (m, 2H), 2.26 – 2.08 (m, 5H), 1.57 (m, 2H), 1.25 (s, 18H), 0.88 (t, *J* = 6.8 Hz, 3H); ¹³C NMR (101 MHz, CDCl₃) δ 170.25, 168.56, 134.07, 132.94, 129.13, 128.66 (2), 127.72 (2), 117.72, 75.01, 74.80, 38.39, 33.61, 32.00, 29.72, 29.71, 29.62, 29.54, 29.45, 29.44, 25.17, 22.77, 20.75, 14.19. [α]_D = -

35.1 ($c = 2.3$, CHCl_3). Spectroscopic data are in agreement with those reported in literature.³¹

(R)-4-Hydroxypentadec-1-en (9):³¹ Compound **8b** (4.2 g, 10.3 mmol) was dissolved in methanol (70 mL), 2 M KOH (aq.) was added slowly and the mixture was heated to 75 °C and stirred overnight. Methanol was removed under reduced pressure before the aqueous solution was acidified with cold 1 M HCl. The solution was extracted with Et_2O , and the combined organic layers were washed with H_2O and brine before drying (Na_2SO_4). Volatiles were removed under reduced pressure and the residue was purified by flash chromatography over silica gel using 10:1 n-pentane-EtOAc. This yielded compound **9** (1.9 g, 8.4 mmol, 82%) as a colorless oil. ^1H NMR (400 MHz, Chloroform- d) δ 5.90 – 5.75 (m, 1H), 5.15 (br d, 1H), 5.11 (s, 1H), 3.67 – 3.60 (m, 1H), 2.34 – 2.25 (m, 1H), 2.14 (dt, $J = 14.0$, 7.8 Hz, 1H), 1.76 (s, 1H), 1.54 – 1.37 (m, 3H), 1.27 (d, $J = 10.2$ Hz, 17H), 0.88 (t, $J = 6.7$ Hz, 3H); ^{13}C NMR (101 MHz, CDCl_3) δ 135.06, 118.03, 70.81, 42.06, 36.94, 32.04, 29.79 (3), 29.74 (2), 29.47, 25.80, 22.80, 14.22. $[\alpha]_D = + 5.8$ ($c = 2.7$, CHCl_3). Spectroscopic data are in agreement with those reported in literature.³¹

(R)-tert-butyltrimethyl(pentadec-1-en-4-yloxy)silane (10):³¹ **9** (1.73 g, 7.7 mmol) and imidazole (0.66g, 9.6 mmol) were dissolved in DMF (4 mL). TBSCl (1.39 g, 9.2 mmol) dissolved in DMF (4 mL) was added, and the mixture was stirred at rt overnight. The reaction mixture was diluted with Et_2O (100 mL). The layers were separated and the organic layer was washed with H_2O and brine. The organic layer was dried (Na_2SO_4), and the solvent was removed under reduced pressure. The residue was further purified by flash chromatography over silica gel using n-pentane. This yielded compound **10** (2.51 g, 7.4 mmol, 96%) as a colorless oil. ^1H NMR (400 MHz, Chloroform- d) δ 5.81 (ddt, $J = 17.5$, 10.4, 7.2 Hz, 1H), 5.08 – 4.97 (m, 2H), 3.67 (q, $J = 5.8$ Hz, 1H), 2.28 – 2.13 (m, 2H), 1.50 – 1.18 (m, 20H), 0.89 (m, 12H), 0.04 (s, 6H); ^{13}C NMR (101 MHz, CDCl_3) δ 135.68, 116.65, 72.23, 42.14, 37.02, 32.12, 29.96, 29.86, 29.84 (2), 29.81, 29.55, 26.08 (3), 25.53, 22.88, 18.32, 14.29, -4.21, -4.35. Spectroscopic data are in agreement with those reported in literature.³¹

(R)-3-(tert-butyltrimethylsilyloxy)tetradecanal (11):³¹ **10** (0.5 g, 1.46 mmol) was dissolved in 1:1 MeOH- CH_2Cl_2 (70 mL). The solution was cooled to -78 °C and ozone was bubbled through the reaction mixture. When the reaction mixture was blue for ~5 min, the ozone flow was stopped. After an additional 15 minutes of stirring the flask was flushed with argon. Me_2S (3.5 mL) and Et_3N were added, the cooling was removed and the reaction was allowed to stir overnight. The volatiles were removed under reduced pressure, and the residue was further purified by flash chromatography over silica gel using 30:1 n-pentane-EtOAc. This yielded aldehyde **11** (0.5 g 1.46 mmol) quantitatively as a colorless oil. ^1H NMR (400 MHz, Chloroform- d) δ 9.81 (t, $J = 2.3$ Hz, 1H), 4.26 – 4.12 (m, 1H), 2.51 (dd, J

= 5.6, 2.3 Hz, 2H), 1.62 – 1.45 (m, 2H), 1.26 (s, 18H), 0.87 (m, 12H), 0.07 (d, $J = 7.0$ Hz, 6H); ^{13}C NMR (101 MHz, CDCl_3) δ 202.40, 68.39, 50.94, 37.97, 32.04, 29.76 (2), 29.72, 29.69 (2), 29.47, 25.88 (3), 25.25, 22.81, 18.09, 14.23, -4.32, -4.59. Spectroscopic data are in agreement with those reported in literature.³¹

(3S,4S)-4-((S)-2-hydroxytridecyl)-3-(6-(trimethylsilyl)hex-5-yn-1-yl)oxetan-2-one (12):³¹

ZnCl_2 (378 mg, 2.78 mmol) was fused under vacuum and allowed to cool to rt under argon before it was suspended in 8.0 mL CH_2Cl_2 . **4** (477 mg, 1.39 mmol) dissolved in CH_2Cl_2 (3 mL) and **11** (704 mg, 1.68 mmol) dissolved in CH_2Cl_2 (4 mL) were added and the suspension was stirred for 65 h at rt. pH 7 phosphate buffer (10 mL) was added, and the mixture was stirred for an additional 45 min. The layers were separated, and the aqueous layer was extracted with CH_2Cl_2 . The combined organic layers were filtered over celite and dried (Na_2SO_4). Volatiles were removed under reduced pressure and the residue was purified by flash chromatography over silica gel using 20:1 n-pentane-EtOAc. This yielded the β -lactone as an inseparable mixture of diastereomers (~10:1 anti/syn) with complete selectivity for the *trans*- β -lactone. Without further purification the mixture of diastereomers was dissolved in acetonitrile (35 mL) and cooled to 0 °C. 48 % HF (3.5 mL) was added drop wise and the mixture was stirred for 2 hours at 0 °C, followed by stirring at rt overnight. The reaction was quenched with saturated NaHCO_3 (aq.), the layers were separated and the organic layer was washed with brine and dried (Na_2SO_4). Volatiles were removed under reduced pressure and the residue was purified by flash chromatography over silica gel using 15:1 n-pentane-EtOAc. This yielded 264 mg, 0.63 mmol, 45% of β -lactone **12** as a colorless oil. ^1H NMR (400 MHz, Chloroform- d) δ 4.49 (dt, $J = 8.5, 4.4$ Hz, 1H), 3.79 (dtd, $J = 9.3, 6.2, 2.8$ Hz, 1H), 3.26 (td, $J = 7.6, 7.2, 4.0$ Hz, 1H), 2.22 (t, $J = 6.6$ Hz, 2H), 1.97 – 1.69 (m, 4H), 1.60 – 1.37 (m, 7H), 1.25 (s, 18H), 0.86 (t, $J = 6.8$ Hz, 3H), 0.13 (s, 9H); ^{13}C NMR (101 MHz, CDCl_3) δ 171.55, 106.86, 85.05, 75.79, 68.58, 56.51, 41.88, 38.25, 32.02, 29.74, 29.73, 29.67, 29.62, 29.45, 28.24, 27.35, 26.02, 25.49, 24.33, 22.79, 19.67, 14.23, 0.26 (3 C). Spectroscopic data are in agreement with those reported in literature.³¹

(3S,4S)-3-(hex-5-yn-1-yl)-4-((S)-2-hydroxytridecyl)oxetan-2-one (13):³¹ Compound **12** (75 mg, 0.18 mmol) was dissolved in 11 mL acetone/ H_2O /2,6-lutidine (1:1:0.1). AgNO_3 (800 mg, 4.7 mmol) was added and the mixture was stirred vigorously for 5 h. 8 mL 1 M KH_2PO_4 (aq.) was added and the yellow suspension was stirred for 30 min before extraction of the aqueous layer with CHCl_3 , the combined organic layers were washed with brine and dried (Na_2SO_4). Volatiles were removed under reduced pressure and the residue was purified by flash chromatography over silica gel using EtOAc followed by a column using 15:1 n-pentane-EtOAc. This yielded compound **13** (50 mg, 0.14 mmol, 79%) as a colorless oil. ^1H NMR (400 MHz, Chloroform- d) δ 4.50 (dt, $J = 8.6, 4.4$ Hz, 1H), 3.83 – 3.76 (m,

1H), 3.28 (td, $J = 7.6, 4.0$ Hz, 1H), 2.20 (td, $J = 6.6, 2.6$ Hz, 2H), 1.99 – 1.77 (m, 4H), 1.74 – 1.38 (m, 8H), 1.25 (s, 18H), 0.87 (t, $J = 6.8$ Hz, 3H); ^{13}C NMR (101 MHz, CDCl_3) δ 171.54, 75.80, 68.82, 68.60, 56.51, 41.87, 38.27, 32.02, 29.81, 29.79, 29.75, 29.73, 29.68, 29.62, 29.45, 28.07, 27.34, 25.94, 25.51, 22.80, 18.24, 14.23 Spectroscopic data are in agreement with those reported in literature.³¹

(S)-(S)-1-((2S,3S)-3-(hex-5-yn-1-yl)-4-oxooxetan-2-yl)tridecan-2-yl 2-formamido-4-methylpentanoate (14):³¹ Alcohol **13** (15 mg, 0.043 mmol), PPh_3 (39 mg, 0.15 mmol) and *N*-formyl-L-leucine (24 mg, 0.15 mmol) were azeotroped with toluene before they were dissolved in THF (1.5 mL). The solution was cooled to 0 °C and DIAD (30 mg, 0.15 mmol) in 0.2 mL THF was added. The mixture was stirred for 30 min at 0 °C and an additional 6 h at rt. The reaction mixture was filtered over a pad of silica before flash chromatography using 4:1 n-pentane-EtOAc. Subsequent HPLC purification yielded **14** (6.1 mg, 0.012 mmol, 30%) as a white solid. ^1H NMR (400 MHz, Chloroform-*d*) δ 8.22 (s, 1H), 5.90 (d, $J = 8.5$ Hz, 1H), 5.09 – 4.98 (m, 1H), 4.68 (td, $J = 8.7, 4.3$ Hz, 1H), 4.35 – 4.25 (m, 1H), 3.24 (td, $J = 7.6, 4.1$ Hz, 1H), 2.27 – 2.12 (m, 3H), 2.06 – 1.98 (m, 1H), 1.96 (t, $J = 2.6$ Hz, 1H), 1.88 – 1.58 (m, 8H), 1.56 – 1.46 (m, 3H), 1.25 (s, 18H), 1.00 – 0.94 (m, 6H), 0.88 (t, $J = 6.8$ Hz, 3H); ^{13}C NMR (101 MHz, CDCl_3) δ 172.06, 170.63, 160.76, 74.84, 72.83, 68.91, 57.00, 49.80, 41.66, 38.90, 34.25, 32.05, 29.76, 29.69, 29.58, 29.53, 29.49, 29.45, 29.40, 28.11, 27.25, 25.88, 25.25, 25.04, 23.03, 22.83, 21.89, 18.25, 14.28. $[\alpha]_{\text{D}} = -31.1$ ($c = 0.12$, CHCl_3); HRMS (ESI+) m/z : calculated for $\text{C}_{29}\text{H}_{49}\text{NO}_5$ ($m + \text{H}$) 492.368, found 492.368; ($m + \text{Na}$) calculated 514.350, found 514.350. Spectroscopic data are in agreement with those reported in literature.³¹

MB064 (15): 14 (5.0 mg, 0.010 mmol) and azido-bodipy acid (4.7 mg, 0.010 mmol) were dissolved in CH_2Cl_2 , sodium ascorbate (10 mg, 0.010 mmol) and CuSO_4 (1.5 mg, 0.002 mmol) in 1 mL H_2O were added, and the mixture was stirred vigorously for 4 h. Saturated NaHCO_3 (aq.) was added and the water layer was extracted with CH_2Cl_2 . The combined organic layers were washed with brine and dried (Na_2SO_4). The solvent was removed under reduced pressure and the residue was further purified by flash chromatography over silica gel using EtOAc with 1% acetic acid, subsequent HPLC purification yielded **15** (4.0 mg, 0.003 mmol, 31%) as a purple solid. ^1H NMR (600 MHz, Chloroform-*d*) δ 8.17 (s, 1H), 7.86 (d, $J = 8.8$ Hz, 2H), 7.30 (s, 1H), 7.10 (s, 1H), 6.98 – 6.89 (m, 3H), 6.53 (d, $J = 4.1$ Hz, 1H), 6.40 (d, $J = 8.4$ Hz, 1H), 5.03 – 4.95 (m, 1H), 4.66 (td, $J = 9.0, 4.9$ Hz, 1H), 4.56 (t, $J = 6.7$ Hz, 2H), 4.28 – 4.21 (m, 1H), 3.98 (t, $J = 5.7$ Hz, 2H), 3.21 (td, $J = 7.4, 4.0$ Hz, 1H), 2.77 – 2.67 (m, 4H), 2.57 – 2.48 (m, 5H), 2.41 (h, $J = 7.1, 6.4$ Hz, 2H), 2.22 (s, 3H), 2.14 (m, 1H), 2.00 – 1.92 (m, 1H), 1.87 – 1.50 (m, 11H), 1.27 – 1.22 (m, 18H), 0.94 (dd, $J = 6.3, 4.0$ Hz, 6H), 0.87 (t, $J = 7.0$ Hz, 3H); ^{13}C NMR (151 MHz, CDCl_3) δ 175.61, 172.04, 170.85, 161.26, 159.64, 159.34, 155.50, 147.65, 140.13, 135.14, 134.55, 130.96, 130.93, 130.91, 130.09, 128.12, 126.16, 123.18, 121.82, 118.47, 114.31, 74.79, 72.76, 64.04, 56.92,

49.86, 46.99, 41.44, 38.75, 34.24, 33.68, 32.06, 29.96, 29.78, 29.77, 29.71, 29.60, 29.50, 29.49, 29.10, 27.39, 26.16, 25.27, 25.20, 25.02, 23.06, 22.84, 21.80, 19.49, 14.28, 13.33, 9.82; HRMS (ESI+) m/z : calculated for $C_{52}H_{73}BF_2N_6O_8$ ($m + H$) 959.562, found 959.564; ($m + Na$) calculated 981.544, found 981.545.

MB108 (16). Biotin-Azide (7 mg, 0.019 mmol) and **14** (7 mg, 0.014 mmol), (synthesized as described previously)¹ were dissolved in DMF (1 mL). 44 μ L Sodium ascorbate (1 M in H_2O) and 50 μ L $CuSO_4$ (200 mM in H_2O) were added. The reaction mixture was sonicated in a sonic bath for 2 h at rt. The solvents were removed under reduced pressure and the residue was purified by flash chromatography over silica gel using $CH_2Cl_2/MeOH$ (90:10) as the eluent (3x). This yielded **16** (4.6 mg, 0.005 mmol, 38%) as a white solid. 1H NMR (850 MHz, MeOD) δ 8.11 (s, 1H), 7.74 (s, 1H), 5.06 – 5.00 (m, 1H), 4.51 – 4.46 (m, 2H), 4.36 (dd, $J = 14.8, 7.7$ Hz, 2H), 4.30 (dt, $J = 8.0, 4.1$ Hz, 1H), 3.39 (td, $J = 7.4, 4.1$ Hz, 1H), 3.24 – 3.10 (m, 5H), 2.95 – 2.88 (m, 2H), 2.77 – 2.67 (m, 3H), 2.23 – 2.13 (m, 4H), 2.09 – 2.01 (m, 1H), 1.95 – 1.87 (m, 2H), 1.83 – 1.76 (m, 2H), 1.76 – 1.57 (m, 12H), 1.50 (ddd, $J = 18.7, 14.7, 7.3$ Hz, 4H), 1.43 (ddd, $J = 19.5, 9.9, 6.7$ Hz, 4H), 1.39 – 1.19 (m, 20H), 0.98 (d, $J = 6.5$ Hz, 3H), 0.94 (d, $J = 6.5$ Hz, 3H), 0.90 (t, $J = 7.1$ Hz, 3H). ^{13}C NMR (214 MHz, MeOD) δ 175.96, 173.18, 172.98, 166.10, 163.65, 148.82, 123.20, 76.32, 73.65, 63.40, 61.63, 57.55, 57.03, 52.40, 51.29, 51.17, 41.46, 41.04, 40.24, 40.16, 39.61, 36.83, 35.29, 33.08, 30.76, 30.74, 30.65, 30.58, 30.47, 30.40, 30.21, 30.13, 29.79, 29.52, 28.32, 27.31, 27.14, 26.93, 26.14, 26.02, 25.92, 23.73, 23.25, 21.80, 14.43. HRMS (ESI+) m/z : calculated for $C_{45}H_{77}N_7O_7S$ ($M + H^+$) 860.5678; found 860.5683.

6-phenylhexanal (33): A solution of DMSO (0.75 g, 10 mmol) in CH_2Cl_2 was added drop-wise to a solution of oxalyl chloride (0.64 g, 5 mmol) in CH_2Cl_2 (5 mL) at $-78^\circ C$. The mixture was stirred for 1 h before 6-phenylhexan-1-ol (297 mg, 1.67 mmol) in CH_2Cl_2 (1 mL) was added drop-wise. After addition, the mixture was stirred overnight, and Et_3N (1.7 mL, 16 mmol) was added drop-wise. The mixture was allowed to warm to rt and washed with 1 M HCl. The aqueous layer was extracted with CH_2Cl_2 , and the combined organic layers were washed with brine and subsequently dried (Na_2SO_4). Volatiles were removed under reduced pressure and the residue was purified by flash chromatography over silica gel using 4:1 n-pentane-EtOAc. This yielded compound **33** (289 mg, 1.65 mmol, 99 %) as a colorless oil. 1H NMR (400 MHz, $CDCl_3$) δ 9.62 (t, $J = 1.6$ Hz, 1H), 7.05-7.17 (m, 5H), 2.51 (t, $J = 7.6$ Hz, 2H), 2.29 (dt, $J = 1.6, 7.6$ Hz, 2H), 1.50-1.56 (m, 4H), 1.24-1.28 (m, 2H); ^{13}C NMR (101 MHz, $CDCl_3$) δ 202.66, 142.38, 128.37, 128.23, 125.60, 43.79, 35.69, 31.21, 28.73, 21.89. Spectroscopic data are in agreement with those reported.³²

2-hydroxy-7-phenylheptanenitrile (34): To a solution of 6-phenylhexanal **33** (290 mg, 1.6 mmol) in (1:1) THF: H_2O (100 mL) was added potassium cyanide (1.2 g, 18 mmol). The reaction mixture was stirred at rt for 72 h. H_2O (10 mL) and Et_2O (10 mL) were added, and

the layers were separated. The aqueous layer was extracted with Et₂O and the combined organic layers were washed with saturated NaHCO₃ (aq.) and brine before drying (Na₂SO₄). Volatiles were removed under reduced pressure and the residue was purified by flash chromatography over silica gel using 5:1 n-pentane-EtOAc with 1 % Et₃N. This yielded compound **34** (213 mg, 1.0 mmol, 64 %) as a colorless oil. ¹H NMR (400 MHz, CDCl₃) δ 7.22-7.36 (m, 5H), 4.45 (dt, J = 6.0, 6.0 Hz, 1H), 3.71 (d, J = 4.8 Hz, 1H), 2.67 (t, J = 7.6 Hz, 2H), 1.85 (q, J = 8.4 Hz, 2H), 1.70 (quint, J = 7.6 Hz, 2H), 1.56 (quint, J = 7.2 Hz, 2H), 1.43 (quint, J = 7.2 Hz, 2H); ¹³C NMR (101 MHz, CDCl₃) δ 142.38, 128.40, 128.32, 125.74, 120.17, 61.07, 35.68, 34.90, 31.12, 28.47, 24.40.

1-(oxazolo[4,5-b]pyridin-2-yl)-6-phenylhexan-1-ol (37): A mixture of CHCl₃ (2 mL) and ethanol (2 mL) was cooled to 0°C before acetyl chloride (2 mL) was added dropwise. The mixture was stirred for 30 minutes, and 2-hydroxy-7-phenylheptanenitrile **34** (60 mg, 0.28 mmol) in CHCl₃ (2 mL) was added. The mixture was stirred for another 1.5 h and the solvent was removed under reduced pressure while keeping the temperature below 25 °C. The residue was taken up in ethanol (6.5 mL) ethoxyethanol (1 mL), 2-amino-3-hydroxypyridine (26 mg, 0.24 mmol) was added and the reaction mixture was heated to 130 °C for 6 h. The solvent was removed under reduced pressure, and the residue was dissolved in EtOAc (30 mL) and 1 M NaOH (10 mL) was added. The layers were separated, and the aqueous layer was extracted with EtOAc. The combined organic layers were washed with brine and dried (Na₂SO₄). Volatiles were removed under reduced pressure and the residue was further purified by flash chromatography over silica gel using 1:1 pentane-EtOAc with 1 % Et₃N. This yielded compound **37** (3.0 mg, 0.01 mmol, 3.5 %) as a yellow solid. ¹H NMR (400 MHz, CDCl₃) δ 8.57 (d, J = 3.7 Hz, 2H), 7.84 (d, J = 8.0 Hz, 2H), 7.73 – 7.22 (m, 3H), 7.18 – 7.14 (m, 2H), 5.00 (t, J = 6.2 Hz, 1H), 3.03 (bs, 1H), 2.60 (t, J = 7.7 Hz, 2H), 2.15 – 1.90 (m, 2H), 1.70 – 1.36 (m, 6H); ¹³C APT NMR (101 MHz, CDCl₃) δ 171.10, 154.90, 146.68, 142.55, 128.41, 128.28, 125.67, 124.81, 120.34, 118.67, 68.21, 35.81, 31.27, 29.73, 28.89, 24.72; Purity > 90 % as determined by LCMS; mass (M+H) = 297.07 m/z

1-(benzo[d]oxazol-2-yl)-6-phenylhexan-1-ol (35): A mixture of CHCl₃ (2.5 mL) and ethanol (2.5 mL) was cooled to 0°C before acetyl chloride (2.5 mL) was added dropwise. The mixture was stirred for 30 minutes, and 2-hydroxy-7-phenylheptanenitrile **34** (319 mg, 1.57 mmol) in CHCl₃ (2.5 mL) was added. The mixture was stirred for another 1.5 h and the solvent was removed under reduced pressure while keeping the temperature below 25 °C. The residue was taken up in ethanol (6.5 mL), and 2-aminophenol (170 mg, 1.56 mmol) was added. The mixture was refluxed for 6 h. Volatiles were removed under reduced pressure and the residue was purified by flash chromatography over silica gel using 1:1 n-pentane-EtOAc. This yielded compound **35** (263 mg, 0.89 mmol, 57 %) as a brown solid. ¹H NMR (400 MHz, CDCl₃) δ 7.71 (m, 1H), 7.28 (m, 1H), 7.34 (m, 2H), 7.29-7.23 (m,

2H), 7.19-7.13 (m, 3H), 4.96 (dd, $J = 5.2, 2.0$ Hz, 1H), 3.15 (bs, 1H), 2.59 (t, $J = 7.6$ Hz, 2H), 2.11 – 1.91 (m, 2H), 1.64 (quint, $J = 8.0$ Hz, 2H), 1.52 (quint, $J = 7.6$ Hz, 2H), 1.44 – 1.36 (m, 2H); ^{13}C APT NMR (101 MHz, CDCl_3) δ 167.95, 150.95, 142.70, 140.42, 128.52, 128.38, 125.77, 125.37, 124.73, 120.11, 110.95, 68.22, 35.94, 35.64, 31.38, 29.05, 24.90. HRMS (ESI+) m/z : calculated for $\text{C}_{19}\text{H}_{21}\text{NO}_2$ ($m + \text{H}$) 296.165, found 296.164.

1-(oxazolo[4,5-b]pyridin-2-yl)-6-phenylhexan-1-one (38):³³ Alcohol **37** (3.0 mg, 0.01 mmol) was dissolved in CH_2Cl_2 (2 mL), and Dess-Martin periodinane (6.8 mg, 0.016 mmol) was added. The mixture was stirred at rt overnight. Saturated NaHCO_3 (aq.) was added and the mixture was stirred for an additional 15 minutes. The layers were separated and the aqueous layer was extracted with CH_2Cl_2 . The combined organic layers were washed with brine, and dried (Na_2SO_4). Volatiles were removed under reduced pressure and the residue was further purified by preparative HPLC. This yielded compound **38** (1.3 mg, 4.4 μmol , 44 %) as a yellow solid. ^1H NMR (400 MHz, CDCl_3) δ 8.76 (dd, $J = 4.7, 1.1$ Hz, 1H), 8.00 (dd, $J = 8.3, 1.3$ Hz, 1H), 7.50 (dd, $J = 8.3, 4.8$ Hz, 1H), 7.31 – 7.24 (m, 2H), 7.22 – 7.12 (m, 3H), 3.28 (t, $J = 7.4$ Hz, 2H), 2.64 (t, $J = 7.7$ Hz, 2H), 1.82 (quint, $J = 7.6, 2\text{H}$), 1.70 (quint, $J = 8.0$ Hz, 2H), 1.51 – 1.41 (m, 2H); ^{13}C NMR (101 MHz, CDCl_3) δ 190.24, 158.48, 154.14, 148.70, 143.58, 142.33, 128.35, 128.24, 125.66, 123.11, 120.20, 39.71, 35.66, 31.09, 28.65, 23.64. Purity > 95 % as determined by LCMS; mass ($M + \text{H}$) = 295.07 m/z . Spectroscopic data are in agreement with those reported.³³

1-(benzo[d]oxazol-2-yl)-6-phenylhexan-1-one (36): Alcohol **35** (44 mg, 0.15 mmol) was dissolved in CH_2Cl_2 . Dess-Martin periodinane (96 mg, 0.23 mmol) was added, and the reaction mixture was stirred for 3.5 h. Volatiles were removed under reduced pressure, and the residue was purified by flash chromatography over silica gel using 9:1 n-pentane-EtOAc. This yielded compound **36** (43 mg, 0.15 mmol, 98 %) as a white solid. ^1H NMR (400 MHz, Chloroform- d) δ 7.89 (d, $J = 8.0$ Hz, 1H), 7.65 (d, $J = 8.2$ Hz, 1H), 7.53 (t, $J = 7.7$ Hz, 1H), 7.46 (t, $J = 7.7$ Hz, 1H), 7.31 – 7.22 (m, 3H), 7.18 (d, $J = 6.9$ Hz, 3H), 3.22 (t, $J = 7.4$ Hz, 3H), 2.68 – 2.57 (m, 2H), 1.85 (p, $J = 7.5$ Hz, 2H), 1.76 – 1.62 (m, 2H), 1.48 (h, $J = 7.2, 6.5$ Hz, 2H); ^{13}C APT NMR (101 MHz, CDCl_3) δ 190.37, 157.25, 150.83, 142.54, 140.62, 128.61, 128.51, 128.39, 125.86, 125.80, 122.3, 112.07, 39.58, 35.84, 31.30, 28.83, 23.81. HRMS (ESI+) m/z : calculated for $\text{C}_{19}\text{H}_{19}\text{NO}_2$ ($m + \text{H}$) 294.149, found 294.149.

Biochemical methods

Preparation of the different constructs. Full length human cDNA was purchased from Biosource and cloned into mammalian expression vector pcDNA3.1, containing genes for ampicillin and neomycin resistance. hDAGL- α and a truncated version of hDAGL- α , containing only the first 687 amino acids were cloned into pcDNA3.1. For the proteins having a FLAG-tag, a FLAG-linker was made from primers and cloned into the vector at the C-terminus of hDAGL- α and the truncated version of hDAGL- α . Two step PCR

mutagenesis was performed to substitute the active site serine for an alanine in the hDAGL- α -FLAG, to obtain hDAGL- α -S472A-FLAG. All plasmids were grown in XL-10 Z-competent cells and prepped (Maxi Prep, Qiagen). The sequences were confirmed by sequence analysis at the Leiden Genome Technology Centre.

Cell culture and membrane preparation. HEK293T cells were grown in DMEM with stable glutamine and phenolred (PAA) with 10% New Born Calf serum, penicillin and streptomycin. Cells were passaged every 2-3 days by resuspending in medium and seeding them to appropriate confluence. Membranes were prepared from transiently transfected HEK293T cells. One day prior to transfection 10^7 cells were seeded in a 15 cm petri dish. Cells were transfected by the addition of a 3:1 mixture of polyethyleneimine (60 μ g) and plasmid DNA (20 μ g) in 2 mL serum free medium. The medium was refreshed after 24 hours, and after 72 h the cells were harvested by suspending them in 20 mL medium. The suspension was centrifuged for 10 min at 1000 rpm, and the supernatant was removed. The cell pellet was stored at -80 °C until use.

Cell pellets were thawed on ice and suspended in lysis buffer A (20 mM Hepes, 2 mM DTT, 0.25 M sucrose, 1 mM MgCl₂, 1x Cocktail (Roche cOmplete EDTA free), 25U/ μ L Benzonase). The suspension was homogenized by polytrone (3 \times 7 sec) and incubated for 30 min on ice. The suspension was subjected to ultracentrifugation (93.000 \times g, 30 min, 4 °C, Beckman Coulter, Type Ti70 rotor) to yield the cytosolic fraction in the supernatant and the membrane fraction as a pellet. The pellet was resuspended in lysis buffer B (20 mM Hepes, 2 mM DTT, 1x Cocktail (Roche cOmplete EDTA free)). The protein concentration was determined with Quick Start Bradford assay (Biorad). The protein fractions were diluted to a total protein concentration of 1 mg/mL and stored in small aliquots at -80 °C until use.

Biochemical DAGL activity assay. The biochemical hDAGL- α activity assay is based on the hydrolysis of para-nitrophenylbutyrate (PNP-butyrate) (Figure S1A-D) by membrane preparations from HEK293T cells transiently transfected with hDAGL- α . 200 μ L reactions were performed in flat bottom Greiner 96-wells plates in a 50 mM pH 7.2 Hepes buffer.. Membrane protein fractions from HEK293T cells transiently transfected with hDAGL- α (0.05 μ g/ μ L final concentration) were used as hDAGL- α source. Inhibitors were introduced in 5 μ L DMSO. The mixtures were incubated for 20-30 minutes before 5.0 μ L 12 mM PNP-butyrate (final concentration 0.3 mM) in DMSO was added (final DMSO concentration 5.0%). Kinetics were followed immediately after addition of PNP-butyrate on a plate reader (TECAN GENios microplate reader), by measuring the OD₄₂₀ every 60 seconds, for 20 minutes at 37°C. The slope of the linear region from 5-15 minutes was determined, and all experiments were performed at N=2, n=2 for experimental measurements and N=2, n=4 for controls.

Data analysis: Z' -factor of each plate was determined for the validation of each experiment, using the following formula $Z' = 1 - 3(\sigma_{pc} + \sigma_{nc}) / (\mu_{pc} - \mu_{nc})$. The slope from 5-15 minutes of the positive control (pc: DAGL DMSO), and the negative control (nc: mock DMSO) was used. Plates were accepted for further analysis when $Z' > 0.6$. Kinetic measurements were corrected for the average absorption of the negative control (mock DMSO). The slope of the linear region from 5-15 minutes was determined. The average, standard deviation (SD) and standard error of mean (SEM) were calculated and normalized to the corrected positive control. Data was exported to Graphpad Prism 5.0 for the calculation of the IC₅₀ using a non-linear dose-response analysis.

Profiling LEI104 activity in intact SHSY5Y cells. This experiment was performed as described previously.²⁶

Preparation of mouse brain membrane proteome. Mouse brains were isolated according to guidelines approved by the ethical committee of Leiden University (DEC#10095). Mouse brains were thawed on ice and homogenized by polytrone (3 × 5 sec.) in pH 7.2 lysis buffer A (20 mM Hepes, 2 mM DTT, 0.25 M sucrose, 1 mM MgCl₂, 25 u/mL Benzonase) and incubated for 15 minutes on ice, followed by low speed spin (2500 × g, 3 min. at 4 °C) to remove debris. The supernatant was subjected to ultracentrifugation (100.000 × g, 45 min. 4 °C, Beckman Coulter, Type Ti70 rotor) to yield the cytosolic fraction in the supernatant and the membrane fraction as a pellet. The pellet was resuspended in lysis buffer B (20 mM Hepes, 2 mM DTT). The total protein concentration was determined with Quick Start Bradford assay (Biorad). Membranes and supernatant were stored in small aliquots at -80 °C until use.

Preparation of mouse kidney, heart, testes, liver and lung membrane proteome. Mouse organs were isolated according to guidelines approved by the ethical committee of Leiden University (DEC#10095). The organs were thawed on ice and Dounce-homogenized in pH 7.2 lysis buffer A (20 mM Hepes, 2 mM DTT, 1 mM MgCl₂, 25 u/mL Benzonase) and incubated for 15 minutes on ice, followed by low speed spin (2500 × g, 1 min, 4 °C) to remove debris. The supernatant was subjected to ultracentrifugation (100.000 × g, 45 min. at 4 °C, Beckman Coulter, Type Ti70 rotor) to yield the cytosolic fraction in the supernatant and the membrane fraction as a pellet. The pellet was resuspended in lysis buffer B (20 mM Hepes, 2 mM DTT). The total protein concentration was determined with Quick Start Bradford assay (Biorad). Membranes and supernatant were stored in small aliquots at -80 °C until use.

Activity based protein profiling. For gel based ABPP experiments, transiently transfected HEK293T cell membrane fractions (2 mg/mL, 20 µL) or mouse brain proteome (2.5 mg/mL, 20 µL) were preincubated for 30 min with vehicle (DMSO) or inhibitor in 0.5 µL

DMSO at rt. And subsequently treated with 250 nM (final concentration) ABP MB064 or 500 nM (final concentration) TAMRA-FP (TAMRA-FP was bought at Thermo Fischer) for 15 minutes at rt. The reactions were quenched with 10 μ L standard 3 \times SDS PAGE sample buffer. The samples were directly loaded and resolved on SDS PAGE gel (10 % acrylamide). The gels were scanned with a Typhoon Variable Mode Imager (Amersham Biosciences) using Cy3/TAMRA settings (excitation wavelength 532 nm, emission wavelength 580 nm) and analyzed using (ImageJ).

DAGL- α screen of mouse organs. Mouse organ membrane proteome (2 μ g/ μ L) was incubated with MB064 (250 nM) for 10 minutes. The samples were quenched with standard 3 \times SDS PAGE sample buffer. The samples were directly loaded and resolved on SDS PAGE gel (10% acrylamide). The gels were scanned with a Typhoon Variable Mode Imager (Amersham Biosciences) using Cy3/TAMRA settings (excitation wavelength 532 nm, emission wavelength 580 nm) and analyzed using (ImageJ). A cutout of the gel at the molecular weight of DAGL- α is depicted in Figure.

Western BLOT. Proteins were transferred from gel to a membrane using a Trans-Blot[®] Turbo (BioRad). FLAG-tagged enzymes were stained using rabbit anti-FLAG as primary antibody, and goat-anti-rabbit HRP as secondary antibody. The blot was developed in the dark using a 10 mL luminal solution, 100 μ L ECL enhancer and 3 μ L H₂O₂. Chemiluminescence was visualized using a ChemiDoc XRS (BioRad).

ABPP activity measurements. IC₅₀ determination of inhibitors against endogenously expressed DAGL- α in the mouse brain membrane proteome. Inhibitors were incubated at the indicated concentrations (total volume 20 μ L) for 30 min at rt, prior to incubation with MB064 for 10 min at rt. The reaction was quenched with 10 μ L standard 3 \times SDS PAGE sample buffer, and resolved on 10 % SDS-PAGE. The gels were scanned with a Typhoon Variable Mode Imager (Amersham Biosciences) using Cy3/TAMRA settings (excitation wavelength 532 nm, emission wavelength 580 nm) and analyzed using (ImageJ). The percentage activity remaining was determined by measuring the integrated optical intensity of the bands using ImageJ software. IC₅₀ values were determined from a dose-response curve generated using Prism software (GraphPad).

Quantification of protein bands for the determination of off-target activity of THL, LEI-103 and LEI-104. The percentage activity remaining was determined by measuring the integrated optical intensity of the bands using ImageJ software. This activity was corrected for the total protein loading per lane as determined by coomassie stain and imaging with a Biorad GS800 densitometer, followed by determination of the integrated optical intensity per lane by using ImageJ software. The intensity of the protein bands from the protein samples treated with vehicle was set to 100%. The results are depicted in Table

S5 and S6 and the corresponding numbering of the protein bands is depicted in Figure S9 and S10.

Proteomics

Pulldown with MB108. Mouse brain membrane proteome (150 μ L, 2.5 mg/mL in pH 7.2 HEPES buffer) was incubated with vehicle (DMSO) or THL (20 μ M) for 30 minutes at rt. THL was used to differentiate between specific interactions with the ABP and background proteins. Followed by incubation with biotin probe MB108 (10 μ M) for 30 minutes at rt. The samples were denaturated with a 10% (wt/vol) SDS solution to a final SDS concentration of 2 %, followed by chloroform/methanol precipitation as described previously.³⁴ The cell pellet was dried for 5 minutes and dissolved in 25 μ L 2% (wt/vol) SDS to a clear solution. The sample was diluted stepwise with pH 7.2 HEPES/ 50 mM NaCl to a final SDS concentration of 0.05% (wt/vol). Streptavidin magnetic beads 1.0 mg (prewashed 3 times with pH 7.2 HEPES/ 50 mM NaCl buffer) were added. The proteins were incubated for 3 h at 4.0 °C while shaking. The beads were washed with 4 M urea, 0.1% (wt/vol) SDS (2x), 150 mM NaCl (2x), 50 mM NaCl (2x) and pH 7.2 HEPES (2x). Followed by overnight on bead digest with sequencing grade trypsin (promega) in 100 μ L Pd buffer (100 mM Tris, 100 mM NaCl, 1 mM CaCl_2 , 2 % ACN and 250 ng trypsin) at 37 °C with vigorous shaking. The pH was adjusted with formic acid to pH 3, followed by desalting and sample preparation as described previously.³⁴

Reduction and alkylation of the cysteines was not performed and the following variable modifications were used for the database search: Acetyl (N-term), Deamidated (NQ), Gln->pyro-Glu (N-term Q), Glu->pyro-Glu (N-term E), Oxidation (M).

Tryptic peptides were analyzed on a Surveyor nanoLC system (Thermo) hyphenated to a LTQ-Orbitrap mass spectrometer (Thermo). Gold and carbon coated emitters (OD/ID = 360/25 mm tip ID = 5 μ m), trap column (OD/ID = 360/ 100 μ m packed with 25 mm robust Poros10R2/ 15 mm BioSphere C18 5 μ m 120 Å) and analytical columns (OD/ID = 360/75 μ m packed with 20 cm BioSphere C18 5 mm 120 Å) were from Nanoseparations (Nieuwkoop, The Netherlands). The mobile phases (A: 0.1% FA/H₂O, B: 0.1% FA/ACN) were made with ULC/MS grade solvents (Biosolve). The emitter tip was coupled end-to-end with the analytical column via a 15 mm long TFE Teflon tubing sleeve (OD/ID 0.3 3 1.58 mm, Supelco, USA) and installed in a stainless steel holder mounted in a nano-source base (Upchurch scientific, IDEX, USA). General mass spectrometric conditions were as follows: an electrospray voltage of 1.8 kV was applied to the emitter, no sheath and auxiliary gas flow, ion transfer tube temperature 150 °C, capillary voltage 41 V, tube lens voltage 150 V. Internal mass calibration was performed with air-borne protonated polydimethylcyclsiloxane (m/z = 445.12002) and the plasticizer protonated dioctyl phthalate ions (m/z = 391.28429) as lock mass. For shotgun proteomics analysis, 10 μ l of the samples was pressure loaded on the trap column with a 10 μ l/min flow for 5 min

followed by peptide separation with a gradient of 35 min 5%–30% B, 15 min 30%–60% B, 5 min A at a flow of 300 ml/min split to 250 nl/min by the LTQ divert valve. For each data-dependent cycle, one full MS scan (300–2000 m/z) acquired at high mass resolution (60,000 at 400 m/z, AGC target 1×10^6 , maximum injection time 1000 ms) in the Orbitrap was followed by three MS/MS fragmentations in the LTQ linear ion trap (AGC target 5×10^3 , maximum injection time 120 ms) from the three most abundant ions. MS2 settings were as follows: collision gas pressure 1.3 mT, normalized collision energy 35%, ion selection threshold of 500 counts, activation $q = 0.25$ and activation time of 30 ms. Fragmented precursor ions that were measured twice within 10 s were dynamically excluded for 60 s and ions with $z < 2$ or unassigned were not analyzed.

After LC-MS analysis, peak lists were extracted from the .raw files using the DTA supercharge software. The peak lists were searched against a recent mouse protein database (niprot reference mouse_proteome_2013_06) using the Mascot software (Matrix science) and the mouse decoy database. To ensure statistic reliability of the results, protein hits presented show a false discovery rate (%FDR) lower than 1% and a mascot peptide score >40. In addition, we validated the results in a separate experiment in which a pre-incubation of THL with mouse brain homogenate was performed, followed by the pull down. The proteins, which were identified in this control experiment were considered as a-selective binders and were not listed in Table 1. All experiments were performed in duplicate.

References

1. Bisogno, T.; Howell, F.; Williams, G.; Minassi, A.; Cascio, M. G.; Ligresti, A.; Matias, I.; Schiano-Moriello, A.; Paul, P.; Williams, E. J.; Gangadharan, U.; Hobbs, C.; Di Marzo, V.; Doherty, P. *J. Cell. Biol.* **2003**, *163*, 463.
2. Reisenberg, M.; Singh, P. K.; Williams, G.; Doherty, P. *Philos. Trans. R. Soc. Lond. B. Biol. Sci.* **2012**, *367*, 3264.
3. Katona, I.; Freund, T. F. *Annu. Rev. Neurosci.* **2012**.
4. Di Marzo, V. *Nat. Neurosci.* **2011**, *14*, 9.
5. Nomura, D. K.; Morrison, B. E.; Blankman, J. L.; Long, J. Z.; Kinsey, S. G.; Marcondes, M. C.; Ward, A. M.; Hahn, Y. K.; Lichtman, A. H.; Conti, B.; Cravatt, B. F. *Science* **2011**, *334*, 809.
6. Bisogno, T.; Burston, J. J.; Rai, R.; Allara, M.; Saha, B.; Mahadevan, A.; Razdan, R. K.; Wiley, J. L.; Di Marzo, V. *ChemMedChem* **2009**, *4*, 946.
7. Bisogno, T.; Cascio, M. G.; Saha, B.; Mahadevan, A.; Urbani, P.; Minassi, A.; Appendino, G.; Saturnino, C.; Martin, B.; Razdan, R.; Di Marzo, V. *Biochim. Biophys. Acta.* **2006**, *1761*, 205.
8. Johnston, M.; Bhatt, S. R.; Sikka, S.; Mercier, R. W.; West, J. M.; Makriyannis, A.; Gatley, S. J.; Duclos, R. I., Jr. *Bioorg. Med. Chem. Lett.* **2012**, *22*, 4585.
9. Ortar, G.; Bisogno, T.; Ligresti, A.; Morera, E.; Nalli, M.; Di Marzo, V. *J. Med. Chem.* **2008**, *51*, 6970.
10. Hsu, K. L.; Tsuboi, K.; Adibekian, A.; Pugh, H.; Masuda, K.; Cravatt, B. F. *Nat. Chem. Biol.* **2012**, *8*, 999.
11. Marrs, W. R.; Blankman, J. L.; Horne, E. A.; Thomazeau, A.; Lin, Y. H.; Coy, J.; Bodor, A. L.; Muccioli, G. G.; Hu, S. S.; Woodruff, G.; Fung, S.; Lafourcade, M.; Alexander, J. P.; Long, J. Z.; Li, W.; Xu, C.; Moller, T.; Mackie, K.; Manzoni, O. J.; Cravatt, B. F.; Stella, N. *Nat. neurosci.* **2010**, *13*, 951.
12. Bisogno, T.; Mahadevan, A.; Coccurello, R.; Chang, J. W.; Allara, M.; Chen, Y.; Giacobuzzo, G.; Lichtman, A.; Cravatt, B.; Moles, A.; Di Marzo, V. *Br. J. Pharmacol.* **2013**, *169*, 784.
13. Moellering, R. E.; Cravatt, B. F. *Chem. Biol.* **2012**, *19*, 11.
14. Long, J. Z.; Cravatt, B. F. *Chem. Rev.* **2011**, *111*, 6022.
15. Hoover, H. S.; Blankman, J. L.; Niessen, S.; Cravatt, B. F. *Bioorg. Med. Chem. Lett.* **2008**, *18*, 5838.
16. Rusch, M.; Zimmermann, T. J.; Burger, M.; Dekker, F. J.; Gormer, K.; Triola, G.; Brockmeyer, A.; Janning, P.; Bottcher, T.; Sieber, S. A.; Vetter, I. R.; Hedberg, C.; Waldmann, H. *Angew. Chem. Int. Ed.* **2011**, *50*, 9838.
17. Hedberg, C.; Dekker, F. J.; Rusch, M.; Renner, S.; Wetzels, S.; Vartak, N.; Gerding-Reimers, C.; Bon, R. S.; Bastiaens, P. I.; Waldmann, H. *Angew. Chem. Int. Ed.* **2011**, *50*, 9832.

18. Dekker, F. J.; Rocks, O.; Vartak, N.; Menninger, S.; Hedberg, C.; Balamurugan, R.; Wetzel, S.; Renner, S.; Gerauer, M.; Scholermann, B.; Rusch, M.; Kramer, J. W.; Rauh, D.; Coates, G. W.; Brunsveld, L.; Bastiaens, P. I.; Waldmann, H. *Nat. Chem. Biol.* **2010**, *6*, 449.
19. Bottcher, T.; Sieber, S. A. *Angew. Chem. Int. Ed.* **2008**, *47*, 4600.
20. Wang, Z.; Gu, C.; Colby, T.; Shindo, T.; Balamurugan, R.; Waldmann, H.; Kaiser, M.; van der Hoorn, R. A. *Nat. Chem. Biol.* **2008**, *4*, 557.
21. Yang, P. Y.; Liu, K.; Ngai, M. H.; Lear, M. J.; Wenk, M. R.; Yao, S. Q. *J. Am. Chem. Soc.* **2010**, *132*, 656.
22. Verdoes, M.; Florea, B. I.; Hillaert, U.; Willems, L. I.; van der Linden, W. A.; Sae-Heng, M.; Filippov, D. V.; Kisselev, A. F.; van der Marel, G. A.; Overkleeft, H. S. *Chembiochem* **2008**, *9*, 1735.
23. Pedicord, D. L.; Flynn, M. J.; Fanslau, C.; Miranda, M.; Hunihan, L.; Robertson, B. J.; Pearce, B. C.; Yu, X. C.; Westphal, R. S.; Blat, Y. *Biochem. Biophys. Res. Commun.* **2011**, *411*, 809.
24. Leung, D.; Hardouin, C.; Boger, D. L.; Cravatt, B. F. *Nat. Biotechnol.* **2003**, *21*, 687.
25. Pedicord, D. L.; Flynn, M. J.; Fanslau, C.; Miranda, M.; Hunihan, L.; Robertson, B. J.; Pearce, B. C.; Yu, X. C.; Westphal, R. S.; Blat, Y. *Biochem. Biophys. Res. Commun.* **2011**, *411*, 809.
26. Bisogno, T.; Howell, F.; Williams, G.; Minassi, A.; Cascio, M. G.; Ligresti, A.; Matias, I.; Schiano-Moriello, A.; Paul, P.; Williams, E. J.; Gangadharan, U.; Hobbs, C.; Di Marzo, V.; Doherty, P. *J. Cell Biol.* **2003**, *163*, 463.
27. Boger, D. L.; Sato, H.; Lerner, A. E.; Hedrick, M. P.; Fecik, R. A.; Miyauchi, H.; Wilkie, G. D.; Austin, B. J.; Patricelli, M. P.; Cravatt, B. F. *Proc. Natl. Acad. Sci. U. S. A.* **2000**, *97*, 5044.
28. Bisogno, T.; Mahadevan, A.; Coccurello, R.; Chang, J. W.; Allara, M.; Chen, Y. G.; Giacomazzo, G.; Lichtman, A.; Cravatt, B.; Moles, A.; Di Marzo, V. *Br. J. Pharmacol.* **2013**, *169*, 784.
29. Lichtman, A. H.; Leung, D.; Shelton, C. C.; Saghatelian, A.; Hardouin, C.; Boger, D. L.; Cravatt, B. F. *J. Pharmacol. Exp. Ther.* **2004**, *311*, 441.
30. Boger, D. L.; Miyauchi, H.; Hedrick, M. P. *Bioorg. Med. Chem. Lett.* **2001**, *11*, 1517.
31. Yang, P. Y.; Liu, K.; Ngai, M. H.; Lear, M. J.; Wenk, M. R.; Yao, S. Q. *J. Am. Chem. Soc.* **2010**, *132*, 656.
32. Murphy, J. A.; Schoenebeck, F.; Findlay, N. J.; Thomson, D. W.; Zhou, S. Z.; Garnier, J. *J. Am. Chem. Soc.* **2009**, *131*, 6475.
33. Boger, D. L.; Sato, H.; Lerner, A. E.; Hedrick, M. P.; Fecik, R. A.; Miyauchi, H.; Wilkie, G. D.; Austin, B. J.; Patricelli, M. P.; Cravatt, B. F. *Proc. Natl. Acad. Sci. U. S. A.* **2000**, *97*, 5044.

34. Li, N.; Kuo, C. L.; Paniagua, G.; van den Elst, H.; Verdoes, M.; Willems, L. I.; van der Linden, W. A.; Ruben, M.; van Genderen, E.; Gubbens, J.; van Wezel, G. P.; Overkleeft, H. S.; Florea, B. I. *Nat. Protoc.* **2013**, 8, 1155.

CHAPTER 4

A highly Selective, Reversible Inhibitor Identified by Comparative Chemoproteomics Modulates Diacylglycerol Lipase Activity in Neurons*

Introduction

Endocannabinoids are endogenous signaling lipids that activate the cannabinoid CB₁ and CB₂ receptor. They play an essential role in human health and disease, regulating processes, such as immunomodulation, energy balance and neurotransmission.¹ There are two main endocannabinoids: anandamide and 2-arachidonoylglycerol (2-AG).²⁻⁴ Both endocannabinoids are often found together, but their levels vary between species, tissue type, developmental stage and pathological condition.⁵ Although selective inhibitors of their metabolic pathways have provided information about the biological function of the endocannabinoids, it is still unclear to a large extent which endocannabinoid is responsible for specific cannabinoid CB₁ receptor dependent (patho)physiological effects.^{6,7} Selective inhibition of the formation of anandamide and 2-AG would be instrumental to determine which endocannabinoid is responsible for specific CB₁-mediated physiological effects. However, pathway-selective inhibitors for 2-AG and anandamide biosynthesis are currently lacking.

2-AG is mainly formed by the action of two diacylglycerol lipases (DAGL- α and DAGL- β).⁸ DAGLs are intracellular, multi-domain integral membrane proteins. The DAGLs share extensive homology, but differ in size: ~120 and ~70 kDa for DAGL- α and DAGL- β respectively.^{8,9}

*Baggelaar, M. P.; Chameau, P. J.; Kantae, V.; Hummel, J.; Hsu, K. L.; Janssen, F. J.; van der Wel, T.; Soethoudt, M.; Deng, H.; den Dulk, H.; Allarà, M.; Florea, B. I.; Di Marzo, V.; Wadman, W. J.; Kruse, C. G.; Overkleeft, H. S.; Hankemeier, T.; Werkman, T. R.; Cravatt, B. F.; van der Stelt, M.; Highly Selective, Reversible Inhibitor Identified by Comparative Chemoproteomics Modulates Diacylglycerol Lipase Activity in Neurons. *J. Am. Chem. Soc.* **2015**, *137*, 8851–8857

DAGLs belong to the class of serine hydrolases that employ the typical Ser-His-Asp catalytic triad to hydrolyze the ester bond of acyl chains from arachidonate-containing diacylglycerols in a *sn*-1 specific manner. Studies with DAGL knock-out mice have shown that DAGL- α controls to a large extent the formation of 2-AG in the central nervous system, whereas DAGL- β appears to partake in 2-AG production in the periphery during inflammation.^{5,10} Importantly, also basal anandamide levels were reduced in DAGL- α knock-out mice. Selective inhibitors for DAGLs, which can be used in an acute and temporal fashion and do not modulate anandamide levels, would, therefore, constitute an important counterpart of the DAGL knock-out mice, and allow the examination of acute versus congenital inhibition.

Although, several classes of DAGL inhibitors have been described in literature,^{8,11-15} these inhibitors are based on the natural substrates and/or have reactive chemical warheads, and are not selective over other serine hydrolases that modulate endocannabinoid signaling (e.g. α , β -hydrolase domain-containing protein 6 and 12 (ABHD6 and ABHD12), monoacylglycerol lipase (MAGL) or fatty acid amide hydrolase (FAAH)). Therefore highly selective DAGL inhibitors are needed to study the cellular role of the biosynthetic enzymes.

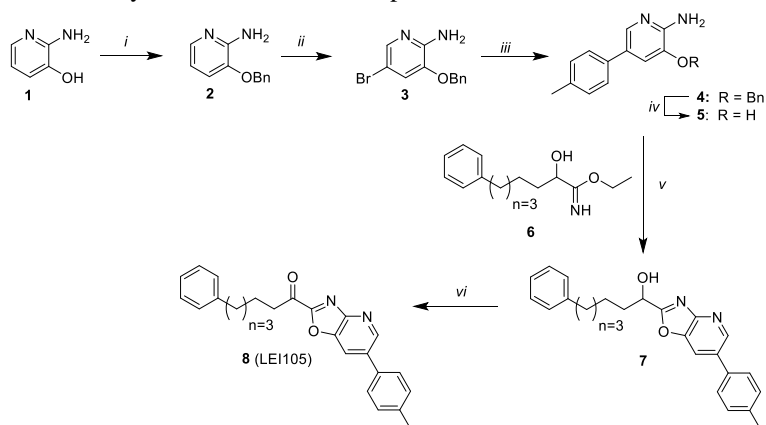
Activity-based protein profiling (ABPP) has emerged as a powerful technique for discovering selective enzyme inhibitors acting in their native physiological context.¹⁶ ABPP hinges on the use of activity-based probes (ABPs) to report on enzyme activity in cells, tissue or animals.¹⁷ An ABP normally consists of a covalent, irreversible enzyme inhibitor featuring a reporter entity (fluorophore, biotin, bioorthogonal tag) to label the active site of the enzyme or enzyme family at hand. ABPP is unique in its ability to rapidly identify inhibitor activity and selectivity within large enzyme families in complex proteome samples. The prototypical ABP for serine hydrolases is based on a fluorophosphonate (FP)-warhead.¹⁸ However, this probe does not recognize DAGL- α and the signals for MAGL and ABHD6 cannot be unequivocally established because not all gel bands can be clearly resolved in the brain proteome.¹⁹ The design, synthesis and characterization of a specific β -lactone-containing ABP (MB064) for the detection of DAGL- α activity was described in Chapter 3.^{20,21} Using this ABP, 1-(oxazolo[4,5-*b*]pyridin-2-yl)-6-phenylhexan-1-one (LEI104, Figure 1) was identified as DAGL- α inhibitor. This inhibitor belongs to the class of α -ketoheterocycles and is the first reversible inhibitor for DAGL- α . LEI104 was, however, weakly active in a cellular assay and not selective over FAAH, the enzyme responsible for the metabolism of the other endocannabinoid anandamide (AEA).^{22,23} Moreover, activity of LEI104 on DAGL- α was not studied, but in view of the high homology between DAGL- α and DAGL- β it is likely that there is cross-reactivity. To apply α -ketoheterocycles as chemical tools to study 2-AG signaling, it is important to increase their cellular activity, to have selectivity over FAAH and to assess their activity on endogenous DAGL- β .

Here, a structure-guided approach to optimize LEI104, employing a homology-model of DAGL- α is reported. In addition, it was discovered that the β -lactone probe MB064 could also label DAGL- β in cells and tissues. Using these tools LEI105 was characterized as a cellular active, dual DAGL- α/β inhibitor. Comparative chemoproteomics revealed that LEI105 is selective for DAGL- α/β over ABHD6, ABHD12, MAGL and FAAH. Furthermore, targeted lipidomics revealed that LEI105 is able to reduce 2-AG levels in a concentration dependent manner in neuronal cells without affecting AEA levels. With LEI105 cannabinoid CB₁-receptor-dependent short-term synaptic plasticity in a hippocampal slice model can be reduced. In summary, comparative and competitive chemoproteomics was applied to characterize the most selective DAGL inhibitor to date. This inhibitor can be used to study DAGL function in an acute and temporal manner in a neuronal context.

Results & discussion

Structure-guided modeling to identify LEI105 as DAGL- α inhibitor

Previously, the α -ketoheterocycle, 1-(oxazolo[4,5-*b*]pyridin-2-yl)-6-phenylhexan-1-one (LEI104, Figure 1A) was identified as an inhibitor of DAGL- α . To improve the potency of LEI104 a structure-guided modeling approach was used. The binding pose of LEI104 in DAGL- α was investigated in detail using a molecular dynamics simulation in a previously generated homology model.²¹ From this analysis, an additional hydrophobic pocket close to the catalytic site that did not appear to be occupied by LEI104 was identified (Figure 1B). Introduction of a phenyl substituent at the 6-position of the oxazolopyridine allowed probing this pocket with the aim of increasing potency and/or selectivity. A α -ketoheterocycle with a para-toluyyl group at the 6-position of LEI104 was synthesized and termed LEI105. The synthesis of LEI105 is depicted in scheme 1.



Scheme 1. Synthesis of LEI105. *i*) BnBr, Cs₂CO₃, DMF. *ii*) NBS, ACN, 0 °C. *iii*) 4-methylphenylboronic acid, Pd(dppf)Cl₂, DME/H₂O (20:1). *iv*) Pd/C, MeOH. *v*) EtOH, pyridine, 80 °C, microwave. *vi*) Dess-Martin periodinane, CH₂Cl₂.

Compound **2** was obtained by benzylation of 1-amino-2-hydroxypyridine **1**. The benzyl protection of the alcohol was required in the next step for a high yielding selective bromination in the para position with respect to the amine. The bromination was performed using *N*-bromosuccinimide and resulted in aromatic building block **3**. This compound was used to couple *p*-tolylboronic acid by a Suzuki cross coupling. Subsequent removal of the benzyl protecting group provided building block **5**. The Suzuki cross coupling was performed before the alcohol was deprotected, because the cross coupling with the free alcohol resulted in poor yields. 1-Amino-2-hydroxypyridine **5** was coupled to imidate **6** (synthesized as described in Chapter 3), which resulted in alcohol **7**. Oxidation of **7** using Dess-Martin periodinane afforded final α -ketoheterocycle **8** (LEI105).

The activity of LEI105 was tested on human DAGL- α in a colorimetric assay using *para*-nitrophenylbutyrate as a surrogate substrate.²⁴ LEI105 proved to be a potent inhibitor with a pIC_{50} of 8.5 ± 0.06 ($N=2$, $n=2$), thus some 10-fold more potent than LEI104 (7.4 ± 0.05 ; $N=2$, $n=2$).²¹ To confirm that LEI105 was also able to block conversion of the natural substrate 1-stearoyl-2-arachidonoyl-*sn*-glycerol of DAGL- α to the endocannabinoid 2-AG, the real-time fluorescence-based assay was employed.²⁵ In this assay LEI105 inhibited recombinant human DAGL- α with a pIC_{50} of 7.9 ± 0.08 ($N=2$, $n=2$) (Figure 1E), which is a 40-fold increase compared to LEI104 (pIC_{50} 6.3 ± 0.1 ($N=2$, $n=2$)). The inhibitory activity of LEI105 was confirmed in a radiometric assay using 1-[^{14}C]oleoyl-2-arachidonoyl-*sn*-glycerol ($1.0 \text{ mCi mmol}^{-1}$, $20 \text{ }\mu\text{m}$) as substrate (pIC_{50} of 6.6 ; $n = 2$).⁸

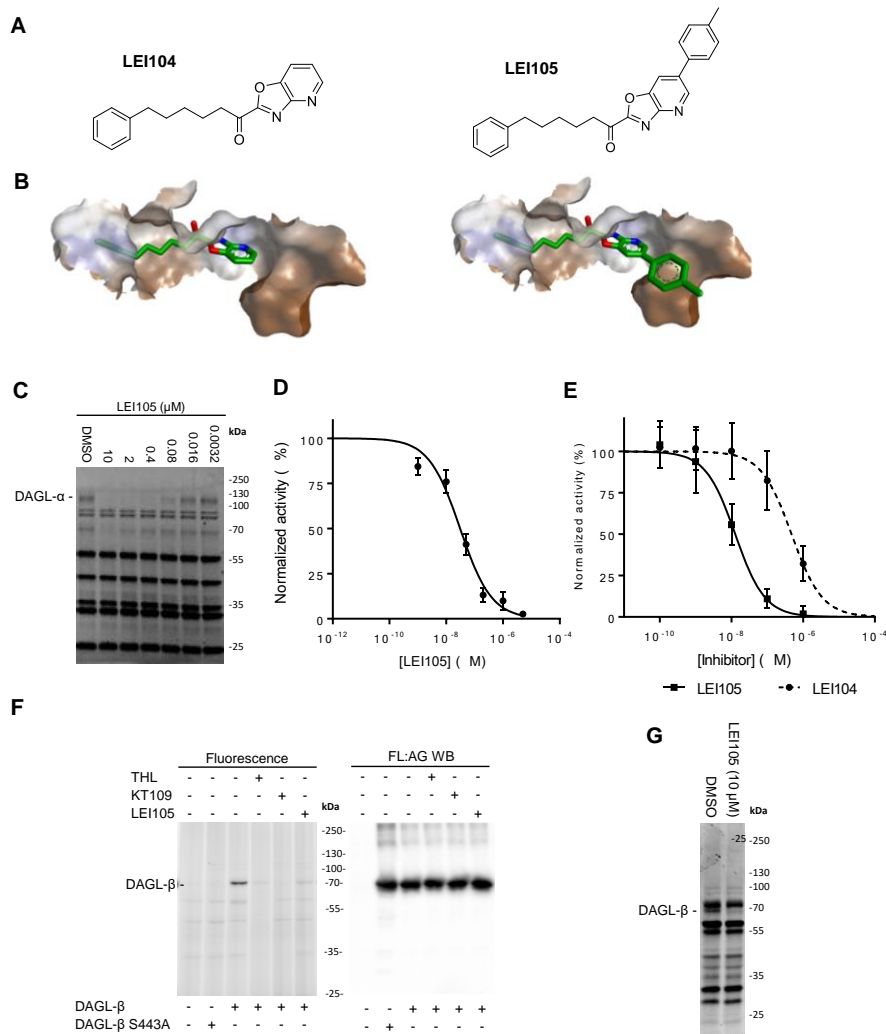


Figure 1. Structure-guided modeling and biochemical characterization of LEI105. (A) Structures of α -ketoheterocycle based DAGL inhibitors LEI104 and LEI105. (B) LEI104 and LEI105 in a homology model of DAGL- α . (C) Representative fluorescent ABPP gel showing dose dependent inhibition of MB064 (250 nM) labeling of endogenous DAGL- α labeling by LEI105 in the mouse brain membrane proteome. (* = DAGL- α breakdown product). (D) Dose response curve of DAGL- α inhibition as determined with competitive ABPP (pIC_{50} 7.5 ± 0.07 ($\text{IC}_{50} = 32$ nM); $n = 3$). (E) Dose response curve of DAGL- α inhibition by LEI104 (pIC_{50} 6.3 ± 0.1 ($\text{IC}_{50} = 501$ nM); $N=2$, $n=2$) and LEI105 (pIC_{50} 7.9 ± 0.08 nM ($\text{IC}_{50} = 13$ nM); $N=2$, $n=2$) as determined with a glycerol based natural substrate assay. (F) ABPP using MB064 (1 μM) with different hDAGL- β constructs and anti-FLAG western blot of the same gel. (G) Competitive ABPP in the mouse spleen membrane proteome using MB064 (1.0 μM) in competition with LEI105 (10 μM), LEI105 can block labeling of endogenously expressed DAGL- β in the mouse spleen membrane proteome.

Determining endogenous DAGL activity using MB064 as ABP

To test the activity of LEI105 on endogenously expressed DAGL- α in mouse membrane proteome, a previously reported ABPP method with MB064 was used.²¹ A competitive concentration response experiment with LEI105 in the mouse brain membrane proteome using MB064 revealed a pIC_{50} of 7.5 ± 0.07 ($n=3$) against DAGL- α (Figure 1C, D).

In view of the high homology between DAGL- α and DAGL- β the activity of LEI105 was also assessed on native DAGL- β . To this end, it was tested whether ABP MB064 was also able to label DAGL- β . MB064 was incubated with membranes from mock and hDAGL- β transfected HEK293T cells. MB064 labeled a protein at the expected molecular weight of DAGL- β , which was not present in the control membranes, or in S443A-hDAGL- β transfected cells, in which the catalytic serine is replaced by alanine using site-directed mutagenesis (Figure 1F). Thus, MB064 can also detect DAGL- β . Labeling of hDAGL- β was inhibited by LEI105 with a pIC_{50} of 7.4 ± 0.07 ($n=3$) (Figure 2).

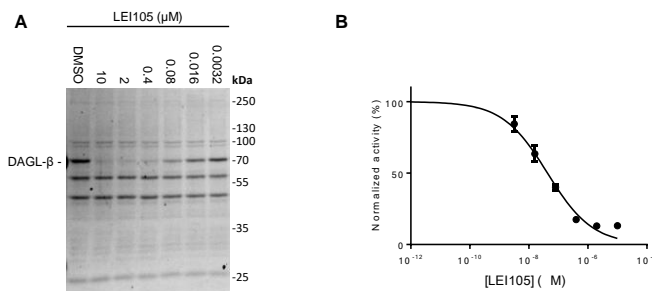


Figure 2. Dose-response of LEI105 as determined by competitive ABPP using ABP MB064 (1 μ M) against recombinant hDAGL- β . (A) Representative gel of the dose response of LEI105 against DAGL- β . (B) Dose-response curve of recombinantly expressed DAGL- β inhibition by LEI105. LEI105 inhibited hDAGL- β with a pIC_{50} of 7.4 ± 0.07 ($n=3$).

The activity of LEI105 on human DAGL- β was confirmed using a biochemical assay with *para*-nitrophenylbutyrate as a surrogate substrate (pIC_{50} of 8.1 ± 0.07 , $n=4$; Figure 3).

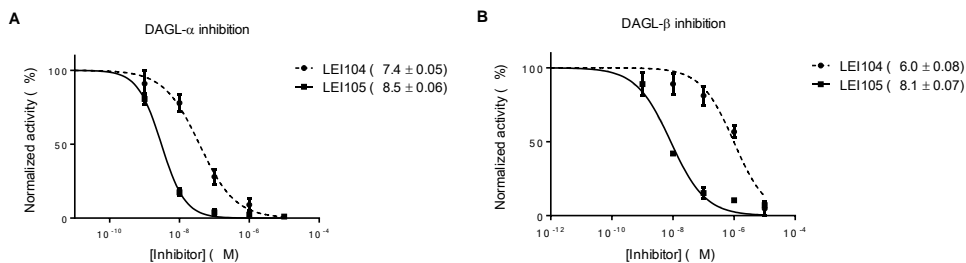


Figure 3. Dose-response curves of LEI104 and LEI105 against hDAGL- α and hDAGL- β as determined with a colorimetric assay based on the hydrolysis of PNP butyrate (A). Dose-response of LEI104 (pIC_{50} 7.4 ± 0.05 ; $N=2$, $n=2$) and LEI105 (pIC_{50} of 8.5 ± 0.06 ; $N=2$, $n=2$) against hDAGL- α . (B) Dose-response of LEI104 (pIC_{50} 8.1 ± 0.07 ; $N=2$, $n=2$) and LEI105 (pIC_{50} of 6.0 ± 0.08 ; $N=2$, $n=2$) against hDAGL- β .

Next, ABP MB064 was used to profile endogenous DAGL- β activity in twelve tissues from wild-type and DAGL- β knock-out mice. Spleen tissue was found to display the highest DAGL- β activity (Figure 4). This activity could be inhibited by LEI105 (Figure 1G).

Reduction of the α -keto group of LEI105 to the corresponding alcohol (compound 7, scheme 1) led to a ~ 150 fold drop of activity against DAGL- α , thereby indicating that the α -carbonyl in LEI105 reacts with the active site serine hydroxyl to form a covalent, though reversible, enzyme-inhibitor hemiketal adduct. To determine the mode of action (reversible versus irreversible) of LEI105, an experiment in which human DAGL- α membranes were pre-incubated at the IC_{80} concentration of LEI105 or the irreversible DAGL inhibitor KT109 was performed (Figure 5).¹⁵ The protein was separated from small molecule inhibitors via size exclusion column chromatography and remaining enzyme activity was visualized with MB064. No recovery of DAGL- α activity was found for KT109, whereas MB064 labeled DAGL- α exposed to LEI105 with similar intensity compared to DMSO treated DAGL- α (Figure 5). This indicates that LEI105 is a reversible inhibitor of DAGL- α .

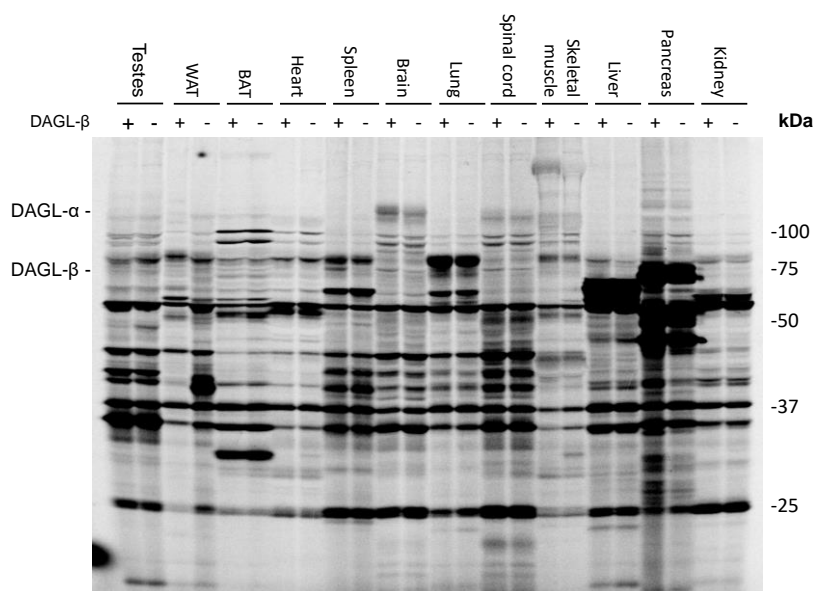


Figure 4. Screen of DAGL- β WT and KO tissues. DAGL- β WT and KO tissues were screened to obtain a tissue wide overview of DAGL- β activity. Mouse membrane proteome was incubated with 1 μ M MB064 for min 30 at rt. A band at the molecular weight (~ 70 kD) of DAGL- β was present in the WT spleen tissue but absent in its KO counterpart. This indicates that MB064 can visualize DAGL- β activity in the spleen membrane proteome. (Abbreviations WAT: white adipose tissue; BAT: brown adipose tissue; (+) WT tissue and (-) DAGL- β KO tissue).

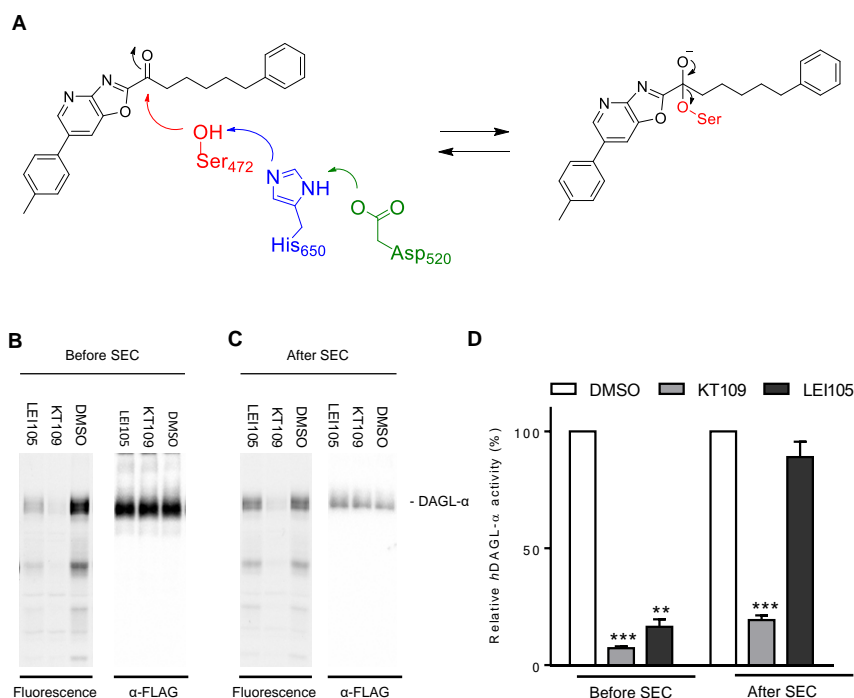


Figure 5. Reversibility assay against human recombinant DAGL-α. (A) Proposed mechanism of covalent reversible inhibition of DAGL-α by LEI105. (B) Fluorescence gel of DAGL-α labeling after treatment with KT109 and LEI105 before size exclusion chromatography (SEC) and anti-FLAG western blot of the same gel to control for protein loading. (C) Fluorescence gel of DAGL-α labeling after SEC of the same protein samples. DAGL-α labeling is regained after LEI105 treatment but still absent after treatment. (D) Schematic representation of the size exclusion chromatography (SEC) experiment that shows reversibility of LEI105 in recombinant DAGL-α (n = 3, full fluorescent gel and western blot are given in the supporting information). Statistical analysis: 2-way ANOVA (***) = p < 0.001; ** = p < 0.01 vs vehicle).

Determining proteome-wide selectivity of LEI105 using comparative and competitive chemoproteomics

To investigate the selectivity of LEI105 in the mouse brain proteome, comparative and competitive ABPP with a broad-spectrum FP-based probe (TAMRA-FP) and the DAGL-α targeting ABP, MB064 was used. As a reference, the widely used β-lactone-based DAGL-inhibitors THL and OMDM-188, two highly potent non-selective covalent and irreversible serine hydrolase inhibitors were used.^{8,14} In our experimental setup, both compounds blocked labeling of at least 4 serine hydrolases at concentrations as low as 1 μM, including ABHD6 and ABHD12, enzymes involved in 2-AG metabolism in the brain (Figure 6 A,B).

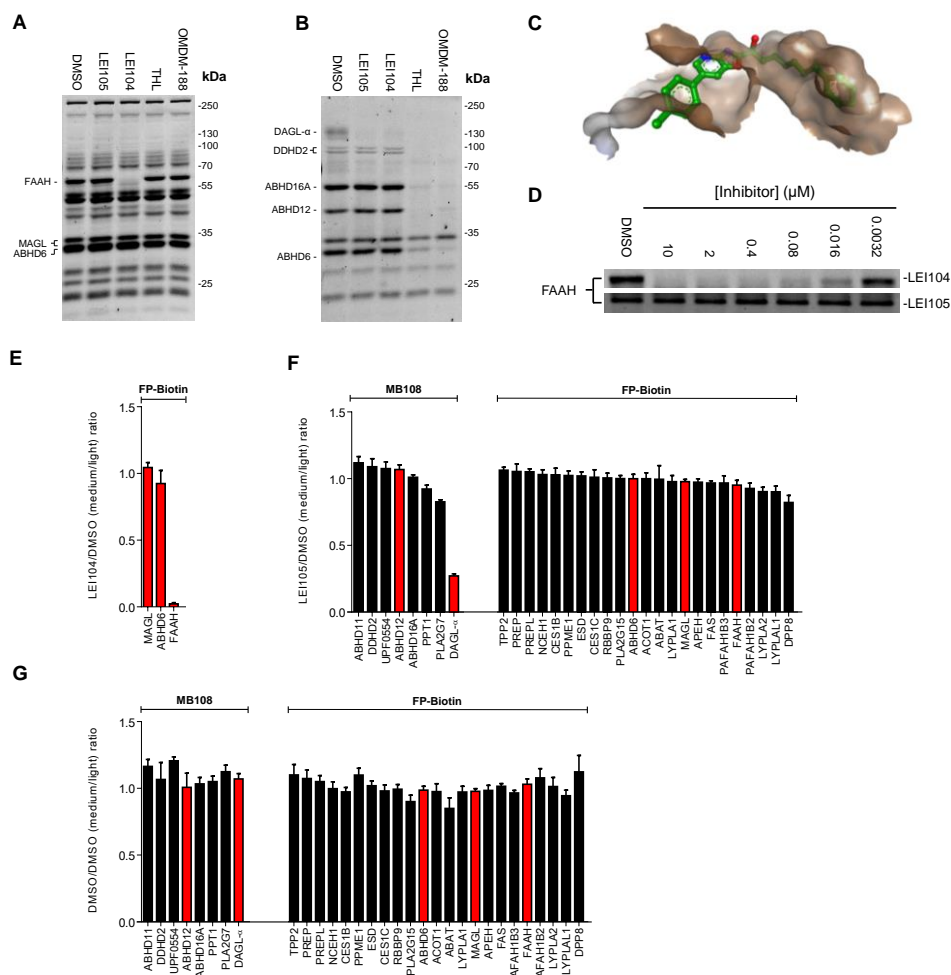


Figure 6. Selectivity of LEI105. (A) Competitive ABPP in the mouse brain membrane proteome with LEI104 (10 μ M), LEI105 (10 μ M), OMDM188 (1 μ M) and THL (1 μ M) using TAMRA-FP (500 nM). (B) Same experiment as in (a) with THL based ABP MB064 (250 nM) showing excellent selectivity of LEI105 at 10 μ M compared to THL and OMDM188. (C) One possible LEI105-like conformer in a previously reported co-crystal structure of FAAH, showing a steric clash between the toluyl group and FAAH. (D) Activity of LEI104 and LEI105 against FAAH in a concentration response experiment in the mouse brain membrane proteome using TAMRA-FP (500 nM, full gels are given in the supporting information). (E) Chemoproteomic competition between LEI104 (10 μ M) and FP-biotin (5 μ M) for FAAH, MAGL and ABHD6, showing that the chemoproteomic settings using FP-biotin are compatible with reversible α -ketoheterocycles. (F) MB108 and FP-biotin based chemoproteomic analysis of serine hydrolase activities in the mouse brain membrane proteome treated with LEI105 (10 μ M). DAGL- α labeling is reduced to over 70%. (G) Chemoproteomic control experiment shows equal isotopic labeling and detection of peptides from MB108 and FP-biotin labeled serine hydrolases. Enzymes known to be directly involved in endocannabinoid biosynthesis and metabolism are highlighted in red. (n = 3-4 independent chemoproteomics experiments; Error bars represent \pm s.e.m. of medium over light ratios of quantified peptides (minimum of two unique peptides per enzyme). Only unique proteins are given for MB108, all detected proteins including proteins

overlapping between the probes are given in the supporting information. See supplementary data set 1 for complete proteomic data.

In previous studies, fatty acid amide hydrolase (FAAH) was identified as a major off-target for LEI104. In stark contrast to LEI104, which inhibited FAAH labeling with a pIC_{50} of 7.8 ± 0.04 ($n=3$) (Figure 6A, 7), LEI105 did not block FAAH labeling up to a concentration of $10 \mu M$ ($n=3$) (Figure 6A, D). Of note, LEI105 did not inhibit labeling of any other band either, it can be concluded that LEI105 is highly selective at least within the panel of serine hydrolases labeled by TAMRA-FP and MB064. To explain this remarkable selectivity of LEI105 for DAGL α/β over FAAH, a detailed investigation using a co-crystal structure of FAAH with OL-135 (pdb: 2WJ1 and 2WJ2) was performed.²⁶ *In silico* modification of the heterocyclic part of OL-135, in the presence of the protein receptor, to a LEI105 like conformer revealed a steric clash of the toluoyl moiety of LEI105 with the substrate channel of FAAH, thereby possibly explaining the high selectivity of LEI105 over FAAH compared to its analog LEI104 (Figure 6C).

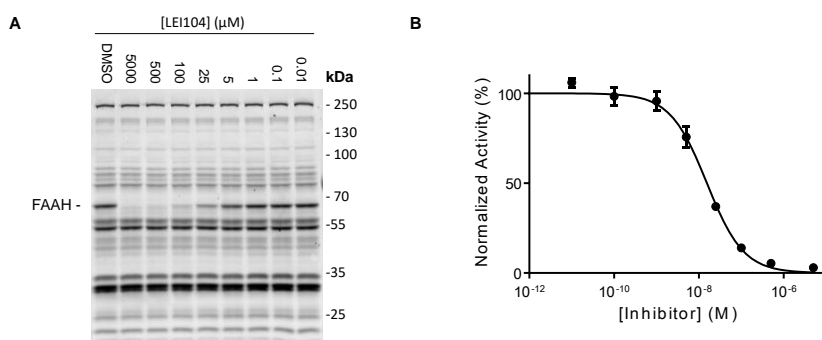


Figure 7. Activity of LEI104 against FAAH. (A). Dose-response of LEI104 against FAAH in the mouse brain membrane proteome as determined by competitive ABPP using ABP TAMRA-FP (500 nM for 20 min at rt). (B). Dose-response curve of gel based FAAH inhibition assay pIC_{50} 7.8 ± 0.04 ($n = 3$).

Considering that the human serine hydrolase family contains approximately 200 family members,²⁷ the selectivity of LEI105 in the brain proteome was examined in a broader and more detailed manner. To this end, a semi-quantitative chemoproteomics protocol was adapted. This protocol was previously applied to determine the selectivity profile of the irreversible inhibitor KT-109. MB108 and FP-Biotin, a biotinylated version of MB064 and TAMRA-FP respectively, were used for this method. This methodology allows for a more accurate quantification avoiding band overlap (as observed with gel-based assays) and enables screening over a broader range of specified serine hydrolases. First, equal isotopic labeling and detection of light and medium peptides from proteins targeted by both ABPs was validated (Figure 6G). Next, the selectivity of LEI105 in this chemoproteomic assay was investigated. LEI105 ($10 \mu M$, 30 min) did not reduce labeling of the detected serine

hydrolases by more than 20%, except for DAGL- α (Figure 6F). In addition, LEI105 was tested in biochemical assays using recombinant human ABHD6 and MAGL and in a cannabinoid CB₁ receptor radioligand displacement assay. No significant interaction ($pK_i < 5$) with these proteins of the endocannabinoid system was found (Figure 8). Together these results indicate that LEI105 is a highly selective DAGL inhibitor.

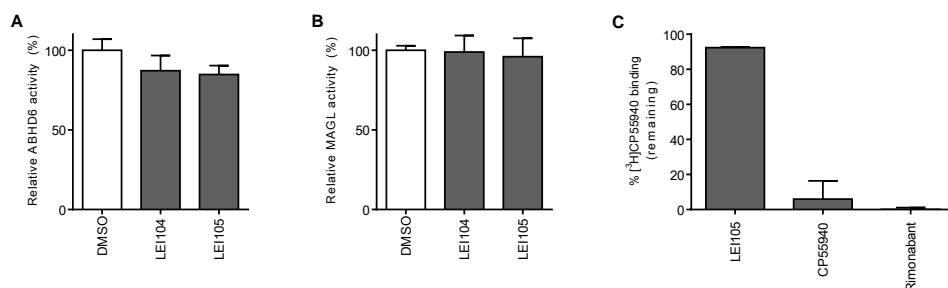


Figure 8. Selectivity of LEI105. (A). Relative MAGL activity in the presence of 10 μ M LEI104 or LEI105 as determined with the glycerol-based natural substrate assay. (B). Relative ABHD6 activity in the presence of 10 μ M LEI104 or LEI105 as determined with the glycerol-based natural substrate assay (C) Radioligand displacement assay for the CB₁ receptor. LEI105 (10 μ M) shows no affinity for the CB₁ receptor.

LEI105 reduces 2-AG levels in Neuro2A cells

To test the cellular activity of LEI105, Neuro2A cells were used. Neuro2A is a mouse neuroblastoma cell line known to express both DAGL- α and DAGL- β .²⁸ First, the presence of the mRNA transcripts of both DAGLs was confirmed. Interestingly, it was found that DAGL- β mRNA levels are ~128-fold higher, compared to DAGL- α , as determined by qPCR. In line, DAGL- α protein activity was below the detection limit of our ABPP assay, whereas a fluorescent band at the expected molecular weight of DAGL- β was detected using MB064. The identity of the band at ~70 kD was confirmed by competition with three DAGL inhibitors with a different chemotype (THL, LEI105 and KT109), all 3 inhibitors blocked labeling of the band at ~70 kD, while the control inhibitor for KT109 (KT195, Supporting Figure 1) developed by Hsu *et al.*¹⁵ did not block labeling of the band at ~70 kD. This confirmed the identity of the band as DAGL- β (Figure 9).

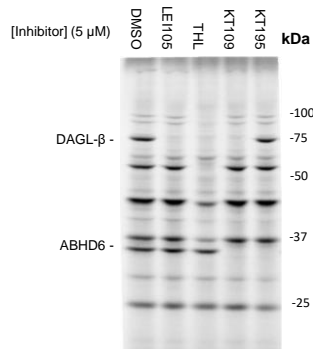


Figure 9. Validation of endogenous DAGL- β labeling by MB064 in Neuro2A cells. Labeling of Neuro2A membrane fractions by MB064 (2 μ M, 20 min at rt) showed a fluorescent band at \sim 70 kDa corresponding to the molecular weight of DAGL- β . This signal was inhibited by DAGL inhibitors THL, LEI105 and KT109. The signal at \sim 70 kDa was not inhibited by the reported control probe for KT109.⁵ These data together indicate that the fluorescent band at \sim 70 kDa corresponds with the enzyme DAGL- β . No fluorescent band was observed at \sim 120 kDa, the molecular weight of DAGL- α .

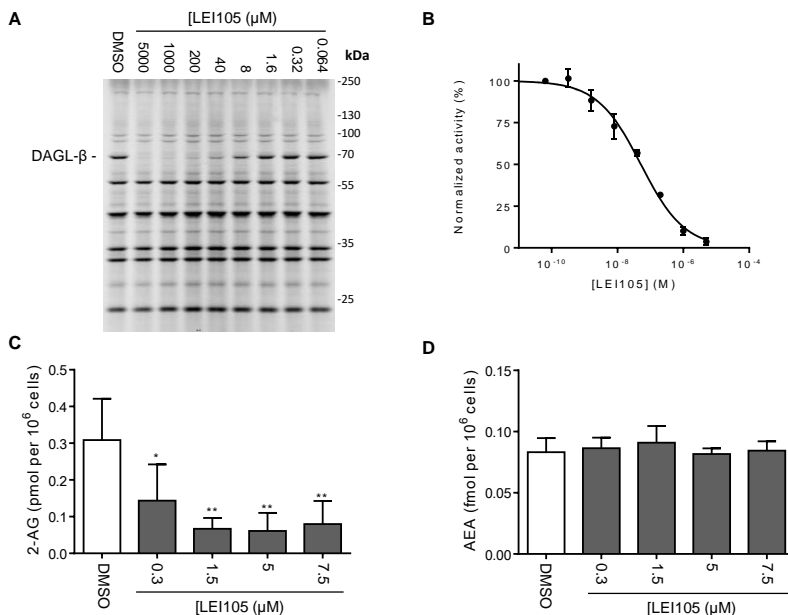


Figure 10. Cellular activity of LEI105. (A) Representative gel of concentration dependent inhibition of endogenous DAGL- β in vitro in the Neuro2A proteome as determined with ABP MB064. (B) Dose response curve of DAGL- β inhibition as determined with competitive ABP MB064 (\pm SEM, $n = 3$). (C) *In situ* treatment of Neuro2A cells (1h, 37 $^{\circ}$ C) dose dependently decreased basal 2-AG levels while keeping anandamide (AEA) levels constant (mean \pm SEM; $n = 4$). Statistical analysis: 2-way ANOVA (*** = $p < 0.001$; ** = $p < 0.01$; * = $p < 0.05$ vs vehicle).

LEI105 selectively reduced DAGL- β labeling in a concentration dependent manner with a pIC_{50} of 7.3 ± 0.07 (Figure 10A, B). Of note, no inhibition of ABHD6 was observed. Next, in a targeted lipidomics experiment the effect of LEI105 on the cellular levels of 2-AG and anandamide was determined. A concentration-dependent reduction of 2-AG was found in Neuro2A cells, whereas anandamide levels were unaffected (Figure 10C, D). To test the activity of LEI105 in a human cell line, the PC3 cell line was used. DAGL β activity in PC3 cells was confirmed in the same manner as in Neuro2A cells. All 3 DAGL inhibitors (THL, LEI105 and KT109) blocked MB064 labeling of a band at ~ 70 kD, while KT195 did not, confirming that the band at ~ 70 kD is DAGL- β (Figure 11). LEI105 reduced 2-AG levels, but no change in *sn*-1-stearoyl-2-arachidonoyl-glycerol substrate levels of DAGL was detected, which may suggest that DAG species are rapidly converted into other membrane constituents, such as phosphatidic acid by DAG-kinases. Interestingly, arachidonic acid levels were reduced by LEI105 treatment of PC3 cells (Figure 11C). This may indicate that downstream metabolic pathways of 2-AG signaling are also affected and that the biosynthesis of 2-AG is the rate-limiting step. This is in line with a previously reported reduction of arachidonic acid levels in DAGL- α knockout mice and after inhibition with KT109 in mouse liver.^{15, 5}

LEI105 reduces synaptic transmission in hippocampus

To demonstrate a physiological effect of the inhibition of 2-AG biosynthesis by LEI105, the attention was focused on hippocampal slice preparations in which depolarization-induced suppression of inhibition (DSI) is thought to be mediated via 2-AG-induced activation of presynaptic cannabinoid CB₁ receptors.^{29,30} Experimental evidence, which supports a role of DAGL- α in DSI, has been obtained through the use of genetically engineered mice that constitutively lack DAGL- α . DSI was absent in these DAGL- α knock-out mice, but not in their DAGL- β knock-out counterparts.^{5,10} Of note, anandamide levels were also reduced in these DAGL- α knock-out mice. Acute DAGL inhibition studies with chemical tools would, therefore, provide an additional line of evidence to verify the role of DAGL- α in DSI. Pharmacological intervention studies with the two highly potent non-selective DAGL inhibitors, THL and OMDM-188, however, have challenged the unequivocal role of the DAGLs in DSI. Multiple groups reported a suppression of DSI by THL and/or OMDM-188,³¹⁻³⁶ whereas other groups did not find any inhibitory effect of THL and/or OMDM-188.^{37,38} The discrepancy between the genetic model and the pharmacological studies, led to the alternative hypothesis that 2-AG is released from pre-formed lipid stores instead of the ‘on demand’ production of 2-AG.^{39,40}

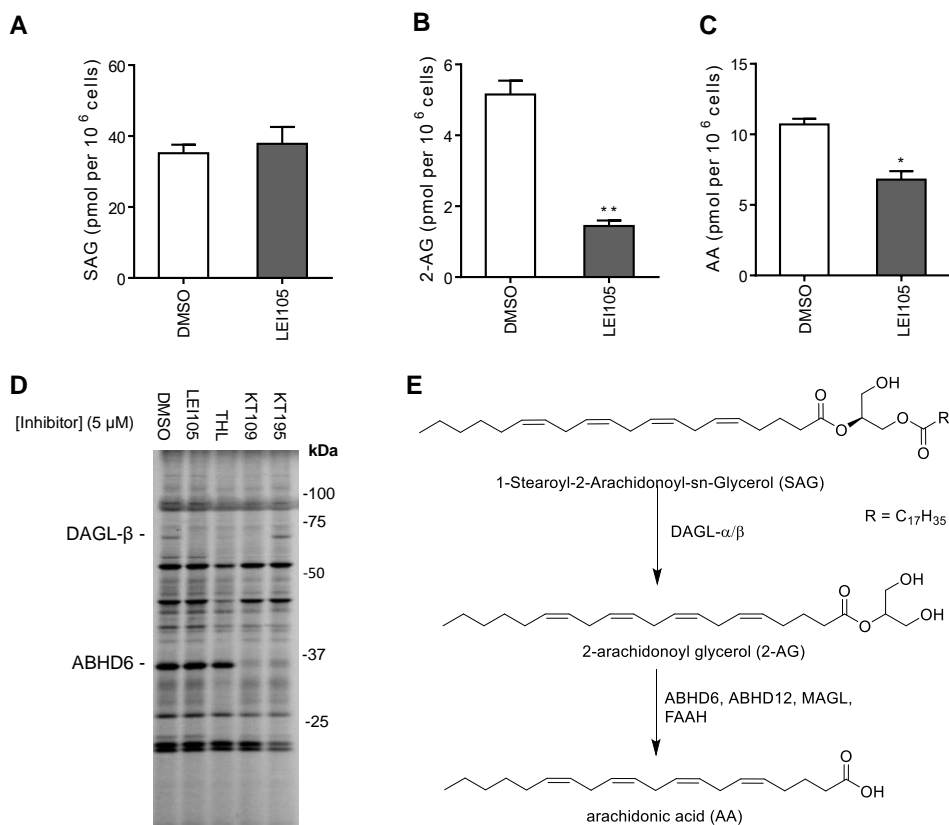


Figure 11. Cellular activity of LEI105 in PC3 cells. (A) In situ treatment of PC3 cells with LEI105 (7.5 μ M for 4h; 37 °C) did not affect SAG levels but decreased basal 2-AG (B) and AA (C) levels. (D) Labeling of PC3 membrane fractions by MB064 (2 μ M, 20 min at rt) showed a fluorescent band at ~70 kDa, the molecular weight of DAGL- β . This signal could be inhibited by DAGL inhibitors THL, LEI105 and KT109. The signal at ~70 kDa was not inhibited by the reported control probe for KT109.⁵ These data together indicate that the fluorescent band at ~70 kDa corresponds with the enzyme DAGL- β , and that DAGL- β is expressed and active in the PC3 cell line. No fluorescent band was observed at ~120 kDa, the molecular weight of DAGL- α . (E) Schematic representation of the current model of 2-AG biosynthesis and degradation. Statistical analysis: 2-way ANOVA (*** = $p < 0.001$; ** = $p < 0.01$; * = $p < 0.05$ vs vehicle).

Here, cannabinoid CB₁ receptor-dependent DSI in CA1 pyramidal neurons in hippocampal slices with the selective DAGL inhibitor was investigated. Pre-incubation and continuous application of 10 μ M LEI105 had no effect on the amplitude of the stimulus-evoked inhibitory post-synaptic currents (IPSC) (271 ± 22 pA) compared to control (276 ± 32 pA). In control conditions, a DSI response could be evoked which decayed back with an exponential time course ($\tau = 34$ sec) to baseline levels. DSI was quantified as the reduction in IPSC amplitude averaged over the first 15 sec after its induction. DSI evoked in slices treated with LEI105 was smaller than DSI induced in control slices ($18 \pm 7\%$, $n=15$ and

36 ± 4%, n=18, respectively; $p < 0.05$, Student's t-test) (Figure 12). However, it is clear that DSI is not completely blocked in the presence of LEI105, which suggests that in addition to on demand 2-AG synthesis, the recruitment of 2-AG pools may contribute to DSI.⁴⁰ Alternatively, other endocannabinoids (e.g. anandamide) may be involved. Of note, at 10 μ M LEI105 was still selective in our experimental set up and did not displace ³H-CP55940 from the CB₁ receptor (Figure 8), a result that excludes direct antagonism of the CB₁ receptor by LEI105. Thus, the data support the hypothesis of a major, but not exclusive, role of 'on demand' production of 2-AG, which is responsible for the cannabinoid CB₁ receptor-mediated synaptic plasticity.³³

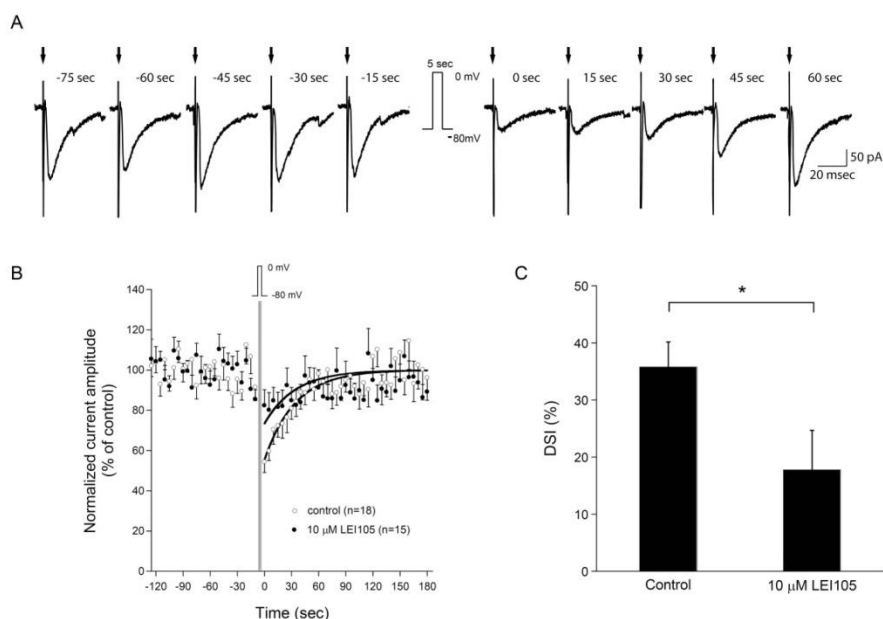


Figure 12. DSI is reduced in hippocampal slices treated with 10 μ M LEI105. (A) Example of a typical whole-cell voltage-clamp recording of evoked inhibitory post-synaptic currents (IPSCs) in a CA1 pyramidal neuron under control conditions. IPSCs are evoked every 5 seconds, but for clarity, IPSCs shown here are representative traces recorded every 15 seconds. DSI is induced with a 5-sec duration depolarization from -80 mV to 0 mV and is observed as a marked and brief reduction of IPSC amplitude following the depolarization. (B) Averaged IPSC amplitude recorded every 5 seconds in CA1 neurons from vehicle-treated slices (DMSO) and from slices pre-incubated at least 30 minutes and in the continuous presence of LEI 105 (10 μ M). The dark lines represent the single exponential fit of the recovery phase following the depolarizing step. (C) Initial DSI amplitude under control conditions (DMSO) and in the presence of LEI105 (10 μ M). (* $p < 0.05$ vs vehicle)

Conclusions

In conclusion, comparative and competitive chemproteomics using a DAGL- α targeting ABP (MB064) in combination with the broad-spectrum probe (TAMRA-FP) was applied to identify and characterize the reversible DAGL inhibitor LEI105. This inhibitor was found to be an excellent tool to study the enzymatic role of DAGL- α in a neuronal setting and provides a critical counterpart to currently available DAGL knock-out mice. This was exemplified in Neuro2A cells (where LEI105 reduced 2-AG levels, but not AEA levels) and in intact hippocampal brain slices (where a clear suppression of DSI was observed in the presence of LEI105). Using this combination of activity-based probes in a chemoproteomic setting many lipases involved in the regulation of endocannabinoid levels (e.g. DAGL- α , ABHD6, ABHD12, MAGL and FAAH) in the brain are targeted with high affinity. This opens the door to broadly apply this methodology to identify and characterize not only covalent irreversible inhibitors, but also reversible inhibitors that target DAGL and other enzymes involved in 2-AG biosynthesis and metabolism. Identification of reversible inhibitors is important, because covalent irreversible inhibitors can potentially lead to toxicity and immunogenicity of covalent inhibitor-protein complexes and selectivity issues using reactive covalent warheads. Reversible inhibitors have the additional intrinsic advantage to enable a better control of partial inhibition of their target enzyme. This is especially important with respect to endocannabinoid signaling in the CNS, since complete blockade of cannabinoid CB₁ receptor signaling in the CNS may lead to severe side effects.⁴¹ Thus, this feature can play an important factor in the development of clinical candidates to provide therapeutic solutions for diseases, such as obesity, related metabolic disorders and neuroinflammation, in which excessive 2-AG signaling or its metabolites play an important factor.

Experimental Methods

Synthetic procedures

General remarks

All reactions were performed using oven or flame-dried glassware and dry solvents. Reagents were purchased from Sigma Aldrich, Acros and Merck and used without further purification unless noted otherwise. All moisture sensitive reactions were performed under an argon atmosphere. Traces of water were removed from starting compounds by co-evaporation with toluene.

^1H - and ^{13}C -NMR spectra were recorded on a Bruker AV 400 MHz spectrometer at 400.2 (^1H) and 100.6 (^{13}C) MHz or a Bruker DMX-600 spectrometer 600 (^1H) and 150 (^{13}C) MHz using CDCl_3 or CD_3OD as solvent, unless stated otherwise. Chemical shift values are reported in ppm with tetramethylsilane or solvent resonance as the internal standard (CDCl_3 δ 7.26 for ^1H , δ 77.0 for ^{13}C , CD_3OD : δ 3.31 for ^1H). Data are reported as follows: chemical shifts (δ), multiplicity (s = singlet, d = doublet, dd = double doublet, td = triple doublet, t = triplet, q = quartet, quint = quint, br = broad, m = multiplet), coupling constants J (Hz), and integration. HPLC purification was performed on a preparative LC-MS system (Agilent 1200 serie) with an Agilent 6130 Quadrupole MS detector. High-resolution mass spectra (HRMS) were recorded on a Thermo Scientific LTQ Orbitrap XL. Flash chromatography was performed using SiliCycle silica gel type SiliaFlash P60 (230 – 400 mesh). TLC analysis was performed on Merck silica gel 60/Kieselguhr F254, 0.25 mm. Compounds were visualized using either Seebach's reagent (a mixture of phosphomolybdic acid (25 g), cerium (IV) sulfate (7.5 g), H_2O (500 mL) and H_2SO_4 (25 mL)) or a KMnO_4 stain (K_2CO_3 (40 g), KMnO_4 (6 g), H_2O (600 mL) and 10% NaOH (5 mL)).

3-(benzyloxy)pyridin-2-amine (2): Benzylbromide (2.2 mL, 18.2 mmol) was dissolved in DMF (90 mL), 2-hydroxy-3-aminopyridine (2.0 g, 18.2 mmol) and Cs_2CO_3 (6.4 g, 18.2 mmol) were added and the reaction mixture was stirred over weekend. The reaction mixture was diluted with $\text{EtOAc}/\text{H}_2\text{O}$ (1:1, 100 mL), the layers were separated and the water layer was extracted with EtOAc . The combined organic layers were washed with H_2O and brine before they were dried on MgSO_4 , filtered and concentrated under reduced pressure. The residue was purified by flash chromatography over silica gel using pentane/ethyl acetate (20:80) with 1% Et_3N . This yielded **2** (2.0 g, 10.2 mmol, 56%) as a pale yellow solid. ^1H NMR (400 MHz, CDCl_3) δ 7.67 (d, J = 5.1 Hz, 1H), 7.46 – 7.31 (m, 5H), 6.96 (d, J = 7.8 Hz, 1H), 6.59 (dd, J = 7.8, 5.1 Hz, 1H), 5.06 (s, 2H), 4.73 (s, 2H). ^{13}C NMR (101 MHz, CDCl_3) δ 150.33, 141.58, 139.10, 136.36, 128.78 (2C), 128.38, 127.67 (2C), 116.90, 113.69, 70.28. IR: 3468.6, 3290.3, 3130.7, 1626.5, 1485.7, 1452.2, 1205.9, 738.3, 697.

3-(benzyloxy)-5-bromopyridin-2-amine (3): (2.0 g, 9.99 mmol) was dissolved in ACN and cooled to 0°C. N-bromosuccinimide (1.79 g, 10 mmol) was added in portions. The reaction mixture was stirred for 15 minutes before the solvent was removed under reduced pressure. The residue was taken up in EtOAc/H₂O (1:1) and the layers were separated. The organic layer was washed with saturated NaHCO₃ (aq.) and brine before it was dried on MgSO₄, filtered and concentrated under reduced pressure. This yielded **3** (2.2 g, 8.0 mmol, 80%). ¹H NMR (400 MHz, CDCl₃) δ 7.73 (d, *J* = 1.9 Hz, 1H), 7.44 – 7.33 (m, 5H), 7.08 (d, *J* = 1.9 Hz, 1H), 5.04 (s, 2H), 4.77 (s, 2H). ¹³C NMR (101 MHz, CDCl₃) δ 149.07, 141.86, 139.32, 135.59, 128.88 (2C), 128.67, 127.82(2C), 119.65, 106.95, 70.68. Spectroscopic data are in agreement with those reported.⁹

3-(benzyloxy)-5-(p-tolyl)pyridin-2-amine (4): 4-methylphenylboronic acid (120 mg, 0.88 mmol), **3** (200 mg, 0.72 mmol), Na₂CO₃ (228 mg, 2.16 mmol) and Pd(dppf)Cl₂ (5 mg, 0.006 mmol) were dissolved in 5 mL 1,2-dimethoxyethane/H₂O (20:1). The mixture was heated for 8h to 150 °C using microwave irradiation. The reaction mixture was diluted with EtOAc and washed with H₂O and brine. The organic layer was dried on MgSO₄, filtered and concentrated under reduced pressure. The residue was purified by flash chromatography using pentane/ethyl acetate (70:30) with 1% Et₃N. This yielded **4** (138 mg, 0.48mmol, 66%) as a brown solid. ¹H NMR (400 MHz, CDCl₃) δ 7.90 (d, *J* = 1.8 Hz, 1H), 7.48 – 7.34 (m, 8H), 7.22 – 7.19 (m, 2H), 5.14 (s, 2H), 4.84 (s, 2H), 2.38 (s, 3H). ¹³C NMR (101 MHz, CDCl₃) δ 149.24, 141.68, 136.88, 136.48, 136.20, 135.66, 129.71 (2C), 128.86 (2C), 128.52, 127.82 (2C), 127.68, 126.44 (2C), 116.08, 70.52, 21.20.

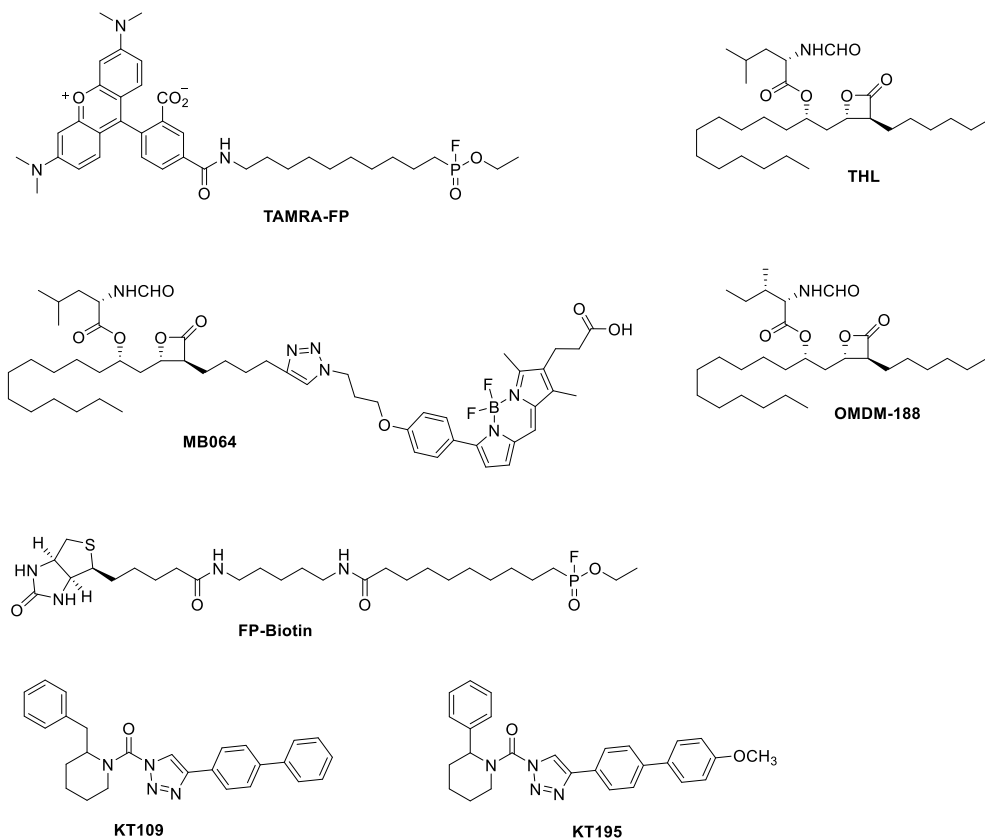
2-amino-5-(p-tolyl)pyridin-3-ol (5): Compound **4** (170 mg, 0.59 mmol) was dissolved in MeOH. Pd/C (50 mg) was added and the mixture was stirred for 1h under a H₂ atmosphere. The reaction mixture was filtered over celite and concentrated under reduced pressure. The residue was purified by flash chromatography over silica gel using CH₂Cl₂/MeOH (90:10). This yielded **5** (77 mg, 0.38 mmol, 65%) as a green solid. ¹H NMR (400 MHz, MeOD) δ 7.61 (d, *J* = 1.9 Hz, 1H), 7.37 (d, *J* = 8.1 Hz, 2H), 7.20 (d, *J* = 7.9 Hz, 2H), 7.16 (d, *J* = 2.0 Hz, 1H), 2.34 (s, 3H). ¹³C NMR (101 MHz, MeOD) δ 150.69, 142.66, 137.81, 136.50, 133.21, 130.54 (2C), 128.77, 126.98 (2C), 119.09, 21.08. IR: 3339.8, 2974.3, 2886.6, 1648.4, 1380.7, 1087.5, 1045.3, 879.6, 615.3.

Ethyl 2-hydroxy-7-phenylheptanimidate (6): Acetyl chloride (1 mL, 14 mmol) was added drop-wise to a mixture of EtOH/CHCl₃ (1:1) at 0 °C, and the solution was subsequently stirred for 30 min. 2-hydroxy-7-phenylheptanenitrile (213 mg, 1.05 mmol) dissolved in CHCl₃ (1.0 mL) was added drop-wise at 0°C. After the reaction mixture was stirred for 2h it was allowed to warm to rt and the solvents were removed at 25°C under reduced pressure. The obtained solid imidate (**6**) was directly used for the next reaction.

6-phenyl-1-(6-(p-tolyl)oxazolo[4,5-b]pyridin-2-yl)hexan-1-ol (7): Compound **5** (77 mg, 0.38 mmol) dissolved in EtOH (2 mL) was added to a sealed microwave tube. Pyridine (0.04 mL, 0.49 mmol) was added and the mixture was heated for 15 min to 80 °C using microwave irradiation. Imidate **6** (123 mg, 0.49 mmol) dissolved in EtOH (1.0 mL) was added and the mixture was heated to 80 °C for 6h using microwave irradiation. The reaction mixture was concentrated under reduced pressure and purified by flash chromatography over silica gel using CH₂Cl₂/MeOH (95:5). This yielded compound **7** (32 mg, 0.082 mmol; 17%) as a brown solid. ¹H NMR (400 MHz, MeOD) δ 8.69 (d, *J* = 1.8 Hz, 1H), 8.20 (d, *J* = 1.9 Hz, 1H), 7.55 (d, *J* = 7.9 Hz, 2H), 7.29 (d, *J* = 7.8 Hz, 2H), 7.23 – 7.17 (m, 2H), 7.13 – 7.08 (m, 3H), 4.96 – 4.90 (m, 1H), 2.57 (t, *J* = 7.7 Hz, 2H), 2.37 (s, 3H), 1.98 (p, 2H), 1.66 – 1.53 (m, 2H), 1.48 – 1.35 (m, 2H). ¹³C NMR (101 MHz, MeOD) δ 173.16, 154.99, 145.94, 145.00, 143.77, 139.61, 136.36, 135.57, 130.97 (2C), 129.38 (2C), 129.24 (2C), 128.44 (2C), 126.63, 118.55, 68.80, 36.76, 36.14, 32.60, 29.91, 26.05, 21.17. IR: 3351.4 (br), 3030.3, 2923.0, 2859.6, 1478.6, 1378.5, 1265.5, 1103.1, 813.3, 740.2, 694.8. HRMS (ESI+) *m/z*: calculated for C₂₅H₂₆N₂O₂ (M + H⁺) 387.2067; found 387.2072.

6-phenyl-1-(6-(p-tolyl)oxazolo[4,5-b]pyridin-2-yl)hexan-1-one(8, LEI105): To a solution of **7** (21 mg, 0.05 mmol) in CH₂Cl₂ (2 mL) was added Dess-Martin periodinane (35 mg, 0.075 mmol) and the reaction mixture was stirred under argon atmosphere overnight. The reaction mixture was quenched with saturated NaHCO₃ (aq). The layers were separated and the organic layer was extracted with CH₂Cl₂. The combined organic layers were washed with brine, dried on MgSO₄, filtered and concentrated under reduced pressure. The residue was purified by flash chromatography over silica gel using toluene/ethyl acetate (90:10) with 1% Et₃N. This yielded compound **8** (LEI105) (14 mg, 0.036 mmol, 73%) as a white solid. ¹H NMR (400 MHz, CDCl₃) δ 8.97 (d, *J* = 2.0 Hz, 1H), 8.09 (d, *J* = 2.0 Hz, 1H), 7.54 (d, *J* = 8.1 Hz, 2H), 7.34 (d, *J* = 8.0 Hz, 2H), 7.31 – 7.22 (m, 2H), 7.22 – 7.13 (m, 3H), 3.29 (t, *J* = 7.4 Hz, 2H), 2.64 (d, *J* = 8.0 Hz, 2H), 2.44 (s, 3H), 1.93 – 1.81 (m, 2H), 1.71 (dt, *J* = 15.4, 7.6 Hz, 2H), 1.55 – 1.44 (m, 2H). ¹³C NMR (101 MHz, CDCl₃) δ 190.20, 158.58, 152.99, 148.15, 144.05, 142.37, 138.98, 137.48, 133.95, 130.09 (2C), 128.37 (2C), 128.26 (2C), 127.49 (2C), 125.67, 117.68, 39.69, 35.69, 31.15, 28.69, 23.71, 21.20. IR: 3029.9, 2921.6, 2857.0, 1705.9, 1529.6, 1371.5, 1232.4, 1000.0, 819.7, 749.7, 697.2. HRMS (ESI+) *m/z*: calculated for C₂₅H₂₄N₂O₂ (M + H⁺) 385.1911; found 385.1914. LCMS purity > 95%, retention time: 7.23, method: CH₃CN/H₂O 50-90%.

Biochemical methods



Additional Figure 1. Structures of inhibitors and probes used throughout the chapter. TAMRA-FP (Thermo fisher scientific), MB064¹, FP-Biotin (Santa Cruz Biotechnology), THL (Sigma Aldrich), OMDM-188⁸, KT109 and KT195¹⁵.

hDAGL- α / β plasmids. Full length human cDNA was purchased (Biosource) and cloned into mammalian expression vector pcDNA3.1, containing genes for ampicillin and neomycin resistance. hDAGL- α constructs were obtained as reported previously.¹³ For proteins containing a FLAG-tag, a FLAG-linker was made from primers and cloned into the vector at the C-terminus of hDAGL- α or hDAGL- β . Two step PCR mutagenesis was performed to substitute the active site serine for an alanine in the hDAGL- β -FLAG, to obtain hDAGL- β -S443A-FLAG. All plasmids were grown in XL-10 Z-competent cells and prepped (Maxi Prep, Qiagen). Sequence analysis for the confirmation of the sequences was performed at the Leiden Genome Technology Centre.

Cell culture and membrane preparation. Cell culture and membrane preparation were performed as previously described.¹³ In brief, HEK293T cells were grown in DMEM with

stable glutamine and phenolred (PAA), 10% New Born Calf serum, penicillin and streptomycin. Cell passage was performed every 2-3 days by resuspension in medium and seeding them to appropriate confluence. Membranes were prepared from transiently transfected HEK293T cells. 24h prior to transfection 10^7 cells were seeded in a 15 cm petri dish. A 3:1 mixture of polyethyleneimine (60 μ g) and plasmid DNA (20 μ g) in 2 mL serum free medium was added. The medium was refreshed after 24 hours, and after 72h the cells were harvested in 20 mL medium. Cells were isolated by centrifugation for 10 min at 1000 rpm and subsequent aspiration of the medium. The cell pellet was flash frozen in liquid nitrogen and stored at -80 °C until use.

Cell pellets were slowly thawed on ice and suspended in lysis buffer (20 mM HEPES pH 7.2, 2 mM DTT, 0.25 M sucrose, 1 mM MgCl₂, 1x protease inhibitor cocktail (Roche cOmplete EDTA free), 25 U/mL Benzonase). Three pulses with a polytrone (3 \times 7 sec) were used to homogenize the suspension. After homogenization, the suspension was allowed to incubate for 10 min on ice. Ultracentrifugation (100,000 \times g, 30 min, 4 °C, Beckman Coulter, Type Ti70 rotor) was used to separate the cytosolic fraction and the membrane fraction. The pellet (membrane fraction) was resuspended in storage buffer (20 mM HEPES pH 7.2, 2 mM DTT, 1x protease inhibitor cocktail (Roche cOmplete EDTA free)). The total protein concentration was determined with Quick Start Bradford assay (Biorad) or QubitTM protein assay (Invitrogen). The protein concentration was adjusted to 1 mg/mL before it was flash frozen in liquid nitrogen and stored at -80 °C until use.

Biochemical DAGL activity assay. The biochemical hDAGL- α assay was performed as reported previously.¹³ In brief, the biochemical hDAGL- α activity assay is based on the hydrolysis of para-nitrophenylbutyrate (PNP-butyrate) by membrane preparations from HEK293T cells transiently transfected with hDAGL- α . Reactions were performed in 50 mM HEPES pH 7.2 buffer with 0.05 μ g/ μ L (final protein concentration) hDAGL- α transfected membrane fractions. The colorimetric assay for DAGL- β activity was performed using the same methodology as for the DAGL- α assay, but hDAGL- β transfected HEK293T cell membranes were used.

Radioligand displacement assay. [³H]CP55940 (specific activity 141.2 Ci/mmol) and GF-C filters were purchased from Perkin Elmer (Waltham, MA). Bicinchoninic acid (BCA) and BCA protein assay reagent were obtained from Pierce Chemical Company (Rochford, IL). The cell line stably expressing the hCB₁ receptor (CHOK1hCB1_{bgal}) was obtained from DiscoveRx.

Cell culture and membrane preparation for the radioligand displacement assay. CHOK1hCB1_{bgal} cells were cultured in Ham's F12 Nutrient Mixture supplemented with 10% fetal calf serum, 1 mM glutamine, 50 μ g/mL penicillin, 50 μ g/mL streptomycin, 300 mg/mL hygromycin and 800 μ g/mL geneticin in a humidified atmosphere at 37°C and 5%

CO₂. Cells were subcultured twice a week at a ratio of 1:20 on 10-cm ø plates by trypsinization. For membrane preparation the cells were subcultured 1:10 and transferred to large 15-cm diameter plates.

[³H]CP55940 displacement assay. [³H]CP55940 displacement assays to determine the cannabinoid CB1 binding affinity were performed as reported previously,³ with the following changes: Membrane aliquots containing 5 µg (CHOK1hCB₁_bgal) of membrane protein in 100 µL assay buffer (50 mM Tris-HCl, 5 mM MgCl₂, 0.1% BSA, pH 7.4) were incubated at 30°C for 1 hr. Non-specific binding was determined in the presence of 10 µM AM630. Filtration was performed on GF/C filters, presoaked for 30 min with 0.25% PEI, using a Brandel harvester. Filter-bound radioactivity was determined in a β-counter.

Preparation of mouse tissue proteome. Mouse tissue were isolated according to guidelines approved by the ethical committee of Leiden University (DEC#13191). Mouse tissues were dounce homogenized in pH 7.2 lysis buffer A (20 mM HEPES pH 7.2, 2 mM DTT, 1 mM MgCl₂, 25 U/mL Benzonase) and incubated for 5 minutes on ice. The suspension was centrifuged (2500 × g, 3 min, 4 °C) to remove debris. The supernatant was collected and subjected to ultracentrifugation (100.000 × g, 45 min, 4 °C, Beckman Coulter, Type Ti70 rotor). This yielded the membrane fraction as a pellet and the cytosolic fraction in the supernatant. The membrane fraction was suspended in storage buffer (20 mM HEPES pH 7.2, 2 mM DTT). The total protein concentration was determined with Quick Start Bradford assay (Biorad) or QubitTM protein assay (Invitrogen). Membranes and supernatant were flash frozen in liquid nitrogen and stored in aliquots at -80 °C until use.

Activity based protein profiling on transiently transfected HEK293T cells. HEK293T cells were transfected with hDAGL-α-FLAG, hDAGL-β-FLAG or hDAGL-β-S443A-FLAG and the membranes were isolated following a protocol reported previously.¹ For DAGL-α ABPP assays, the membrane proteome (1 mg/mL, 20 µL) was incubated at rt with vehicle (DMSO) or inhibitor in 0.5 µL DMSO for 30 min. The sample was subsequently treated for 15 min with 250 nM (final concentration) ABP MB064 or 500 nM (final concentration) TAMRA-FP. The incubation protocols for DAGL-β constructs was similar except for the probe concentration and incubation time of MB064 (20 min, 2 µM final concentration). The reactions were quenched with 10 µL standard 3 × SDS PAGE sample buffer. The samples were directly loaded and resolved on SDS PAGE gel (10 % acrylamide). The gels were scanned using a ChemiDoc MP system (Cy3 settings, 605/50 filter) and analyzed using Image lab 4.1.

Activity based protein profiling in Neuro2A cells. Neuro2A cells were grown in DMEM with stable glutamine and phenolred, 10% New Born Calf serum, penicillin and streptomycin. Cells were passaged every 2-3 days by resuspension in medium and seeding

them to appropriate confluence. Before harvest, the Neuro2A cells were washed with serum free medium (3x). The cells were suspended in serum free medium and centrifuged at 1000 rpm for 10 min to pellet the cells. The cell pellets were flash frozen in liquid nitrogen and stored at -80 until lysis. The Neuro2A cells were suspended in lysis buffer (20 mM HEPES pH 7.2, 2 mM DTT, 1 mM MgCl₂, 25u/mL Benzonase) and dounce homogenized. The protein concentration was determined by QubitTM protein assay (invitrogen) or Quick Start Bradford assay (Biorad) and samples were subsequently flash frozen and stored at -80 °C until use. Neuro2A proteome (2 mg/mL) was incubated with vehicle (DMSO) or inhibitor in 0.5 μ L DMSO for 30 min at rt. The sample was subsequently treated with ABP MB064 (2 μ M) for 20 min at rt before the reaction was quenched with standard 3 \times SDS PAGE sample buffer. Gels were scanned using a ChemiDoc MP system (Cy3 settings, 605/50 filter) and analyzed using image lab 4.1. PC3 cells were maintained in F12K medium and subcultured and analyzed using the same protocol as for the Neuro2A cells.

Activity based protein profiling in mouse tissue. Tissue proteome (2 mg/mL) was incubated with vehicle (DMSO) or inhibitor in 0.5 μ L DMSO for 30 min at rt and subsequently incubated for 15 min. with ABP MB064 (250 nM (final concentration) for DAGL- α detection or for 20 min. with 2 μ M ABP MB064 (final concentration) for DAGL- β detection). The proteins were resolved and visualized using the same procedure as for the Neuro2A cells.

Western BLOT. Western blot procedure was performed as reported previously.¹³ In brief, Proteins were transferred from gel to a PVDF membrane using a Trans-Blot[®] Turbo (BioRad). Enzymes containing a FLAG-tag were stained using rabbit anti-FLAG as primary antibody, and goat-anti-rabbit HRP as secondary antibody. The blot was developed in the dark using a 10 mL luminal solution, 100 μ L ECL enhancer and 3 μ L H₂O₂. Chemiluminescence was visualized using a ChemiDoc XRS (BioRad).

qPCR. For qPCR experiments, iTaqTM Universal SYBR[®] Green Supermix (BioRad) was used following the manufacturers protocol.

ABPP inhibitor activity measurements. The percentage of activity remaining was determined by measuring the integrated optical intensity of the fluorescent protein bands using Image lab 4.1. The relative intensity was compared to the vehicle treated proteins, which were set to 100%. IC₅₀ and IC₈₀ values were determined by plotting a log(inhibitor) vs. normalized response (variable slope) dose-response curve generated using Prism software (GraphPad).

Natural substrate based fluorescence assay. The natural substrate assay for DAGL- α , MAGL and ABHD6 activity were performed as reported previously.²⁵

Size exclusion chromatography. Membrane fractions of DAGL- α -FLAG transfected HEK293T (1 mg/mL; 0.5 mL) cells were incubated with vehicle (DMSO), pIC₈₀ concentration of LEI105 (6.5 ± 0.12) or the pIC₈₀ concentration of KT109 (6.8 ± 0.19) for 30 minutes at rt. Small molecules were separated from proteins using 2 mL Zeba spin desalting columns (Thermo scientific) using the manufacturers protocol (3 \times). DAGL- α activity of the samples before and after size exclusion chromatography were analyzed using the ABPP method as described above. Western blot of the FLAG-tag signal was used to control for equal protein loading.

Lipid analysis PC3 cells. PC3 cells were cultured as described above. Before inhibitor treatment, the culture medium was removed and the cells were washed with warm (37 °C) serum-free medium (3x). The cells were treated with vehicle (DMSO) or inhibitor for 4h at 37 °C in serum-free medium. After 4h of incubation medium was removed and the cells were washed with cold (4°C) DPBS (3x) and subsequently suspended in DPBS and pelleted. The cell pellet metabolome was extracted and analyzed as described previously.⁵

Lipid analysis Neuro2A cells. Neuro2A cells were cultured as described above. Before inhibitor treatment, the culture medium was removed and the cells were washed with warm (37 °C) serum free medium (3x). The cells were treated with vehicle (DMSO) or inhibitor for 1h at 37 °C in serum free medium. After 1h of incubation medium was removed and the cells were washed with cold (4°C) PBS (3x) and subsequently suspended in PBS and pelleted. The PBS was removed and the cell pellet was flash frozen and stored at -80 ° until endocannabinoid extraction.

Cell pellets were suspended in 100 μ L 0.5% NaCl (aq.), and 510 μ L 0.2% formic acid (vol/vol) in ACN containing internal standards (d₈-anandamide (6 pmol) and d₈-2-arachidonoyl glycerol (60 pmol)). The mixture was vortexed and loaded on a captiva ND lipid column (A5300635, Agilent technologies). Positive pressure was applied and the flow through was collected. The elution step was subsequently repeated with 500 μ L and 250 μ L 0.2% formic acid (vol/vol) in ACN/H₂O 95:5 (vol/vol). The combined elutes were concentrated in a speedvac and reconstituted in H₂O/MeOH 1:1 (vol/vol) for LC/MS analysis.

LC-Chip-MS/MS analysis. Endocannabinoids were measured using a chip-based nano liquid chromatography (LC) system coupled to a triple quadrupole mass spectrometer. The HPLC-Chip is inserted into the HPLC-Chip-MS interface, which mounts directly on the MS source. It includes a miniature camera for spray visualization, the loading mechanism for chip positioning, the microvalve for flow switching, and fluid connection ports for the nano-LC and microwell- plate autosampler.

Chromatographic conditions were achieved on a 1100 series LC-chip system (Agilent technologies, Walbronn, Germany) consisting of a nanoflow pump, a capillary pump, a micro well plate auto sampler with thermostat and a LC-Chip/MS interface (chipcube). The chromatographic separations were performed on an ultra-high capacity chip including a 360 nL enrichment column and a 150 mm \times 75 μ m analytical column, both packed with a Polaris-HR-chip 3 μ m C18 phase (Agilent Technologies). The mobile phase was composed of 10mM formic acid/water (A) and ACN (B). The analytical gradient was performed in two steps: first, the 8 μ L sample was loaded on the enrichment column during an isocratic enrichment phase using the capillary pump delivering a mobile phase in isocratic mode composed of 40%B at a flow rate of 2 μ L/min. The column was flushed with two wash cycles for 8min at 100%B to remove unretained components. Then, after the valve switches, a gradient starts at 45%B that linearly increases up to 80% B in 12min at a flow rate of 400nL/min. The column was then rinsed with 95%B for 2 minutes before returning to 45% B. The column was re-equilibrated for 5min prior to the next injection. The total analysis time was 20min for each run. During the analysis, the needle was washed with ACN/H₂O (1/1, v/v) commanded by an injection program.

A 6440 Triple quadrupole equipped with a nanoESI source operating in positive mode (Agilent technologies, Walbronn, Germany) was used for MS detection. Capillary voltage was set to 1800V. The drying gas was set at a flow rate of 4 L/min and the source temperature was maintained at 365°C. Quantification was obtained using static MRM (multiple reaction monitoring) mode of the transitions at m/z 379.3 \rightarrow 287.2 for 2-AG, 348.3 \rightarrow 62.2 for AEA and 387.3 \rightarrow 294.2 for 2-AG-d8, 356.3 \rightarrow 62.2 for AEA-d8 (internal standards). Mass hunter workstation (Agilent technologies) was used for instrument control. Raw MS data were processed using mass hunter quantitative analysis work station (Agilent technologies). AEA and 2AG was quantified by using an matrix matched internal standard calibration curve.

Proteomics

A schematic representation of the proteomic experiment is given in figure S2. Mouse brain proteome (500 μ L, 2.0 mg/mL) membrane or soluble fraction was incubated with vehicle (DMSO) or inhibitor (10 μ M) in DMSO for 30 minutes at rt. The proteome was labeled with MB108 (2.5 μ M, 30 minutes, rt) or FP-Biotin (5 μ M, 30 minutes, 37 °C). Subsequently the labeling reaction was quenched and excess probe was removed by chloroform methanol precipitation. Precipitated proteome was suspended in 500 μ L 6M Urea/25 mM ammonium bicarbonate and allowed to incubate for 15 minutes. 5 μ L (1 M DTT) was added and the mixture was heated to 65 °C for 15 minutes. The sample was allowed to cool to rt before 40 μ L (0.5 M) iodoacetamide was added and the sample was alkylated for 30 minutes in the dark. 140 μ L 10% (wt/vol) SDS was added and the proteome was heated for 5 minutes at 65 °C. The sample was diluted with 6 mL PBS. 100

μL of 50% slurry of Avidin–Agarose from egg white (Sigma-Aldrich) was washed with PBS and added to the proteome sample. The beads were incubated with the proteome > 2h. The beads were isolated by centrifugation and washed with 0.5% (wt/vol) SDS and PBS (3x). The proteins were digested overnight with sequencing grade trypsin (Promega) in 100 μL Pd buffer (100 mM Tris, 100 mM NaCl, 1 mM CaCl_2 , 2 % ACN and 500 ng trypsin) at 37 °C with vigorous shaking. The pH was adjusted with formic acid to pH 3 and the beads were removed. The peptides were isotopically labeled by on stage tip dimethyl labeling.

On–stage tip dimethyl labeling (adapted from Li, Kuo *et al.* 2013⁶). The stage tips were made by inserting C_{18} material in a 200 μL pipet. The stepwise procedure given in the table below was followed for stage tip desalting and dimethyl labeling. The solutions were eluted by centrifugal force and the constitutions of the reagents are given below.

Step	Solution	Centrifugation speed
Conditioning	Methanol (50 μL)	2 min 600g
Conditioning	Stage tip solution B (50 μL)	2 min 600g
Conditioning	Stage tip solution A (50 μL)	2 min 600g
Loading	Load samples on stage tips	2.5 min 800g
Washing	Stage tip solution A (100 μL)	2.5 min 800g
Dimethyl labeling	Load 20 μL L or M reagents on stage tip (5X)	5 min 400g
Washing	Stage tip solution A (100 μL)	2.5 min 800g
Elution	Stage tip solution B (100 μL)	2.5 min 800g

Stage tip solution A: Stage tip solution A is 0.5% (vol/vol) FA in H_2O . (Freshly prepared solution)

Stage tip solution B: Stage tip solution B is 0.5% (vol/vol) FA in 80% (vol/vol) ACN/ H_2O . (Freshly prepared solution).

Dimethyl labeling reagents

Light labeling reagent	Final concentration	Volume
Phosphate buffer (50 mM; pH 7.5)		900 μL
CH_2O (light)		50 μL
NaBH_3CN (0.6 M)	0.03 M	50 μL

Medium labeling reagent	Final concentration	Volume
Phosphate buffer (50 mM; pH 7.5)		900 μL
CD_2O (Medium)		50 μL
NaBH_3CN (0.6 M)	0.03 M	50 μL

After the final elution step, the desired heavy and light samples were combined and concentrated on a speedvac to remove the ACN. The residue was reconstituted in 95:3:0.1 H₂O/ACN/FA (vol/vol) before LC/MS analysis.

Tryptic peptides were analyzed on a Surveyor nanoLC system (Thermo) hyphenated to a LTQ-Orbitrap mass spectrometer (Thermo) as previously described.¹ Briefly, emitter, trap and analytical column (C18, 120 Å) were purchased from Nanoseparations (Nieuwkoop, The Netherlands) and mobile phases (A: 0.1% formic acid/H₂O, B: 0.1% formic acid/ACN) were made with ULC/MS grade solvents (Biosolve). General mass spectrometric conditions were: electrospray voltage of 1.8–2.5 kV, no sheath and auxiliary gas flow, capillary voltage 40 V, tube lens voltage 155 V and ion transfer tube temperature 150 °C. Polydimethylcyclsiloxane (*m/z* = 445.12002) and dioctyl phthalate ions (*m/z* = 391.28429) from the milieu were used as lock mass. Some 10 µl of the samples was pressure loaded on the trap column for 5 min with a 10 µl/min flow and separated with a gradient of 35 min 5%–30% B, 15 min 30%–60% B, 5 min A at a flow of 300 µl/min split to 250 nl/min by the LTQ divert valve. Full MS scans (300–2000 *m/z*) acquired at high mass resolution (60,000 at 400 *m/z*, maximum injection time 1000 ms, AGC 106) in the Orbitrap was followed by three MS/MS fragmentations in the LTQ linear ion trap (AGC 5x10³, max inj time 120 ms) from the three most abundant ions. MS/MS settings were: collision gas pressure 1.3 mT, normalized collision energy 35%, ion selection threshold of 750 counts, activation *q* = 0.25 and activation time 30 ms. Ions of *z* < 2 or unassigned were not analyzed and fragmented precursor ions were measured twice within 10 s and were dynamically excluded for 60 s. Data analysis was performed using Maxquant with acetylation (protein N term) and oxidation (M) as variable modifications. The false discovery rate was set at 1% and the peptides were screened against mouse proteome (Uniprot). Serine hydrolases that were identified in at least two repetitive experiments and for which at least 2 unique peptides were identified were considered as valid quantifiable hits.

Computational Chemistry

Docking of LEI104 in a previously reported homology model of DAGL-α was performed as described previously.¹³ The structure of LEI104 was *in silico* modified to LEI105. The geometry was optimized using a fast Dreiding-like forcefield in the presence of the protein receptor. Depicted is one possible representative LEI105-like conformer.

The active conformation of OL-135 in the previously published co-crystal structure of FAAH with OL-135 (pdb: 2WJ2)⁷ was *in silico* modified to the corresponding LEI105 heterocycle. The geometry was optimized using a fast Dreiding-like forcefield in the presence of the protein receptor. Depicted is one possible representative LEI105-like conformer.

DSI protocol

Horizontal slices (300 μm) of the hippocampus were obtained from male C57BL/6 mice (Harlan, the Netherlands) aged 14-19 days postnatal. Experiments were approved by the animal welfare committee of the University of Amsterdam. Animals were killed by decapitation, their brains quickly removed and placed in oxygenated (95% O_2 – 5% CO_2) ice cold (4 $^\circ\text{C}$) adapted artificial cerebrospinal fluid (aACSF), containing in mM: 120 choline chloride, 3.5 KCl, 0.5 CaCl_2 , 6 MgSO_4 , 1.25 NaH_2PO_4 , 25 D-glucose, 25 NaHCO_3 . Slices were cut in aACSF on a vibratome (VT1200S, Leica, Germany) and placed for 30 min in regular ACSF (containing in mM: 120 NaCl, 3.5 KCl, 25 NaHCO_3 , 25 D-glucose, 2.5 CaCl_2 , 1.3 MgSO_4 , 1.25 NaH_2PO_4) at 32 $^\circ\text{C}$. Prior to recording, slices were kept at room temperature for at least one hour. Whole-cell voltage clamp recordings were made at 32 $^\circ\text{C}$ from the soma of CA1 pyramidal neurons (holding potential $V_H = -80$ mV). Recording pipettes were pulled from borosilicate glass (Science Products, Germany) and had a resistance of 2-3 $\text{M}\Omega$ when filled with pipette solution, containing in mM: 110 KGluconate, 30 KCl, 0.5 EGTA, 10 4-(2-hydroxyethyl)-1-piperazineethanesulfonic acid (HEPES), 4 Mg-ATP, 0.5 Na-GTP. Inhibitory postsynaptic currents (IPSCs) were evoked with a glass stimulus electrode (filled with ACSF) positioned in the stratum radiatum, close to the recorded neuron. With 200- μs biphasic stimulus pulses of half-maximal intensity the IPSCs were evoked every 5 sec. 20 μM 6-cyano-7-nitroquinoxaline-2,3-dione (CNQX) and 10 μM (2*R*)-amino-5-phosphonovaleric acid (AP5) were added to the ACSF to block glutamatergic synaptic currents and 5 μM carbachol to enhance inhibitory input. Recordings were made using an Axopatch 200B (Molecular Devices, USA) and in-house software running under Matlab (MathWorks, USA). Signals were low-pass filtered at 5 kHz and sampled at 10 kHz. Series resistance ranged from 5–15 $\text{M}\Omega$ and was compensated to ~65%. Voltage signals were corrected for liquid junction potential.

Stock solutions (10 mM) of LEI105 were made in dimethylsulfoxide (DMSO), which was diluted to the final concentration (10 μM) in ACSF. Recordings were made from CA1 neurons in slices that were pre-incubated with 10 μM LEI105 for at least 30 min; during the experiment this concentration was continuously present. Control experiments were performed on neurons recorded in slices pre-incubated with and in the continuous presence of 0.1% DMSO.

For each CA1 neuron IPSCs were evoked with 5 sec intervals during a 2-min baseline period, prior to the stimulus evoking depolarization-induced suppression of inhibition (DSI). The maximum amplitude of each IPSC was determined and the mean value of the IPSC amplitudes over this period was calculated and used to normalize the evoked synaptic response. DSI was induced by depolarizing the neuron from -80 to 0 mV for 5 sec. The normalized IPSC current amplitudes as a function of time were averaged and used for comparison between both treatments (Fig. 4B; control, $n=18$ neurons; LEI105, $n=15$ neurons). In control conditions the DSI protocol induced a short-lasting reduction of the

IPSC amplitude, which returned to baseline level with a single exponential time course. This recovery phase of the DSI response was fitted with a single exponential function and the time constant value obtained from this fit ($\tau = 34$ sec) also correctly fitted the decay measured in the neurons treated with LEI105. DSI was then quantified as the relative reduction in the mean IPSC amplitude during the first 15 sec after DSI induction (Fig. 4C). DSI amplitudes were compared with Student's t-test, using $p < 0.05$ to indicate a significant difference.

References

1. Katona, I.; Freund, T. F. *Annu. Rev. Neurosci.* **2012**, *35*, 529.
2. Devane, W. A.; Hanus, L.; Breuer, A.; Pertwee, R. G.; Stevenson, L. A.; Griffin, G.; Gibson, D.; Mandelbaum, A.; Etinger, A.; Mechoulam, R. *Science* **1992**, *258*, 1946.
3. Sugiura, T.; Kondo, S.; Sukagawa, A.; Nakane, S.; Shinoda, A.; Itoh, K.; Yamashita, A.; Waku, K. *Biochem. Biophys. Res. Commun.* **1995**, *215*, 89.
4. Mechoulam, R.; Ben-Shabat, S.; Hanus, L.; Ligumsky, M.; Kaminski, N. E.; Schatz, A. R.; Gopher, A.; Almog, S.; Martin, B. R.; Compton, D. R.; Pertwee R.G.; Griffin G.; Bayewitch M.; Barg J.; Vogel Z. *Biochem. Pharmacol.* **1995**, *50*, 83.
5. Gao, Y.; Vasilyev, D. V.; Goncalves, M. B.; Howell, F. V.; Hobbs, C.; Reisenberg, M.; Shen, R.; Zhang, M. Y.; Strassle, B. W.; Lu, P.; Mark, L.; Piesla, M. J.; Deng, K.; Kouranova, E. V.; Ring, R. H.; Whiteside, G. T.; Bates, B.; Walsh, F. S.; Williams, G.; Pangalos, M. N.; Samad, T. A.; Doherty, P. *J. Neurosci.* **2010**, *30*, 2017.
6. Di Marzo, V. *Nat. rev. Drug disc.* **2008**, *7*, 438.
7. Blankman, J. L.; Cravatt, B. F. *Pharmacol. Rev.* **2013**, *65*, 849.
8. Bisogno, T.; Howell, F.; Williams, G.; Minassi, A.; Cascio, M. G.; Ligresti, A.; Matias, I.; Schiano-Moriello, A.; Paul, P.; Williams, E. J.; Gangadharan, U.; Hobbs, C.; Di Marzo, V.; Doherty, P. *J. Cell Biol.* **2003**, *163*, 463.
9. Reisenberg, M.; Singh, P. K.; Williams, G.; Doherty, P. *Philos. Trans. R. Soc. Lond., B, Biol. Sci.* **2012**, *367*, 3264.
10. Tanimura, A.; Yamazaki, M.; Hashimoto, Y.; Uchigashima, M.; Kawata, S.; Abe, M.; Kita, Y.; Hashimoto, K.; Shimizu, T.; Watanabe, M.; Sakimura, K.; Kano, M. *Neuron* **2010**, *65*, 320.
11. Appiah, K. K.; Blat, Y.; Robertson, B. J.; Pearce, B. C.; Pedicord, D. L.; Gentles, R. G.; Yu, X. C.; Mseeh, F.; Nguyen, N.; Swaffield, J. C.; Harden, D. G.; Westphal, R. S.; Banks, M. N.; O'Connell, J. C. *J. Biomol. Screen.* **2014**, *19*, 595.
12. Janssen, F. J.; Deng, H.; Baggelaar, M. P.; Allara, M.; van der Wel, T.; den Dulk, H.; Ligresti, A.; van Esbroeck, A. C. M.; McGuire, R.; Di Marzo, V.; Overkleeft, H. S.; van der Stelt, M. *J. Med. Chem.* **2014**, *57*, 6610.
13. Bisogno, T.; Mahadevan, A.; Coccurello, R.; Chang, J. W.; Allara, M.; Chen, Y.; Giacobuzzo, G.; Lichtman, A.; Cravatt, B.; Moles, A.; Di Marzo, V. *Br. J. Pharmacol.* **2013**, *169*, 784.
14. Ortar, G.; Bisogno, T.; Ligresti, A.; Morera, E.; Nalli, M.; Di Marzo, V. *J. Med. Chem.* **2008**, *51*, 6970.
15. Hsu, K. L.; Tsuboi, K.; Adibekian, A.; Pugh, H.; Masuda, K.; Cravatt, B. F. *Nat. Chem. Biol.* **2012**, *8*, 999.

16. Niphakis, M. J.; Cravatt, B. F. *Annu. Rev. Biochem.* **2014**, *83*, 341.
17. Heal, W. P.; Dang, T. H.; Tate, E. W. *Chem. Soc. Rev.* **2011**, *40*, 246.
18. Liu, Y.; Patricelli, M. P.; Cravatt, B. F. *Proc. Natl. Acad. Sci. U. S. A.* **1999**, *96*, 14694.
19. Hoover, H. S.; Blankman, J. L.; Niessen, S.; Cravatt, B. F. *Bioorg. Med. Chem. Lett.* **2008**, *18*, 5838.
20. Yang, P. Y.; Liu, K.; Ngai, M. H.; Lear, M. J.; Wenk, M. R.; Yao, S. Q. *J. Am. Chem. Soc.* **2010**, *132*, 656.
21. Baggelaar, M. P.; Janssen, F. J.; van Esbroeck, A. C.; den Dulk, H.; Allara, M.; Hoogendoorn, S.; McGuire, R.; Florea, B. I.; Meeuwenoord, N.; van den Elst, H.; van der Marel, G. A.; Brouwer, J.; Di Marzo, V.; Overkleeft, H. S.; van der Stelt, M. *Angew. Chem. Int. Ed.* **2013**, *52*, 12081.
22. Fowler, C. J. *Fundam. Clin. Pharmacol.* **2006**, *20*, 549.
23. Boger, D. L.; Sato, H.; Lerner, A. E.; Hedrick, M. P.; Fecik, R. A.; Miyauchi, H.; Wilkie, G. D.; Austin, B. J.; Patricelli, M. P.; Cravatt, B. F. *Proc. Natl. Acad. Sci. U. S. A.* **2000**, *97*, 5044.
24. Pedicord, D. L.; Flynn, M. J.; Fanslau, C.; Miranda, M.; Hunihan, L.; Robertson, B. J.; Pearce, B. C.; Yu, X. C.; Westphal, R. S.; Blat, Y. *Biochem. Biophys. Res. Commun.* **2011**, *411*, 809.
25. van der Wel, T.; Janssen, F. J.; Baggelaar, M. P.; Deng, H.; den Dulk, H.; Overkleeft, H. S.; van der Stelt, M. *J. Lipid Res.* **2015**, *56*, 927.
26. Mileni, M.; Garfinkle, J.; DeMartino, J. K.; Cravatt, B. F.; Boger, D. L.; Stevens, R. C. *J. Am. Chem. Soc.* **2009**, *131*, 10497.
27. Bachovchin, D. A.; Ji, T.; Li, W.; Simon, G. M.; Blankman, J. L.; Adibekian, A.; Hoover, H.; Niessen, S.; Cravatt, B. F. *Proc. Natl. Acad. Sci. U. S. A.* **2010**, *107*, 20941.
28. Jung, K. M.; Astarita, G.; Thongkham, D.; Piomelli, D. *Mol. Pharmacol.* **2011**, *80*, 60.
29. Ohno-Shosaku, T.; Maejima, T.; Kano, M. *Neuron* **2001**, *29*, 729.
30. Wilson, R. I.; Nicoll, R. A. *Nature* **2001**, *410*, 588.
31. Hashimotodani, Y.; Ohno-Shosaku, T.; Kano, M. *J. Neurosci.* **2007**, *27*, 1211.
32. Hashimotodani, Y.; Ohno-Shosaku, T.; Maejima, T.; Fukami, K.; Kano, M. *Neuropharmacol.* **2008**, *54*, 58.
33. Hashimotodani, Y.; Ohno-Shosaku, T.; Tanimura, A.; Kita, Y.; Sano, Y.; Shimizu, T.; Di Marzo, V.; Kano, M. *J. Physiol.* **2013**, *591*, 4765.
34. Edwards, D. A.; Zhang, L. H.; Alger, B. E. *Proc. Natl. Acad. Sci. U. S. A.* **2008**, *105*, 8142.
35. Zhang, L. H.; Wang, M. N.; Bisogno, T.; Di Marzo, V.; Alger, B. E. *Plos One* **2011**, *6*.

36. Szabo, B.; Urbanski, M. J.; Bisogno, T.; Di Marzo, V.; Mendiguren, A.; Baer, W. U.; Freiman, I. *J. Physiol.* **2006**, 577, 263.
37. Edwards, D. A.; Kim, J.; Alger, B. E. *J. Neurophysiol.* **2006**, 95, 67.
38. Min, R.; Testa-Silva, G.; Heistek, T. S.; Canto, C. B.; Lodder, J. C.; Bisogno, T.; Di Marzo, V.; Brussaard, A. B.; Burnashev, N.; Mansvelder, H. D. *J. Neurosci.* **2010**, 30, 2710.
39. Min, R.; Di Marzo, V.; Mansvelder, H. D. *Neuroscientist* **2010**, 16, 608.
40. Alger, B. E.; Kim, J. *Trends Neurosci.* **2011**, 34, 304.
41. Kunos, G.; Tam, J. *Br. J. Pharmacol.* **2011**, 163, 1423.

CHAPTER 5

Structure Activity Relationship of LEI105*

Introduction

Diacylglycerol lipase- α and - β (DAGL- α and DAGL- β) are the two main enzymes responsible for the production of the endocannabinoid 2-arachidonoylglycerol (2-AG). Both isoforms have a tissue specific contribution to 2-AG biosynthesis. DAGL- α is the main enzyme responsible for the production of 2-AG in the CNS, while DAGL- β has a more pronounced role in the periphery.^{1,2} In addition to congenital knockout of DAGL- α , small molecule inhibitors that acutely inhibit DAGL- α activity are required to study the physiological role of DAGL- α . The DAGL inhibitors known to date can be divided in six different chemotypes (for review see Janssen *et al.*)³. Bis-oximino-carbamates,⁴ β -lactones,^{4,5} fluorophosphonates^{6,7} and 1,2,3-triazole ureas^{8,9} can be classified as irreversible inhibitors. Glycine sulfonamides^{10,11} and α -ketoheterocycles¹²⁻¹⁴ are reversible inhibitors. In chapters 3 and 4, LEI104 and LEI105 are described as α -ketoheterocycle-based DAGL inhibitors, which display high potency and selectivity over other serine hydrolases.^{13,14} They have a reversible mode-of-action, which results in a lower probability of inducing idiosyncratic toxic effects. This makes the α -ketoheterocycles a promising chemotype for further development of DAGL inhibitors.

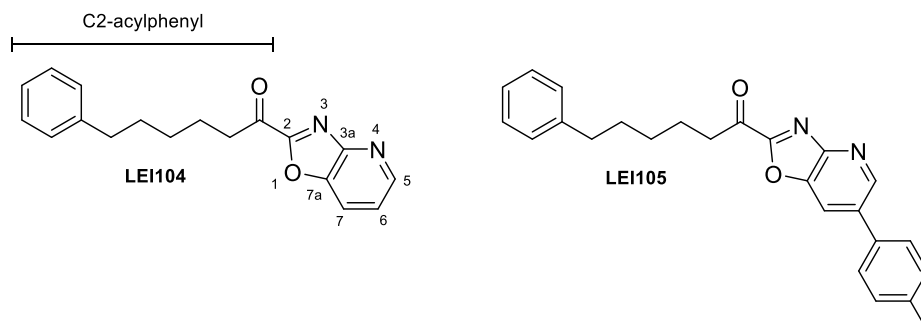


Figure 1. Structure of α -ketoheterocyclic DAGL inhibitors LEI104 and LEI105.

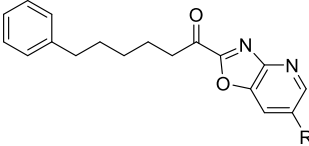
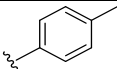
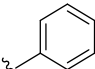
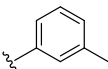
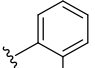
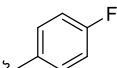
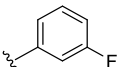
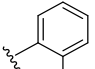
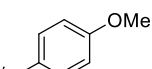
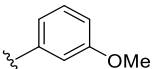
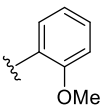
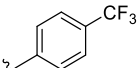
*Published as part of: Janssen, F. J.; Baggelaar, M. P.; Hummel, J. J. A.; van Boeckel, C. A. A.; van der Stelt, M. Pharmaceutically active compounds as DAG-lipase inhibitors, European patent Number EP15169052.6. Filing date 23 May 2016; publication date 22 November 2016.

Janssen *et al.*¹⁴ investigated the structural requirements for the interaction of α -ketoheterocycles with DAGL- α . A 1040-membered focused library of FAAH inhibitors, mainly consisting of previously published α -ketoheterocycles and their corresponding precursors, was screened for DAGL- α inhibition. In addition, 19 new α -ketoheterocycles were synthesized to complement the structure activity relationships. The focused library included benzoxazole, benzothiazole, benzimidazole and their 4-pyridine analogs. The screen revealed that the oxazolo-4N-pyridine was the most potent scaffold for DAGL- α inhibition. Investigation of the C2-acylphenyl spacer length revealed that the inhibitor with a 5-carbon spacer with a distal phenyl group showed the highest lipophilic efficiency (LipE: calculated as $\text{LipE} = \text{pIC}_{50} - \text{cLogP}$). In summary, this study revealed that LEI104 was the most optimal DAGL- α inhibitor from a 1059 member α -ketoheterocycle-based focused library (Figure 1). Introduction of a *para*-tolyl group at the 6-position of the oxazolopyridine of LEI104 produced the highly potent and selective dual DAGL- α/β inhibitor LEI105,¹³ as described in the previous chapter. It was observed that a *p*-tolyl group completely removed cross-reactivity with fatty acid amide hydrolase (FAAH), the enzyme responsible for the degradation of the other endocannabinoid anandamide. However, little is known about the effect of different substituents at the C6 position of LEI104. Therefore, the structure activity relationship of substituents at this position was investigated.

Results and Discussion

A similar strategy as the synthesis towards LEI105, as described in chapter 4, was used for the synthesis of α -ketoheterocycles **1** to **18**. The inhibitory potency of the compounds against *h*DAGL- α was tested in a concentration-response experiment using a colorimetric DAGL- α activity assay based on the hydrolysis of *para*-nitrophenylbutyrate.¹² The activity of the inhibitors against native mouse DAGL- α was evaluated in an orthogonal assay using activity-based protein profiling with MB064 in mouse brain membrane proteome.¹² Inhibitor selectivity was investigated by pre-incubation of mouse brain membrane proteome with inhibitor (10 μM) and subsequent labeling with MB064 (250 nM) or TAMRA-FP (500 nM) as described in chapter 4. A summary of the results of these assays is given in Table 1. The biological characterization revealed that replacing the *p*-tolyl group of LEI105 with a phenyl **1** had no effect on the inhibitory potency on DAGL- α in the ABPP assay. However, this inhibitor (10 μM) showed slightly reduced labeling of FAAH as measured with TAMRA-FP in mouse brain proteome. This is in line with the hypothesis in the previous chapter that the methyl group of LEI105 has a steric clash with FAAH. Changing the position of the methyl group to the *ortho*- **3** or *meta*- **2** position, or replacement of the methyl groups by fluorides on the *para*- **4**, *meta*- **5** or *ortho*-position **6** had little effect on the inhibitory potency against DAGL- α compared to LEI105 in the ABPP and PNP-assay. A methoxy group at the *meta*- or *para*-position reduced the potency of the inhibitors in the

Table 1. Summary of the biological characterization of the inhibitors described in this chapter.

<div>  </div>						
Compound	R	PNP assay pIC ₅₀ ± SEM (N = 2, n = 2)	ABPP pIC ₅₀ ± SEM (n = 3)	ABPP FAAH % inhibition ± SD [10 μM] (n = 3)	cLogP ^a	LipE (PNP- assay)
LEI105		8.5 ± 0.06	7.5 ± 0.1	2 ± 5	6.5	2.1
1		9.2 ± 0.05	7.5 ± 0.1	20 ± 2	6.0	3.2
2		8.8 ± 0.03	7.2 ± 0.1	15 ± 6	6.5	2.3
3		8.5 ± 0.06	7.5 ± 0.1	41 ± 1	6.2	2.3
4		8.4 ± 0.08	7.5 ± 0.1	3 ± 4	6.1	2.3
5		8.7 ± 0.10	7.4 ± 0.1	5 ± 8	6.1	2.6
6		8.7 ± 0.08	7.4 ± 0.1	23 ± 2.8	6.1	2.6
7		8.6 ± 0.04	7.1 ± 0.1	11 ± 4	6.0	2.6
8		8.7 ± 0.05	7.1 ± 0.1	29 ± 35	6.0	2.7
9		8.5 ± 0.06	7.6 ± 0.1	50 ± 4	5.4	3.1
10		9.0 ± 0.03	7.5 ± 0.1	12 ± 13	6.8	2.2

Compound	R	PNP assay pIC ₅₀ ± SEM (N = 2, n = 2)	ABPP pIC ₅₀ ± SEM (n = 3)	ABPP FAAH % inhibition ± SD [10 µM] (n = 3)	cLogP*	LipE (PNP- assay)
11		8.5 ± 0.10	6.5 ± 0.2	3 ± 5	5.9	2.6
12		8.7 ± 0.04	7.3 ± 0.1	67 ± 9	5.4	3.3
13		8.5 ± 0.03	7.1 ± 0.1	31 ± 12	5.4	3.1
14		8.8 ± 0.03	7.6 ± 0.1	24 ± 11	5.4	3.4
15		9.0 ± 0.05	7.5 ± 0.08	40 ± 4	5.6	3.4
16		9.0 ± 0.04	7.7 ± 0.05	17 ± 4	5.5	3.5
17		6.5 ± 0.26	6.9 ± 0.1	66 ± 3	4.5	2.0
18		8.7 ± 0.04	6.9 ± 0.03	84 ± 2	5.3	3.4

*cLogP was estimated with ChemBioDraw Ultra, version 14.0.0.117.

ABPP assay. Remarkably, the activity of the inhibitor with a methoxy group on the *ortho*-position **9** remained similar to LEI105 with a pIC₅₀ of 7.6 ± 0.02 in the ABPP assay. However, **9** also showed the highest activity towards FAAH. A trend emerges that compounds featuring substituents at the *ortho*-position show the highest, and substituents at the *para*-position the lowest activity against FAAH (Figure 2). Introduction of an electron withdrawing CF₃ group at the *para*-position did not influence inhibitor activity, while introduction of an electron donating ester group at the same position decreased the inhibitory activity as measured with the ABPP assay. Introduction of a cyano substituent at the *ortho*- or *para*-position had little effect on the potency against DAGL-α, while at the

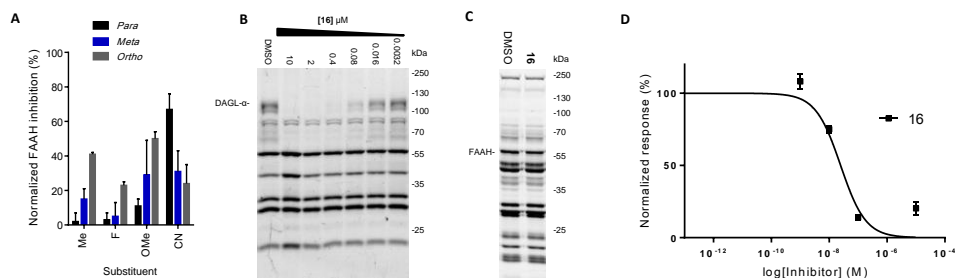


Figure 2. A) Effect of substituents at the ortho, meta or para position on the labeling of FAAH by the fluorophosphonate-based ABP (TAMRA-FP). Substituents: Me = methyl, F = fluoro, OMe = methoxy, CN = Cyano. B) Example of a dose response gel using ABP MB064 (250 nM) and inhibitor **16** in the mouse brain membrane proteome. C) Example gel of the selectivity assay, 30 min. preincubation with **16** (10 μ M) in the mouse brain membrane proteome, followed by labeling with TAMRA-FP (500 nM) for 15 minutes. D) Dose response curve of **16** in a real-time, fluorescent natural substrate-based assay.

meta-position it reduced the pIC_{50} to 7.1 ± 0.03 in the ABPP assay. Interestingly, the cyano group at the *para*-position showed the highest activity against FAAH, compared to the same substituent at the *ortho*- or *meta*-position (Figure 2). Double substituted inhibitor **15** showed good potency in both the ABPP assay and the colorimetric assay, but reduced FAAH labeling by 40%. Compound **16** showed an improved potency in both the colorimetric assay and the ABPP assay, compared to LEI105, while reducing FAAH activity with only 17% at 10 μ M. Introduction of a pyridine **17** or a N-methyl pyrrole **18**, decreased activity against DAGL- α and increased activity against FAAH compared to LEI105. Compound **16** displayed the highest lipophilic efficiency (LiPE) and reduced labeling of FAAH with less than 25% at 10 μ M. Therefore, this compound was analyzed further in a real-time, fluorescent natural substrate-based assay as described previously.¹⁵ The inhibitor showed high activity in the natural substrate assay with a pIC_{50} of 7.6 ± 0.1 (Figure 2).

Conclusions

This chapter described the synthesis and the structure activity relationship of a series of LEI105 analogues. Variations have been made on the *p*-toluyl group of LEI105. None of the substituents tested in this chapter completely abolished activity against DAGL- α , this might indicate that the *p*-toluyl group of LEI105 and the R-groups tested in this chapter reside in a large binding pocket of DAGL- α . A general trend for FAAH off-target activity (*ortho* > *meta* > *para*) was observed, except for cyano substituted phenyls.

Compound **16** showed the highest activity in the ABPP activity assay and had the highest LiPE in the colorimetric assay and reduced labeling of FAAH with less than 25% at 10 μ M. The newly identified inhibitor has a LiPE of 3.5, which is a strong improvement compared to LEI105 with a LiPE of 2.1. The activity of **16** against *h*DAGL- α was tested in

a natural substrate assay and proved to be potent in this assay (pIC_{50} **16**: 7.6 ± 0.1). In view of this attractive pharmacological profile, further *in situ* and *in vivo* studies are warranted.

Experimental Methods

Synthetic procedures

General remarks

All reactions were performed using oven or flame-dried glassware and dry solvents. Reagents were purchased from Sigma Aldrich, Acros and Merck and used without further purification unless noted otherwise. All moisture sensitive reactions were performed under an argon atmosphere. Traces of water were removed from starting compounds by co-evaporation with toluene.

^1H - and ^{13}C -NMR spectra were recorded on a Bruker AV 400 MHz spectrometer at 400.2 (^1H) and 100.6 (^{13}C) MHz or a Bruker DMX-600 spectrometer 600 (^1H) and 150 (^{13}C) MHz using CDCl_3 or CD_3OD as solvent, unless stated otherwise. Chemical shift values are reported in ppm with tetramethylsilane or solvent resonance as the internal standard (CDCl_3 δ 7.26 for ^1H , δ 77.0 for ^{13}C , CD_3OD : δ 3.31 for ^1H). Data are reported as follows: chemical shifts (δ), multiplicity (s = singlet, d = doublet, dd = double doublet, td = triple doublet, t = triplet, q = quartet, quint = quint, br = broad, m = multiplet), coupling constants J (Hz), and integration. HPLC purification was performed on a preparative LC-MS system (Agilent 1200 serie) with an Agilent 6130 Quadrupole MS detector. High-resolution mass spectra (HRMS) were recorded on a Thermo Scientific LTQ Orbitrap XL. Flash chromatography was performed using SiliCycle silica gel type SiliaFlash P60 (230 – 400 mesh). TLC analysis was performed on Merck silica gel 60/Kieselguhr F254, 0.25 mm. Compounds were visualized using either Seebach's reagent (a mixture of phosphomolybdic acid (25 g), cerium (IV) sulfate (7.5 g), H_2O (500 mL) and H_2SO_4 (25 mL)) or a KMnO_4 stain (K_2CO_3 (40 g), KMnO_4 (6 g), H_2O (600 mL) and 10% NaOH (5 mL)).

2-amino-5-(o-tolyl)pyridin-3-ol (19): 2-methylphenylboronic acid (400 mg, 2.96 mmol), 2-amino-5-bromopyridin-3-ol (558 mg, 2 mmol) and Cs_2CO_3 (845 mg, 2.6 mmol) were dissolved in 10 mL DME/ H_2O (10:1). The mixture was degassed under a flow of argon. $\text{Pd}(\text{Ph}_3)_4$ (116 mg, 0.1 mmol) was added and the mixture was stirred at 85 °C for 12 h. The reaction mixture was allowed to cool to rt and H_2O (10 mL) was added. The reaction mixture was extracted with EtOAc. The organic layer was dried NaSO_4 and concentrated under reduced pressure. The residue was taken up in pentane/ EtOAc (1:1) and filtered over a pad of silica. The filtrate was concentrated and the crude 3-(benzyloxy)-5-(o-tolyl)pyridin-2-amine was used for the next reaction.

The crude 3-(benzyloxy)-5-(o-tolyl)pyridin-2-amine was dissolved in MeOH (20 mL) and 0.1 equivalent 10% Pd/C was added. The mixture was stirred under H_2 atmosphere for 12 h at rt. The reaction mixture was filtered over celite and concentrated under reduced pressure. The residue was purified by flash chromatography over silica gel using $\text{CH}_2\text{Cl}_2/\text{MeOH}$ (9:1). This yielded 2-amino-5-(o-tolyl)pyridin-3-ol (165 mg, 0.82 mmol,

41% over two steps). ^1H NMR (400 MHz, DMSO) δ 7.42 (d, J = 1.9 Hz, 1H), 7.32 – 7.20 (m, 3H), 7.19 – 7.13 (m, 1H), 7.06 (d, J = 1.9 Hz, 1H), 2.24 (s, 3H). ^{13}C NMR (101 MHz, DMSO) δ 148.18, 140.20, 137.37, 135.13, 130.73, 130.47, 129.52, 127.50, 126.11, 125.65, 120.88, 20.15.

6-phenyl-1-(6-(o-tolyl)oxazolo[4,5-b]pyridin-2-yl)hexan-1-ol (20): Compound **19** (70 mg, 0.35 mmol) was dissolved in EtOH (4 mL), Pyridine (28 μL , 0.35 mmol) was added and the mixture was heated for 15 min to 85 $^\circ\text{C}$ using. Imidate **7** (174 mg, 0.70 mmol) dissolved in EtOH (1.0 mL) was added and the mixture was heated to 85 $^\circ\text{C}$ for 12 h. The reaction mixture was concentrated under reduced pressure and purified by flash chromatography over silica gel using

Pentane/EtOAc (3:1) \rightarrow (2:1). This yielded **27** (16 mg, 0.04 mmol; 6.0 %) as a colorless oil. ^1H NMR (400 MHz, CDCl_3) δ 8.52 (d, J = 1.6 Hz, 1H), 7.78 (d, J = 1.8 Hz, 1H), 7.33 (dt, J = 7. , 3.8 Hz, 2H), 7.29 – 7.22 (m, 3H), 7.19 – 7.12 (m, 4H), 5.14 – 4.92 (m, 1H), 2.60 (t, J = 17.2, 9.4 Hz, 2H), 2.28 (s, 3H), 2.19 – 1.93 (m, 2H), 1.73 – 1.49 (m, 4H), 1.49 – 1.30 (m, 2H). ^{13}C NMR (101 MHz, CDCl_3) δ 171.24, 153.65, 147.16, 142.84, 142.51, 137.42, 135.75, 134.96, 130.71, 130.21, 128.42 (2C), 128.36 (2C), 128.23, 126.20, 125.63, 119.10, 68.20, 35.78, 35.41, 31.21, 28.88, 24.76, 20.42.

6-phenyl-1-(6-(o-tolyl)oxazolo[4,5-b]pyridin-2-yl)hexan-1-one (3): To a solution of **20** (15 mg, 0.04 mmol) in CH_2Cl_2 (2 mL) was added Dess-Martin periodinane (25 mg, 0.06 mmol) and the reaction mixture was stirred under argon atmosphere overnight. The reaction mixture was quenched with saturated NaHCO_3 (aq). The layers were separated and the organic layer was extracted with CH_2Cl_2 . The combined organic layers were washed with brine, dried on MgSO_4 , filtered and concentrated under reduced pressure. The residue was purified by flash chromatography over silica gel using toluene/ethyl acetate (90:10) with 1% Et₃N. This yielded **3** (12 mg, 0.031 mmol, 78%) as a colorless oil. (^1H NMR (400 MHz, CDCl_3) δ 8.73 (s, 1H), 7.93 (d, J = 1.8 Hz, 1H), 7.41 – 7.26 (m, 6H), 7.19 (d, J = 7.3 Hz, 3H), 3.30 (t, J = 7.4 Hz, 2H), 2.71 – 2.59 (m, 2H), 2.30 (s, 3H), 1.95 – 1.83 (m, 2H), 1.70 (dd, J = 15.4, 7.7 Hz, 2H), 1.50 (dd, J = 12.5, 5.2 Hz, 2H). ^{13}C NMR (101 MHz, CDCl_3) δ 190.41, 158.86, 153.04, 149.86, 143.60, 142.54, 138.10, 137.11, 135.84, 131.03, 130.30, 128.96, 128.55 (2C), 128.44 (2C), 126.51, 125.85, 120.45, 39.89, 35.85, 31.29, 28.84, 23.89, 20.55. HRMS (ESI+) m/z : calculated for $\text{C}_{25}\text{H}_{24}\text{N}_2\text{O}_2$ ($M + H$) 385.1911; found 385.1914. Purity \geq 95% as determined by LC/MS.

2-amino-5-phenylpyridin-3-ol (21): The title compound was synthesized from 2-amino-5-bromopyridin-3-ol (500 mg, 1.8 mmol) and phenylboronic acid (262 mg, 2.2 mmol) according to the procedures described for compound **19**. This yielded 2-amino-5-phenylpyridin-3-ol (200 mg, 1.1 mmol, 61%). ^1H NMR (400 MHz, DMSO) δ 9.70 (s, 1H), 7.78 (d, J = 2.0 Hz, 1H), 7.51 (d, J = 7.3 Hz, 2H), 7.41 (t, J = 7.7 Hz, 2H), 7.34 – 7.19 (m,

2H), 7.13 (d, $J = 2.0$ Hz, 1H), 5.66 (s, 1H). ^{13}C NMR (101 MHz, DMSO) δ 150.07, 139.32, 138.33, 135.28, 128.91 (2C), 126.31, 125.53 (2C), 124.97, 116.79.

6-phenyl-1-(6-phenyloxazolo[4,5-b]pyridin-2-yl)hexan-1-ol (22): The title compound was synthesized from **21** (67 mg, 0.36 mmol) according to the procedures described for **20**. This yielded 6-phenyl-1-(6-phenyloxazolo[4,5-b]pyridin-2-yl)hexan-1-ol (38 mg, 0.10 mmol, 28%) ^1H NMR (400 MHz, CDCl_3) δ 8.72 (d, $J = 1.9$ Hz, 1H), 7.97 (d, $J = 1.9$ Hz, 1H), 7.59 – 7.37 (m, 3H), 7.28 – 7.02 (m, 6H), 5.09 – 4.93 (m, 1H), 2.68 – 2.50 (m, 2H), 2.13 – 1.92 (m, 2H), 1.70 – 1.30 (m, 6H). ^{13}C NMR (101 MHz, CDCl_3) δ 172.04, 153.97, 145.48, 143.57, 142.63, 137.31, 134.94, 129.40 (2C), 128.48 (2C), 128.35 (2C), 127.66 (2C), 125.75, 125.73, 117.41, 68.23, 35.92, 35.46, 34.15, 31.38, 29.02.

6-phenyl-1-(6-phenyloxazolo[4,5-b]pyridin-2-yl)hexan-1-one (1): The title compound was synthesized from **22** (35 mg, 0.094 mmol) according to the procedure described for **3**. This yielded 6-phenyl-1-(6-phenyloxazolo[4,5-b]pyridin-2-yl)hexan-1-one (27 mg, 0.072 mmol, 78%) ^1H NMR (400 MHz, CDCl_3) δ 8.99 (d, $J = 2.0$ Hz, 1H), 8.12 (d, $J = 2.0$ Hz, 1H), 7.65 (dd, $J = 5.3, 3.4$ Hz, 2H), 7.58 – 7.51 (m, 2H), 7.48 (ddd, $J = 7.3, 3.6, 1.3$ Hz, 1H), 7.33 – 7.22 (m, 2H), 7.22 – 7.12 (m, 3H), 3.29 (t, $J = 7.4$ Hz, 2H), 2.71 – 2.60 (m, 2H), 1.88 (dt, $J = 15.1, 7.5$ Hz, 2H), 1.71 (dt, $J = 15.4, 7.6$ Hz, 2H), 1.57 – 1.41 (m, 2H). ^{13}C NMR (101 MHz, CDCl_3) δ 190.35, 158.88, 153.41, 148.40, 144.16, 142.53, 137.65, 137.03, 129.54 (2C), 129.00, 128.54 (2C), 128.43 (2C), 127.84 (2C), 125.84, 118.18, 39.87, 35.84, 31.29, 28.84, 23.86. HRMS (ESI+) m/z : calculated for $\text{C}_{24}\text{H}_{22}\text{N}_2\text{O}_2$ ($M + H$) 371.1754; found 371.1754. Purity $\geq 95\%$ as determined by LC/MS.

2-amino-5-(*m*-tolyl)pyridin-3-ol (23): The title compound was synthesized from 2-amino-5-bromopyridin-3-ol (418 mg, 1.5 mmol) and *m*-tolylboronic acid (300 mg, 2.2 mmol) according to the procedures described for compound **19**. This yielded 2-amino-5-(*m*-tolyl)pyridin-3-ol (220 mg, 1.1 mmol, 73%). ^1H NMR (400 MHz, DMSO) δ 9.65 (s, 1H), 7.77 (d, $J = 1.8$ Hz, 1H), 7.47 – 7.21 (m, 3H), 7.21 – 6.97 (m, 2H), 5.63 (s, 2H), 2.35 (s, 3H). ^{13}C NMR (101 MHz, DMSO) δ 149.95, 139.25, 138.22, 137.91, 135.20, 128.75, 126.94, 126.16, 125.05, 122.63, 116.82, 21.12.

6-phenyl-1-(6-(*m*-tolyl)oxazolo[4,5-b]pyridin-2-yl)hexan-1-ol (24): The title compound was synthesized from **23** (107 mg, 0.53 mmol) according to the procedures described for **20**. This yielded 6-phenyl-1-(6-(*m*-tolyl)oxazolo[4,5-b]pyridin-2-yl)hexan-1-ol (76 mg, 0.20 mmol, 37%). ^1H NMR (400 MHz, CDCl_3) δ 8.70 (d, $J = 1.7$ Hz, 1H), 7.91 (d, $J = 1.7$ Hz, 1H), 7.43 – 7.28 (m, 3H), 7.28 – 7.18 (m, 3H), 7.14 (t, $J = 6.9$ Hz, 3H), 5.13 – 4.98 (m, 1H), 2.65 – 2.52 (m, 2H), 2.42 (s, 3H), 2.11 – 1.91 (m, 2H), 1.73 – 1.46 (m, 4H), 1.46 – 1.30 (m, 2H). ^{13}C NMR (101 MHz, CDCl_3) δ 171.65, 154.05, 145.56, 143.41, 142.63,

139.02, 137.40, 134.76, 129.20, 129.10, 128.43 (2C), 128.32, 128.30 (2C), 125.68, 124.71, 117.02, 68.14, 35.88, 35.42, 31.33, 29.03, 24.95, 21.59.

6-phenyl-1-(6-(m-tolyl)oxazolo[4,5-b]pyridin-2-yl)hexan-1-one (2): The title compound was synthesized from **24** (60 mg, 0.16 mmol) according to the procedure described for **3**. This yielded 6-phenyl-1-(6-(m-tolyl)oxazolo[4,5-b]pyridin-2-yl)hexan-1-one (45 mg, 0.12 mmol, 76%). ^1H NMR (400 MHz, CDCl_3) δ 8.97 (d, $J = 1.9$ Hz, 1H), 8.09 (d, $J = 2.0$ Hz, 1H), 7.47 – 7.39 (m, 3H), 7.32 – 7.23 (m, 3H), 7.17 (dd, $J = 10.9, 4.4$ Hz, 3H), 3.28 (dd, $J = 9.4, 5.4$ Hz, 2H), 2.69 – 2.57 (m, 2H), 2.46 (s, 3H), 1.87 (dt, $J = 15.1, 7.5$ Hz, 2H), 1.70 (dt, $J = 15.4, 7.6$ Hz, 2H), 1.55 – 1.43 (m, 2H). ^{13}C NMR (101 MHz, CDCl_3) δ 190.30, 158.80, 153.29, 148.38, 144.13, 142.50, 139.29, 137.76, 136.97, 129.71, 129.40, 128.51 (2C), 128.40 (2C), 125.81, 124.93, 118.09, 39.83, 35.81, 31.26, 28.81, 23.83, 21.64. HRMS (ESI+) m/z : calculated for $\text{C}_{25}\text{H}_{24}\text{N}_2\text{O}_2$ ($M + H$) 385.1911; found 385.1914. Purity $\geq 95\%$ as determined by LC/MS.

2-amino-5-(4-fluorophenyl)pyridin-3-ol (35): The title compound was synthesized from 2-amino-5-bromopyridin-3-ol (300 mg, 1.08 mmol) and 4-fluorophenylboronic acid (180 mg, 1.3 mmol) according to the procedures described for compound **19**. This yielded 2-amino-5-(4-fluorophenyl)pyridin-3-ol (100 mg, 0.5 mmol, 50%). ^1H NMR (400 MHz, DMSO) δ 9.67 (s, 1H), 7.73 (d, $J = 2.0$ Hz, 1H), 7.62 – 7.44 (m, 2H), 7.37 – 7.13 (m, 2H), 7.07 (d, $J = 2.1$ Hz, 1H), 5.64 (s, 2H). ^{13}C NMR (101 MHz, DMSO) δ 161.16 (d, $J = 242.9$ Hz), 150.05, 139.28, 135.24, 134.87, 127.40 (d, $J = 8.0$ Hz, 2C), 124.02, 116.75, 115.65 (d, $J = 21.2$ Hz, 2C).

1-(6-(4-fluorophenyl)oxazolo[4,5-b]pyridin-2-yl)-6-phenylhexan-1-ol (36): The title compound was synthesized from **25** (70 mg, 0.35 mmol) according to the procedures described for **20**. This yielded 1-(6-(4-fluorophenyl)oxazolo[4,5-b]pyridin-2-yl)-6-phenylhexan-1-ol (40 mg, 0.10 mmol, 29%) ^1H NMR (400 MHz, CDCl_3) δ 8.70 (d, $J = 1.8$ Hz, 1H), 7.91 (d, $J = 1.8$ Hz, 1H), 7.60 – 7.46 (m, 2H), 7.31 – 7.07 (m, 7H), 5.11 – 4.96 (m, 1H), 2.70 – 2.50 (m, 2H), 2.04 (pd, $J = 13.8, 6.9$ Hz, 2H), 1.73 – 1.47 (m, 4H), 1.47 – 1.32 (m, 2H). ^{13}C NMR (101 MHz, CDCl_3) δ 171.71, 163.14 (d, $J = 248.6$ Hz), 154.24, 145.58, 143.49, 142.65, 133.81, 133.64 (d, $J = 3.4$ Hz), 129.38 (d, $J = 8.2$ Hz, 2C), 128.49 (2C), 128.37 (2C), 125.77, 117.02, 116.52, 116.30, 68.29, 35.92, 35.49, 31.35, 29.02, 24.91.

1-(6-(4-fluorophenyl)oxazolo[4,5-b]pyridin-2-yl)-6-phenylhexan-1-one (4): The title compound was synthesized from **36** (39 mg, 0.1 mmol) according to the procedures described for **3**. This yielded 1-(6-(4-fluorophenyl)oxazolo[4,5-b]pyridin-2-yl)-6-phenylhexan-1-one (31 mg, 0.08 mmol, 80%). ^1H NMR (400 MHz, CDCl_3) δ 8.94 (d, $J = 2.0$ Hz, 1H), 8.07 (d, $J = 2.0$ Hz, 1H), 7.70 – 7.53 (m, 2H), 7.35 – 7.10 (m, 7H), 3.29 (dd, $J = 9.4, 5.4$ Hz, 2H), 2.72 – 2.54 (m, 2H), 1.97 – 1.79 (m, 2H), 1.71 (dt, $J = 15.5, 7.6$ Hz, 2H), 1.56 – 1.41 (m, 2H). ^{13}C NMR (101 MHz, CDCl_3) δ 190.29, 163.46 (d, $J = 249.5$ Hz),

158.96, 153.45, 148.18, 144.09, 142.52, 136.63, 133.17 (d, $J = 3.3$ Hz), 129.61 (d, $J = 8.4$ Hz, 2C), 128.53 (2C), 128.43 (2C), 125.84, 118.05, 116.63 (d, $J = 21.8$ Hz, 2C), 39.88, 35.84, 31.28, 28.83, 23.84. HRMS (ESI+) m/z : calculated for $C_{24}H_{21}FN_2O_2$ ($M + H$) 389.1660; found 389.1662. Purity $\geq 95\%$ as determined by LC/MS.

2-amino-5-(3-fluorophenyl)pyridin-3-ol (27): The title compound was synthesized from 2-amino-5-bromopyridin-3-ol (300 mg, 1.08 mmol) and 3-fluorophenylboronic acid (179 mg, 1.3 mmol) according to the procedures described for compound **19**. This yielded 2-amino-5-(3-fluorophenyl)pyridin-3-ol (120 mg, 0.59 mmol, 54%). 1H NMR (400 MHz, DMSO) δ 9.70 (s, 1H), 7.81 (d, $J = 2.1$ Hz, 1H), 7.49 – 7.38 (m, 1H), 7.38 – 7.26 (m, 2H), 7.19 – 6.93 (m, 2H), 5.73 (s, 2H). ^{13}C NMR (101 MHz, DMSO) δ 162.73 (d, $J = 242.9$ Hz), 150.58, 140.89 (d, $J = 8.0$ Hz), 139.21, 135.70, 130.75 (d, $J = 8.8$ Hz), 123.45, 121.43 (d, $J = 2.4$ Hz), 116.58, 112.82 (d, $J = 21.1$ Hz), 111.95 (d, $J = 21.9$ Hz).

1-(6-(3-fluorophenyl)oxazolo[4,5-b]pyridin-2-yl)-6-phenylhexan-1-ol (28): The title compound was synthesized from **27** (70 mg, 0.35 mmol) according to the procedures described for **20**. This yielded 1-(6-(3-fluorophenyl)oxazolo[4,5-b]pyridin-2-yl)-6-phenylhexan-1-ol (34 mg, 0.08 mmol, 25%). 1H NMR (400 MHz, $CDCl_3$) δ 8.74 (d, $J = 1.9$ Hz, 1H), 7.95 (d, $J = 1.9$ Hz, 1H), 7.56 – 7.41 (m, 1H), 7.36 (d, $J = 8.1$ Hz, 1H), 7.32 – 7.21 (m, 3H), 7.21 – 7.03 (m, 4H), 5.04 (dd, $J = 13.7, 6.5$ Hz, 1H), 2.70 – 2.44 (m, 2H), 2.20 – 1.91 (m, 2H), 1.74 – 1.48 (m, 4H), 1.47 – 1.31 (m, 2H). ^{13}C NMR (101 MHz, $CDCl_3$) δ 172.04, 163.39 (d, $J = 247.2$ Hz), 154.64, 145.64, 143.50, 142.65, 139.67 (d, $J = 7.7$ Hz), 133.54, 131.01 (d, $J = 8.5$ Hz), 128.50 (2C), 128.38 (2C), 125.77, 123.37 (d, $J = 2.9$ Hz), 117.22, 115.39 (d, $J = 21.1$ Hz), 114.66 (d, $J = 22.4$ Hz), 68.31, 35.92, 35.50, 31.36, 29.02, 24.9.

1-(6-(3-fluorophenyl)oxazolo[4,5-b]pyridin-2-yl)-6-phenylhexan-1-one (5): The title compound was synthesized from **28** (33 mg, 0.085 mmol) according to the procedure described for **3**. This yielded 1-(6-(3-fluorophenyl)oxazolo[4,5-b]pyridin-2-yl)-6-phenylhexan-1-one (28 mg, 0.07 mmol, 85%). 1H NMR (400 MHz, $CDCl_3$) δ 8.96 (d, $J = 1.8$ Hz, 1H), 8.11 (d, $J = 2.0$ Hz, 1H), 7.51 (td, $J = 8.0, 5.8$ Hz, 1H), 7.45 – 7.39 (m, 1H), 7.37 – 7.31 (m, 1H), 7.28 (dt, $J = 6.7, 2.5$ Hz, 2H), 7.22 – 7.11 (m, 4H), 3.29 (dd, $J = 9.4, 5.4$ Hz, 2H), 2.70 – 2.58 (m, 2H), 1.88 (dt, $J = 15.1, 7.5$ Hz, 2H), 1.71 (dt, $J = 15.4, 7.6$ Hz, 2H), 1.56 – 1.42 (m, 2H). ^{13}C NMR (101 MHz, $CDCl_3$) δ 190.25, 163.42 (d, $J = 247.7$ Hz), 159.12, 153.88, 148.19, 144.05, 142.51, 139.18 (d, $J = 7.8$ Hz), 136.29, 131.19 (d, $J = 8.4$ Hz), 128.53 (2C), 128.43 (2C), 125.84, 123.55 (d, $J = 3.0$ Hz), 118.30, 115.93 (d, $J = 21.1$ Hz), 114.85 (d, $J = 22.6$ Hz), 39.90, 35.83, 31.27, 28.82, 23.83. HRMS (ESI+) m/z : calculated for $C_{24}H_{21}FN_2O_2$ ($M + H$) 389.1660; found 389.1664. Purity $\geq 95\%$ as determined by LC/MS.

2-amino-5-(2-fluorophenyl)pyridin-3-ol (29): The title compound was synthesized from 2-amino-5-bromopyridin-3-ol (509 mg, 1.9 mmol) and 2-fluorophenylboronic acid (400 mg, 2.8 mmol) according to the procedures described for compound **19**. This yielded 2-amino-5-(2-fluorophenyl)pyridin-3-ol (70 mg, 0.34 mmol, 18%). ¹H NMR (400 MHz, DMSO) δ 9.70 (s, 1H), 7.64 (s, 1H), 7.44 (td, J = 7.8, 1.5 Hz, 1H), 7.37 – 7.14 (m, 3H), 7.06 (s, 1H), 5.70 (s, 2H). ¹³C NMR (101 MHz, DMSO) δ 159.07 (d, J = 244.6 Hz), 150.19, 138.74, 137.12 (d, J = 3.4 Hz), 129.81 (d, J = 3.8 Hz), 128.41 (d, J = 8.3 Hz), 126.14 (d, J = 13.2 Hz), 124.88 (d, J = 3.4 Hz), 119.58, 118.61 (d, J = 3.7 Hz), 116.02 (d, J = 22.7 Hz).

1-(6-(2-fluorophenyl)oxazolo[4,5-b]pyridin-2-yl)-6-phenylhexan-1-ol (30): The title compound was synthesized from **29** (66 mg, 0.32 mmol) according to the procedures described for **20**. This yielded 1-(6-(2-fluorophenyl)oxazolo[4,5-b]pyridin-2-yl)-6-phenylhexan-1-ol (20 mg, 0.05 mmol, 16%). ¹H NMR (400 MHz, CDCl₃) δ 8.70 (s, 1H), 8.04 (d, J = 18.2 Hz, 1H), 7.56 – 7.36 (m, 2H), 7.34 – 6.99 (m, 7H), 5.10 – 4.96 (m, 1H), 2.65 – 2.57 (m, 2H), 2.18 – 1.91 (m, 2H), 1.63 (tt, J = 12.6, 6.2 Hz, 2H), 1.58 – 1.47 (m, 2H), 1.48 – 1.31 (m, 2H). ¹³C NMR (101 MHz, CDCl₃) δ 171.88, 159.92 (d, J = 248.7 Hz), 154.33, 146.95, 143.15, 142.67, 130.93 (d, J = 2.8 Hz), 130.44 (d, J = 8.2 Hz), 129.15, 128.52 (2C), 128.39 (2C), 125.78, 125.02 (d, J = 3.7 Hz), 119.26, 116.58 (d, J = 22.3 Hz), 68.34, 35.93, 35.55, 31.36, 29.03, 24.90.

1-(6-(2-fluorophenyl)oxazolo[4,5-b]pyridin-2-yl)-6-phenylhexan-1-one (6): The title compound was synthesized from **30** (19 mg, 0.049 mmol) according to the procedure described for **3**. This yielded 1-(6-(2-fluorophenyl)oxazolo[4,5-b]pyridin-2-yl)-6-phenylhexan-1-one (17 mg, 0.04 mmol, 89%). ¹H NMR (400 MHz, CDCl₃) δ 8.92 (s, 1H), 8.16 (t, J = 1.7 Hz, 1H), 7.48 (dddd, J = 9.9, 7.1, 6.4, 1.7 Hz, 2H), 7.35 – 7.24 (m, 5H), 7.20 – 7.13 (m, 3H), 3.29 (t, J = 7.4 Hz, 2H), 2.70 – 2.60 (m, 2H), 1.88 (dt, J = 15.1, 7.5 Hz, 2H), 1.71 (dt, J = 15.4, 7.6 Hz, 2H), 1.49 (ddd, J = 18.4, 8.9, 6.5 Hz, 2H). ¹³C NMR (101 MHz, CDCl₃) δ 190.34, 159.94 (d, J = 249.3 Hz), 153.55, 149.44 (d, J = 2.9 Hz), 143.73, 143.60, 142.54, 132.02, 131.01, 130.92, 128.55 (2C), 128.44 (2C), 125.85, 125.16 (d, J = 3.7 Hz), 124.83 (d, J = 13.4 Hz), 120.43 (d, J = 4.1 Hz), 116.74 (d, J = 22.3 Hz), 39.92, 35.85, 31.29, 28.84, 23.86. HRMS (ESI+) m/z : calculated for C₂₄H₂₁FN₂O₂ (M + H) 389.1660; found 389.1662. Purity \geq 95% as determined by LC/MS.

2-amino-5-(4-methoxyphenyl)pyridin-3-ol (31): The title compound was synthesized from 2-amino-5-bromopyridin-3-ol (300 mg, 1.08 mmol) and 4-methoxyphenylboronic acid (198 mg, 1.3 mmol) according to the procedures described for compound **19**. This yielded 2-amino-5-(4-methoxyphenyl)pyridin-3-ol (148 mg, 0.69 mmol, 63%). ¹H NMR (400 MHz, DMSO) δ 9.62 (s, 1H), 7.71 (d, J = 2.1 Hz, 1H), 7.53 – 7.28 (m, 2H), 7.07 (d, J = 2.1 Hz, 1H), 7.02 – 6.89 (m, 2H), 5.54 (s, 2H), 3.78 (s, 3H). ¹³C NMR (101 MHz, DMSO) δ 158.07, 149.49, 139.27, 134.73, 130.79, 126.63 (2C), 124.89, 116.68, 114.34 (2C), 55.09.

1-(6-(4-methoxyphenyl)oxazolo[4,5-b]pyridin-2-yl)-6-phenylhexan-1-ol (32): The title compound was synthesized from **31** (52 mg, 0.24 mmol) according to the procedures described for **20**. This yielded 1-(6-(4-methoxyphenyl)oxazolo[4,5-b]pyridin-2-yl)-6-phenylhexan-1-ol (28 mg, 0.07 mmol, 29%). ¹H NMR (400 MHz, CDCl₃) δ 8.70 (d, *J* = 1.9 Hz, 1H), 7.90 (d, *J* = 1.9 Hz, 1H), 7.49 (t, *J* = 5.8 Hz, 2H), 7.25 (dd, *J* = 8.7, 6.5 Hz, 2H), 7.15 (t, *J* = 6.8 Hz, 3H), 7.06 – 6.92 (m, 2H), 5.09 – 4.92 (m, 1H), 3.86 (s, 3H), 2.66 – 2.53 (m, 2H), 2.14 – 1.89 (m, 2H), 1.72 – 1.58 (m, 2H), 1.58 – 1.45 (m, 2H), 1.46 – 1.33 (m, 2H). ¹³C NMR (101 MHz, CDCl₃) δ 171.27, 160.02, 153.70, 145.42, 143.57, 142.67, 134.46, 129.90, 128.76 (2C), 128.49 (2C), 128.36 (2C), 125.75, 116.56, 114.83 (2C), 68.26, 55.53, 35.92, 35.48, 31.36, 29.03, 24.92.

1-(6-(4-methoxyphenyl)oxazolo[4,5-b]pyridin-2-yl)-6-phenylhexan-1-one (7): The title compound was synthesized from **32** (25 mg, 0.062 mmol) according to the procedure described for **3**. This yielded 1-(6-(4-methoxyphenyl)oxazolo[4,5-b]pyridin-2-yl)-6-phenylhexan-1-one (18 mg, 0.045 mmol, 72%). ¹H NMR (400 MHz, CDCl₃) δ 8.95 (d, *J* = 1.3 Hz, 1H), 8.05 (d, *J* = 2.0 Hz, 1H), 7.63 – 7.53 (m, 2H), 7.28 (dt, *J* = 6.7, 2.9 Hz, 2H), 7.17 (dd, *J* = 10.7, 4.3 Hz, 3H), 7.09 – 7.02 (m, 2H), 3.88 (s, 3H), 3.28 (dd, *J* = 9.4, 5.4 Hz, 2H), 2.70 – 2.58 (m, 2H), 1.87 (dt, *J* = 15.2, 7.5 Hz, 2H), 1.70 (dt, *J* = 15.5, 7.6 Hz, 2H), 1.55 – 1.43 (m, 2H). ¹³C NMR (101 MHz, CDCl₃) δ 190.33, 160.48, 158.66, 152.87, 148.10, 144.26, 142.53, 137.35, 129.34, 128.97 (2C), 128.53 (2C), 128.41 (2C), 125.82, 117.41, 115.01 (2C), 55.59, 39.82, 35.83, 31.28, 28.83, 23.86. HRMS (ESI+) *m/z*: calculated for C₂₅H₂₄N₂O₃ (M + H) 401.1860; found 401.1852. Purity ≥95% as determined by LC/MS.

2-amino-5-(3-methoxyphenyl)pyridin-3-ol (33): The title compound was synthesized from 2-amino-5-bromopyridin-3-ol (367 mg, 1.3 mmol) and 3-methoxyphenylboronic acid (237 mg, 1.6 mmol) according to the procedures described for compound **19**. This yielded 2-amino-5-(3-methoxyphenyl)pyridin-3-ol (80 mg, 0.37 mmol, 28%). ¹H NMR (400 MHz, MeOD) δ 7.63 (d, *J* = 2.0 Hz, 1H), 7.26 (t, *J* = 8.0 Hz, 1H), 7.13 (d, *J* = 2.0 Hz, 1H), 7.06 – 6.90 (m, 2H), 6.81 (dd, *J* = 8.2, 2.4 Hz, 1H), 3.78 (s, 3H). ¹³C NMR (101 MHz, MeOD) δ 152.09, 141.65, 132.98, 131.49, 124.65, 121.42, 119.11, 110.05, 109.59, 103.66, 103.36, 46.17.

1-(6-(3-methoxyphenyl)oxazolo[4,5-b]pyridin-2-yl)-6-phenylhexan-1-ol (34): The title compound was synthesized from **33** (96 mg, 0.45 mmol) according to the procedures described for **20**. This yielded 1-(6-(3-methoxyphenyl)oxazolo[4,5-b]pyridin-2-yl)-6-phenylhexan-1-ol (35 mg, 0.09 mmol, 19%) ¹H NMR (400 MHz, CDCl₃) δ 8.74 (d, *J* = 1.9 Hz, 1H), 7.95 (d, *J* = 2.0 Hz, 1H), 7.41 (t, *J* = 8.0 Hz, 1H), 7.31 – 7.21 (m, 2H), 7.20 – 7.04 (m, 5H), 7.03 – 6.92 (m, 1H), 5.10 – 4.93 (m, 1H), 3.87 (s, 3H), 2.69 – 2.57 (m, 2H), 2.13 –

1.93 (m, 2H), 1.71 – 1.46 (m, 4H), 1.45 – 1.32 (m, 2H). ^{13}C NMR (101 MHz, CDCl_3) δ 171.73, 160.30, 154.22, 145.69, 143.48, 142.65, 138.88, 134.65, 130.44, 128.48 (2C), 128.35 (2C), 125.74, 125.71, 120.07, 117.24, 113.63, 113.55, 68.25, 35.92, 35.48, 31.37, 29.03, 24.93.

1-(6-(3-methoxyphenyl)oxazolo[4,5-b]pyridin-2-yl)-6-phenylhexan-1-one (8): The title compound was synthesized from **34** (35 mg, 0.087 mmol) according to the procedure described for **3**. This yielded 6-phenyl-1-(6-phenyloxazolo[4,5-b]pyridin-2-yl)hexan-1-one (20 mg, 0.05 mmol, 57%) ^1H NMR (400 MHz, CDCl_3) δ 8.98 (s, 1H), 8.11 (d, J = 2.0 Hz, 1H), 7.45 (t, J = 8.0 Hz, 1H), 7.28 (dt, J = 6.6, 1.6 Hz, 2H), 7.24 – 7.12 (m, 5H), 7.01 (ddd, J = 8.3, 2.5, 0.7 Hz, 1H), 3.90 (s, 3H), 3.29 (t, J = 7.4 Hz, 2H), 2.71 – 2.55 (m, 2H), 1.87 (dt, J = 15.2, 7.5 Hz, 2H), 1.70 (dq, J = 15.7, 7.8 Hz, 2H), 1.55 – 1.43 (m, 2H). ^{13}C NMR (101 MHz, CDCl_3) δ 190.33, 160.43, 158.91, 153.51, 148.40, 144.12, 142.53, 138.45, 137.53, 130.63, 128.54 (2C), 128.43 (2C), 125.84, 120.23, 118.24, 114.14, 113.75, 55.59, 39.87, 35.84, 31.29, 28.83, 23.85. Purity \geq 95% as determined by LC/MS, m/z : calculated for $\text{C}_{25}\text{H}_{24}\text{N}_2\text{O}_3$ ($M + H$) 401.19; found 401.00. HRMS (ESI+) m/z : calculated for $\text{C}_{25}\text{H}_{24}\text{N}_2\text{O}_3$ ($M + H$) 401.1860; found 401.1852.

2-amino-5-(2-methoxyphenyl)pyridin-3-ol (35): The title compound was synthesized from 2-amino-5-bromopyridin-3-ol (300 mg, 1.08 mmol) and 2-methoxyphenylboronic acid (198 mg, 1.3 mmol) according to the procedures described for compound **20**. This yielded 2-amino-5-(2-methoxyphenyl)pyridin-3-ol (135 mg, 0.63 mmol, 58%). ^1H NMR (400 MHz, DMSO) δ 9.52 (s, 1H), 7.54 (d, J = 1.7 Hz, 1H), 7.25 (ddd, J = 13.0, 8.1, 3.8 Hz, 2H), 7.01 (dt, J = 14.6, 5.7 Hz, 3H), 5.51 (s, 2H), 3.75 (s, 3H). ^{13}C NMR (101 MHz, DMSO) δ 156.18, 149.35, 138.28, 137.20, 129.64, 128.03, 127.55, 122.87, 120.77, 119.85, 111.66, 55.43.

1-(6-(2-methoxyphenyl)oxazolo[4,5-b]pyridin-2-yl)-6-phenylhexan-1-ol (36): The title compound was synthesized from **35** (77 mg, 0.36 mmol) according to the procedures described for **20**. This yielded 1-(6-(2-methoxyphenyl)oxazolo[4,5-b]pyridin-2-yl)-6-phenylhexan-1-ol (25 mg, 0.06 mmol, 17%) ^1H NMR (400 MHz, CDCl_3) δ 8.65 (d, J = 1.8 Hz, 1H), 8.02 (d, J = 1.8 Hz, 1H), 7.48 – 6.95 (m, 9H), 5.01 (dt, J = 20.7, 10.3 Hz, 1H), 3.81 (d, J = 9.2 Hz, 3H), 2.70 – 2.43 (m, 2H), 2.17 – 1.90 (m, 2H), 1.76 – 1.33 (m, 6H). ^{13}C NMR (101 MHz, CDCl_3) δ 171.39, 156.61, 153.55, 147.45, 142.99, 131.83, 131.07, 130.00, 128.50 (2C), 128.36 (2C), 126.43, 125.74, 125.71, 121.30, 119.84, 111.47, 68.28, 55.66, 35.93, 35.53, 31.37, 29.04, 24.91.

1-(6-(2-methoxyphenyl)oxazolo[4,5-b]pyridin-2-yl)-6-phenylhexan-1-one (9): The title compound was synthesized from **36** (23 mg, 0.057 mmol) according to the procedure described for **3**. This yielded 1-(6-(2-methoxyphenyl)oxazolo[4,5-b]pyridin-2-yl)-6-phenylhexan-1-one (15 mg, 0.037 mmol, 66%) ^1H NMR (400 MHz, CDCl_3) δ 8.88 (d, J =

1.9 Hz, 1H), 8.17 (d, J = 1.9 Hz, 1H), 7.48 – 7.36 (m, 2H), 7.33 – 7.23 (m, 2H), 7.17 (dd, J = 10.8, 4.4 Hz, 3H), 7.11 (td, J = 7.5, 1.0 Hz, 1H), 7.05 (d, J = 8.3 Hz, 1H), 3.85 (s, 3H), 3.29 (t, J = 7.4 Hz, 2H), 2.69 – 2.58 (m, 2H), 1.87 (dt, J = 15.1, 7.5 Hz, 2H), 1.70 (dq, J = 14.8, 7.3 Hz, 2H), 1.55 – 1.42 (m, 2H). ^{13}C NMR (101 MHz, CDCl_3) δ 190.47, 158.68, 156.66, 152.76, 150.19, 143.66, 142.54, 134.82, 131.06, 130.49, 128.53 (2C), 128.41 (2C), 125.98, 125.82, 121.40, 120.87, 111.56, 55.70, 39.84, 35.85, 31.30, 28.84, 23.90. HRMS (ESI+) m/z : calculated for $\text{C}_{25}\text{H}_{24}\text{N}_2\text{O}_3$ ($M + H$) 401.1860; found 401.1858. Purity \geq 95% as determined by LC/MS.

2-amino-5-(4-(trifluoromethyl)phenyl)pyridin-3-ol (37): The title compound was synthesized from 2-amino-5-bromopyridin-3-ol (300 mg, 1.08 mmol) and 4-(trifluoromethyl)phenylboronic acid (244 mg, 1.3 mmol) according to the procedures described for compound **19**. This yielded 2-amino-5-(4-(trifluoromethyl)phenyl)pyridin-3-ol (140 mg, 0.55 mmol, 51%). ^1H NMR (400 MHz, DMSO) δ 9.80 (s, 1H), 7.95 – 7.82 (m, 1H), 7.74 (s, 4H), 7.18 (d, J = 1.8 Hz, 1H), 5.85 (s, 2H). ^{13}C NMR (101 MHz, DMSO) δ 150.95, 142.41, 139.34, 136.06, 125.90, 125.74, 125.71, 123.07, 116.45. ^{13}C NMR (101 MHz, DMSO) δ 150.95, 142.41, 139.34, 136.06, 126.63, 126.32, 125.90 (2C), 125.72 (q, J = 3.6 Hz, 2C), 123.07, 116.45.

6-phenyl-1-(6-(4-(trifluoromethyl)phenyl)oxazolo[4,5-b]pyridin-2-yl)hexan-1-ol (38): The title compound was synthesized from **37** (96 mg, 0.38 mmol) according to the procedures described for **20**. This yielded 6-phenyl-1-(6-(4-(trifluoromethyl)phenyl)oxazolo[4,5-b]pyridin-2-yl)hexan-1-ol (35 mg, 0.08 mmol, 21%) ^1H NMR (400 MHz, CDCl_3) δ 8.79 (d, J = 1.9 Hz, 1H), 8.00 (d, J = 1.9 Hz, 1H), 7.76 (d, J = 8.4 Hz, 2H), 7.73 – 7.65 (m, 2H), 7.33 – 7.02 (m, 5H), 5.12 – 4.98 (m, 1H), 2.68 – 2.50 (m, 2H), 2.15 – 1.93 (m, 2H), 1.71 – 1.32 (m, 6H). ^{13}C NMR (101 MHz, CDCl_3) δ 172.42, 154.81, 145.70, 143.50, 142.64 (d, J = 5.4 Hz), 140.95, 133.35, 130.75, 130.48, 128.49 (2C), 128.39 (2C), 128.03 (2C), 126.37 (q, J = 3.7 Hz, 2C), 125.78 (d, J = 2.4 Hz), 117.46, 68.32, 35.92, 35.50, 31.35, 29.00, 24.92.

6-phenyl-1-(6-(4-(trifluoromethyl)phenyl)oxazolo[4,5-b]pyridin-2-yl)hexan-1-one (10): The title compound was synthesized from **38** (33 mg, 0.075 mmol) according to the procedure described for **3**. This yielded 6-phenyl-1-(6-(4-(trifluoromethyl)phenyl)oxazolo[4,5-b]pyridin-2-yl)hexan-1-one (28 mg, 0.064 mmol, 85%). ^1H NMR (400 MHz, CDCl_3) δ 8.99 (d, J = 2.0 Hz, 1H), 8.15 (d, J = 2.0 Hz, 1H), 7.78 (q, J = 8.4 Hz, 4H), 7.33 – 7.23 (m, 2H), 7.17 (dd, J = 10.4, 4.3 Hz, 3H), 3.30 (t, J = 7.4 Hz, 2H), 2.69 – 2.60 (m, 2H), 1.88 (dt, J = 15.1, 7.5 Hz, 2H), 1.71 (dt, J = 15.4, 7.6 Hz, 2H), 1.55 – 1.43 (m, 2H). ^{13}C NMR (101 MHz, CDCl_3) δ 190.22, 159.26, 154.16, 148.21, 144.02, 142.50, 140.56, 136.05, 131.10 (q, J = 32.9 Hz), 128.54 (2C), 128.44 (2C), 128.24 (2C), 126.51 (q, J = 3.6 Hz, 2C), 125.86, 125.40, 118.54, 39.93, 35.84, 31.28, 28.82, 23.81.

HRMS (ESI+) m/z : calculated for $C_{25}H_{21}F_3N_2O_2$ ($M + H$) 439.1628; found 439.1626. Purity $\geq 95\%$ as determined by LC/MS.

methyl 4-(6-amino-5-hydroxypyridin-3-yl)benzoate (39): The title compound was synthesized from 2-amino-5-bromopyridin-3-ol (300 mg, 1.08 mmol) and 4-methoxycarbonylphenylboronic acid (234 mg, 1.3 mmol) according to the procedures described for compound **19**. This yielded methyl 4-(6-amino-5-hydroxypyridin-3-yl)benzoate (150 mg, 0.61 mmol, 57%). 1H NMR (400 MHz, DMSO) δ 9.85 (s, 1H), 7.97 (d, $J = 8.5$ Hz, 2H), 7.88 (d, $J = 2.1$ Hz, 1H), 7.66 (d, $J = 8.5$ Hz, 2H), 7.19 (d, $J = 2.1$ Hz, 1H), 5.90 (s, 2H), 3.85 (s, 3H). ^{13}C NMR (101 MHz, DMSO) δ 166.08, 150.80, 142.87, 139.41, 135.70, 129.85, 127.09, 125.33, 123.24, 116.43, 52.02.

methyl 4-(2-(1-hydroxy-6-phenylhexyl)oxazolo[4,5-b]pyridin-6-yl)benzoate (40): The title compound was synthesized from **39** (34 mg, 0.14 mmol) according to the procedures described for **20**. This yielded methyl 4-(2-(1-hydroxy-6-phenylhexyl)oxazolo[4,5-b]pyridin-6-yl)benzoate (14 mg, 0.032 mmol, 23%). 1H NMR (400 MHz, $CDCl_3$) δ 8.80 (s, 1H), 8.16 (d, $J = 8.3$ Hz, 2H), 8.01 (d, $J = 1.3$ Hz, 1H), 7.66 (d, $J = 8.3$ Hz, 2H), 7.26 (t, $J = 7.5$ Hz, 2H), 7.16 (t, $J = 6.9$ Hz, 3H), 5.10 – 4.95 (m, 1H), 4.00 – 3.88 (m, 3H), 2.67 – 2.55 (m, 2H), 2.18 – 1.95 (m, 2H), 1.74 – 1.48 (m, 4H), 1.48 – 1.34 (m, 2H). ^{13}C NMR (101 MHz, $CDCl_3$) δ 171.98, 166.76, 154.88, 145.88, 143.51, 142.64, 141.89, 133.57, 130.64 (2C), 130.06, 128.50 (2C), 128.39 (2C), 127.62 (2C), 125.79, 117.24, 68.35, 52.46, 35.92, 35.52, 31.36, 29.01, 24.89.

Methyl 4-(2-(6-phenylhexanoyl)oxazolo[4,5-b]pyridin-6-yl)benzoate (11): The title compound was synthesized from **40** (13 mg, 0.03 mmol) according to the procedure described for **3**. This yielded methyl 4-(2-(6-phenylhexanoyl)oxazolo[4,5-b]pyridin-6-yl)benzoate (7.2 mg, 0.017 mmol, 57%). 1H NMR (400 MHz, $CDCl_3$) δ 9.01 (s, 1H), 8.22 – 8.18 (m, 2H), 8.16 (d, $J = 2.0$ Hz, 1H), 7.77 – 7.66 (m, 2H), 7.28 (dt, $J = 6.5, 1.5$ Hz, 2H), 7.17 (dd, $J = 10.4, 4.3$ Hz, 3H), 3.97 (s, 3H), 3.30 (t, $J = 7.4$ Hz, 2H), 2.70 – 2.56 (m, 2H), 1.88 (dt, $J = 15.1, 7.5$ Hz, 2H), 1.71 (dt, $J = 15.5, 7.6$ Hz, 2H), 1.49 (ddd, $J = 18.2, 8.8, 6.4$ Hz, 2H). ^{13}C NMR (101 MHz, $CDCl_3$) δ 190.24, 166.63, 159.20, 154.05, 148.28, 144.06, 142.51, 141.31, 136.39, 130.75 (2C), 130.57, 128.53 (2C), 128.43 (2C), 127.83 (2C), 125.85, 118.44, 52.53, 39.93, 35.85, 31.29, 28.84, 23.84. HRMS (ESI+) m/z : calculated for $C_{26}H_{24}N_2O_4$ ($M + H$) 429.1809; found 429.1809. Purity $\geq 95\%$ as determined by LC/MS.

4-(6-amino-5-hydroxypyridin-3-yl)benzonitrile (41): The title compound was synthesized from 2-amino-5-bromopyridin-3-ol (350 mg, 1.25 mmol) and 4-cyanophenylboronic acid (276 mg, 1.9 mmol) according to the procedures described for compound **19**. This yielded 4-(6-amino-5-hydroxypyridin-3-yl)benzonitrile (87 mg, 0.41 mmol, 33%). 1H NMR (400 MHz, DMSO) δ 9.81 (s, 1H), 7.89 (d, $J = 2.0$ Hz, 1H), 7.82 (d,

$J = 8.3$ Hz, 2H), 7.71 (d, $J = 8.4$ Hz, 2H), 7.15 (d, $J = 2.0$ Hz, 1H), 5.90 (s, 2H). ^{13}C NMR (101 MHz, DMSO) δ 151.22, 142.96, 139.29, 136.44, 132.79, 125.88 (2C), 122.61, 119.13, 116.18, 108.33.

4-(2-(1-hydroxy-6-phenylhexyl)oxazolo[4,5-b]pyridin-6-yl)benzonitrile (42): The title compound was synthesized from **41** (87 mg, 0.41 mmol) according to the procedures described for **20**. This yielded 4-(2-(1-hydroxy-6-phenylhexyl)oxazolo[4,5-b]pyridin-6-yl)benzonitrile (33 mg, 0.08 mmol, 20%) ^1H NMR (400 MHz, CDCl_3) δ 8.77 (d, $J = 2.0$ Hz, 1H), 8.00 (d, $J = 2.0$ Hz, 1H), 7.79 (d, $J = 8.4$ Hz, 2H), 7.70 (d, $J = 8.4$ Hz, 2H), 7.34 – 7.20 (m, 2H), 7.20 – 7.08 (m, 3H), 5.03 (ddd, $J = 19.1, 12.3, 3.6$ Hz, 1H), 2.65 – 2.53 (m, 2H), 2.15 – 1.95 (m, 2H), 1.72 – 1.58 (m, 2H), 1.58 – 1.48 (m, 2H), 1.48 – 1.34 (m, 2H). ^{13}C NMR (101 MHz, CDCl_3) δ 172.47, 155.25, 145.65, 143.41, 142.57, 141.94, 133.12 (2C), 132.61, 128.45 (2C), 128.35 (2C), 128.27 (2C), 125.76, 118.51, 117.26, 112.21, 68.25, 35.88, 35.46, 31.34, 28.98, 24.91.

4-(2-(6-phenylhexanoyl)oxazolo[4,5-b]pyridin-6-yl)benzonitrile (12): The title compound was synthesized from **42** (33 mg, 0.83 mmol) according to the procedure described for **3**. This yielded (3-(2-(6-phenylhexanoyl)oxazolo[4,5-b]pyridin-6-yl)benzonitrile (26 mg, 0.066 mmol, 80%). ^1H NMR (400 MHz, CDCl_3) δ 9.00 (t, $J = 7.4$ Hz, 1H), 8.15 (d, $J = 2.0$ Hz, 1H), 7.91 – 7.81 (m, 2H), 7.80 – 7.73 (m, 2H), 7.33 – 7.22 (m, 2H), 7.17 (dd, $J = 10.2, 4.2$ Hz, 3H), 3.30 (t, $J = 7.4$ Hz, 2H), 2.73 – 2.58 (m, 2H), 1.88 (dt, $J = 15.1, 7.5$ Hz, 2H), 1.71 (dt, $J = 15.4, 7.6$ Hz, 2H), 1.56 – 1.43 (m, 2H). ^{13}C NMR (101 MHz, CDCl_3) δ 190.15, 159.41, 155.96, 154.46, 148.05, 143.96, 142.47, 141.44, 135.42, 133.27 (2C), 128.51 (2C), 128.42 (2C), 125.85 (2C), 118.53, 118.38, 112.85, 39.94, 35.81, 31.26, 28.79, 23.77. Purity $\geq 95\%$ as determined by LC/MS, m/z : calculated for $\text{C}_{25}\text{H}_{21}\text{N}_3\text{O}_2$ ($M + H$) 396.17; found 396.00. HRMS (ESI+) m/z : calculated for $\text{C}_{25}\text{H}_{21}\text{N}_3\text{O}_2$ ($M + H$) 396.1707; found 396.1703.

3-(6-amino-5-hydroxypyridin-3-yl)benzonitrile (43): The title compound was synthesized from 2-amino-5-bromopyridin-3-ol (347 mg, 1.24 mmol) and 3-cyanophenylboronic acid (181 mg, 1.24 mmol) according to the procedures described for compound **19**. This yielded 3-(6-amino-5-hydroxypyridin-3-yl)benzonitrile (82 mg, 0.39 mmol, 31%). ^1H NMR (400 MHz, DMSO) δ 9.75 (s, 1H), 7.98 (s, 1H), 7.85 (t, $J = 4.9$ Hz, 2H), 7.70 (d, $J = 7.7$ Hz, 1H), 7.58 (dd, $J = 17.6, 9.8$ Hz, 1H), 7.13 (d, $J = 2.0$ Hz, 1H), 5.80 (s, 2H). ^{13}C NMR (101 MHz, DMSO) δ 150.88, 139.59, 139.26, 136.02, 130.15, 130.09, 129.72, 128.80, 122.62, 118.94, 116.46, 112.00.

3-(2-(1-hydroxy-6-phenylhexyl)oxazolo[4,5-b]pyridin-6-yl)benzonitrile (44): The title compound was synthesized from **43** (82 mg, 0.39 mmol) according to the procedures described for **20**. This yielded 3-(2-(1-hydroxy-6-phenylhexyl)oxazolo[4,5-b]pyridin-6-yl)benzonitrile (10 mg, 0.025 mmol, 6.4%) ^1H NMR (400 MHz, CDCl_3) δ 8.77 (t, $J = 6.1$

Hz, 1H), 7.99 (dd, $J = 9.4, 1.9$ Hz, 1H), 7.93 – 7.79 (m, 2H), 7.78 – 7.69 (m, 1H), 7.31 – 7.21 (m, 2H), 7.17 (dd, $J = 10.4, 4.6$ Hz, 4H), 5.11 – 4.95 (m, 1H), 2.67 – 2.53 (m, 2H), 2.14 – 1.93 (m, 2H), 1.74 – 1.60 (m, 2H), 1.60 – 1.48 (m, 2H), 1.47 – 1.35 (m, 2H). ^{13}C NMR (101 MHz, CDCl_3) δ 173.27, 172.22, 155.19, 145.69, 143.47, 138.94, 132.00, 131.86, 131.16, 130.31, 128.51 (2C), 128.40 (2C), 125.81, 118.44, 117.19, 115.64, 113.74, 68.35, 35.92, 35.53, 31.36, 29.00, 24.89.

3-(2-(6-phenylhexanoyl)oxazolo[4,5-b]pyridin-6-yl)benzonitrile (13): The title compound was synthesized from **44** (10 mg, 0.025 mmol) according to the procedure described for **3**. This yielded 3-(2-(6-phenylhexanoyl)oxazolo[4,5-b]pyridin-6-yl)benzonitrile (5 mg, 0.013 mmol, 51%). ^1H NMR (400 MHz, CDCl_3) δ 8.96 (d, $J = 1.6$ Hz, 1H), 8.12 (d, $J = 2.0$ Hz, 1H), 7.92 (d, $J = 1.3$ Hz, 1H), 7.90 – 7.85 (m, 1H), 7.78 (dd, $J = 6.5, 1.2$ Hz, 1H), 7.72 – 7.63 (m, 1H), 7.31 – 7.22 (m, 2H), 7.17 (dd, $J = 10.1, 4.3$ Hz, 3H), 3.30 (t, $J = 7.4$ Hz, 2H), 2.70 – 2.59 (m, 2H), 1.88 (dt, $J = 15.1, 7.5$ Hz, 2H), 1.71 (dt, $J = 15.4, 7.6$ Hz, 2H), 1.49 (ddd, $J = 18.4, 8.9, 6.5$ Hz, 2H). ^{13}C NMR (101 MHz, CDCl_3) δ 190.19, 159.39, 154.35, 147.99, 143.98, 142.50, 138.43, 135.17, 132.36, 132.13, 131.31, 130.48, 128.54 (2C), 128.45 (2C), 125.87, 118.48, 118.27, 113.98, 39.96, 35.84, 31.28, 28.82, 23.80. Purity $\geq 95\%$ as determined by LC/MS, m/z : calculated for $\text{C}_{25}\text{H}_{21}\text{N}_3\text{O}_2$ (M + H) 396.17; found 396.00. HRMS (ESI+) m/z : calculated for $\text{C}_{25}\text{H}_{21}\text{N}_3\text{O}_2$ (M + H) 396.1707; found 396.1704.

2-(6-amino-5-hydroxypyridin-3-yl)benzonitrile (45): The title compound was synthesized from 2-amino-5-bromopyridin-3-ol (380 mg, 1.4 mmol) and 2-cyanophenylboronic acid (300 mg, 2.0 mmol) according to the procedures described for compound **19**. This yielded 2-(6-amino-5-hydroxypyridin-3-yl)benzonitrile (90 mg, 0.42 mmol, 30%). ^1H NMR (400 MHz, DMSO) δ 9.90 (s, 1H), 8.02 – 7.82 (m, 1H), 7.74 (td, $J = 7.7, 1.4$ Hz, 1H), 7.66 (d, $J = 2.1$ Hz, 1H), 7.55 (d, $J = 7.3$ Hz, 1H), 7.50 (td, $J = 7.6, 1.1$ Hz, 1H), 7.09 (t, $J = 4.6$ Hz, 1H), 5.90 (s, 2H). ^{13}C NMR (101 MHz, DMSO) δ 151.38, 142.88, 139.22, 137.62, 134.38, 133.98, 129.97, 127.75, 122.78, 119.35, 118.53, 109.99.

2-(2-(1-hydroxy-6-phenylhexyl)oxazolo[4,5-b]pyridin-6-yl)benzonitrile (46): The title compound was synthesized from **45** (45 mg, 0.21 mmol) according to the procedures described for **20**. This yielded 2-(2-(1-hydroxy-6-phenylhexyl)oxazolo[4,5-b]pyridin-6-yl)benzonitrile (22 mg, 0.06 mmol, 26%). ^1H NMR (400 MHz, CDCl_3) δ 8.67 (d, $J = 1.7$ Hz, 1H), 8.08 (d, $J = 1.8$ Hz, 1H), 7.89 – 7.78 (m, 1H), 7.78 – 7.67 (m, 1H), 7.56 (t, $J = 7.4$ Hz, 2H), 7.33 – 7.21 (m, 2H), 7.21 – 7.04 (m, 3H), 5.03 (dd, $J = 23.5, 18.1$ Hz, 1H), 2.67 – 2.59 (m, 2H), 2.12 – 1.95 (m, 2H), 1.73 – 1.51 (m, 4H), 1.50 – 1.36 (m, 2H). ^{13}C NMR (101 MHz, CDCl_3) δ 172.59, 155.28, 146.72, 142.84, 142.66, 141.30, 134.15, 133.43, 131.31, 130.60, 128.86, 128.50 (2C), 128.36 (2C), 125.74, 119.06, 118.15, 111.93, 68.31, 55.51, 35.93, 35.51, 31.37, 29.03, 24.92.

2-(2-(6-phenylhexanoyl)oxazolo[4,5-b]pyridin-6-yl)benzonitrile (14): The title compound was synthesized from **46** (22 mg, 0.055 mmol) according to the procedure described for **3**. This yielded 2-(2-(6-phenylhexanoyl)oxazolo[4,5-b]pyridin-6-yl)benzonitrile (15 mg, 0.038 mmol, 69%) ^1H NMR (400 MHz, CDCl_3) δ 8.89 (s, 1H), 8.24 (t, $J = 7.2$ Hz, 1H), 7.93 – 7.84 (m, 1H), 7.77 (td, $J = 7.8, 1.3$ Hz, 1H), 7.60 (ddd, $J = 7.6, 4.0, 1.2$ Hz, 2H), 7.34 – 7.24 (m, 2H), 7.17 (dd, $J = 11.1, 4.5$ Hz, 3H), 3.30 (t, $J = 7.4$ Hz, 2H), 2.72 – 2.53 (m, 2H), 1.88 (dt, $J = 15.1, 7.5$ Hz, 2H), 1.71 (dt, $J = 15.5, 7.6$ Hz, 2H), 1.50 (ddd, $J = 18.5, 8.9, 6.4$ Hz, 2H). ^{13}C NMR (101 MHz, CDCl_3) δ 190.19, 159.52, 154.52, 149.04, 142.52, 140.80, 134.28, 134.11, 133.51, 130.60, 129.31, 128.55 (2C), 128.44 (2C), 125.85, 120.45, 117.91, 112.16, 39.98, 35.84, 31.29, 28.81, 23.82. Purity $\geq 95\%$ as determined by LC/MS, m/z : calculated for $\text{C}_{25}\text{H}_{21}\text{N}_3\text{O}_2$ ($\text{M} + \text{H}$) 396.17; found 396.13. HRMS (ESI+) m/z : calculated for $\text{C}_{25}\text{H}_{21}\text{N}_3\text{O}_2$ ($\text{M} + \text{H}$) 396.1707; found 396.1700.

2-Amino-5-(4-fluoro-2-methoxyphenyl)pyridin-3-ol (47) The title compound was synthesized from 3-(benzyloxy)-5-bromopyridin-2-amine (320 mg, 1.15 mmol) according to the procedures described for compound **19**. This yielded 2-amino-5-(4-fluoro-2-methoxyphenyl)pyridin-3-ol (129 mg, 0.55 mmol, 48%, 2 steps). ^1H NMR (MeOD, 400 MHz): δ 7.47 (d, $J = 1.9$ Hz, 1H), 7.23 (dd, $J = 8.4, 6.7$ Hz, 1H), 7.12 (d, $J = 1.9$ Hz, 1H), 6.84 (dd, $J = 11.1, 2.5$ Hz, 1H), 6.76 – 6.68 (m, 1H), 3.80 (s, 3H). ^{13}C BBDEC NMR (MeOD, 101 MHz): δ 164.43 (d, $J = 244.6$ Hz), 159.20 (d, $J = 9.9$ Hz), 150.24, 141.75, 135.00, 133.04 (d, $J = 10.1$ Hz), 131.83 (d, $J = 9.9$ Hz), 125.31, 120.67, 114.60, 107.93 (d, $J = 21.4$ Hz), 100.51 (d, $J = 26.2$ Hz), 56.28.

1-(6-(4-fluoro-2-methoxyphenyl)oxazolo[4,5-b]pyridin-2-yl)-6-phenylhexan-1-ol (48): The title compound was synthesized from **47** (150 mg, 0.69 mmol) according to the procedures described for **20**. This yielded 1-(6-(4-fluoro-2-methoxyphenyl)oxazolo[4,5-b]pyridin-2-yl)-6-phenylhexan-1-ol (66 mg, 0.16 mmol, 25%). ^1H NMR (500 MHz, CDCl_3) δ 8.62 (d, $J = 1.8$ Hz, 1H), 7.99 (d, $J = 1.8$ Hz, 1H), 7.32 – 7.13 (m, 6H), 6.83 – 6.74 (m, 2H), 5.16 – 4.88 (m, 1H), 3.84 (d, $J = 8.1$ Hz, 3H), 2.64 (dd, $J = 21.0, 13.8$ Hz, 2H), 2.22 – 1.94 (m, 2H), 1.75 – 1.33 (m, 6H). ^{13}C NMR (126 MHz, CDCl_3) δ 171.63, 163.88 (d, $J = 248.0$ Hz), 157.81 (d, $J = 9.9$ Hz), 153.56, 147.34, 142.81 (d, $J = 35.4$ Hz), 131.85 (d, $J = 10.0$ Hz), 131.03, 128.50, 128.37, 125.76, 122.41 (d, $J = 3.4$ Hz), 119.79, 111.07, 107.78 (d, $J = 21.4$ Hz), 99.82 (d, $J = 25.9$ Hz), 68.25, 55.93, 35.92, 35.50, 31.36, 29.03, 24.92.

1-(6-(4-fluoro-2-methoxyphenyl)oxazolo[4,5-b]pyridin-2-yl)-6-phenylhexan-1-one (15): The title compound was synthesized from **48** (66 mg, 0.16 mmol) according to the procedure described for **3**. This yielded 1-(6-(4-fluoro-2-methoxyphenyl)oxazolo[4,5-b]pyridin-2-yl)-6-phenylhexan-1-one (19 mg, 0.045 mmol, 28%). ^1H NMR (400 MHz, CDCl_3) δ 8.81 (d, $J = 18.6$ Hz, 1H), 7.93 (t, $J = 5.8$ Hz, 1H), 7.34 – 7.23 (m, 2H), 7.21 – 7.09 (m, 3H), 6.88 – 6.81 (m, 1H), 6.41 (dt, $J = 12.8, 6.4$ Hz, 1H), 6.33 – 6.25 (m, 1H), 3.75

(s, 3H), 3.28 (t, $J = 7.4$ Hz, 2H), 2.63 (dd, $J = 17.9, 10.2$ Hz, 2H), 1.87 (dt, $J = 15.1, 7.5$ Hz, 2H), 1.69 (dq, $J = 15.8, 7.8$ Hz, 2H), 1.55 – 1.45 (m, 2H). ^{13}C NMR (126 MHz, CDCl_3) δ 190.41, 164.18 (d, $J = 248.8$ Hz), 158.77, 157.95 (d, $J = 10.0$ Hz), 152.82, 150.00, 143.69, 142.53, 133.99, 131.91 (d, $J = 10.1$ Hz), 128.53 (2C), 128.42 (2C), 125.83, 122.05 (d, $J = 3.4$ Hz), 120.80, 108.00 (d, $J = 21.5$ Hz), 99.99 (d, $J = 25.9$ Hz), 56.01, 39.86, 35.85, 31.29, 28.84, 23.90. Purity $\geq 95\%$ as determined by LC/MS, m/z : calculated for $\text{C}_{25}\text{H}_{23}\text{FN}_2\text{O}_3$ (M + H) 419.18; found 419.13. HRMS (ESI+) m/z : calculated for $\text{C}_{25}\text{H}_{23}\text{FN}_2\text{O}_3$ (M + H) 419.1765; found 419.1762.

2-(6-amino-5-hydroxypyridin-3-yl)-5-fluorobenzonitrile (49): The title compound was synthesized from 2-amino-5-bromopyridin-3-ol (279 mg, 1.0 mmol) and 2-cyano-4-fluorobenzeneboronic acid pinacol ester (250 mg, 1.0 mmol) according to the procedures described for compound **19**. This yielded 2-(6-amino-5-hydroxypyridin-3-yl)-5-fluorobenzonitrile (80 mg, 0.35 mmol, 35%). ^1H NMR (400 MHz, MeOD) δ 7.66 – 7.52 (m, 3H), 7.48 (td, $J = 8.5, 2.7$ Hz, 1H), 7.11 (d, $J = 2.0$ Hz, 1H). ^{13}C NMR (101 MHz, MeOD) δ 162.58 (d, $J = 248.0$ Hz), 152.21, 141.52, 140.47, 136.96, 133.10 (d, $J = 8.4$ Hz), 124.44, 121.87 (d, $J = 21.6$ Hz), 121.25 (d, $J = 25.2$ Hz), 119.97, 118.48, 113.83 – 112.52.

5-fluoro-2-(2-(1-hydroxy-6-phenylhexyl)oxazolo[4,5-b]pyridin-6-yl)benzonitrile (50): The title compound was synthesized from **49** (78 mg, 0.34 mmol) according to the procedures described for **20**. This yielded 5-fluoro-2-(2-(1-hydroxy-6-phenylhexyl)oxazolo[4,5-b]pyridin-6-yl)benzonitrile (48 mg, 0.12 mmol, 35%). ^1H NMR (400 MHz, CDCl_3) δ 8.63 (d, $J = 1.8$ Hz, 1H), 8.04 (d, $J = 1.9$ Hz, 1H), 7.54 (dt, $J = 7.4, 3.7$ Hz, 2H), 7.44 (td, $J = 8.2, 2.6$ Hz, 1H), 7.31 – 7.20 (m, 2H), 7.20 – 7.08 (m, 3H), 5.15 – 4.96 (m, 1H), 2.59 (dd, $J = 17.8, 10.1$ Hz, 2H), 2.18 – 1.94 (m, 2H), 1.71 – 1.29 (m, 6H). ^{13}C NMR (101 MHz, CDCl_3) δ 172.83, 161.98 (d, $J = 252.6$ Hz), 155.36, 142.78, 142.64, 137.70 (d, $J = 3.8$ Hz), 132.63 (d, $J = 8.4$ Hz), 130.31, 128.49 (2C), 128.35 (2C), 125.74, 121.18 (d, $J = 21.3$ Hz), 120.86 (d, $J = 24.8$ Hz), 119.06, 116.95 (d, $J = 2.8$ Hz), 113.36 (d, $J = 9.4$ Hz), 68.27, 35.90, 35.47, 31.36, 29.00, 24.89.

5-fluoro-2-(2-(6-phenylhexanoyl)oxazolo[4,5-b]pyridin-6-yl)benzonitrile (16): The title compound was synthesized from **50** (48 mg, 0.12 mmol) according to the procedure described for **3**. This yielded 5-fluoro-2-(2-(6-phenylhexanoyl)oxazolo[4,5-b]pyridin-6-yl)benzonitrile (12 mg, 0.029 mmol, 24%). ^1H NMR (400 MHz, CDCl_3) δ 8.87 (d, $J = 14.0$ Hz, 1H), 8.22 (dd, $J = 15.0, 1.9$ Hz, 1H), 7.67 – 7.53 (m, 2H), 7.49 (td, $J = 8.2, 2.7$ Hz, 1H), 7.38 – 7.23 (m, 2H), 7.22 – 7.08 (m, 3H), 3.30 (t, $J = 7.4$ Hz, 2H), 2.64 (dd, $J = 16.5, 8.7$ Hz, 2H), 1.96 – 1.82 (m, 2H), 1.70 (dq, $J = 14.8, 7.3$ Hz, 2H), 1.49 (dt, $J = 15.3, 7.6$ Hz, 2H). ^{13}C NMR (101 MHz, CDCl_3) δ 190.12, 162.24 (d, $J = 253.3$ Hz), 159.55, 154.59, 148.89, 143.29, 142.48, 137.16 (d, $J = 3.8$ Hz), 133.05, 132.64 (d, $J = 8.5$ Hz), 128.52 (2C), 128.41 (2C), 125.83, 121.18, 121.17 (d, $J = 45.3$ Hz), 120.45, 116.73 (d, $J = 2.7$ Hz),

113.62 (d, $J = 9.3$ Hz), 39.97, 35.82, 31.29, 28.79, 23.77. Purity $\geq 95\%$ as determined by LC/MS, m/z : calculated for $C_{25}H_{20}FN_3O_2$ (M + H) 414.16; found 414.13. HRMS (ESI+) m/z : calculated for $C_{25}H_{20}FN_3O_2$ (M + H) 414.1612; found 414.608.

5-(benzyloxy)-[3,3'-bipyridin]-6-amine (51): The title compound was synthesized from 2-amino-5-bromopyridin-3-ol (305 mg, 1.1 mmol) and 3-pyridineboronic acid (1.2 eq., 161 mg, 1.3 mmol) according to the procedures described for compound **19**. This yielded 5-(benzyloxy)-[3,3'-bipyridin]-6-amine (200 mg, 0.73 mmol, 66%). 1H NMR (400 MHz, $CDCl_3$): $\delta = 8.72$ (s, 1H), 8.52 (d, $J = 4.8, 1.5$ Hz, 1H), 7.84 (s, 1H), 7.74 (d, $J = 8.0, 1.9$ Hz, 1H), 7.48 – 7.26 (m, 6H), 7.15 (s, 1H), 5.42 (br s, 2H), 5.12 (s, 2H). ^{13}C NMR (101 MHz, $CDCl_3$): $\delta = 150.43, 147.79, 147.27, 141.62, 136.21, 135.76, 134.07, 133.60, 128.73, 128.43, 127.63, 123.64, 123.30, 115.26, 70.38$. HR-MS (ESI+): $m/z = \text{calc. for } C_{17}H_{15}N_3O [M + H]^+ 278.1288$. Found 278.1287.

6-phenyl-1-(6-(pyridin-3-yl)oxazolo[4,5-b]pyridin- 2-yl)hexan-1-ol (52): The title compound was synthesized from **51** (96 mg, 0.5 mmol) according to the procedures described for **20**. This yielded 6-phenyl-1-(6-(pyridin-3-yl)oxazolo[4,5-b]pyridin- 2-yl)hexan-1-ol (72 mg, 0.19 mmol, 38%). 1H NMR (400 MHz, MeOD): $\delta = 8.91$ (d, $J = 2.3$ Hz, 1H), 8.81 (d, $J = 2.0$ Hz, 1H), 8.61 (dd, $J = 4.9, 1.5$ Hz, 1H), 8.41 (d, $J = 2.0$ Hz, 1H), 8.21 (dt, $J = 8.1, 1.9$ Hz, 1H), 7.59 (dd, $J = 8.0, 4.9$ Hz, 1H), 7.29 – 7.05 (m, 5H), 4.95 (t, $J = 7.7, 5.8$ Hz, 1H), 2.59 (t, $J = 7.7$ Hz, 2H), 1.80 – 1.69 (m, 2H), 1.68 – 1.52 (m, 2H), 1.52 – 1.24 (m, 4H). ^{13}C NMR (101 MHz, MeOD): $\delta = 180.63, 149.76, 148.86, 146.15, 143.86, 137.20, 132.49, 129.38, 129.23, 126.63, 125.68, 119.20, 68.79, 36.81, 35.57, 32.67, 30.06, 25.95$.

6-phenyl-1-(6-(pyridin-3-yl)oxazolo[4,5-b]pyridin- 2-yl)hexan-1-one(17): The title compound was synthesized from 6-phenyl-1-(6-(pyridin-3-yl)oxazolo[4,5-b]pyridin- 2-yl)hexan-1-ol (49 mg, 0.13mmol) according to the procedure described for **3**. This yielded 6-phenyl-1-(6-(pyridin-3-yl)oxazolo[4,5-b]pyridin- 2-yl)hexan-1-one (20 mg, 0.05 mmol, 39%). 1H NMR (400 MHz, $CDCl_3$): $\delta = 8.98$ (d, $J = 2.0$ Hz, 1H), 8.93 (s, 1H), 8.74 (d, $J = 4.8$ Hz, 1H), 8.16 (d, $J = 2.0$ Hz, 1H), 7.98 (dt, $J = 8.1, 1.8$ Hz, 1H), 7.51 (dd, $J = 7.9, 4.8$ Hz, 1H), 7.32 – 7.25 (m, 2H), 7.22 – 7.14 (m, 3H), 3.30 (t, $J = 7.4$ Hz, 2H), 2.65 (t, $J = 7.7$ Hz, 2H), 1.88 (p, $J = 7.5$ Hz, 2H), 1.71 (p, $J = 7.5$ Hz, 2H), 1.55 – 1.44 (m, 2H). ^{13}C NMR (101 MHz, $CDCl_3$): $\delta = 190.18, 159.18, 154.14, 149.92, 148.48, 148.02, 143.99, 142.47, 135.25, 134.08, 132.93, 128.51, 128.41, 25.83, 124.21, 118.41, 39.92, 35.82, 31.28, 28.80, 23.78$. HR-MS (ESI+): $m/z = \text{calc. for } C_{23}H_{21}N_3O_2 [M + H]^+ 372.1707$. Found 372.1711. Purity $\geq 95\%$ as determined by LC/MS.

2-amino-5-(1-methyl-1H-pyrrol-2-yl)pyridin-3-ol (53): The title compound was synthesized from 2-amino-5-bromopyridin-3-ol (1.59 g, 5.7 mmol) and 1-methyl-2-

pyrroleboronic acid pinacol ester (895 mg, 7.1 mmol) according to the procedures described for compound **19** using DMF as the solvent for the suzuki coupling. This yielded 2-amino-5-(1-methyl-1H-pyrrol-2-yl)pyridin-3-ol (117 mg, 0.61 mmol, 11%). ¹H NMR (500 MHz, MeOD) δ 7.33 (d, *J* = 1.8 Hz, 1H), 7.06 (d, *J* = 1.8 Hz, 1H), 6.69 (dd, *J* = 2.5, 2.0 Hz, 1H), 6.04 (ddd, *J* = 6.4, 3.6, 2.3 Hz, 2H), 3.56 (s, 3H). ¹³C NMR (126 MHz, MeOD) δ 149.38, 143.05, 130.69, 129.12, 125.20, 121.92, 121.15, 109.83, 108.67, 35.03.

1-(6-(1-methyl-1H-pyrrol-2-yl)oxazolo[4,5-b]pyridin-2-yl)-6-phenylhexan-1-ol (54):

The title compound was synthesized from **53** (128 mg, 0.67 mmol) according to the procedures described for **20**. This yielded 1-(6-(1-methyl-1H-pyrrol-2-yl)oxazolo[4,5-b]pyridin-2-yl)-6-phenylhexan-1-ol (44 mg, 0.12 mmol, 18%). ¹H NMR (500 MHz, CDCl₃) δ 8.59 (s, 1H), 7.96 – 7.66 (m, 1H), 7.27 – 7.23 (m, 3H), 7.16 – 7.11 (m, 2H), 6.80 (d, *J* = 1.7 Hz, 1H), 6.40 – 6.16 (m, 2H), 5.13 – 4.89 (m, 1H), 3.69 (s, 3H), 2.65 – 2.51 (m, *J* = 17.1, 9.2 Hz, 2H), 2.12 – 1.92 (m, 2H), 1.72 – 1.32 (m, 6H). ¹³C NMR (126 MHz, CDCl₃) δ 171.61, 153.37, 146.65, 143.15, 142.65, 130.21, 128.50 (2C), 128.37 (2C), 126.97, 125.77, 125.23, 118.24, 110.71, 108.60, 68.26, 35.93, 35.49, 35.25, 31.38, 29.02, 24.93.

1-(6-(1-methyl-1H-pyrrol-2-yl)oxazolo[4,5-b]pyridin-2-yl)-6-phenylhexan-1-one (18):

The title compound was synthesized from **54** (44 mg, 0.12 mmol) according to the procedure described for **3**. This yielded 1-(6-(1-methyl-1H-pyrrol-2-yl)oxazolo[4,5-b]pyridin-2-yl)-6-phenylhexan-1-one (19 mg, 0.051 mmol, 42%). ¹H NMR (500 MHz, CDCl₃) δ 8.81 (d, *J* = 23.2 Hz, 1H), 7.92 (dd, *J* = 14.2, 1.9 Hz, 1H), 7.41 – 7.23 (m, 2H), 7.23 – 7.10 (m, 3H), 6.84 (dd, *J* = 2.4, 1.9 Hz, 1H), 6.48 – 6.35 (m, 1H), 6.35 – 6.15 (m, 1H), 3.73 (s, 3H), 3.28 (t, *J* = 7.4 Hz, 2H), 2.70 – 2.56 (m, 2H), 1.92 – 1.81 (m, 2H), 1.75 – 1.66 (m, 2H), 1.49 (ddd, *J* = 18.1, 8.8, 6.6 Hz, 2H). ¹³C NMR (126 MHz, CDCl₃) δ 190.25, 158.68, 152.51, 149.18, 143.84, 142.53, 129.97, 129.76, 128.54 (2C), 128.43 (2C), 126.16, 125.84, 118.48, 111.58, 109.00, 39.85, 35.85, 35.46, 31.29, 28.85, 23.90. Purity ≥95% as determined by LC/MS, *m/z*: calculated for (M + H) C₂₃H₂₄N₃O₂ 374.18 found 374.20. HRMS (ESI+) *m/z*: calculated for C₂₃H₂₃N₃O₂ (M + H) 374.1863; found 374.1863.

Biochemical methods

The colorimetric hDAGL-α assay based on the hydrolysis of PNP-butyrate was performed as described in Chapter 4.

Concentration response analysis of the inhibitors against native DAGL-α in the mouse brain membrane proteome using competitive ABPP with MB064 (250 nM) were performed as described in chapter 4 and 5.

Selectivity in the mouse brain membrane proteome using TAMRA-FP (500 nM) and MB064 (250 nM) were performed as describes in chapter 4.

The fluorescence based DAGL- α natural substrate assay was performed as reported previously.¹⁵

References

1. Gao, Y.; Vasilyev, D. V.; Goncalves, M. B.; Howell, F. V.; Hobbs, C.; Reisenberg, M.; Shen, R.; Zhang, M. Y.; Strassle, B. W.; Lu, P. M.; Mark, L.; Piesla, M. J.; Deng, K. W.; Kouranova, E. V.; Ring, R. H.; Whiteside, G. T.; Bates, B.; Walsh, F. S.; Williams, G.; Pangalos, M. N.; Samad, T. A.; Doherty, P. *J. Neurosci.* **2010**, *30*, 2017.
2. Tanimura, A.; Yamazaki, M.; Hashimotodani, Y.; Uchigashima, M.; Kawata, S.; Abe, M.; Kita, Y.; Hashimoto, K.; Shimizu, T.; Watanabe, M.; Sakimura, K.; Kano, M. *Neuron* **2010**, *65*, 320.
3. Janssen, F. J.; van der Stelt, M. *Bioorg. Med. Chem. Lett.* **2016**, *26*, 3831.
4. Bisogno, T.; Howell, F.; Williams, G.; Minassi, A.; Cascio, M. G.; Ligresti, A.; Matias, I.; Schiano-Moriello, A.; Paul, P.; Williams, E. J.; Gangadharan, U.; Hobbs, C.; Di Marzo, V.; Doherty, P. *J. Cell Biol.* **2003**, *163*, 463.
5. Ortar, G.; Bisogno, T.; Ligresti, A.; Morera, E.; Nalli, M.; Di Marzo, V. *J. Med. Chem.* **2008**, *51*, 6970.
6. Bisogno, T.; Cascio, M. G.; Saha, B.; Mahadevan, A.; Urbani, P.; Minassi, A.; Appendino, G.; Saturnino, C.; Martin, B.; Razdan, R.; Di Marzo, V. *Biochim. biophys. acta, mol. cell. biol. lipids* **2006**, *1761*, 205.
7. Bisogno, T.; Mahadevan, A.; Coccurello, R.; Chang, J. W.; Allara, M.; Chen, Y. G.; Giacobuzzo, G.; Lichtman, A.; Cravatt, B.; Moles, A.; Di Marzo, V. *Br. J. Pharmacol.* **2013**, *169*, 784.
8. Ogasawara, D.; Deng, H.; Viader, A.; Baggelaar, M. P.; Breman, A.; den Dulk, H.; van den Nieuwendijk, A. M.; Soethoudt, M.; van der Wel, T.; Zhou, J.; Overkleeft, H. S.; Sanchez-Alavez, M.; Mo, S.; Nguyen, W.; Conti, B.; Liu, X.; Chen, Y.; Liu, Q. S.; Cravatt, B. F.; van der Stelt, M. *Proc. Natl. Acad. Sci. U. S. A.* **2016**, *113*, 26.
9. Hsu, K. L.; Tsuboi, K.; Chang, J. W.; Whitby, L. R.; Speers, A. E.; Pugh, H.; Cravatt, B. F. *J. Med. Chem.* **2013**, *56*, 8270.
10. Janssen, F. J.; Deng, H.; Baggelaar, M. P.; Allara, M.; van der Wel, T.; den Dulk, H.; Ligresti, A.; van Esbroeck, A. C.; McGuire, R.; Di Marzo, V.; Overkleeft, H. S.; van der Stelt, M. *J. Med. Chem.* **2014**, *57*, 6610.
11. Appiah, K. K.; Blat, Y.; Robertson, B. J.; Pearce, B. C.; Pedicord, D. L.; Gentles, R. G.; Yu, X. C.; Mseeh, F.; Nguyen, N.; Swaffield, J. C.; Harden, D. G.; Westphal, R. S.; Banks, M. N.; O'Connell, J. C. *J. Biomol. Screen.* **2014**, *19*, 595.
12. Baggelaar, M. P.; Janssen, F. J.; van Esbroeck, A. C.; den Dulk, H.; Allara, M.; Hoogendoorn, S.; McGuire, R.; Florea, B. I.; Meeuwenoord, N.; van den Elst, H.; van der Marel, G. A.; Brouwer, J.; Di Marzo, V.; Overkleeft, H. S.; van der Stelt, M. *Angew. Chem. Int. Ed.* **2013**, *52*, 12081.

13. Baggelaar, M. P.; Chameau, P. J.; Kantae, V.; Hummel, J.; Hsu, K. L.; Janssen, F.; van der Wel, T.; Soethoudt, M.; Deng, H.; den Dulk, H.; Allara, M.; Florea, B. I.; Di Marzo, V.; Wadman, W. J.; Kruse, C. G.; Overkleeft, H. S.; Hankemeier, T.; Werkman, T. R.; Cravatt, B. F.; van der Stelt, M. *J. Am. Chem. Soc.* **2015**, *137*, 8851.
14. Janssen, F. J.; Baggelaar, M. P.; Hummel, J. J.; Overkleeft, H. S.; Cravatt, B. F.; Boger, D. L.; van der Stelt, M. *J. Med. Chem.* **2015**, *58*, 9742.
15. van der Wel, T.; Janssen, F. J.; Baggelaar, M. P.; Deng, H.; den Dulk, H.; Overkleeft, H. S.; van der Stelt, M. *J. Lipid Res.* **2015**, *56*, 927.

CHAPTER 6

Chemical Proteomics Maps Brain Region Specific Activity of Endocannabinoid Hydrolases*

Introduction

The endocannabinoid system consists of the cannabinoid type 1 and 2 (CB₁ and CB₂) receptors, lipid messengers termed endocannabinoids, and the hydrolytic enzymes responsible for the biosynthesis and catabolism of these lipid signaling molecules. 2-Arachidonoylglycerol (2-AG) and anandamide (AEA) are the two main endocannabinoids.¹ The CB₁ receptor is highly expressed in the central nervous system, while the CB₂ receptor is more abundant in immune cells. The CB₁ receptor is among the most abundant G-protein coupled receptors in the brain and modulates a wide variety of signaling events, including inhibition of adenylate cyclase activity, stimulation of ERK activation, closure of voltage-sensitive Ca²⁺ channels and opening of K⁺ channels.^{2,3} Activation of the CB₁ receptor is associated with multiple physiological processes, such as energy balance, learning and memory, pain sensation, and neuro-inflammation.⁴⁻⁷ Unlike classical polar neurotransmitters, which are stored in presynaptic vesicles, 2-AG and AEA are synthesized “on-demand” from post-synaptic membranes and act as retrograde messengers activating presynaptic CB₁ receptors, thereby modulating neurotransmitter release. This implies that the biosynthetic and catabolic machinery of the endocannabinoids tightly regulates CB₁ receptor activation.⁸

*Baggelaar, M. P.; van Esbroeck, A. C. M.; van Rooden, E.; Florea, B. I.; Overkleeft, H. S.; Marsicano, G.; Chaoulloff, F.; van der stelt, M. Chemical Proteomics Maps Brain Region Specific Activity Of Endocannabinoid Hydrolases. *ACS Chem. Biol.* **2017**, DOI: 10.1021/acscchembio.6b01052.

Several biosynthetic and catabolic endocannabinoid hydrolases control 2-AG and AEA levels (Figure 1). Diacylglycerol lipase- α and - β (DAGL- α and DAGL- β) are the main enzymes producing 2-AG. They display a tissue specific distribution and studies using mice with congenital deletion of DAGL- α or DAGL- β have identified DAGL- α as the primary enzyme responsible for the biosynthesis of 2-AG in the brain.^{9,10} α,β -Hydrolase domain-containing protein 6 and 12 (ABHD6 and ABHD12) and monoacylglycerol lipase (MAGL) inactivate 2-AG by hydrolysis to give arachidonic acid (AA) and glycerol. MAGL is responsible for the bulk hydrolysis of 2-AG, while ABHD6 and ABHD12 play a more distinct role in specific cell populations.¹¹

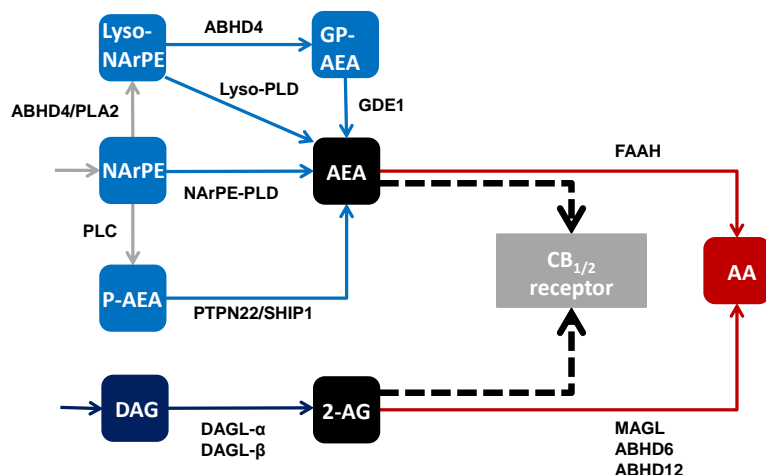


Figure 1. Biosynthetic and catabolic pathways of 2-AG and AEA.

The biosynthetic pathways towards AEA appear to be more complex compared with those of 2-AG.^{4,6} *N*-arachidonoyl-phosphatidylethanolamine (NArPE) is a key intermediate in AEA biosynthesis. NArPE can be converted via multiple phospholipase-dependent pathways to AEA: (a) hydrolysis by *N*-acylphosphatidylethanolamine-phospholipase D (NAPE-PLD), a metallo- β -lactamase, producing AEA and a phosphatidic acid in one step.¹² (b) phospholipase A₂ (PLA₂) and α,β -hydrolase domain-containing protein 4 (ABHD4) mediated conversion to lyso-NArPE, followed by the action of an unknown lysophospholipase D (PLD). Of note, lyso-NArPE can also be converted in a two-step sequence by ABHD4 to glycerophospho-AEA (GP-AEA) and subsequently hydrolyzed to AEA by glycerophosphodiesterase 1 or 4 (GDE1 or GDE4),^{13,14} (c) in macrophages NArPE serves as a substrate for an unidentified phospholipase C yielding phospho-AEA. Hydrolysis of the phosphate group by phosphatases PTPN22 or SHIP1 provides AEA.^{15,16} The enzymatic inactivation of AEA is less complex and is primarily

mediated by fatty acid amide hydrolase (FAAH), which hydrolyses AEA towards arachidonic acid and ethanolamine.^{4,17}

Monitoring the activity of the different endocannabinoid hydrolases in various brain regions is key to gain insight in spatiotemporal control of CB₁ receptor activation and its physiological role. The existence of a feedback mechanism in anterograde neurotransmitter systems through presynaptic “autoreceptors” to control the release of the neurotransmitters has led to the hypothesis that such an autoregulatory mechanism could also be present in retrograde systems, such as the endocannabinoid system.¹⁸⁻²⁰ Previous studies have investigated the effect of CB₁ receptor modulation on basal endocannabinoid levels. Several studies observed changes in AEA and/or 2-AG levels²¹⁻²⁵, whereas others did not.^{18,26} Interestingly, Maccarrone *et al.* found that the endocannabinoid system of CB₁ knockout mice adapted with age by upregulating AEA catabolism.^{23,24} Recently, Belluomo *et al.* reported that MAGL inhibitor JZL-195 reduced 2-AG accumulation rates in the frontal cortex of mice lacking the CB₁ receptor in glutamatergic neurons and an increase of 2-AG accumulation under the same conditions in mice with congenital deletion of the CB₁ receptor in astrocytes.¹⁸ In addition, chronic elevation of 2-AG levels by genetic deletion of MAGL or repeated administration of JZL184 led to CB₁ receptor desensitization.²⁷ These observations suggest that there is a crosstalk between the CB₁ receptor and the endocannabinoid regulatory machinery. The pre- and postsynaptic autoregulatory mechanisms controlling endocannabinoid levels are, however, poorly understood.

Studying changes in bulk endocannabinoid levels will not reveal which biosynthetic or catabolic pathways are responsible for the regulation of CB₁ receptor activity.^{18,26} To this end, the activity of each hydrolytic enzyme should be studied. Over the years a brain region and cell type resolved map of the molecular distribution of endocannabinoid hydrolases has been generated by *in situ* hybridization and global proteomics.²⁸⁻³⁰ These studies provided a detailed understanding of the molecular composition of the endocannabinoid system in different brain regions at the mRNA and protein level. However, actual enzymatic activity does not always correlate with mRNA and protein levels in specific brain regions due to post-transcriptional and post-translational processes.^{31,32} The activity of DAGL- α is, for example, regulated by CaMKII-mediated phosphorylation and MAGL activity can be modulated by sulfenylation of specific cysteines.^{33,34} Consequently, it is important to measure actual enzyme activity in the various brain regions.

Conventional enzyme activity assays rely on radiolabeled substrates and LC/MS-based methods.³⁵ These assays are expensive, time consuming and measure the activity of one enzyme at a time. Others and we have recently applied comparative activity-based protein profiling (ABPP) and chemo-proteomics to measure serine hydrolase activity in complex proteomes.³⁶⁻³⁹ ABPP is a technique, which relies on active site directed chemical probes that form a covalent bond with the catalytic nucleophile of targeted enzymes and have a fluorescent or biotin reporter group for visualization and identification,

respectively.³⁶ Many enzymes regulating brain endocannabinoid levels (i.e. MAGL, DAGL, FAAH, ABHD4, ABHD6 and ABHD12) belong to the serine hydrolase family, therefore they have conserved structural features, which allow for their targeting by specific activity-based probes (ABPs), such as FP-TAMRA and MB064. Here, we have used ABPP to map the relative activity of endocannabinoid hydrolases in different brain regions, such as cerebellum, frontal cortex, hippocampus and striatum. We applied this method to investigate the existence of an autoregulatory feedback mechanism of the CB₁ receptor on the endocannabinoid hydrolase activity by comparing the brains of CB₁ receptor knockout mice versus wild-type mice.

Results

Gel-based brain region comparison

Previously, a β -lactone (MB064) and fluorophosphonate (FP-TAMRA) were applied as tools to study the selectivity of DAGL inhibitors LEI104, LEI105 and DH376.^{38,40} The use of two ABPs extends the range of enzymes, because the probes have orthogonal warheads and different recognition elements, leading to a different interaction profile. Here, both ABPs were used to map brain region dependent activity of endocannabinoid hydrolases by comparative ABPP. Global assessment of serine hydrolase activity across four different brain regions was performed using a gel-based assay. Membrane and soluble proteomes from mouse cerebellum, frontal cortex, hippocampus or striatum were incubated with the fluorescent ABP MB064 (250 nM) or FP-TAMRA (500 nM), resolved on SDS-PAGE and followed by in-gel fluorescence detection. Coomassie staining was used as protein loading control. Using MB064, 9 intense bands were identified in the membrane fractions of the mouse brain regions, and the identity of endocannabinoid hydrolase bands could be established using reference inhibitors and KO tissue as previously reported.^{38,40}

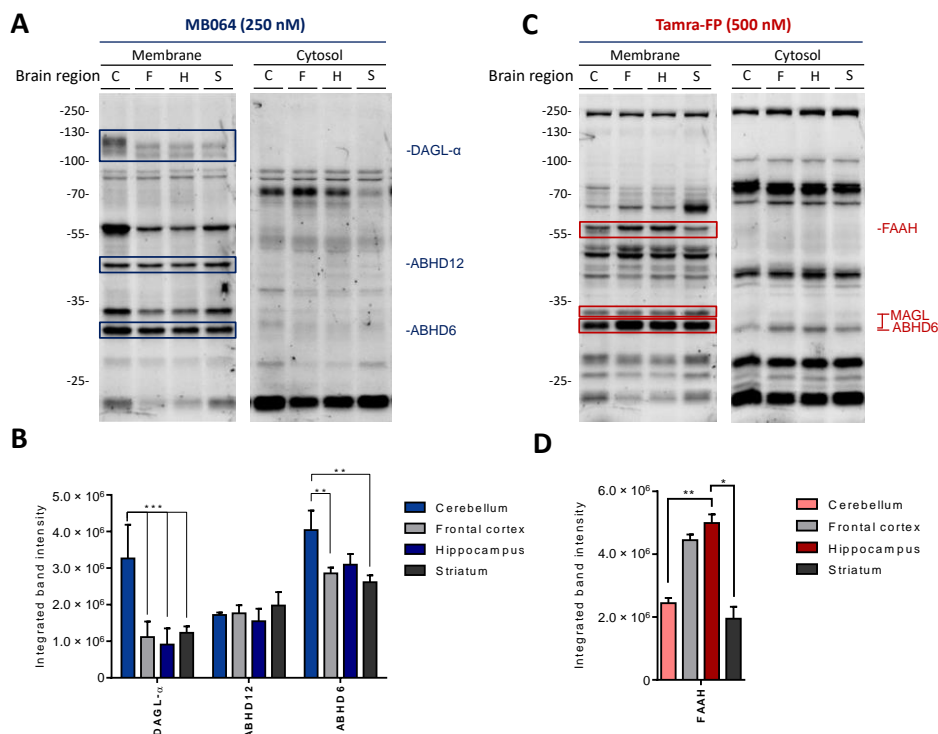


Figure 2. Gel based mapping of brain region dependent hydrolase activity. (A) Activity-based protein profiling with MB064 in 4 mouse brain regions. (B) Quantification of endocannabinoid hydrolase activity as determined with MB064. (C) Activity-based protein profiling with FP-TAMRA in 4 mouse brain regions. (D) Quantification of FAAH activity as measured with ABP FP-TAMRA. Statistical analysis was performed by means of 2-way ANOVA with Turkey multiple comparisons test (* $P \leq 0.05$; ** $P \leq 0.01$; *** $P \leq 0.001$) (C = cerebellum, F = frontal cortex, H = hippocampus, S = striatum)

In this manner the bands at 120 kDa, 45 kDa and 30 kDa were ascribed to DAGL- α , ABHD12 and ABHD6, respectively. FP-TAMRA labelled FAAH (64 kDa), MAGL (35 and 30 kDa) and ABHD6 (30 kDa). All identified endocannabinoid proteins were present in the four brain regions, but several hydrolases demonstrated pronounced region-dependent activity (Figure 2). For example, DAGL- α activity was ~3 times higher in the cerebellum compared to the frontal cortex, hippocampus and striatum (Figure 2A, B). Interestingly, the fluorescent protein band corresponding to DAGL- α in the cerebellum was shifted towards a higher molecular weight compared to the hippocampus, striatum and frontal cortex. This could indicate that DAGL- α carries a post-translational modification. The activity of ABHD12 was similar in all four brain regions, while the activity of ABHD6 was ~25% higher in the cerebellum compared to the frontal cortex, hippocampus and the striatum. The fluorophosphonate-based ABP revealed the the activity of FAAH to be ~2 times higher in the frontal cortex and the hippocampus. The signals of MAGL and ABHD6 as measured

with this activity-based probe are overlapping and could not be quantified accurately (Figure 2C).

Chemoproteomic brain region comparison

To analyze the relative activities in depth, ABPP was coupled to high resolution mass spectrometry. This methodology enables direct identification of the enzymes and provides a more accurate quantification by avoiding band overlap, and yields a broader range of hydrolases due to a higher sensitivity. Membrane and soluble proteomes from cerebellum, hippocampus, frontal cortex or striatum were separately incubated with MB108 or FP-biotin, biotinylated versions of MB064 and FP-TAMRA, respectively. Targeted enzymes were enriched by avidin chromatography, followed by on-bead digest using sequencing grade trypsin. Tryptic peptides from different brain regions were equipped with a different isotopic label by reductive dimethylation with deuterated or non-deuterated formaldehyde. After 1:1 mixing of the differentially labeled brain regions, samples were measured by high resolution MS/MS and analyzed using Maxquant software. (a schematic overview of the chemoproteomic workflow is given in Figure 3a).⁴¹

Using this chemoproteomic methodology, the relative activity of 34 different hydrolases was quantified in all brain regions, including DAGL- α , FAAH, ABHD12, MAGL, ABHD6 and ABHD4 (See Figure 3 for a heat map). Eleven enzymes reacted with both probes. A high correlation was found between the quantified enzymatic activities for each probe (pearson's correlation of 0.86 ($P < 0.0001$)), indicating probe-independent protein activity was measured (Figure 3). The fluorophosphonate-based ABP targeted 14 unique proteins, including MAGL and FAAH, whereas the β -lactone-based ABP MB108 targeted 7 unique proteins including ABHD4, ABHD12 and DAGL- α . ABHD4 showed an equal activity across all brain regions, while FAAH had the highest activity in the hippocampus and frontal cortex. The activity of DAGL- α in the cerebellum was ~2-fold higher compared to the striatum, hippocampus and frontal cortex. Interestingly, MAGL-activity was lowest in the cerebellum. The results from the chemoproteomic analysis were in line with the gel-based ABPP method, except for ABHD6, which is likely to be caused by band overlap in the gel-based assay. Further detailed analysis showed that overall relative enzymatic activities followed the same trends as observed for the protein abundance derived from a global proteomics data set published by Sharma *et al.*²⁹ (See supporting figure 1).

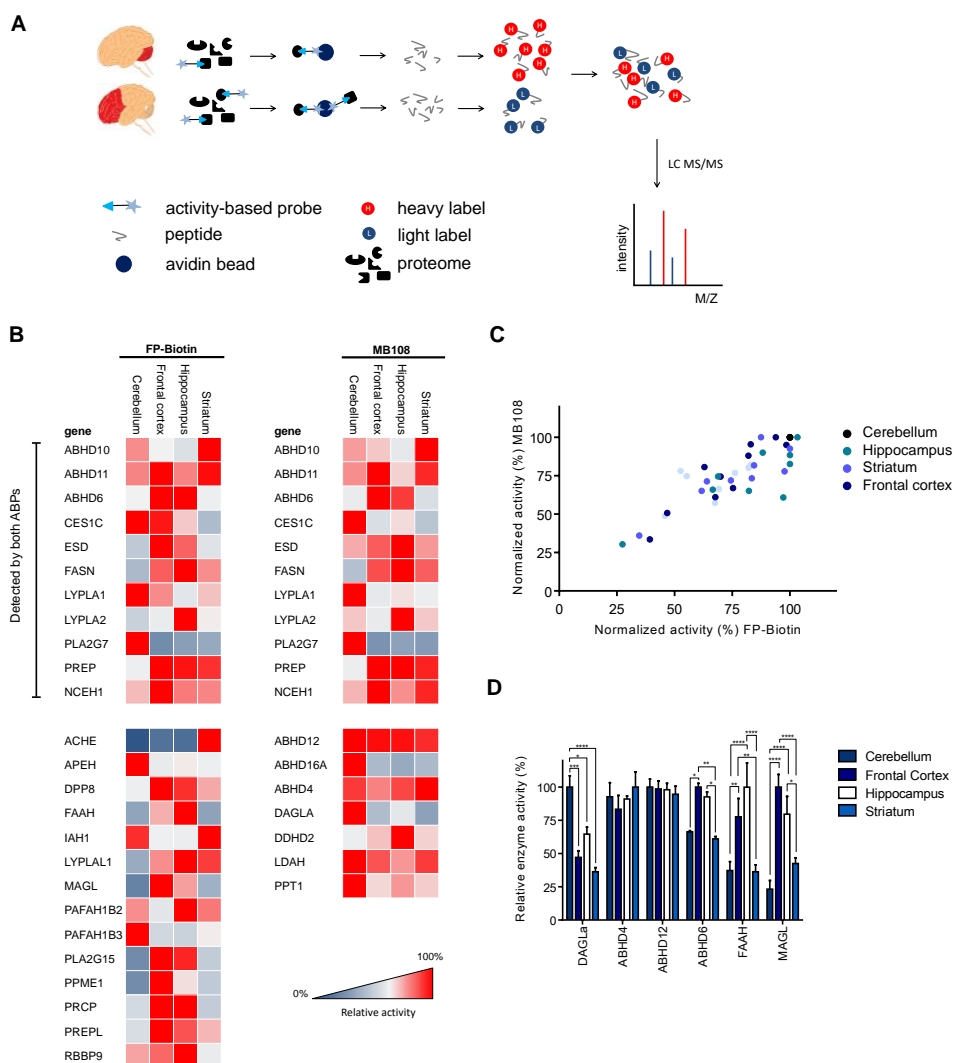


Figure 3. Brain region dependent chemoproteomic mapping of relative hydrolase activity. (A) Schematic representation of the chemoproteomic workflow. (B) Heat map of relative enzyme activity as measured by a fluorophosphonate (FP) based activity-based probe conjugated to a biotin reporter tag (FP-biotin) and a β -lactone based activity-based probe conjugated to a biotin reporter tag (MB108). Data is calculated from the mean ratios of the comparison between cerebellum and striatum, frontal cortex and striatum, and cerebellum and hippocampus. Each comparison was performed in 3 biological replicates. The relative enzyme activity in the brain region in which the serine hydrolase displayed highest activity was set to 100%. (C) Correlation graph for enzymes detected by both MB108 and FP-biotin. (D) Endocannabinoid regulating enzymes show significant difference between the studied brain regions. Statistical analysis was performed by means of 2 way ANOVA with Turkey multiple comparisons test (* $P \leq 0.05$; ** $P \leq 0.01$; *** $P \leq 0.001$) (C = cerebellum, F = frontal cortex, H = hippocampus, S = striatum)

Of note, several pronounced differences were detected. These different intensity profiles for activity and protein abundance may suggest that protein activity is regulated by post-translational modifications. For example, the activity of ABHD12 was equally distributed over the four brain regions, while ABHD12 abundance in the hippocampus was twice as high as in the cerebellum, frontal cortex and striatum. These different profiles might be explained by a down regulation of ABHD12 activity in the hippocampus. DAGL- α activity was highest in the cerebellum, while its relative activity in the frontal cortex was $47.2 \pm 8.6 \%$, $64.6 \pm 9.0\%$ in the hippocampus and $36.3 \pm 5.4\%$ in the striatum. In contrast, global proteomics data showed the highest abundance of DAGL- α in the hippocampus, while less than 30% was found in the cerebellum, frontal cortex and striatum. To investigate this apparent discrepancy, we have performed a western blot analysis to check the DAGL- α protein levels in the 4 brain regions of our mice. We observed relatively high DAGL- α abundance in the cerebellum (Figure 4), which matched the relative activity as measured with our ABPP method.

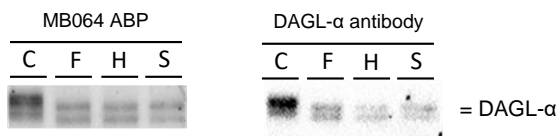


Figure 4. Activity based protein profiling and anti DAGL- α western blot in the mouse (C = cerebellum, F = frontal cortex, H = hippocampus, S = striatum)

Many other serine hydrolases were detected next to the endocannabinoid hydrolases (Figure 3). Marked differences in activity between the brain regions were observed for some of these enzymes. For example, acetylcholinesterase (ACHE), which is responsible for acetylcholine hydrolysis, showed over 10-fold activity in the striatum compared to the other three brain regions. ABHD16A, which is a phosphatidylserine lipase producing lysophosphatidyl-serine⁴², demonstrated a ~2-fold increased activity in the cerebellum compared to other brain regions. Platelet-activating factor acetylhydrolase (PLA2G7), which cleaves the *sn*-2 acetyl of acetyl-glycerol-ether-phosphorylcholine, showed an approximate 3-fold higher activity in the cerebellum compared to the other brain regions.⁴³

Comparison of CB₁^{+/+} and CB₁^{-/-} brain regions

Next, the regulatory control of the CB₁ receptor over basal production and degradation of endocannabinoids was investigated. To this end, the enzymatic activity of hydrolases involved in endocannabinoid biosynthesis and degradation in the cerebellum, hippocampus, frontal cortex and striatum of CB₁ receptor knockout mice was compared to their wild-type counterparts. Fluorescent scanning of gels from ABPP experiments using MB064 and FP-TAMRA did not reveal any difference in labeling patterns in the brain regions (Figure 5).

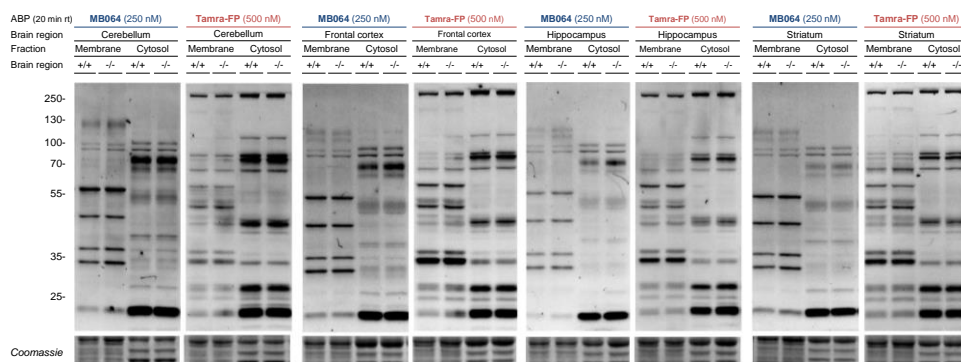


Figure 5. Gel based CB1^{+/+} vs CB1^{-/-} comparison. Study of enzyme activity in CB1^{+/+} and CB1^{-/-} mouse brain regions as measured by two activity based probes (MB064 and TAMRA-FP). No difference in enzyme activity between CB1^{-/-} and CB1^{+/+} was observed.

To investigate in depth the effect of CB₁ receptor deletion on serine hydrolase activity, the chemo-proteomic assay in the four mouse brain regions was performed. The relative activities of 36 different serine hydrolases were detected and quantified. No difference in the enzymatic activity of the 2-AG biosynthetic enzyme (DAGL- α) and the 2-AG catabolic enzymes ABHD6, ABHD12 and MAGL were observed in the cerebellum, frontal cortex, hippocampus or striatum. Nor were any changes observed in ABHD4 and FAAH activities.

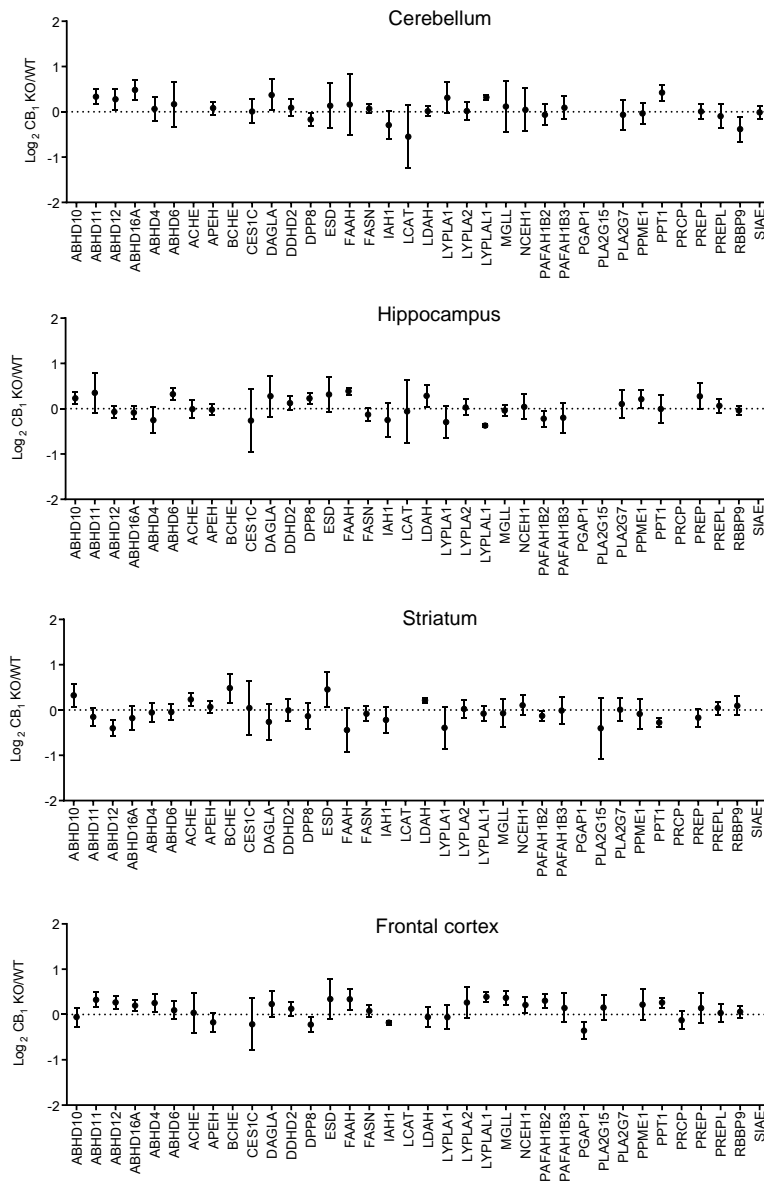


Figure 6. Comparison of enzyme activity in $\text{CB}_1^{+/+}$ and $\text{CB}_1^{-/-}$ mouse brain regions. Log_2 ratio of enzyme activity in $\text{CB}_1^{-/-}$ brain regions compared to $\text{CB}_1^{+/+}$. Activity is measured by activity-based proteomics using FP-biotin (10 μM) and MB108 (10 μM). Combined data from both activity based probes ($n = 4$ for each brain region). Statistical analysis by means of one-way ANOVA, each $\text{CB}_1 \text{ WT/KO}$ ratio was compared to a Log_2 ratio of 0, subsequently the p values were subjected to Benjamini Hochberg correction. Setting the false discovery rate at 10%.

Discussion

The enzymes responsible for endocannabinoid biosynthesis and degradation tightly regulate cannabinoid CB₁ receptor activation. In this Chapter, a fluorescence and chemoproteomic assay were employed to quantify the activity of hydrolases in the cerebellum, hippocampus, striatum and frontal cortex to gain more insight in the spatiotemporal control of CB₁ receptor-mediated physiology. The gel-based fluorescence assay has relatively short experiment time (~3h) and has the ability to retrieve information on differences in protein migration on SDS-PAGE caused by e.g. phosphorylation, glycosylation or proteolysis. Chemoproteomic methodology is complementary and directly reports on the identity and activity of a large number of enzymes in parallel in their native environment with all post-translational modifications in place.

Previous studies have indicated the importance of analyzing different brain regions when studying the endocannabinoid system. Endocannabinoid levels have been shown to vary between brain regions. Moreover, the CB₁ receptor and the endocannabinoid regulatory machinery do not present a homogenous expression across brain regions.^{1,26,29,44} These variations are confirmed in the comparative ABPP approach using cerebellum, hippocampus, frontal cortex and striatum. Significant differences were found in enzyme activity of DAGL- α , MAGL, ABHD6 and FAAH between different brain regions. For instance, highest FAAH activity was observed in the hippocampus, which is in line with previous reports indicating that the hippocampus has the highest FAAH expression levels, highest AEA levels and turnover rate compared to other brain regions.^{18,21,26} These observations suggest that AEA has an important physiological role in the hippocampus, such as providing “on demand” CB₁ receptor-dependent neuroprotection against excitotoxicity.⁴⁵ Next to its role as an endocannabinoid, AEA functions also as an endogenous agonist of the TRPV1 ion channel.⁴⁶ It could be envisioned that FAAH, not only terminates CB₁ receptor signaling, but also limits TRPV1 signaling by AEA in the hippocampus. In this respect, it would be interesting to investigate whether TRPV1 mediates crosstalk between AEA and 2-AG biosynthesis as was previously observed in the striatum.⁴⁷ Of note, FAAH does not only inactivate AEA, but uses a wide range of long chain fatty acid amides as substrates. The physiological role of these endogenous signaling lipids is poorly understood, but the hippocampus would be an excellent brain region to investigate their biological role.

DAGL- α activity was ~2 fold higher in the cerebellum compared to the frontal cortex, striatum and hippocampus. The activity of MAGL in the cerebellum was only 23.3 \pm 11% of the total MAGL activity in the frontal cortex. In addition, no relative compensatory activity of ABHD6 and ABHD12 was observed in the cerebellum (Figure 2). Yet, 2-AG levels are not substantially higher in the cerebellum.^{21,26,48} This may suggest that 2-AG levels and CB₁ receptor activity are controlled by MAGL, rather than by 2-AG

biosynthesis, or that other catabolic pathways, such as oxidative catabolism, could play a role in this brain region.

Comparison of the activity-based proteomics data with protein expression values from literature showed an overall correlation. For several enzymes (e.g. ABHD16A, ABHD10, ABHD12), however, the activity profile did not match protein abundance profile as reported in a global proteomics data set.²⁹ This may indicate that the activity of these proteins is regulated by post-translational modifications or could result from differences in the protein expression due to variation in age and mouse species analyzed in the various studies (as observed with DAGL- α).

Previous studies have investigated the effect of CB₁ receptor modulation by pharmacological or genetic means on endocannabinoid levels.^{18,21-26} Here, this question was revisited and the ABPP-methodology was employed to study the effect of genetic deletion of the CB₁ receptor on endocannabinoid hydrolase activity in various brain regions. No significant differences in the activity of endocannabinoid biosynthetic and catabolic enzymes between CB₁ KO and WT brain regions were observed. These results are in line with previous reports.^{26,18} Yet, it cannot be excluded that specific CB₁ receptor populations might increase production and/or degradation whilst others might decrease it, leading to a lack of change when removing all these receptor populations. In support of this hypothesis is the observation that within the frontal cortex the turnover of 2-AG is decreased and increased in mutant mice lacking CB₁ receptors on principal neurons (possibly glutamatergic) and on astrocytes, respectively.¹⁸

Although the proteomics assay is capable to detect a wide array of hydrolases that play an important role in regulation of endocannabinoid signaling, this methodology is not compatible with enzymes that do not form a covalent intermediate with their substrate, such as the β -metallo-lactamase NAPE-PLD. In addition, other mechanisms that regulate endocannabinoid signaling, such as the putative endocannabinoid transporter proteins and oxidative metabolism of endocannabinoids towards eicosanoids, are not taken into account by the ABPP-method.

In conclusion an ABPP method was employed that can measure the activity of six different enzymes with endocannabinoid hydrolase activity in their native setting in a single experiment without having the need of radioactive substrate assays for each individual enzyme. This methodology was used to map endocannabinoid hydrolase activity in the cerebellum, striatum, frontal cortex and cerebellum. This revealed brain region specific differences in endocannabinoid hydrolase activity. The method was applied to study the effect of genetic deletion of the CB₁ receptor in these brain regions. The results indicate that the CB₁ does not exert regulatory control over the basal production and degradation of endocannabinoids and that genetic deletion of the CB₁ receptor does not induce any compensatory mechanism in endocannabinoid hydrolase activity.

Experimental Methods

Animals

The experiments were conducted in strict compliance with European directives and French laws on animal experimentation (authorization number C33 12024 to F.C. from the French Ministry of Agriculture). The experiments were conducted on brains of male CB1 WT and KO mice that were sacrificed at the age of 8-9 weeks. The mice were bred at the NeuroCentre INSERM U862.

Preparation of mouse tissue proteome. The mouse brain regions; hippocampus, striatum, cerebellum and frontal cortex were slowly thawed on ice. The thawed mouse brain regions were dounce homogenized in cold (4 °C) pH 7.2 lysis buffer A (20 mM HEPES pH 7.2, 2 mM DTT, 1 mM MgCl₂, 25 U/mL Benzonase) and incubated for 5 minutes on ice. The suspension was centrifuged (2500 × g, 3 min, 4 °C) to remove debris. The supernatant was collected and subjected to ultracentrifugation (100.000 × g, 45 min. 4 °C, Beckman Coulter, Type Ti70 rotor). This yielded the membrane fraction as a pellet and the cytosolic fraction in the supernatant. The supernatant was collected and the membrane fraction was suspended in storage buffer (20 mM HEPES pH 7.2, 2 mM DTT). The total protein concentration was determined with Quick Start Bradford assay (Biorad) or QubitTM protein assay (Invitrogen). Membranes and supernatant fractions were both diluted to a total protein concentration of 0.5 mg/mL and were used directly or flash frozen in liquid nitrogen and stored in aliquots at -80 °C until use.

Activity-based protein profiling

Mouse hippocampus, striatum, cerebellum or frontal cortex (0.5 mg/mL) was incubated with activity-based probe MB064 (250 nM) or TAMRA-FP (500 nM) for 20 min at rt. Laemmli buffer was added to quench the protein activity and the mixture was allowed to stand at rt for 30 min before the the samples were loaded and resolved on SDS PAGE gel (10 % acrylamide). The gels were scanned using a ChemiDoc MP system (Cy3 settings, 605/50 filter) and analyzed using Image lab 4.1. After fluorescent scanning, the gels were stained with a coomassie staining solution. After destaining the gels were scanned and protein loading was quantified using image lab 4.1. Gel fluorescence intensities were corrected for protein abundance (loading control).

Western blot

Proteins were transferred from gel to a PVDF membrane using a Trans-Blot[®] Turbo (BioRad). The membrane was treated with a blocking solution (5% milk in TBST) for 1 h. The blot was subsequently incubated with the primary antibody rb-anti-DAGLa (D3G8H) (1:1000 in 5% BSA-TBST, 4C, O/N). After washing the blot was incubated with the secondary antibody gt-anti-rb-HRP (1:5000 in 5% BSA-TBST, RT, 1h)). After washing the

blot was developed in the dark using a 10 mL luminal solution, 100 μ L ECL enhancer and 3 μ L H_2O_2 . Chemiluminescence was visualized using a ChemiDoc XRS (BioRad).

Actin was used as a control using the same procedure, but using ms-anti-actin (1:5000 in 5% Milk-TBST, 4C, O/N) as primary antibody and gt-anti-ms-HRP (1:5000 in 5% BSA-TBST, RT, 1h) as secondary antibody.

Proteomics

Mouse brain region (250 μ L, 0.5 mg/mL) membrane or soluble proteome was incubated with vehicle MB108 (μ M) or FP-Biotin (10 μ M) for 60 min at rt. Subsequently the labeling reaction was quenched and excess probe was removed by chloroform/methanol precipitation. Precipitated proteome was suspended in 500 μ L 6M Urea/25 mM ammonium bicarbonate and allowed to incubate for 15 minutes. 5 μ L (1 M DTT) was added and the mixture was heated to 65 °C for 15 minutes. The sample was allowed to cool to rt before 40 μ L (0.5 M) iodoacetamide was added and the sample was alkylated for 30 minutes in the dark. 140 μ L 10% (wt/vol) SDS was added and the proteome was heated for 5 minutes at 65 °C. The sample was diluted with 6 mL PBS. 100 μ L (50 μ L for NPC^{+/+} and NPC^{-/-} mouse brains) of 50% slurry of Avidin-Agarose from egg white (Sigma-Aldrich) was washed with PBS and added to the proteome sample. The beads were incubated with the proteome > 2h.

The beads were isolated by centrifugation and washed with 0.5% (wt/vol) SDS and PBS (3x). The proteins were digested overnight with sequencing grade trypsin (Promega) in 100 μ L Pd buffer (100 mM Tris pH 7, 100 mM NaCl, 1 mM CaCl_2 , 2 % ACN and 500 ng trypsin) at 37 °C with vigorous shaking. The pH was adjusted with formic acid to pH 3 and the beads were removed. The peptides were isotopically labeled by on stage tip dimethyl labeling.

Brain regions were differently labeled with isotopic dimethyl labeling and combined after labeling to allow comparison.

On-stage tip dimethyl labeling

The stage tips were made by inserting C_{18} material in a 200 μ L pipet. The stepwise procedure given in the table below was followed for stage tip desalting and dimethyl labeling. The solutions were eluted by centrifugal force and the constitutions of the reagents are given below.

Step	Solution	Centrifugation speed
Conditioning	Methanol (50 μ L)	2 min 600g
Conditioning	Stage tip solution B (50 μ L)	2 min 600g
Conditioning	Stage tip solution A (50 μ L)	2 min 600g
Loading	Load samples on stage tips	2.5 min 800g
Washing	Stage tip solution A (100 μ L)	2.5 min 800g
Dimethyl labeling	Load 20 μ L L or M reagents on stage tip	5 min 400g
	Load 40 μ L L or M reagents on stage tip	5 min 400g
	Load 40 μ L L or M reagents on stage tip	5 min 400g
	Load 40 μ L L or M reagents on stage tip	5 min 400g
	Load 40 μ L L or M reagents on stage tip	5 min 400g
	Load 30 μ L L or M reagents on stage tip	5 min 400g
	Load 30 μ L L or M reagents on stage tip	5 min 400g
Washing	Stage tip solution A (100 μ L)	2.5 min 800g
Elution	Stage tip solution B (100 μ L)	2.5 min 800g

Stage tip solution A: Stage tip solution A is 0.5% (vol/vol) FA in H₂O. (Freshly prepared solution)

Stage tip solution B: Stage tip solution B is 0.5% (vol/vol) FA in 80% (vol/vol) ACN/H₂O. (Freshly prepared solution).

Dimethyl labeling reagents

Light labeling reagent	Final concentration	Volume
Phosphate buffer (50 mM; pH 7.5)		900 μ L
CH ₂ O (light)		50 μ L
NaBH ₃ CN (0.6 M)	0.03 M	50 μ L

Medium labeling reagent	Final concentration	Volume
Phosphate buffer (50 mM; pH 7.5)		900 μ L
CD ₂ O (Medium)		50 μ L
NaBH ₃ CN (0.6 M)	0.03 M	50 μ L

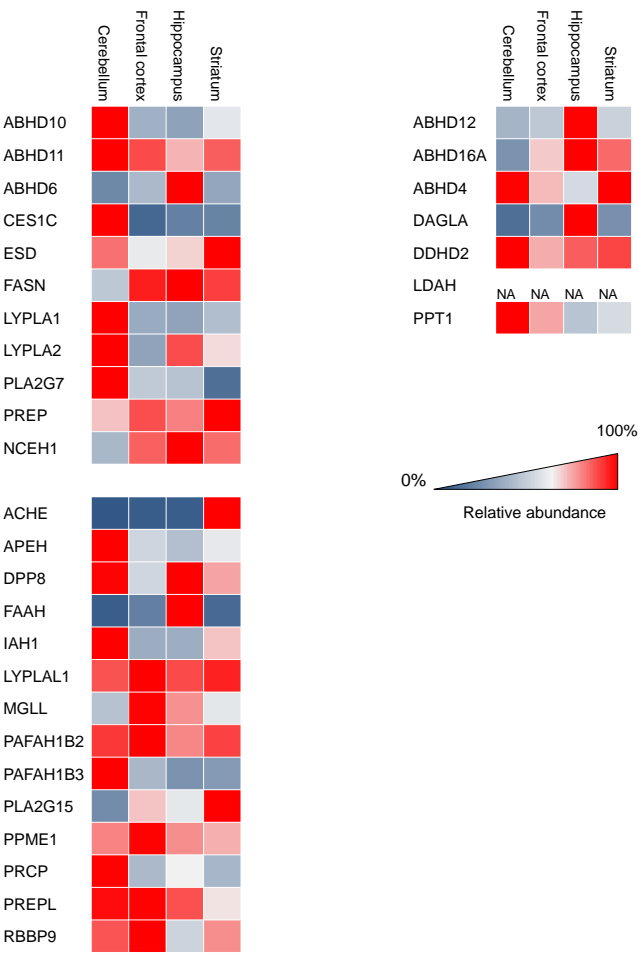
After the final elution step, the desired heavy and light samples were combined and concentrated on a speedvac to remove the ACN. The residue was reconstituted in 95:3:0.1 H₂O/ACN/FA (vol/vol) before LC/MS analysis.

Tryptic peptides were analyzed on a Surveyor nanoLC system (Thermo) hyphenated to a LTQ-Orbitrap mass spectrometer (Thermo) as previously described.¹ Briefly, emitter, trap

and analytical column (C18, 120 Å) were purchased from Nanoseparations (Nieuwkoop, The Netherlands) and mobile phases (A: 0.1% formic acid/H₂O, B: 0.1% formic acid/ACN) were made with ULC/MS grade solvents (Biosolve). General mass spectrometric conditions were: electrospray voltage of 1.8–2.5 kV, no sheath and auxiliary gas flow, capillary voltage 40 V, tube lens voltage 155 V and ion transfer tube temperature 150 °C. Polydimethylcyclsiloxane ($m/z = 445.12002$) and dioctyl phthalate ions ($m/z = 391.28429$) from the milieu were used as lock mass. Some 10 µl of the samples was pressure loaded on the trap column for 5 min with a 10 µl/min flow and separated with a gradient of 35 min 5%–30% B, 15 min 30%–60% B, 5 min A at a flow of 300 µl/min split to 250 nl/min by the LTQ divert valve. Full MS scans (300–2000 m/z) acquired at high mass resolution (60,000 at 400 m/z , maximum injection time 1000 ms, AGC 106) in the Orbitrap was followed by three MS/MS fragmentations in the LTQ linear ion trap (AGC 5x10³, max inj time 120 ms) from the three most abundant ions. MS/MS settings were: collision gas pressure 1.3 mT, normalized collision energy 35%, ion selection threshold of 750 counts, activation $q = 0.25$ and activation time 30 ms. Ions of $z < 2$ or unassigned were not analyzed and fragmented precursor ions were measured twice within 10 s and were dynamically excluded for 60 s. Data analysis was performed using Maxquant with acetylation (protein N term) and oxidation (M) as variable modifications. The false discovery rate was set at 1% and the peptides were screened against mouse proteome (Uniprot). Serine hydrolases that were identified in at least two repetitive experiments and for which at least 2 unique peptides were identified were considered as valid quantifiable hits. The activities of proteins were relatively quantified by setting the protein with highest activity at 100%.

Statistical analysis for CB₁^{+/+} and CB₁^{-/-} comparison.

For proteins identified by both probes, the normalized ratios from Maxquant were combined for further analysis. Using GraphPad Prism 7.0 software the binary logarithm of each ratio was compared to 0 with one way ANOVA. The resulting p values were subjected to a Benjamini-Hochberg correction, setting the false discovery rate at 10% ($q=0.1$). Briefly, the p-values of all quantifiable hits were ordered from lowest to highest, and the Benjamini-Hochberg statistic was calculated as $q * (\text{position in the list})$ divided by the number of tests. Subsequently, the proteins for which the p-value is smaller than the BH statistic are controlled for a FDR of $q*10\%$.



Supporting Figure 1. Relative abundance of the hydrolases determined with untargeted proteomics, retrieved from literature.²⁹

References

1. Mechoulam, R.; Parker, L. A. *Annu. Rev. Physiol.* **2013**, *64*, 21.
2. Dalton, G. D.; Howlett, A. C. *Br. J. Pharmacol.* **2012**, *165*, 2497.
3. Howlett, A. C.; Barth, F.; Bonner, T. I.; Cabral, G.; Casellas, P.; Devane, W. A.; Felder, C. C.; Herkenham, M.; Mackie, K.; Martin, B. R.; Mechoulam, R.; Pertwee, R. G. *Pharmacol. Rev.* **2002**, *54*, 161.
4. Ahn, K.; McKinney, M. K.; Cravatt, B. F. *Chem. Rev.* **2008**, *108*, 1687.
5. Di Marzo, V. *Nat. Neurosci.* **2011**, *14*, 9.
6. Piomelli, D. *Neuropharmacol.* **2014**, *76 Pt B*, 228.
7. Pacher, P.; Batkai, S.; Kunos, G. *Pharmacol. Rev.* **2006**, *58*, 389.
8. Di Marzo, V.; Bifulco, M.; De Petrocellis, L. *Nat. Rev. Drug Discov.* **2004**, *3*, 771.
9. Gao, Y.; Vasilyev, D. V.; Goncalves, M. B.; Howell, F. V.; Hobbs, C.; Reisenberg, M.; Shen, R.; Zhang, M. Y.; Strassle, B. W.; Lu, P.; Mark, L.; Piesla, M. J.; Deng, K.; Kouranova, E. V.; Ring, R. H.; Whiteside, G. T.; Bates, B.; Walsh, F. S.; Williams, G.; Pangalos, M. N.; Samad, T. A.; Doherty, P. J. *Neurosci.* **2010**, *30*, 2017.
10. Tanimura, A.; Yamazaki, M.; Hashimotodani, Y.; Uchigashima, M.; Kawata, S.; Abe, M.; Kita, Y.; Hashimoto, K.; Shimizu, T.; Watanabe, M.; Sakimura, K.; Kano, M. *Neuron* **2010**, *65*, 320.
11. Murataeva, N.; Straiker, A.; Mackie, K. *Br. J. Pharmacol.* **2014**, *171*, 1379.
12. Di Marzo, V.; Fontana, A.; Cadas, H.; Schinelli, S.; Cimino, G.; Schwartz, J. C.; Piomelli, D. *Nature* **1994**, *372*, 686.
13. Sun, Y. X.; Tsuboi, K.; Okamoto, Y.; Tonai, T.; Murakami, M.; Kudo, I.; Ueda, N. *Biochem. J.* **2004**, *380*, 749.
14. Tsuboi, K.; Okamoto, Y.; Rahman, I. A.; Uyama, T.; Inoue, T.; Tokumura, A.; Ueda, N. *Biochim. Biophys. Acta* **2015**, *1851*, 537.
15. Liu, J.; Wang, L.; Harvey-White, J.; Huang, B. X.; Kim, H. Y.; Luquet, S.; Palmiter, R. D.; Krystal, G.; Rai, R.; Mahadevan, A.; Razdan, R. K.; Kunos, G. *Neuropharmacol.* **2008**, *54*, 1.
16. Rahman, I. A. S.; Tsuboi, K.; Uyama, T.; Ueda, N. *Pharmacol. Res.* **2014**, *86*, 1.
17. Cravatt, B. F.; Giang, D. K.; Mayfield, S. P.; Boger, D. L.; Lerner, R. A.; Gilula, N. B. *Nature* **1996**, *384*, 83.
18. Belluomo, I.; Matias, I.; Pernegre, C.; Marsicano, G.; Chaouloff, F. *J. Neurochem.* **2015**, *133*, 26.
19. Starke, K.; Gothert, M.; Kilbinger, H. *Physiological reviews* 1989, *69*, 864.
20. Langer, S. Z. *Trends Pharmacol. Sci.* **1997**, *18*, 95.
21. Di Marzo, V.; Breivogel, C. S.; Tao, Q.; Bridgen, D. T.; Razdan, R. K.; Zimmer, A. M.; Zimmer, A.; Martin, B. R. *J. Neurochem.* **2000**, *75*, 2434.

22. Di Marzo, V.; Berrendero, F.; Bisogno, T.; Gonzalez, S.; Cavaliere, P.; Romero, J.; Cebeira, M.; Ramos, J. A.; Fernandez-Ruiz, J. J. *J. Neurochem.* **2000**, *74*, 1627.
23. Maccarrone, M.; Attina, M.; Bari, M.; Cartoni, A.; Ledent, C.; Finazzi-Agro, A. *J. Neurochem.* **2001**, *78*, 339.
24. Maccarrone, M.; Valverde, O.; Barbaccia, M. L.; Castane, A.; Maldonado, R.; Ledent, C.; Parmentier, M.; Finazzi-Agro, A. *Eur. J. Neurosci.* **2002**, *15*, 1178.
25. Bequet, F.; Uzabiaga, F.; Desbazeille, M.; Ludwiczak, P.; Maftouh, M.; Picard, C.; Scatton, B.; Le Fur, G. *Eur. J. Neurosci.* **2007**, *26*, 3458.
26. Leishman, E.; Cornett, B.; Spork, K.; Straiker, A.; Mackie, K.; Bradshaw, H. B. *Pharmacological Research* **2016**.
27. Schlosburg, J. E.; Blankman, J. L.; Long, J. Z.; Nomura, D. K.; Pan, B.; Kinsey, S. G.; Nguyen, P. T.; H.; Cravatt, B. F. *Nat. Neurosci.* **2010**, *13*, 1113.
28. Kang, H. J.; Kawasaki, Y. I.; Cheng, F.; Zhu, Y.; Xu, X. M.; Li, M. F.; Sousa, A. M. M.; Pletikos, M.; Meyer, K. A.; Sedmak, G.; Guennel, T.; Shin, Y.; Johnson, M. B.; Krsnik, Z.; Mayer, S.; Fertuzinhos, S.; Umlauf, S.; Lisgo, S. N.; Vortmeyer, A.; Weinberger, D. R.; Mane, S.; Hyde, T. M.; Huttner, A.; Reimers, M.; Kleinman, J. E.; Sestan, N. *Nature* 2011, *478*, 483.
29. Sharma, K.; Schmitt, S.; Bergner, C. G.; Tyanova, S.; Kannaiyan, N.; Manrique-Hoyos, N.; Kongi, K.; Cantuti, L.; Hanisch, U. K.; Philips, M. A.; Rossner, M. J.; Mann, M.; Simons, M. *Nat. Neurosci.* **2015**, *18*, 1819.
30. Lein, E. S.; Hawrylycz, M. J.; Ao, N.; Ayres, M.; Bensinger, A.; Bernard, A.; Boe, A. F.; Boguski, M. S.; Brockway, K. S.; Byrnes, E. J.; Chen, L.; Chen, L.; Chen, T. M.; Chin, M. C.; Chong, J.; Crook, B. E.; Czaplinska, A.; Dang, C. N.; Datta, S.; Dee, N. R.; Desaki, A. L.; Desta, T.; Diep, E.; Dolbeare, T. A.; Donelan, M. J.; Dong, H. W.; Dougherty, J. G.; Duncan, B. J.; Ebbert, A. J.; Eichele, G.; Estlin, L. K.; Faber, C.; Facer, B. A.; Fields, R.; Fischer, S. R.; Fliss, T. P.; Frensley, C.; Gates, S. N.; Glattfelder, K. J.; Halverson, K. R.; Hart, M. R.; Hohmann, J. G.; Howell, M. P.; Jeung, D. P.; Johnson, R. A.; Karr, P. T.; Kaval, R.; Kidney, J. M.; Knapik, R. H.; Kuan, C. L.; Lake, J. H.; Laramie, A. R.; Larsen, K. D.; Lau, C.; Lemon, T. A.; Liang, A. J.; Liu, Y.; Luong, L. T.; Michaels, J.; Morgan, J. J.; Morgan, R. J.; Mortrud, M. T.; Mosqueda, N. F.; Ng, L. L.; Ng, R.; Orta, G. J.; Overly, C. C.; Pak, T. H.; Parry, S. E.; Pathak, S. D.; Pearson, O. C.; Puchalski, R. B.; Riley, Z. L.; Rickett, H. R.; Rowland, S. A.; Royall, J. J.; Ruiz, M. J.; Sarno, N. R.; Schaffnit, K.; Shapovalova, N. V.; Sivasay, T.; Slaughterbeck, C. R.; Smith, S. C.; Smith, K. A.; Smith, B. I.; Sordt, A. J.; Stewart, N. N.; Stumpf, K. R.; Sunkin, S. M.; Sutram, M.; Tam, A.; Teemer, C. D.; Thaller, C.; Thompson, C. L.; Varnam, L. R.; Visel, A.; Whitlock, R. M.; Wornoutka, P. E.; Wolkey, C. K.; Wong, V. Y. *Nature* **2007**, *445*, 168.
31. Vogel, C.; Marcotte, E. M. *Nat. Rev. Genet.* **2012**, *13*, 227.
32. Kobe, B.; Kemp, B. E. *Nature* **1999**, *402*, 373.

33. Dotsey, E. Y.; Jung, K. M.; Basit, A.; Wei, D.; Daglian, J.; Vacondio, F.; Armirotti, A.; Mor, M.; Piomelli, D. *Chem. Biol.* **2015**, 22, 619.
34. Shonesy, B. C.; Wang, X.; Rose, K. L.; Ramikie, T. S.; Cavener, V. S.; Rentz, T.; Baucum, A. J., 2nd; Jalan-Sakrikar, N.; Mackie, K.; Winder, D. G.; Patel, S.; Colbran, R. J. *Nat. Neurosci.* **2013**, 16, 456.
35. Bisogno, T.; Howell, F.; Williams, G.; Minassi, A.; Cascio, M. G.; Ligresti, A.; Matias, I.; Schiano-Moriello, A.; Paul, P.; Williams, E. J.; Gangadharan, U.; Hobbs, C.; Di Marzo, V.; Doherty, P. *J. Cell Biol.* **2003**, 163, 463.
36. Cravatt, B. F.; Wright, A. T.; Kozarich, J. W. *Annu. Rev. Biochem.* **2008**, 77, 383.
37. Niphakis, M. J.; Cravatt, B. F. *Annu. Rev. Biochem.* **2014**, 83, 341.
38. Baggelaar, M. P.; Chameau, P. J.; Kantae, V.; Hummel, J.; Hsu, K. L.; Janssen, F.; van der Wel, T.; Soethoudt, M.; Deng, H.; den Dulk, H.; Allara, M.; Florea, B. I.; Di Marzo, V.; Wadman, W. J.; Kruse, C. G.; Overkleeft, H. S.; Hankemeier, T.; Werkman, T. R.; Cravatt, B. F.; van der Stelt, M. *J. Am. Chem. Soc.* **2015**, 137, 8851.
39. Liu, Y.; Patricelli, M. P.; Cravatt, B. F. *Proc. Natl. Acad. Sci. U. S. A.* **1999**, 96, 14694.
40. Baggelaar, M. P.; Janssen, F. J.; van Esbroeck, A. C.; den Dulk, H.; Allara, M.; Hoogendoorn, S.; McGuire, R.; Florea, B. I.; Meeuwenoord, N.; van den Elst, H.; van der Marel, G. A.; Brouwer, J.; Di Marzo, V.; Overkleeft, H. S.; van der Stelt, M. *Angew. Chem. Int. Ed.* **2013**, 52, 12081.
41. Cox, J.; Mann, M. *Nat. Biotechnol.* **2008**, 26, 1367.
42. Kamat, S. S.; Camara, K.; Parsons, W. H.; Chen, D. H.; Dix, M. M.; Bird, T. D.; Howell, A. R.; Cravatt, B. F. *Nat. Chem. Biol.* **2015**, 11, 164.
43. Long, J. Z.; Cravatt, B. F. *Chem. Rev.* **2011**, 111, 6022.
44. Herkenham, M.; Lynn, A. B.; Little, M. D.; Johnson, M. R.; Melvin, L. S.; de Costa, B. R.; Rice, K. C. *Proc. Natl. Acad. Sci. U. S. A.* **1990**, 87, 1932.
45. Marsicano, G.; Goodenough, S.; Monory, K.; Hermann, H.; Eder, M.; Cannich, A.; Azad, S. C.; Cascio, M. G.; Gutierrez, S. O.; van der Stelt, M.; Lopez-Rodriguez, M. L.; Casanova, E.; Schutz, G.; Zieglgansberger, W.; Di Marzo, V.; Behl, C.; Lutz, B. *Science* **2003**, 302, 84.
46. van der Stelt, M.; Trevisani, M.; Vellani, V.; De Petrocellis, L.; Schiano Moriello, A.; Campi, B.; McNaughton, P.; Geppetti, P.; Di Marzo, V. *EMBO J.* **2005**, 24, 3026.
47. Maccarrone, M.; Rossi, S.; Bari, M.; De Chiara, V.; Fezza, F.; Musella, A.; Gasperi, V.; Prosperetti, C.; Bernardi, G.; Finazzi-Agro, A.; Cravatt, B. F.; Centonze, D. *Nat. Neurosci.* **2008**, 11, 152.
48. Buczynski, M. W.; Parsons, L. H. *Br. J. Pharmacol.* **2010**, 160, 423.

CHAPTER 7

Focused Library Screening Using Activity-based Probes Reveals Novel Inhibitors of the α,β -hydrolase Fold Family*

Introduction

The activity-based probes (ABPs) MB064 and MB108 that were initially designed to target diacylglycerol lipase- α are non-specific ABPs that label multiple enzymes. After a close look at their target profiles in chapter 3, 4 and 6 it became apparent that they showed affinity for multiple α,β -hydrolase fold domain (ABHD) containing proteins. These targets

included ABHD6, ABHD12 and ABHD16a, therefore it was hypothesized that MB064 and MB108 could potentially serve as broad-spectrum ABPs for the α,β -hydrolase fold protein superfamily.

The α,β -hydrolase protein fold was discovered 1992 by Ollis *et al.*² This protein family is one of the largest and most diverse protein families, covering most, albeit not all, serine hydrolases. The α,β -hydrolase fold family includes lipases, esterases, epoxidases, peroxide hydrolases and dehalogenases.² The α,β -fold is characterized by 8 β -strands forming a central β -sheet, which is surrounded and

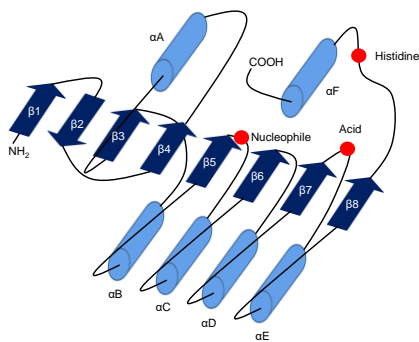


Figure 1. Structure of the α,β -hydrolase fold. B-sheets are denoted as arrows and α -helices are denoted as cylinders. The amino acids of the catalytic triad are depicted in red. Figure is adapted from Nardini and Dijkstra.¹

*Xavier Ruf and Hans den Dulk are kindly acknowledged for the generation of the ABHD constructs and Bogdan I. Florea is kindly acknowledged for the analysis of proteomics samples.

connected by 6 α -helices and several loops (Figure 1).¹ A catalytic triad formed by a catalytic nucleophile, an acidic residue and a histidine is responsible for hydrolase activity. The catalytic nucleophile resides within the nucleophilic elbow, which can be recognized by the consensus motif Sm-X-Nu-X-Sm (Sm = small residue, X = any residue, Nu = nucleophile). A special subgroup of the α,β -hydrolase family are the ABHD proteins, which consists of 22 members. Members sharing the ABHD nomenclature generally have a GX SXG motif.³ Conserved structural features shared by this subfamily predict common roles in lipid biosynthesis and metabolism.³ Dysregulated lipid metabolism is the underlying cause of many human disorders.^{4,5} Despite their potentially important roles in pathological conditions, products and substrates of the ABHD family members and their position in lipid metabolic pathways are largely unknown.

ABHD family members play important roles in various (patho)physiological processes. For example, α,β -hydrolase domain-containing protein 2 (ABHD2) is essential in hepatitis B virus propagation,⁶ and has recently been identified as an enzyme that stimulates sperm activation.⁷ ABHD11 is deleted in the Williams-Beuren syndrome,⁸ and mutations in ABHD12 have been shown to be causative in polyneuropathy, hearing loss, ataxia, retinitis pigmentosa and cataract (PHARC).⁹ The physiological role of many members of this enzyme family is not elucidated. Small molecule inhibitors for these enzymes are likely to provide valuable information on the (patho)physiological functions of these enzymes, and may potentially serve as leads for novel therapeutic agents.

In this chapter ABPs MB108 and MB064 are profiled as broad-spectrum probes for the α,β -hydrolase fold protein family. Broad-spectrum probes are unique in their ability to enable screening of an inhibitor library against multiple enzymes in parallel. A library against library screen of 7 enzymes against 200+ inhibitors facilitated rapid identification of inhibitors for ABHD2 and ABHD3. No inhibitors are currently available for these enzymes. It is anticipated that these new inhibitors will be instrumental to study the (patho)physiological role of ABHD2 and ABHD3.

Results

Identification of α,β -hydrolase fold containing proteins targeted by MB064 and MB108

A large variety in expression for α,β -hydrolase fold family members across different tissue types has been observed by *in-situ* hybridization and in global proteomics studies.^{3,10-12} Therefore, it was investigated whether this tissue specific expression was mirrored in the enzyme activity measured by ABP MB064. The labeling profile of fluorescent ABP MB064 in the mouse cytosol and membrane fractions of the brain, heart, kidney, liver, lung, pancreas, spleen and testes was examined (Figure 2B). A highly diverse labeling pattern across different tissue types was observed, in particular in the membrane fraction. Therefore, the extent of α,β -hydrolase fold family members targeted by a biotinylated

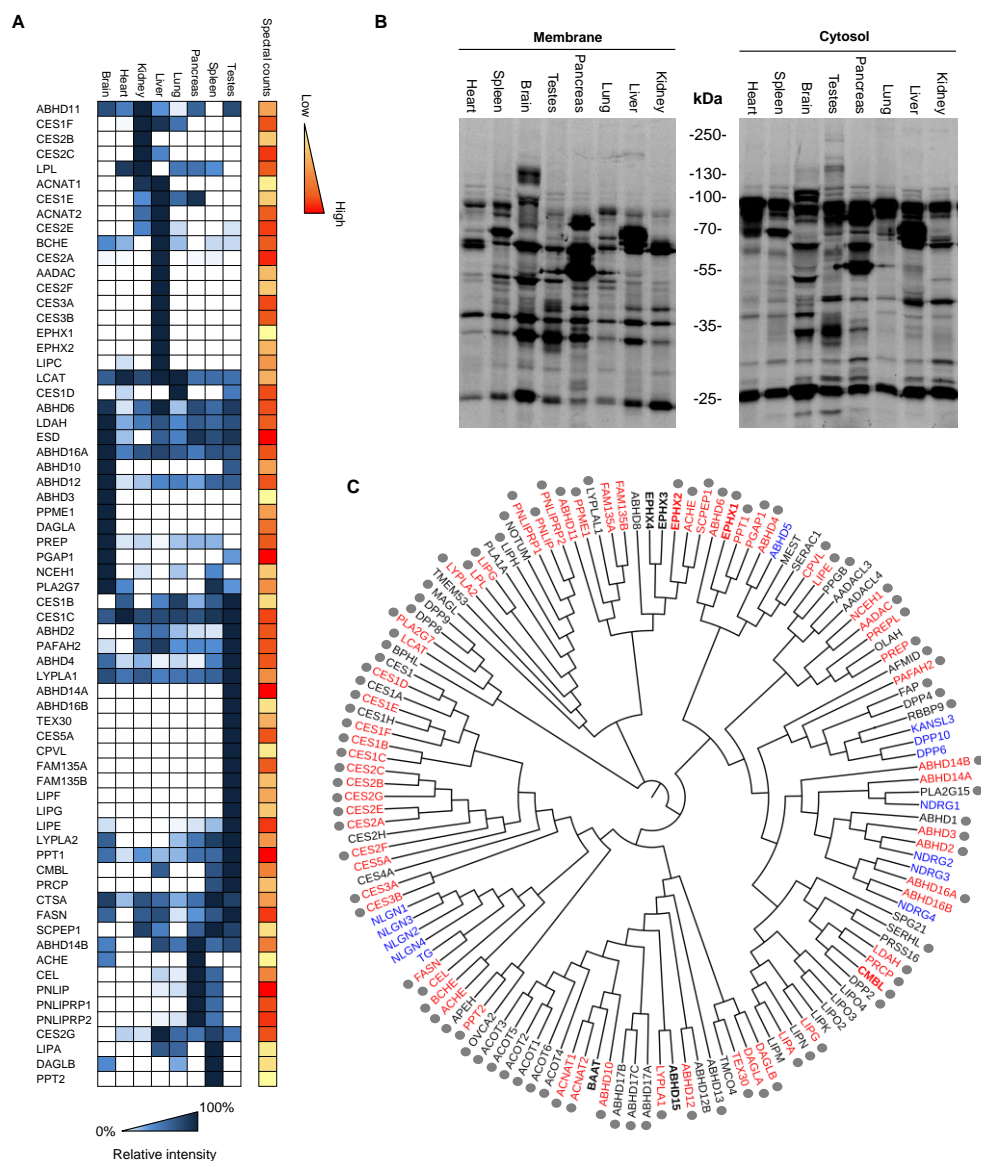


Figure 2. Detection of α,β -hydrolase fold enzyme activity in the mouse brain proteome using β -lactone based ABPs MB064 and MB108. (A) Chemoproteomic screen of α,β hydrolase fold enzyme activity in the mouse proteome using β -lactone based activity-based probe MB108 (10 μ M). Mean of the average spectral counts over three replicate experiments. Heatmap: proteins are ordered by hierarchical clustering. Intensity in blue represents the relative activity per protein in each tissue. Intensity in orange are the spectral counts in the tissue where the protein shows highest activity. (B) Gel based tissue screen with ABP MB064 (2 μ M) in the membrane and cytosolic mouse proteome. (C) Phylogenetic tree of α,β -hydrolase fold proteins generated by multiple sequence alignment (Muscle) and ClustalW2 omega phylogeny.¹⁴ Proteins highlighted in red are targeted by MB108. All proteins are serine hydrolases except those in bold or highlighted in blue. Blue proteins lack a catalytic residue.

Bold proteins have a cysteine or asparagine as a catalytic residue. Grey dots indicate organophosphate targeted proteins.^{10,15}

version of MB064 (MB108) was comprehensively determined in a tissue-wide chemoproteomic screen. MB108 contains the same warhead and recognition element as MB064 and is therefore expected to have a similar target profile.

As a reference for probe targets, a list of α,β -hydrolase fold enzymes was retrieved from the ESTHER database (<http://bioweb.ensam.inra.fr/esther>), which is widely used to monitor proteins containing a α,β -hydrolase fold.¹³ 136 mouse α,β -hydrolase fold containing proteins were retrieved from the database. The sequences of the α,β -hydrolase fold containing proteins were aligned and a phylogenetic tree was generated using multiple sequence alignment (Muscle) and ClustalW2 omega phylogeny (Figure 2C).¹⁴ The α,β -hydrolase fold containing proteins detected in the chemoproteomic screen which were >5 fold enriched (quantification based on spectral counts) compared to heat denaturated controls are highlighted in red. The screen revealed that 66 out of the 136 mouse α,β -hydrolase fold proteins were detected by MB108 in one or more tissues (Figure 2A). In addition, a number of hydrolases and transferases that did not contain the α,β -hydrolase fold motif, but have a catalytic nucleophile that can attack the β -lactone were also targeted. These proteins are given in Supporting Figure 1.

It is well-known that α,β -hydrolase fold proteins react well with organophosphates.¹⁵ Therefore, organophosphate-based ABPs are suitable tools to study α,β -hydrolase fold enzymatic activity. Bachovchin *et al.* have targeted >80% of mammalian metabolic serine hydrolases using a single fluorophosphonate-based ABP.¹⁰ Proteins that are known to interact with organophosphates are marked with a grey dot in Figure 1C. A large overlap between the targets of the organophosphates and MB108 was observed. Importantly, MB108 targeted FAM135, FAM135B, CES5A and ABHD14A, which are not targeted by organophosphate-based probes.^{10,15}

In conclusion, the β -lactone based ABPs, MB108 and its fluorescent analogue MB064 are broad-spectrum ABPs. They are highly versatile and powerful tools to study the activity of many (~50%) of the members of the α,β -hydrolase fold family, including several members that are not detected by organophosphate-based probes.

Gel-based assay for identification α,β -hydrolase family

The biochemical and physiological functions of many members of the α,β -hydrolase fold family are not known and selective small molecule inhibitors for members of this family are scarce. Inhibitors that enable spatiotemporal control over enzyme activity are highly valuable tools to elucidate enzyme function. The α,β -hydrolase fold subfamily sharing the ABHD nomenclature share conserved structural motifs that suggest common roles in lipid metabolism.³ Therefore, a competitive screen between ABHD proteins and a targeted lipase

inhibitor library was envisioned to identify novel modulators for members of this subfamily.

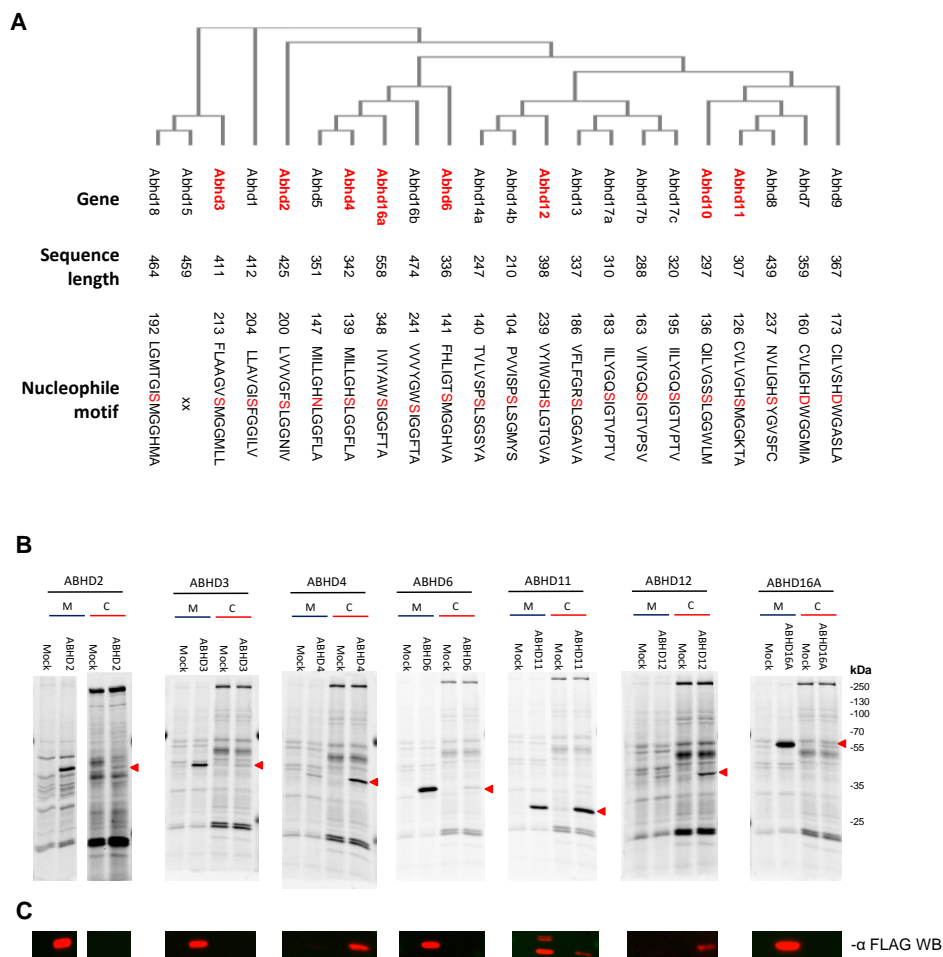


Figure 3. (A) phylogenetic tree of the α,β -hydrolase fold family members sharing the ABHD nomenclature. The tree is generated by multiple sequence alignment (Muscle) and ClustalW2 omega phylogeny.¹⁴ Proteins used for the inhibitor screen are highlighted in red. (B) Labeling of ABHD proteins overexpressed in HEK293T or U2OS cells. Protein labeling of ABHD transfected cells was compared to mock transfected cells in the membrane (M) and cytosolic (C) fractions. Proteins (1 mg/mL) were labeled by ABP MB064 (2 μ M). Overexpressed proteins are marked by a red triangle. (C) Anti-FLAG western blot for confirmation of protein expression and localization of the transfected ABHD. Cutout at the molecular weight indicated by the red triangle is represented.

Chemoproteomic ABPP is highly sensitive and allows the study of native enzymes with relative low abundance and activity in tissues or cell lines. However, chemoproteomics is costly and time consuming, thus not suitable for high throughput screening of inhibitor

libraries. Therefore, a gel-based assay using the fluorescent analogue of MB108, MB064 was employed to identify novel inhibitors for ABHD family members. A gel-based assay is compatible with screening of a considerable number of inhibitors (200+) against multiple enzymes at the same time in one assay. It is important to note that it is challenging to correlate enzymes to specific fluorescent bands on SDS-PAGE in native proteomes. Native enzymes show large variations in labeling intensities and display unequal tissue distribution. Therefore, it is difficult to make a generic assay for multiple proteins of interest in native proteome. Recombinant expression of proteins avoids several of these problems and is highly suitable for generating custom protein libraries for inhibitor screening.

The human enzymes sharing the ABHD nomenclature corresponding to the enzymes that were detected in the chemoproteomic mouse tissue screen were recombinantly expressed in HEK293T or U2OS cells (Figure 3A). The constructs were equipped with a FLAG tag to monitor protein expression and gel migration. Human ABHD3, 4, 6, 11, 12 and 16A were recombinantly expressed in HEK293T cells. ABHD2 was expressed in U2OS cells because the efficiency of overexpression for ABHD2 in HEK293T cells was low. No expression of ABHD10, 14A, 14B and 16B in HEK293T nor U2OS could be achieved for reasons that are not completely understood. Labeling (ABP MB064 (2 μ M)) of lysates from transfected cells and comparison to mock transfected cells was used to monitor protein activity. ABHD2, 3, 6, and 16A showed the highest activity in the membrane fraction, ABHD4 and 12 in the cytosolic fraction and ABHD11 showed high labeling efficiencies in both cytosolic and membrane fractions, with a slightly higher signal in the cytosol.

To establish a multiple protein assay, recombinantly expressed proteins were pooled in custom made protein libraries. ABHD3, 4 and 12 are clustered around a molecular weight of ~40 kD. Therefore, two protein libraries were required resolve all expressed ABHDs on 1D SDS-PAGE. Protein library 1 contained ABHD2, 3 and 12, and protein library 2 consists of ABHD4, 6, 11 and 16A.

The lipase-focused library contained 207 inhibitors, and was divided in three major classes (α -ketoamides, β -ketoamides and 1,2,4-triazole ureas) and a set of unique chemotypes (singletons). The compound library was screened at 10 μ M against the two protein libraries, resulting in the rapid generation of ~1500 protein-inhibitor interaction data points. The screen revealed that all proteins were hit by one or more compounds (Figure 4D). Inhibitors were qualified as a hit when protein labeling was reduced > 70% compared to vehicle-treated control. A clear distinction between target profiles of different inhibitor classes was detected (Figure 4E). The α -ketoamides were practically inactive against all tested ABHD family members. The β -ketoamides provided an excellent chemotype to inhibit ABHD3; 21 hits were identified of which 13 compounds were considered selective (< 50% inhibition of the other ABHDs). Compound **47** and **60** were the most potent inhibitors that remained selective over the other measured ABHDs. Inhibitors from the 1,2,4 triazole-urea class were more reactive. This class effectively targeted ABHD6 and

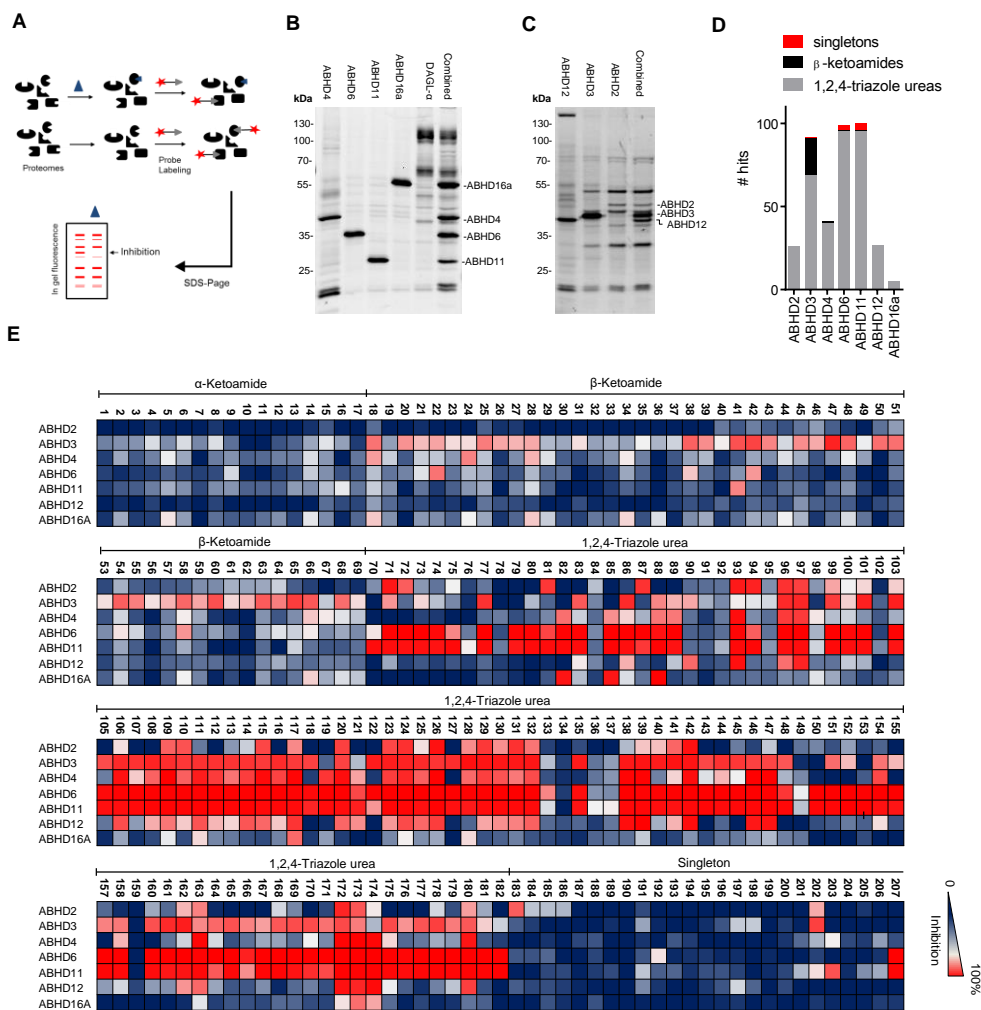


Figure 4. (A) Schematic representation of the gel-based competitive ABPP workflow. (B). Fluorescent labeling (MB064, 2 μ M) of HEK293T lysates that overexpress ABHD4, 6, 11, 16A and DAGL- α , and a combination thereof to form protein library 1. (C) Fluorescent labeling (MB064, 2 μ M) of HEK293T lysates that overexpress ABHD12, 3, 2 and a combination thereof to form protein library 2. (D) Graphical representation of the number of hits per chemotype per enzyme. (E) Heatmap overview of the inhibitor screen.

ABHD11, >70% of the 1,2,4-triazole ureas were classified as hits for these enzymes. Compound **183** from the singleton series reduced labeling of ABHD2 with more than 70% without reducing labeling of other ABHDs with more than 50%. No selective inhibitors were found for ABHD4, 6, 11, 12, or 16A; the non-selective compounds may still represent interesting starting points for hit optimization programs. Since no selective

inhibitors are known for ABHD2 and ABHD3, it was decided to analyze compounds **183**, **47** and **60** in more detail.

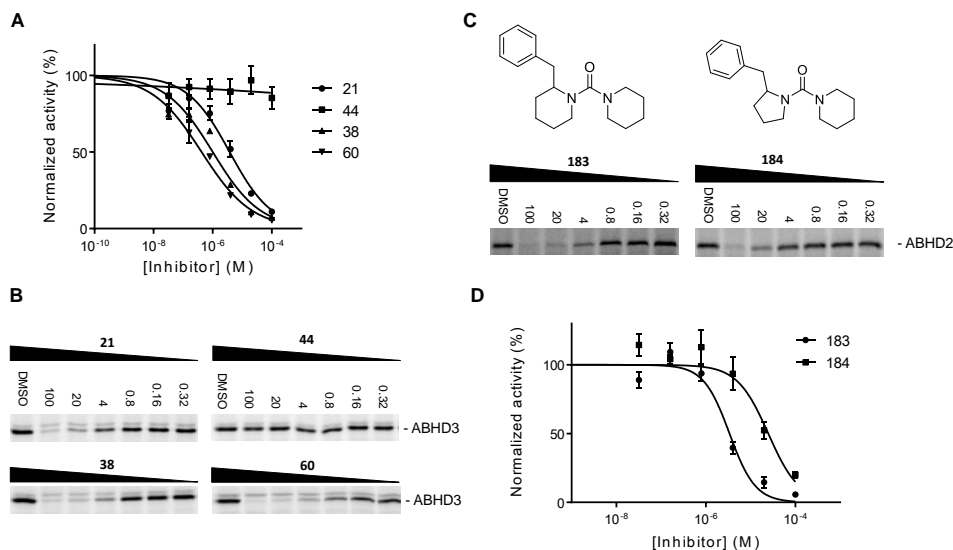


Figure 5. Structure activity of lead inhibitors for ABHD2 and ABHD3. (A) Dose response curves of inhibitor **21**, **44**, **38**, **60**. (B) Dose dependent inhibition of MB064 (2 μ M) of ABHD3 by inhibitor **1**, **5**, **8** and **9** on gel. (C) Dose dependent inhibition of MB064 (2 μ M) labeling of ABHD2 on gel. (D) Dose response curve of inhibitor **183** $pIC_{50} = 5.5 \pm 0.06$ ($n = 3$; \pm SEM) and **184** $pIC_{50} = 4.6 \pm 0.1$ ($n = 3$; \pm SEM). All experiments were performed in triplicate.

Table 1. SAR of β -ketoamides against ABHD3.

Entry ^a	n	X ₁	X ₂	R ₁	R ₂	R ₃	pIC ₅₀
21	2	F	C	H	H	H	5.42 ± 0.07
39^a	2	F	C	H	H	H	5.36 ± 0.08^a
24	1	F	C	H	H	H	N/A
23	2	H	C	H	H	H	N/A
44	2	F	C	Me	H	H	N/A
47	2	F	N	H	H	H	5.64 ± 0.10
53	2	F	C	H	H	CF ₃	4.42 ± 0.22
38	2	F	C	H	F	H	6.00 ± 0.08
60	2	F	C	H	OMe	F	6.38 ± 0.06

^a β -ketone reduced to an alcohol. ^adifluoro β -ketoamides show two peaks on LC/MS, which is hypothesized to be caused by hydration of the ketone.

Compound **183** was found to inhibit ABHD2 with a pIC_{50} of 5.5 ± 0.06 (Figure 5C, D). The structurally related compound **184**, which contains a pyrrolidine instead of a piperidine, showed a 10-fold drop in activity with a pIC_{50} of 4.6 ± 0.1 .

To investigate the structure activity relationship of β -ketoheterocycles against ABHD3, a dose-response analysis on a selected subset of the β -ketoheterocycles identified in the focused library screen was performed. The two most potent selective inhibitors **47** and **60** and structural analogues which could provide important information on the SAR were selected for a more detailed analysis (Table 1). Compound **21** represents the core structure of most active β -ketoheterocyclic ABHD3 inhibitors, and had a pIC_{50} of 5.4 ± 0.07 . Remarkably, compound **39**, where the β -ketone of **21** was replaced by an alcohol was also active on ABHD3. A methyl spacer instead of an ethyl spacer between the β -ketone and phenyl group **24** was not allowed. Compound **44**, which contains an N-methylated amide was inactive and compound **23** which has a hydrogen instead of a fluorine at X_1 was also inactive. The inhibitor where the eastern phenyl group was replaced by a pyridine **47** has a pIC_{50} of 5.64 ± 0.10 . A CF_3 group on the *ortho* position of the eastern phenyl group **53** showed 10-fold less activity compared to **47**. Compound **38** showed considerable activity with a pIC_{50} of 6.00 ± 0.08 , but the inhibitor with an *o*-fluoro-*p*-methoxyphenyl substituent on the eastern side **60** was the most potent inhibitor, with a pIC_{50} of 6.38 ± 0.06 . Therefore, compound **60** was selected for a selectivity assessment.

Inhibitor selectivity

To investigate the selectivity of inhibitors **60** and **150** in native mouse proteome, comparative and competitive ABPP with broad-spectrum FP-based probes (TAMRA-FP and FP-biotin) and the ABPs MB064 and MB108 was employed (Figure 6).¹⁶ The fluorophosphonate was added to broaden the scope of the selectivity profile because it is known to target many serine hydrolases.¹⁰ Since, ABHD3 was only detected in the brain (Figure 1A), the selectivity of compound **60** was tested in this tissue. Gel-based competitive ABPP revealed that **60** (20 μM , 30 min) reduced labeling of a band at ~ 35 kD in the membrane fractions using both ABPs. This band has previously been identified as ABHD6. The identity of the off-target was confirmed by a competitive chemoproteomic assay with FP-biotin.¹⁶⁻¹⁸

The selectivity of ABHD2 inhibitor **183** (20 μM , 30 min) was investigated in mouse testes. Compound **183** reduced labeling of two fluorescent bands in the membrane proteome as determined by MB064. The competitive chemoproteomic assay confirmed ABHD2 inhibition, but no other targets were detected. Together these studies indicate that inhibitor **183** shows a highly selective labeling profile and can be used to inhibit ABHD2 in the testes proteome in an acute fashion with high selectivity.

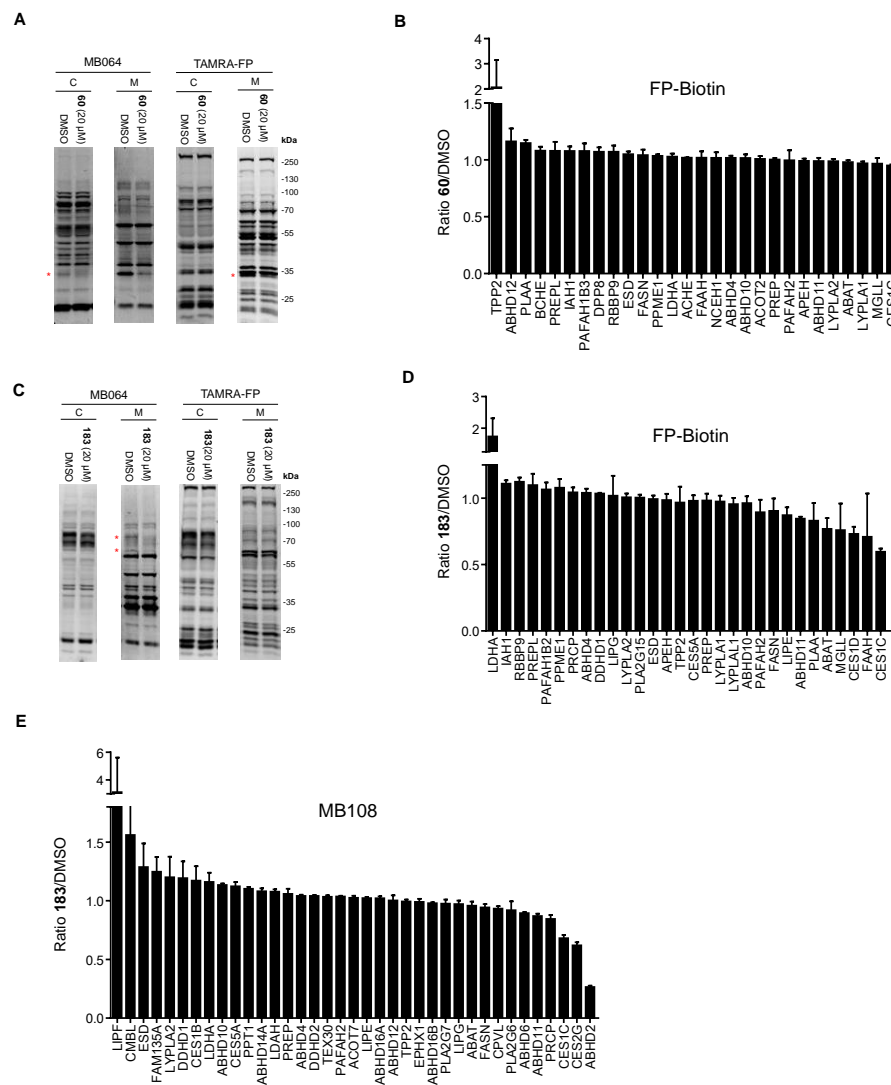


Figure 6. Selectivity of identified inhibitors for ABHD2 and ABHD3. (A) Gel-based competitive ABPP with inhibitor **60** (20 μ M) against TAMRA FP (2 μ M) and MB064 (2 μ M) in the brain cytosolic and membrane fractions (n=3). (B) Competitive chemoproteomic selectivity assay of inhibitor **60** (20 μ M) in the mouse brain proteome using ABP FP-biotin (10 μ M; n=3). (C) Gel-based competitive ABPP with inhibitor **183** (20 μ M) against TAMRA-FP (2 μ M) and MB064 (2 μ M) in the mouse testes cytosolic and membrane fractions (n=3). (D) Competitive chemoproteomic selectivity assay of inhibitor **183** (20 μ M) in the testes proteome using ABP FP-biotin (10 μ M; n=3). (E) Competitive chemoproteomic selectivity assay of inhibitor **183** (20 μ M) in the mouse testes proteome using ABP MB108 (10 μ M; n=3).

Discussion/Conclusion

The target profile of ABP MB108 and MB064 across the mouse proteome (spleen, pancreas, liver, testes, brain, kidney, heart and lung) was mapped. This revealed MB108 and MB064 as highly suitable broad spectrum ABPs to study the activity of α,β -hydrolase fold proteins. The ABPs target ~50% of the α,β -hydrolase fold superfamily, including FAM135A, FAM135B, ABHD14B and CES5A, which are not detected by organophosphates.¹⁰ This remarkably nonspecific target profile demonstrates that it is important to look at the full target profile of an ABP to make optimal use of its properties. The value of MB108 and MB064 as tools for the identification of inhibitors for α,β -hydrolase fold family members was shown by the rapid identification of inhibitors for ABHD2, (**183**) and ABHD3, (**60**).

The biochemical role of ABHD3 has been examined by untargeted metabolomics in ABHD3 knockout mice.¹⁹ ABHD3 is a medium chain (C_{14}) phosphatidylcholine (PC) phospholipase and its genetic deletion elevates $C_{14:18:2}$ -PC, $C_{14:20:4}$ -PC and $C_{14:22:6}$ -PC. In addition, ABHD3 also cleaves phosphatidylcholines (PCs) with shorter acyl chains and oxidatively truncated PCs (oxPCs). These oxPCs are involved in the promotion of cell death and atherosclerosis.^{20,21} Inhibitors can be used to study the effect of acute modulation of ABHD3 activity and its medium chain phospholipid substrates in physiological processes where these lipids have been postulated to be involved in a range of signaling functions.^{22,23}

ABHD2 plays an important role in hepatitis B virus propagation and may serve as a novel drug target for anti-hepatitis-B drug development.⁶ ABHD2 is also associated with chronic diseases that involve monocyte/macrophage recruitment, such as emphysema and atherosclerosis.²⁴⁻²⁶ Recently, 2-AG was identified as a substrate for ABHD2.⁷ The enzyme is highly expressed in spermatozoa and acts as a progesterone-dependent hydrolase. 2-AG inhibits the sperm calcium channel CatSper. 2-AG hydrolysis by ABHD2 leads to calcium influx and sperm activation. Therefore, ABHD2 could be an interesting target for the development of male contraceptives.

The ABHD2 and ABHD3 inhibitors **183** and **60** respectively are likely to become useful tools to study the biological role of ABHD2 and ABHD3. Furthermore they provide excellent leads for further development toward more potent and more selective inhibitors for these enzymes.

Experimental methods

Cell culture. Cell culture was performed as described in chapter 3 and 4. In brief, HEK293T or U2OS cells were grown in DMEM with stable glutamine and phenolred (PAA), 10% New Born Calf serum, penicillin and streptomycin. Cell passage was performed every 2-3 days by resuspension in medium and seeding to appropriate confluence.

Transfection and cell lysis. 24h prior to transfection 10^7 cells were seeded in a 15 cm petri dish. A 3:1 mixture of polyethyleneimine (60 μ g) and plasmid DNA (20 μ g) in 2 mL serum free medium was added. The medium was refreshed after 24 hours, and after 72h HEK293T (48h for U2OS) cells were harvested in 20 mL medium. Cells were isolated by centrifugation for 10 min at 1000 rpm and subsequent aspiration of the medium. The cell pellet was flash frozen in liquid nitrogen and stored at -80 °C until use.

Cell pellets were slowly thawed on ice and suspended in lysis buffer (20 mM HEPES pH 7.2, 2 mM DTT, 0.25 M sucrose, 1 mM MgCl₂, 25 U/mL Benzonase). Three pulses with a polytrone (3 \times 7 sec) were used to homogenize the suspension. After homogenization, the suspension was allowed to incubate for 10 min on ice. Ultracentrifugation (100.000 \times g, 45 min, 4 °C, Beckman Coulter, Type Ti70 rotor) was used to separate the cytosolic and membrane fraction. The pellet (membrane fraction) was resuspended in storage buffer (20 mM HEPES pH 7.2, 2 mM DTT). The total protein concentration was determined with Quick Start Bradford assay (Biorad) or QubitTM protein assay (Invitrogen). The lysates were flash frozen in liquid nitrogen and stored at -80 °C until use.

Preparation of mouse tissue proteome. Mouse tissue were isolated according to guidelines approved by the ethical committee of Leiden University (DEC#13191). Mouse tissues were dounce homogenized in pH 7.2 lysis buffer A (20 mM HEPES pH 7.2, 2 mM DTT, 1 mM MgCl₂, 25 U/mL Benzonase) and incubated for 5 minutes on ice. The suspension was centrifuged (2500 \times g, 3 min, 4 °C) to remove debris. The supernatant was collected and subjected to ultracentrifugation (100.000 \times g, 45 min, 4 °C, Beckman Coulter, Type Ti70 rotor). This yielded the membrane fraction as a pellet and the cytosolic fraction in the supernatant. The membrane fraction was suspended in storage buffer (20 mM HEPES pH 7.2, 2 mM DTT). The total protein concentration was determined with Quick Start Bradford assay (Biorad) or QubitTM protein assay (Invitrogen). Membranes and supernatant were flash frozen in liquid nitrogen and stored in aliquots at -80 °C until use.

Gel-based tissue screen (MB064): The membrane or lysate fraction of mouse brain, heart, kidney, liver, lung, pancreas, spleen or testes was diluted to 1 mg/mL. Proteome (1 mg/mL, 20 μ L) was incubated at 37 °C for 15 min with MB064 (1 μ M, final concentration). After 15 min the reactions were quenched with 10 μ L standard 3 \times SDS-PAGE sample buffer.

The samples were directly loaded and resolved on SDS PAGE gel (10 % acrylamide). The gels were scanned using a ChemiDoc MP system (Cy3 settings, 605/50 filter) and analyzed using Image lab 4.1.

Chemoproteomic tissue screen. The membrane or lysate fraction of mouse brain, heart, kidney, liver, lung, pancreas, spleen or testes was diluted to 2 mg/mL. The proteomes (490 μ L) were incubated with 10 μ L 500 μ M ABP MB108 (final concentration 10 μ M) for 1h at rt. The labeling reaction was quenched and excess probe was removed by chloroform methanol precipitation. Precipitated proteome was suspended in 500 μ L 6M Urea/25 mM ammonium bicarbonate and allowed to incubate for 15 minutes. 5 μ L (1 M DTT) was added and the mixture was heated to 65 °C for 15 minutes. The sample was allowed to cool to rt before 40 μ L (0.5 M) iodoacetamide was added and the sample was alkylated for 30 minutes in the dark. 140 μ L 10% (wt/vol) SDS was added and the proteome was heated for 5 minutes at 65 °C. The sample was diluted with 6 mL PBS. 100 μ L of 50% slurry of Avidin–Agarose from egg white (Sigma-Aldrich) was washed with PBS and added to the proteome sample. The beads were incubated with the proteome for 3h.

Beads were isolated by centrifugation and washed with 0.5% (wt/vol) SDS and PBS (3x). The proteins were digested overnight with sequencing grade trypsin (Promega) in 100 μ L Pd buffer (100 mM Tris Ph 7.0, 100 mM NaCl, 1 mM CaCl_2 , 2 % ACN and 500 ng trypsin) at 37 °C with vigorous shaking. The pH was adjusted with formic acid to pH 3 and the beads were removed. The samples were further purified and measured as described in chapter 3.

Enzyme mixes for inhibitor screen. Protein library 1 is made in standard assay buffer (20 mM HEPES pH 7.2, 2 mM DTT) and contains the following transiently transfected proteins (concentrations are final concentrations). 4 mg/mL cytosolic fraction of ABHD12 transfected HEK293T cell lysate, 0.3 mg/mL membrane fraction ABHD3 transfected HEK293T cell lysate, and 1 mg/mL membrane fraction of ABHD2 transfected U2OS cell lysate.

Protein library 2 is made in standard assay buffer (20 mM HEPES pH 7.2, 2 mM DTT) and contains the following transiently transfected proteins (concentrations are final concentrations). 1 mg/mL cytosolic fraction of ABHD4 transfected HEK293T cell lysate, 0.25 mg/mL membrane fraction ABHD6 and 11 transfected HEK293T cell lysate, 0.2 mg/mL membrane fraction ABHD16A transfected HEK293T cell lysate and finally 0.5 mg/mL membrane fraction DAGL- α transfected HEK293T cell lysate.

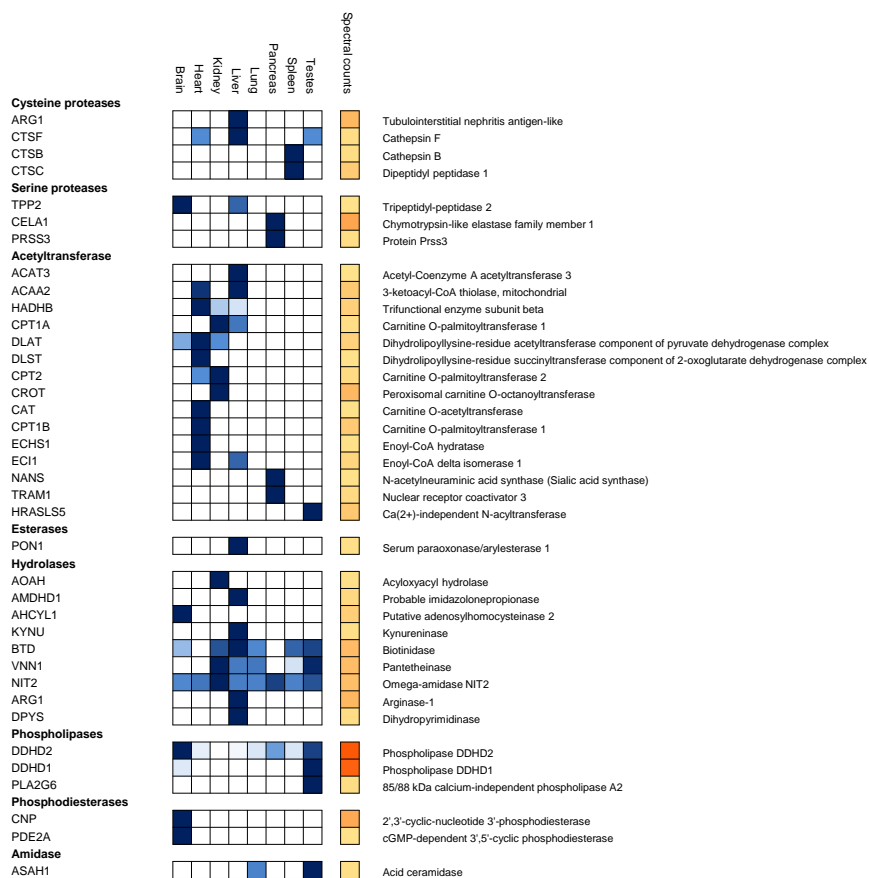
Inhibitor screen. Enzyme mix 1 or 2 (19.5 μ L) was incubated with DMSO (0.5 μ L) or inhibitor (0.5 μ L, 400 μ M; 10 μ M final concentration) for 30 min at 37 °C. Next MB064 (0.5 μ L, 80 μ M; 2 μ M final concentration) was incubated for 15 min at 37 °C. The reactions were quenched with 10 μ L standard 3 \times SDS PAGE sample buffer. The samples

were directly loaded and resolved on SDS PAGE gel (10 % acrylamide). The gels were scanned using a ChemiDoc MP system (Cy3 settings, 605/50 filter) and the percentage inhibition was determined by comparison with DMSO (100%) using Image lab 4.1. Control for protein loading was performed by coomassie staining and adjustment for total lane intensity.

Gel-based dose-response analysis. Dose response analysis was performed as described in chapter 4. In brief, transfected proteome (19.5 μ L) was incubated with DMSO (0.5 μ L) or inhibitor (0.5 μ L) at indicated final concentrations for 30 min at 37 °C. Next MB064 (0.5 μ L, 80 μ M; 2 μ M final concentration) was incubated for 15 min at 37 °C. The reactions were quenched with 10 μ L standard 3 \times SDS PAGE sample buffer. The samples were directly loaded and resolved on SDS PAGE gel (10 % acrylamide). The gels were scanned using a ChemiDoc MP system (Cy3 settings, 605/50 filter) the percentage of activity remaining was determined by measuring the integrated optical intensity of the fluorescent protein bands using Image lab 4.1. The relative intensity was compared to the vehicle treated proteins, which were set to 100%. Correction for protein loading was performed by coomassie staining. IC50 values were determined by plotting log(inhibitor) vs. normalized response (variable slope) dose-response curve generated using Prism software (GraphPad).

Selectivity in native mouse proteome. The gel-based selectivity assay was performed in a similar fashion as described in chapter 4. In brief, mouse testes or brain cytosolic or membrane fractions were diluted to a total protein concentration of 2 mg/mL. Proteome (19.5 μ L) was incubated with DMSO (0.5 μ L) or inhibitor (0.5 μ L, 20 μ M final concentration) for 30 min at 37 °C. Next MB064 or TAMRA-FP (0.5 μ L, 80 μ M; 2 μ M final concentration) was incubated for 15 min at 37 °C. The reactions were quenched with 10 μ L standard 3 \times SDS PAGE sample buffer and analysed as described in chapter 4.

Chemoproteomic selectivity assay in native mouse proteome. Mouse testes or brain cytosolic or membrane fraction was diluted to a total protein concentration of 2 mg/mL. 5 μ L 1 mM inhibitor (20 μ M final concentration) or DMSO was added to 240 μ L proteome and allowed to incubate for 30 min at 37 °C. FP-Biotin or MB108 (5 μ L, 500 μ M) was added and incubated for 30 min at 37 °C. The samples were further processed and analysed as described in chapter 4.



Supporting figure 1. Non α,β -hydrolase fold proteins with hydrolase activity that were detected by MB108. Hydrolases, proteases, transferases, esterases and amidases as classified by panther gene ontology.

References

1. Nardini, M.; Dijkstra, B. W. *Curr. Opin. Struct. Biol.* **1999**, *9*, 732.
2. Ollis, D. L.; Cheah, E.; Cygler, M.; Dijkstra, B.; Frolow, F.; Franken, S. M.; Harel, M.; Remington, S. J.; Silman, I.; Schrag, J. *Protein Eng.* **1992**, *5*, 197.
3. Lord, C. C.; Thomas, G.; Brown, J. M. *Biochim. Biophys. Acta* **2013**, *1831*, 792.
4. Hotamisligil, G. S. *Nature* **2006**, *444*, 860.
5. Nomura, D. K.; Morrison, B. E.; Blankman, J. L.; Long, J. Z.; Kinsey, S. G.; Marcondes, M. C.; Ward, A. M.; Hahn, Y. K.; Lichtman, A. H.; Conti, B.; Cravatt, B. F. *Science* **2011**, *334*, 809.
6. Ding, X.; Yang, J.; Wang, S. *Oligonucleotides* **2011**, *21*, 77.
7. Miller, M. R.; Mannowetz, N.; Iavarone, A. T.; Safavi, R.; Gracheva, E. O.; Smith, J. F.; Hill, R. Z.; Bautista, D. M.; Kirichok, Y.; Lishko, P. V. *Science* **2016**, *352*, 555.
8. Merla, G.; Ucla, C.; Guipponi, M.; Reymond, A. *Hum. Genet.* **2002**, *110*, 429.
9. Fiskerstrand, T.; H'Mida-Ben Brahim, D.; Johansson, S.; M'Zahem, A.; Haukanes, B. I.; Drouot, N.; Zimmermann, J.; Cole, A. J.; Vedeler, C.; Bredrup, C.; Assoum, M.; Tazir, M.; Klockgether, T.; Hamri, A.; Steen, V. M.; Boman, H.; Bindoff, L. A.; Koenig, M.; Knappskog, P. M. *The Am. J. Hum. Genet.* **2010**, *87*, 410.
10. Bachovchin, D. A.; Ji, T.; Li, W.; Simon, G. M.; Blankman, J. L.; Adibekian, A.; Hoover, H.; Niessen, S.; Cravatt, B. F. *Proc. Natl. Acad. Sci. U. S. A.* **2010**, *107*, 20941.
11. Sharma, K.; Schmitt, S.; Bergner, C. G.; Tyanova, S.; Kannaiyan, N.; Manrique-Hoyos, N.; Kongi, K.; Cantuti, L.; Hanisch, U. K.; Philips, M. A.; Rossner, M. J.; Mann, M.; Simons, M. *Nat. Neurosci.* **2015**, *18*, 1819.
12. Uhlen, M.; Fagerberg, L.; Hallstrom, B. M.; Lindskog, C.; Oksvold, P.; Mardinoglu, A.; Sivertsson, A.; Kampf, C.; Sjostedt, E.; Asplund, A.; Olsson, I.; Edlund, K.; Lundberg, E.; Navani, S.; Szgyarto, C. A.; Odeberg, J.; Djureinovic, D.; Takanen, J. O.; Hober, S.; Alm, T.; Edqvist, P. H.; Berling, H.; Tegel, H.; Mulder, J.; Rockberg, J.; Nilsson, P.; Schwenk, J. M.; Hamsten, M.; von Feilitzen, K.; Forsberg, M.; Persson, L.; Johansson, F.; Zwahlen, M.; von Heijne, G.; Nielsen, J.; Ponten, F. *Science* **2015**, *347*, 1260419.
13. Lenfant, N.; Hotelier, T.; Velluet, E.; Bourne, Y.; Marchot, P.; Chatonnet, A. *Nucleic Acids Res.* **2013**, *41*, D423.
14. Edgar, R. C. *Nucleic Acids Res.* **2004**, *32*, 1792.
15. Lenfant, N.; Bourne, Y.; Marchot, P.; Chatonnet, A. *Chem. Biol. Interact.* **2016**.
16. Baggelaar, M. P.; Chameau, P. J.; Kantae, V.; Hummel, J.; Hsu, K. L.; Janssen, F.; van der Wel, T.; Soethoudt, M.; Deng, H.; den Dulk, H.; Allara, M.; Florea, B. I.; Di Marzo, V.; Wadman, W. J.; Kruse, C. G.; Overkleeft, H. S.; Hankemeier, T.;

- Werkman, T. R.; Cravatt, B. F.; van der Stelt, M. *J. Am. Chem. Soc.* **2015**, *137*, 8851.
17. Ogasawara, D.; Deng, H.; Viader, A.; Baggelaar, M. P.; Breman, A.; den Dulk, H.; van den Nieuwendijk, A. M.; Soethoudt, M.; van der Wel, T.; Zhou, J.; Overkleeft, H. S.; Sanchez-Alavez, M.; Mori, S.; Nguyen, W.; Conti, B.; Liu, X.; Chen, Y.; Liu, Q. S.; Cravatt, B. F.; van der Stelt, M. *Proc. Natl. Acad. Sci. U. S. A.* **2016**, *113*, 26.
18. Hsu, K. L.; Tsuboi, K.; Adibekian, A.; Pugh, H.; Masuda, K.; Cravatt, B. F. *Nat. Chem. Biol.* **2012**, *8*, 999.
19. Long, J. Z.; Cisar, J. S.; Milliken, D.; Niessen, S.; Wang, C.; Trauger, S. A.; Siuzdak, G.; Cravatt, B. F. *Nat. Chem. Biol.* **2011**, *7*, 763.
20. Chen, R.; Yang, L.; McIntyre, T. M. *J. Biol. Chem.* **2007**, *282*, 24842.
21. Navab, M.; Ananthramaiah, G. M.; Reddy, S. T.; Van Lenten, B. J.; Ansell, B. J.; Fonarow, G. C.; Vahabzadeh, K.; Hama, S.; Hough, G.; Kamranpour, N.; Berliner, J. A.; Lusa, A. J.; Fogelman, A. M. *J. Lipid Res.* **2004**, *45*, 993.
22. Yea, K.; Kim, J.; Yoon, J. H.; Kwon, T.; Kim, J. H.; Lee, B. D.; Lee, H. J.; Lee, S. J.; Kim, J. I.; Lee, T. G.; Baek, M. C.; Park, H. S.; Park, K. S.; Ohba, M.; Suh, P. G.; Ryu, S. H. *J. Biol. Chem.* **2009**, *284*, 33833.
23. Murakami, N.; Yokomizo, T.; Okuno, T.; Shimizu, T. *J. Biol. Chem.* **2004**, *279*, 42484.
24. Miyata, K.; Oike, Y.; Hoshii, T.; Maekawa, H.; Ogawa, H.; Suda, T.; Araki, K.; Yamamura, K. *Biochem. Biophys. Res. Commun.* **2005**, *329*, 296.
25. Miyata, K.; Nakayama, M.; Mizuta, S.; Hokimoto, S.; Sugamura, K.; Oshima, S.; Oike, Y.; Sugiyama, S.; Ogawa, H.; Yamamura, K. *Biochem. Biophys. Res. Commun.* **2008**, *365*, 207.
26. Jin, S.; Zhao, G.; Li, Z.; Nishimoto, Y.; Isohama, Y.; Shen, J.; Ito, T.; Takeya, M.; Araki, K.; He, P.; Yamamura, K. *Biochem. Biophys. Res. Commun.* **2009**, *380*, 419.

CHAPTER 8

Summary and Future Prospects

The aim of the work described in this thesis is the identification, development and application of chemical tools and methodologies to study the activity of endocannabinoid hydrolases in complex proteomes. Of particular interest were the diacylglycerol lipases. Activity-based protein profiling (ABPP) was used as the main technique for the identification and characterization of small molecule inhibitors for these enzymes.¹

Chapter 1 introduces this technique and its position within the wide landscape of approaches available to scientists to study enzyme function. ABPP is a chemical proteomic technique that revolves around active site directed small molecules, termed “activity-based probes” (ABPs). They consist of a warhead, a linker/recognition region and a reporter tag (Figure 1). The warhead reacts in a mechanism-based fashion, thereby establishing a covalent bond with only the active form of the

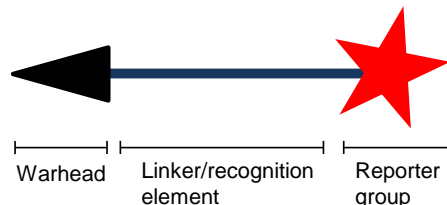


Figure 1. Schematic representation of an activity-based probe (ABP)

target enzyme. The recognition element generally directs the ABP to its target enzyme and the reporter tag ensures readout of the enzymatic activity. ABPP is arguably unique in its ability to directly monitor the activity of proteins in their native environment. This is important because the activity of many proteins is regulated by posttranslational modifications, protein-protein interactions and endogenous inhibitors.² In addition, an ABP that interacts with a specific protein provides a direct activity assay independent of prior annotation of the targeted enzyme. These characteristics makes ABPP, especially when performed with broad-spectrum ABPs, an excellent technique to study and identify inhibitors for proteins with unknown functions in native proteomes.³

The endocannabinoid system is a signaling system that consists of the cannabinoid type 1 and type 2 (CB₁ and CB₂) receptors, lipid messengers termed endocannabinoids and the enzymes responsible for the biosynthesis and metabolism of the

lipid messengers.⁴ 2-Arachidonoylglycerol (2-AG) and anandamide (AEA) are the two main endocannabinoids (Figure 2). The CB₁ receptor is highly expressed in the brain and the CB₂ receptor plays an important role in immune cells. Activation of the cannabinoid receptors by their endogenous ligands plays an important role in various patho(physiological) processes, such as learning and memory,⁵ pain sensation,⁶ energy balance⁷ and inflammation.⁸ Levels of 2-AG and AEA are tightly regulated by the enzymes responsible for their biosynthesis and catabolism.

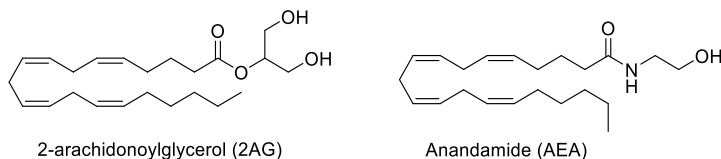


Figure 2. Structures of the endocannabinoids 2-AG and AEA.

Chapter 2 introduces the endocannabinoid system and describes the physiological role of 2-AG in the brain. Modulation of its biosynthesis and catabolism has provided insight in 2-AG-mediated physiology. According to classical models, virtually all physiological processes influenced by 2-AG are mediated by the CB receptors. Although the 2-AG-CB receptor axis is involved in many physiological processes, other biological roles of 2-AG have emerged. 2-AG has been identified as a key metabolic intermediate towards arachidonic acid (AA) and downstream pro-inflammatory prostaglandins. In addition, the function of other proteins, including GPR55, TRPV1, GABA_A and Adenosine A₃, might also be modulated by 2-AG.

In view of the important role of 2-AG in multiple pathological processes, the enzymes responsible for its biosynthesis and degradation are considered interesting drug targets. Novel tools that can selectively target specific enzymes involved in 2-AG biosynthesis and catabolism are highly desired and could serve as leads for the development of small molecule based therapies to treat human diseases, such as metabolic syndrome, pain and neuroinflammation.

Diacylglycerol lipase- α (DAGL- α) is the main enzyme responsible for the production of the endocannabinoid 2-AG in the central nervous system. It is a potential drug target for the treatment of obesity and neurodegenerative diseases.⁹ **Chapter 3** describes the development of MB064 as an ABP for this enzyme (Figure 3).¹⁰ This ABP enables the study of DAGL- α in native proteomes and can serve as a tool to identify new inhibitors for this enzyme.

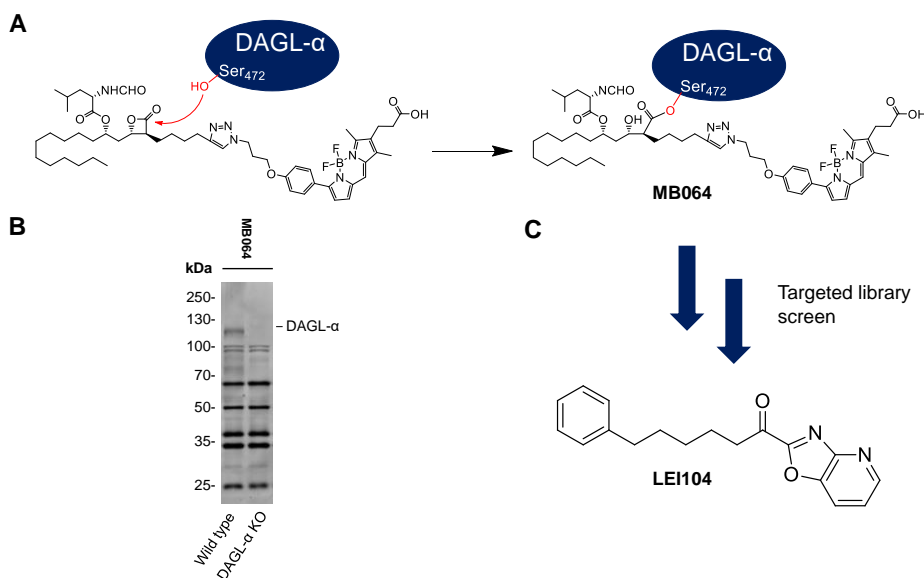


Figure 3. Schematic representation of chapter 3. (A) THL based ABP MB064 covalently labels DAGL- α at catalytic serine 472 by opening of the β -lactone and forming a stable ester bond. (B) Fluorescent labeling of DAGL- α knockout (KO) and wild type (WT) mouse brain membrane proteome by ABP MB064. A fluorescent band at the molecular weight of DAGL- α (~120 kDa) is visible in the WT proteome but absent in the KO, indicating DAGL- α labeling. (C) A targeted library screen led to the identification of the novel DAGL- α inhibitor LEI104.

The design of MB064 is based on THL, which is a known non-specific covalent inhibitor of DAGL- α . THL was equipped with an alkyne handle, and subsequently ligated to a bodipy-based fluorophore for visualization and a biotin group for enrichment and subsequent LC-MS/MS analysis. MB064 labeled recombinantly expressed hDAGL- α at the catalytic Ser-472 (Figure 3). In addition, the ABP also labeled native DAGL- α in the mouse brain proteome. MB064 was used in combination with a biochemical assay to screen a targeted library to identify novel DAGL- α inhibitors. The library consisted of inhibitors that were selected for their ability to inhibit enzymes that recognize similar structures as 2-AG. LEI104 was identified as a covalent reversible α -ketoheterocyclic DAGL- α inhibitor. LEI104 was an *in situ* active and highly selective DAGL- α inhibitor. Fatty acid amide hydrolase (FAAH) was detected as its only off-target. FAAH is the main enzyme responsible for hydrolysis of anandamide (AEA) towards ethanolamine and AA. Selectivity over FAAH is important to dissect the signaling roles of 2-AG and AEA.

Chapter 4 describes identification of a highly selective DAGL inhibitor using a structure-guided and a chemoproteomics strategy to characterize the selectivity of the inhibitor in complex proteomes.¹¹ Key to the success of this approach was the use of comparative and competitive ABPP in which broad-spectrum fluorophosphonate-based and

β -lactone-based ABPs are combined to report on the inhibition of a protein family in its native environment. Competitive ABPP with broad-spectrum fluorophosphonate-based probes and β -lactone-based probes led to the discovery of α -ketoheterocycle LEI105 as a potent, highly selective, and reversible dual DAGL- α /DAGL- β inhibitor. LEI105 did not affect other enzymes involved in endocannabinoid metabolism including α,β -hydrolase domain-containing protein 6 (ABHD6), α,β -hydrolase domain-containing protein 12 (ABHD12), monoacylglycerol lipase (MAGL), FAAH and did not display affinity for the cannabinoid CB₁ receptor. Targeted lipidomics revealed that LEI105 reduced 2-AG levels in a concentration-dependent manner, but did not affect AEA levels, in Neuro2A cells. It was shown that CB₁-receptor-mediated short-term synaptic plasticity in mouse hippocampal slices could be reduced by LEI105. Hereby, LEI105 provided new pharmacological evidence to support the “on demand biosynthesis” hypothesis for retrograde endocannabinoid signaling in the CNS.

Chapter 5 describes the efforts to improve the potency and physicochemical properties of LEI105. A series of LEI105 analogues was made in which the *p*-tolyl group of LEI105 was exchanged for phenyl groups bearing different substituents or replaced by heterocycles. This resulted in the identification of compound **16**. This inhibitor displayed improved activity in the ABPP activity assay compared to LEI105. In addition, it had the highest lipophilic efficiency (LipE) amongst the 18 tested compounds and reduced FAAH labeling with less than 25% at 10 μ M. The inhibitory activity against *h*DAGL- α was tested in a natural substrate assay and **16** had a pIC₅₀ of 7.6 ± 0.1 .

Towards in vivo active inhibitors

It is anticipated that the inhibitors, tools and methodologies developed in Chapters 3, 4 and 5 will enable the advancement of our understanding of the (patho)physiological role of DAGL. This will allow the evaluation of DAGLs as potential drug targets for treatment the metabolic syndrome, drug abuse or neuroinflammatory diseases, such as Alzheimers’s disease, Parkinson’s disease and multiple sclerosis (MS). An important next step to achieve this goal will be to study the *in vivo* activity of the α -ketoheterocyclic inhibitors.

The structures described in chapter 5 are part of a larger collaborative effort to optimize LEI105. A complete list of compounds and their biological activities are described in a patent.¹² A noteworthy modification of LEI105 that is described in this patent and which might improve its pharmacokinetic properties, is the replacement of the phenylpentyl by a 4,4,4-trifluoropropyl tail (Figure 4). This modification significantly improved its lipophilic efficiency. In addition, the 4,4,4-trifluoropropyl group is likely to provide metabolic stability. Although, *in vivo* active inhibitors for DAGL have been reported,¹³ these reversible α -ketoheterocycles are a valuable addition to the currently known irreversible DAGL inhibitors. Covalent irreversible inhibition could lead to idiosyncratic toxicity. In addition, adverse psychiatric side effects upon complete blockade of DAGL- α are a

significant risk.¹⁴ Reversible α -ketoheterocyclic DAGL inhibitors may provide insight whether a therapeutic window for DAGL inhibition can be established.

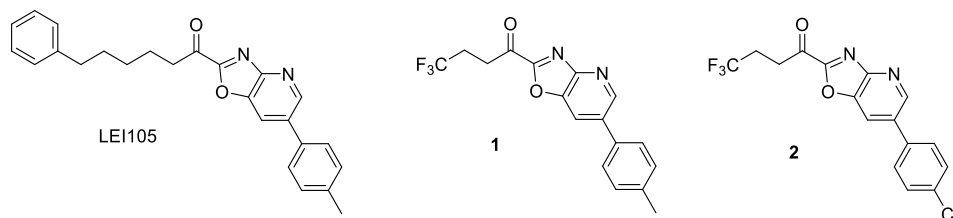


Figure 4. Analogues of LEI105 with potentially better pharmacokinetic and pharmacodynamics properties. LEI105 pIC_{50} 8.52 ± 0.06 , **1** pIC_{50} 7.83 ± 0.13 , **2** pIC_{50} 8.57 ± 0.07 . pIC_{50} was determined by the colorimetric PNP-butyrate *h*DAGL- α assay. N=2; n=2.

DAGL- α and DAGL- β subtype selective inhibitors

DAGL- α and DAGL- β display a tissue specific distribution and appear to regulate different 2-AG pools. DAGL- α , but not DAGL- β , regulates the major forms of 2-AG mediated synaptic plasticity.^{15,16} In addition, DAGL- α has the highest activity in neurons, while DAGL- β showed the highest activity microglia.¹⁷ Interestingly, genetic disruption of DAGL- β attenuates neuro-inflammatory events *in vivo* independently of broader effects on 2-AG levels. Subtype selective inhibitors will be instrumental to investigate the contributions of each subtype to 2-AG biosynthesis in specific (patho)physiological processes.

Subtype specific inhibitors could enable better spatiotemporal control over 2-AG biosynthesis and circumvent or reduce adverse effects. It would be interesting to evaluate DAGL- β specific inhibitors in models of neurodegenerative disorders, such as Parkinson's disease, Alzheimer's disease and Multiple Sclerosis.

In the colorimetric assay based on hydrolysis of *para*-nitro-phenylbutyrate, LEI105 showed a high potency for both DAGL- α (pIC_{50} of 8.5 ± 0.06 ; n=4) and DAGL- β (pIC_{50} 8.1 ± 0.07 ; n=4). The inhibitors synthesized in chapter 5 were, however, not tested for their activity on DAGL- β . It is important to investigate if the inhibitors in these new series show some preference for DAGL- α over DAGL- β or vice-versa. DAGL- α and DAGL- β show an extensive homology, but differ in the length of a C-terminal tail.¹⁸ Currently no crystal structures of DAGL- α and DAGL- β are available to guide the design of subtype selective inhibitors. Crystal structures of DAGL- α and DAGL- β will be an important breakthrough for the design of subtype selective inhibitors. Alternatively, homology models of DAGL- α can be used, but a homology model of DAGL- β is still lacking.

Full interaction landscape of reversible inhibitors

The competitive and comparative chemoproteomic selectivity assay developed in chapter 4 is a powerful technique to study the selectivity of reversible DAGL inhibitors over a broad panel of serine hydrolases. In addition, it provides confirmation of target engagement of reversible inhibitors in native proteomes. Although a good coverage of relevant off-targets is obtained, the technique remains limited to screening proteins that are targeted by the ABPs at hand. Other non-related off-targets can not be excluded. Covalent irreversible inhibitors are commonly equipped with a reporter tag and used as an ABP to monitor all interacting proteins to which the inhibitor covalently binds.¹³ This is not feasible for reversible inhibitors. Photoaffinity-based protein profiling is an alternative method to gain a more comprehensive map of the interaction landscape of reversible inhibitors. This technique does not require a covalent irreversible bond between a catalytic nucleophile of the target protein and the ABP. Instead, photoaffinity labeling utilizes a photoreactive group to establish a covalent bond with target proteins in response to light. Figure 5 depicts two photoaffinity probes based on the structure of LEI105 which could be used to investigate selectivity of LEI105. Photoaffinity probe **PAP1** relies on an aryl azide, and probe **PAP2** on a diazirine as photocrosslinker. These probes can be used to monitor their interaction partners directly, or in a competitive setting. This method is not limited to the targets of MB108 and FP-Biotin, but can also detect interactions with proteins that do not have a catalytic nucleophile, such as transporters and receptors.

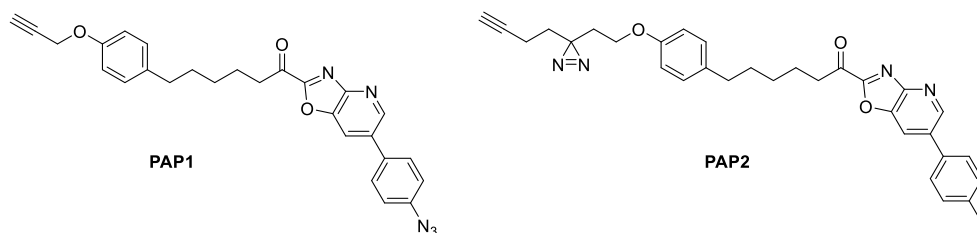


Figure 5. Two proposed photoaffinity-based probes (**PAP1** and **PAP2**) based on LEI105 which could be used to monitor the full interaction landscape of LEI105.

Chapter 6: TAMRA-FP and MB064 do not only detect DAGL- α , but react with multiple endocannabinoid hydrolases. Therefore, they are excellent tools to study the endocannabinoid regulatory machinery. The biosynthetic and metabolic enzymes of the endocannabinoids tightly regulate endocannabinoid-mediated activation of the CB₁ receptor. Monitoring the activity of these endocannabinoid hydrolases in different brain regions is, therefore, key to gain insight in spatiotemporal control of CB₁ receptor-mediated physiology.

Chapter 6 describes the development of a comparative chemical proteomics approach to quantitatively map the activity profile of endocannabinoid hydrolases in

various mouse brain regions at the same time. To this end, two different activity-based probes: fluorophosphonate-biotin (FP-biotin), which quantifies FAAH, ABHD6 and MAG-lipase activity, and MB108 that detects DAGL- α , ABHD4, ABHD6 and ABHD12 were used. Both probes were applied to four different brain regions (frontal cortex, hippocampus, striatum and cerebellum).

Comparison of endocannabinoid hydrolase activity in the four brain regions revealed that FAAH activity was highest in hippocampus, MAGL activity was most pronounced in the frontal cortex, whereas DAGL- α was most active in cerebellum. ABHD4, 6 and 12 activities were equally distributed over all brain regions. The enzyme activity profile was compared to a global proteomics dataset and pronounced differences were found. This could indicate that post-translational modification of the endocannabinoid hydrolases is important to regulate their activities. Measured enzyme activity was compared with protein expression and lipodomics from literature. Since, different age and sample handling could lead to variable outcomes, it would be valuable to perform shotgun proteomics and lipodomics on the same brain regions that were used for the comparative chemoproteomics.

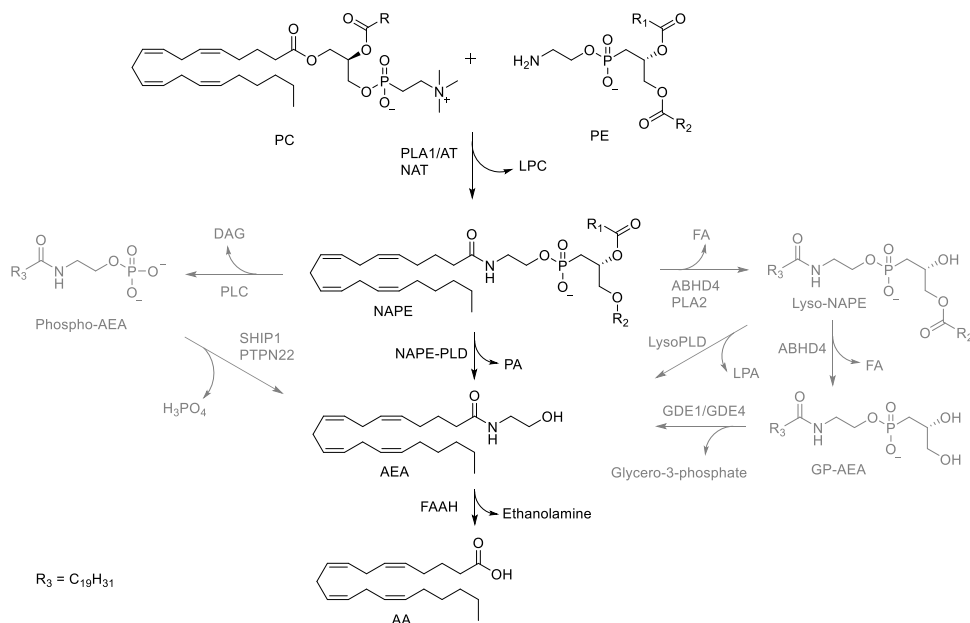
Next, the effect of genetic deletion of the cannabinoid CB₁ receptor on the activity of endocannabinoid hydrolases was studied. No differences in enzymatic activities were observed in the cerebellum, striatum, frontal cortex and hippocampus of CB₁ receptor knockout animals compared to wild type mice. Our results are in line with previous reports and indicate that the CB₁ receptor exerts no regulatory control over the basal production and degradation of endocannabinoids. Genetic deletion of the CB₁ receptor did not induce compensatory mechanisms in endocannabinoid hydrolase activity.

2-AG plays an important role in neuro-inflammation.^{17,19} The comparative chemoproteomic method described in Chapter 6 may be extended to study diseases that have a neuro-inflammatory component. Endocannabinoid hydrolase activity in healthy and diseased tissue can be compared to identify dysregulated enzyme activities. This might ultimately lead to the identification of novel drug targets.

AEA biosynthesis

The comparative chemoproteomic method described in Chapter 6 is an efficient method to monitor the activity of both the major biosynthetic and catabolic enzymes for 2-AG in the brain. However, the biosynthesis of AEA, the other important endocannabinoid, can currently not be monitored. The functions of 2-AG and AEA are strongly intertwined and crosstalk between the two lipids has been suggested.²⁰ In addition, AEA levels decrease when 2-AG biosynthesis is blocked.¹³ The underlying mechanism of this effect remains to be elucidated. The identification of tools to modulate and detect the AEA biosynthetic machinery will be instrumental to dissect AEA and 2-AG signaling and study the (patho)physiological role of each endocannabinoid in the endocannabinoid system. Multiple biosynthetic pathways for AEA have recently been uncovered (Scheme 1),²¹⁻²³ but

the contribution to AEA biosynthesis of each biological pathway during different physiological and pathological conditions is unknown.



Scheme 1. biosynthetic pathways of AEA. PC: Phosphatidylcholine, PE: Phosphatidylethanolamine, PA: Phosphatidic acid, LPA: Lyso-phosphatidic acid, NAT: N-acyltransferase, LPC: Lyso-phosphatidylcholine, FA: Fatty acid, ABHD4: α,β -hydrolase domain-4, PLA2: Phospholipase A2, GDE1 or 4: Glycerophosphodiesterase 1 or 4, GP-AEA: Glycerophospho-AEA, DAG: Diacylglycerol, PLC: Phospholipase C, PTPN22: protein tyrosine phosphatase, non-receptor type 22. NAPE: N-arachidonoylphosphatidylethanolamine, FAAH: Fatty acid amide hydrolase, AA: Arachidonic acid.

The rate limiting step of AEA formation is transacylation, which is performed by N-acyltransferases (NATs). They produce a precursor termed N-arachidonoylphosphatidylethanolamine (NArPE),²⁴ which plays a central role in the current models for AEA generation.²⁴⁻²⁶ There are two types of NATs, Ca^{2+} -dependent NAT, which has recently been identified as cytosolic phospholipase A2 epsilon (PLA2G4E) in mouse brain,²⁷ and Ca^{2+} -independent phospholipase A1/acyltransferases (PLA/AT). It is unknown whether PLA/ATs contribute to NAPE formation in the brain, but they produce AEA in primary sensory neurons in a Ca^{2+} -insensitive manner.²⁸ AEA can be generated from NArPE via different phospholipase-dependent pathways.^{21,29} (a) hydrolysis by N-acylphosphatidylethanolamine-phospholipase D (NArPE-PLD), a metallo- β -lactamase, producing AEA and a phosphatidic acid in one step.³⁰ (b) Phospholipase A₂ (PLA₂) and α,β -hydrolase domain-containing protein 4 (ABHD4)-mediated conversion to lyso-NArPE, followed by the action of an unknown lysophospholipase D (PLD). Of note, lyso-NArPE can also be converted in a two-step sequence by ABHD4 to glycerophospho-AEA (GP-

AEA) and subsequently hydrolyzed to AEA by glycerophosphodiesterase 1 or 4 (GDE1 or GDE4),^{31,32} (c) in macrophages NArPE serves as a substrate for an unidentified phospholipase C yielding phospho-AEA. Hydrolysis of the phosphate group by phosphatases PTPN22 or SHIP1 provides AEA.^{22,33}

Studies with KO mice lacking these different biosynthetic proteins did not yield conclusive evidence for the preferred pathway in the CNS. This is possibly because of the induction of compensatory mechanisms as a result of congenital deletion of these enzymes.^{34,35}

ABPs that monitor and detect activity of the enzymes that catalyze the rate-limiting step towards AEA formation are likely to provide insight in their function and can facilitate inhibitor discovery. In the tissue wide chemoproteomic screen described in Chapter 7, PLA/AT5 activity was detected in the testes, but no other PLA/ATs were found. This could be due to low expression/activity of these enzymes in native proteomes (under basal conditions). Further investigation of the affinity of MB064 for PLA/ATs could lead to the identification of MB064 as a PLA/AT family targeting ABP.

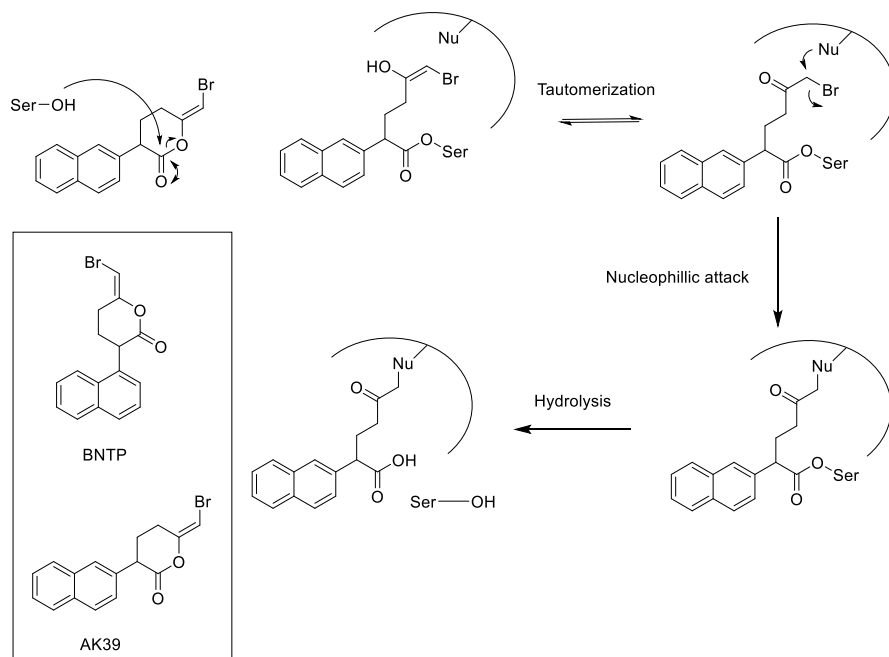
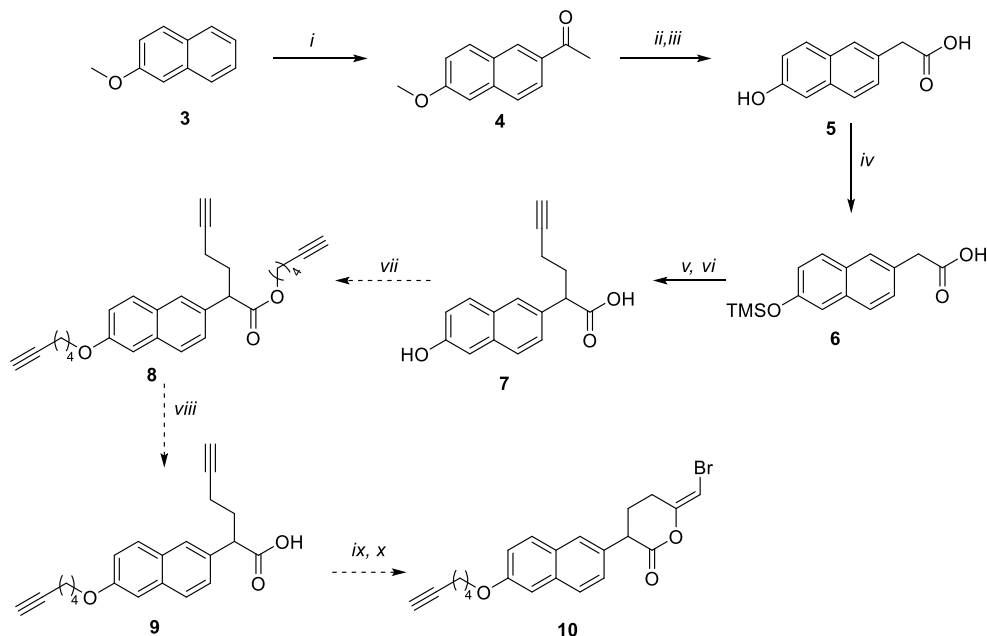


Figure 6. Structures of Ca^{2+} -dependent NAT inhibitors, BNTP and AK39. Proposed mechanism of covalent inhibition of bromoenol lactones.

An ABP or inhibitors for the Ca^{2+} -dependent NAT cannot be based on a THL scaffold, because THL does not inhibit PLA2G4E. Previously, Cadas *et al.* reported the inhibition of Ca^{2+} dependent AEA biosynthesis by the covalent inhibitor (E)-6-(bromomethylene)

tetrahydro-3-(1-naphthalenyl)-2H-pyran-2-one (BTNP) in rat brain (Figure 6). Recombinant PLA2G4E is labeled by the fluorescent fluorophosphonate-based ABP TAMRA-FP. However, the endogenous expression of PLA2GE is very low, therefore a tailored-ABP can be a valuable tool to study endogenous PLA2G4E activity. BNTP can serve as a lead for the development of tailored ABPs for this enzyme. Initial experiments revealed that a BNTP-analogue, AK39, inhibited recombinantly expressed PLA2G4E to over 90% at 10 μ M (unpublished results). Scheme 2 depicts a possible synthetic route towards a proposed PLA2G4E directed ABP.



Scheme 2. Proposed synthetic scheme towards Ca^{2+} dependent NAT (PLA2G4E) ABP. Reagents and conditions. (i) AlCl_3 , acetyl chloride, CH_2Cl_2 , $0^\circ\text{C} \rightarrow \text{rt}$, 28%. (ii) Morpholine, S_8 , pTsOH, 130°C , 4 h. (iii) HCl (37% aq.), AcOH (gl.), TEBA, 100°C , on, 72%. (iv) TMS-Cl, Et_3N , benzene, 80°C , 1.5 h, 44%. (v) LDA, THF, -10°C , 45 min. (vi) 4-bromo-1-butyne, $-10^\circ\text{C} \rightarrow \text{rt}$, 2h, 97%. (vii) K_2CO_3 , DMF, 60°C . (viii) NaOH (5 M aq.), $\text{H}_2\text{O}:\text{MeOH}$ (1:10), rt, 4h. (ix) KHCO_3 , CH_2Cl_2 (x) NBS, H_2O .

Chapters 3-6 have shown that MB064 and MB108 target many hydrolases in the mouse brain proteome. The target profile of the β -lactone-based ABPs was, therefore systematically investigated in **Chapter 7** using proteomes from mouse spleen, kidney, liver, heart, lung, pancreas, brain and testes. This revealed that the ABPs acted as highly effective broad spectrum probes for proteins with a α,β -hydrolase fold. The ABPs targeted $\sim 50\%$ of the α,β -hydrolase fold protein family and multiple other hydrolases and transferases. Therefore, these probes are considered as suitable ABPs for the identification of new inhibitors for the α,β -hydrolase fold protein family. The value of MB108 and MB064 for the identification of new inhibitors was demonstrated. A protein library of

ABHD2, 3, 4, 6, 11, 12, and 16A was compiled and screened against a focused library of 207 lipase inhibitors. This library versus library screen allowed evaluation of both selectivity and activity of the inhibitors in one experiment. The screen led to the identification of compounds **60** and **183** as novel inhibitors for ABHD3 and ABHD2, respectively. Their selectivity was further investigated in native proteome by comparative and competitive ABPP. This revealed that both inhibitors showed a highly restricted off-target profile. It is anticipated that inhibitors **60** and **183** will be instrumental to study the physiological role of ABHD2 and ABHD3.

In conclusion, ABPs MB064 and MB108 are the first tools that enabled the study of DAGL- α activity in native biological systems. These probes in combination with the development of the ABPP-based assays described in this thesis have greatly facilitated the identification and characterization of novel DAGL- α inhibitors. Inhibitors for DAGL- α are potential leads for the development of therapeutics to battle the metabolic syndrome and neurodegenerative diseases such as Parkinson's disease, Alzheimer's disease and Multiple Sclerosis.

ABPs MB064 and MB108 that were designed to target DAGL- α revealed to be broad spectrum probes that target many members of the α , β -hydrolase fold protein family. Therefore they represent powerful tools for the identification for new inhibitors for many members of this enzyme family. This finding demonstrates that it is important to analyze the full target profile of an ABP to optimally exploit its properties.

References

1. Willems, L. I.; Overkleeft, H. S.; van Kasteren, S. I. *Bioconjugate Chem.* **2014**, *25*, 1181.
2. Niphakis, M. J.; Cravatt, B. F. *Annu. Rev. Biochem.* **2014**, *83*, 341.
3. Saghatelian, A.; Cravatt, B. F. *Nat. Chem. Biol.* **2005**, *1*, 130.
4. Murataeva, N.; Straiker, A.; Mackie, K. *Br. J. Pharmacol.* **2014**, *171*, 1379.
5. Marsicano, G.; Lafenetre, P. *Curr. Top. Behav. Neurosci.* **2009**, *1*, 201.
6. Calignano, A.; La Rana, G.; Giuffrida, A.; Piomelli, D. *Nature* **1998**, *394*, 277.
7. Colombo, G.; Agabio, R.; Diaz, G.; Lobina, C.; Reali, R.; Gessa, G. L. *Life sciences* **1998**, *63*, PL113.
8. Rajesh, M.; Pan, H.; Mukhopadhyay, P.; Batkai, S.; Osei-Hyiaman, D.; Hasko, G.; Liaudet, L.; Gao, B.; Pacher, P. *J. Leukoc. Biol.* **2007**, *82*, 1382.
9. Janssen, F. J.; van der Stelt, M. *Bioorg. Med. Chem. Lett.* **2016**, *26*, 3831.
10. Baggelaar, M. P.; Janssen, F. J.; van Esbroeck, A. C. M.; den Dulk, H.; Allara, M.; Hoogendoorn, S.; McGuire, R.; Florea, B. I.; Meeuwenoord, N.; van den Elst, H.; van der Marel, G. A.; Brouwer, J.; Di Marzo, V.; Overkleeft, H. S.; van der Stelt, M. *Angew. Chem. Int. Ed.* **2013**, *52*, 12081.
11. Baggelaar, M. P.; Chameau, P. J.; Kantae, V.; Hummel, J.; Hsu, K. L.; Janssen, F.; van der Wel, T.; Soethoudt, M.; Deng, H.; den Dulk, H.; Allara, M.; Florea, B. I.; Di Marzo, V.; Wadman, W. J.; Kruse, C. G.; Overkleeft, H. S.; Hankemeier, T.; Werkman, T. R.; Cravatt, B. F.; van der Stelt, M. *J. Am. Chem. Soc.* **2015**, *137*, 8851.
12. Janssen, F. J.; Baggelaar, M. P.; Hummel, J. A.; van Boeckel, C. A. A.; van der Stelt, M. Pharmaceutically active compounds as DAG-lipase inhibitors, European patent Number EP15169052.6. Filing date 23 May **2016**; publication date 22 November **2016**.
13. Ogasawara, D.; Deng, H.; Viader, A.; Baggelaar, M. P.; Breman, A.; den Dulk, H.; van den Nieuwendijk, A. M.; Soethoudt, M.; van der Wel, T.; Zhou, J.; Overkleeft, H. S.; Sanchez-Alavez, M.; Mori, S.; Nguyen, W.; Conti, B.; Liu, X.; Chen, Y.; Liu, Q. S.; Cravatt, B. F.; van der Stelt, M. *Proc. Natl. Acad. Sci. U. S. A.* **2016**, *113*, 26.
14. Jenniches, I.; Ternes, S.; Albayram, O.; Otte, D. M.; Bach, K.; Bindila, L.; Michel, K.; Lutz, B.; Bilkei-Gorzo, A.; Zimmer, A. *Biol. Psychiatry* **2016**, *79*, 858.
15. Gao, Y.; Vasilyev, D. V.; Goncalves, M. B.; Howell, F. V.; Hobbs, C.; Reisenberg, M.; Shen, R.; Zhang, M. Y.; Strassle, B. W.; Lu, P.; Mark, L.; Piesla, M. J.; Deng, K.; Kouranova, E. V.; Ring, R. H.; Whiteside, G. T.; Bates, B.; Walsh, F. S.; Williams, G.; Pangalos, M. N.; Samad, T. A.; Doherty, P. J. *Neurosci.* **2010**, *30*, 2017.

16. Tanimura, A.; Yamazaki, M.; Hashimotodani, Y.; Uchigashima, M.; Kawata, S.; Abe, M.; Kita, Y.; Hashimoto, K.; Shimizu, T.; Watanabe, M.; Sakimura, K.; Kano, M. *Neuron* **2010**, *65*, 320.
17. Viader, A.; Ogasawara, D.; Joslyn, C. M.; Sanchez-Alavez, M.; Mori, S.; Nguyen, W.; Conti, B.; Cravatt, B. F. *eLife* **2016**, *5*, e12345.
18. Bisogno, T.; Howell, F.; Williams, G.; Minassi, A.; Cascio, M. G.; Ligresti, A.; Matias, I.; Schiano-Moriello, A.; Paul, P.; Williams, E. J.; Gangadharan, U.; Hobbs, C.; Di Marzo, V.; Doherty, P. *J. Cell Biol.* **2003**, *163*, 463.
19. Nomura, D. K.; Morrison, B. E.; Blankman, J. L.; Long, J. Z.; Kinsey, S. G.; Marcondes, M. C.; Ward, A. M.; Hahn, Y. K.; Lichtman, A. H.; Conti, B.; Cravatt, B. F. *Science* **2011**, *334*, 809.
20. Long, J. Z.; Nomura, D. K.; Vann, R. E.; Walentiny, D. M.; Booker, L.; Jin, X.; Burston, J. J.; Sim-Selley, L. J.; Lichtman, A. H.; Wiley, J. L.; Cravatt, B. F. *Proc. Natl. Acad. Sci. U. S. A.* **2009**, *106*, 20270.
21. Ahn, K.; McKinney, M. K.; Cravatt, B. F. *Chem. Rev.* **2008**, *108*, 1687.
22. Rahman, I. A. S.; Tsuboi, K.; Uyama, T.; Ueda, N. *Pharmacol. Res.* **2014**, *86*, 1.
23. Natarajan, V.; Reddy, P. V.; Schmid, P. C.; Schmid, H. H. *Biochim. Biophys. Acta* **1982**, *712*, 342.
24. Astarita, G.; Ahmed, F.; Piomelli, D. *J. Lipid Res.* **2008**, *49*, 48.
25. Cadas, H.; Gaillet, S.; Beltramo, M.; Venance, L.; Piomelli, D. *J. Neurosci.* **1996**, *16*, 3934.
26. Cadas, H.; di Tomaso, E.; Piomelli, D. *J. Neurosci.* **1997**, *17*, 1226.
27. Ogura, Y.; Parsons, W. H.; Kamat, S. S.; Cravatt, B. F. *Nat. Chem. Biol.* **2016**, *12*, 669.
28. Varga, A.; Jenes, A.; Marczylo, T. H.; Sousa-Valente, J.; Chen, J.; Austin, J.; Selvarajah, S.; Piscitelli, F.; Andreou, A. P.; Taylor, A. H.; Kyle, F.; Yaqoob, M.; Brain, S.; White, J. P.; Csernoch, L.; Di Marzo, V.; Buluwela, L.; Nagy, I. *Pflugers Arch.* **2014**, *466*, 1421.
29. Piomelli, D. *Neuropharmacol.* **2014**, *76 Pt B*, 228.
30. Di Marzo, V.; Fontana, A.; Cadas, H.; Schinelli, S.; Cimino, G.; Schwartz, J. C.; Piomelli, D. *Nature* **1994**, *372*, 686.
31. Sun, Y. X.; Tsuboi, K.; Okamoto, Y.; Tonai, T.; Murakami, M.; Kudo, I.; Ueda, N. *Biochem. J.* **2004**, *380*, 749.
32. Tsuboi, K.; Okamoto, Y.; Rahman, I. A.; Uyama, T.; Inoue, T.; Tokumura, A.; Ueda, N. *Biochim. Biophys. Acta* **2015**, *1851*, 537.
33. Liu, J.; Wang, L.; Harvey-White, J.; Huang, B. X.; Kim, H. Y.; Luquet, S.; Palmiter, R. D.; Krystal, G.; Rai, R.; Mahadevan, A.; Razdan, R. K.; Kunos, G. *Neuropharmacol.* **2008**, *54*, 1.
34. Leung, D.; Saghatelian, A.; Simon, G. M.; Cravatt, B. F. *Biochemistry* **2006**, *45*, 4720.

35. Tsuboi, K.; Okamoto, Y.; Ikematsu, N.; Inoue, M.; Shimizu, Y.; Uyama, T.; Wang, J.; Deutsch, D. G.; Burns, M. P.; Ulloa, N. M.; Tokumura, A.; Ueda, N. *Biochim. Biophys. Acta* **2011**, *1811*, 565.

Samenvatting

Sinds de ontrafeling van het humane genoom is de exacte volgorde van de individuele basenparen van het menselijk DNA bekend, en daarmee zijn vrijwel alle genen die coderen voor de eiwitten in ons lichaam ontdekt. Eiwitten katalyseren biochemische reacties in onze cellen en reguleren de fysiologische functie van onze organen. Het gebrekkig functioneren van eiwitten is de onderliggende oorzaak van veel ziekten. Daarom is inzicht in de functie van eiwitten die betrokken zijn bij ziekten van cruciaal belang voor de ontwikkeling van nieuwe geneesmiddelen. Hoewel een gen de exacte volgorde van de aminozuren bepaalt waaruit een eiwit wordt opgebouwd, kan er slechts beperkte informatie uit worden afgeleid met betrekking tot de biochemische functie van een eiwit. Dit komt doordat kleine verschillen in aminozuur-volgorde grote veranderingen in functie kunnen veroorzaken, wat het voorspellen van de exacte rol van een eiwit moeilijk maakt.

Een van de grote uitdagingen in de chemische biologie is het in kaart brengen van de fysiologische functies van eiwitten. Kennis van de functie van eiwitten kan ons helpen begrijpen hoe het gezonde menselijk lichaam werkt, maar ook welke processen verstoord zijn tijdens een ziekte. Het verwijderen van een gen of het verhinderen van de vorming van het eiwit in de cel zijn veel toegepaste methoden om de functies van eiwitten te ontrafelen. Deze methodes maken het mogelijk om fysiologische veranderingen in een cel als gevolg van de afwezigheid van het eiwit te bestuderen. Genetische methodes zijn zeer waardevol, omdat ze heel specifiek zijn voor een bepaald eiwit, breed toepasbaar en onafhankelijk van het biologische systeem kunnen worden ingezet. Ze hebben echter ook enkele nadelen. Er wordt bijvoorbeeld geen onderscheid gemaakt tussen de katalytische en structurele functies van een eiwit. Tevens is het niet mogelijk om het eiwit slechts tijdelijk uit te schakelen, maar alleen permanent. Hierdoor heeft de cel de mogelijkheid om alternatieve biochemische routes in te schakelen ter compensatie van de functie van het verwijderde gen.

De toepassing van kleine moleculen is een tweede methode om de rol van eiwitten in de cel te bestuderen. Met behulp van kleine moleculen kunnen enkele nadelen van genetische technieken worden omzeild. Deze methode maakt het bijvoorbeeld mogelijk om de functie van eiwitten tijdelijk te moduleren. Tevens bieden deze stoffen aanknopingspunten voor de ontwikkeling van potentiële medicijnen. Een nadeel is dat de stoffen vaak niet specifiek zijn en dus de functie van meerdere eiwitten tegelijkertijd moduleren. Dit kan bijwerkingen veroorzaken.

Dit proefschrift beschrijft een nieuwe methode om kleine moleculen voor eiwitten te identificeren die zeer specifiek zijn voor een bepaald eiwit en dus zo min mogelijk bijwerkingen vertonen. Het proefschrift focust op diacylglycerol lipases die behoren tot de eiwitfamilie van de α,β -hydrolases, en die verantwoordelijk zijn voor de productie van

2-arachidonoylglycerol (2-AG). 2-AG is een endocannabinoïde, een soort van lichaamseigen marihuana dat betrokken is bij vele functies in de hersenen, zoals geheugen vorming, het voelen van pijn en het reguleren van het lichaamsgewicht. Het is de verwachting dat diacylglycerol lipases betrokken zijn bij veel uiteenlopende ziekten, zoals ontstekingen in de hersenen en overgewicht. Om dit te bestuderen is het daarom van belang om kleine moleculen te vinden die heel specifiek de activiteit van diacylglycerol lipases kunnen remmen.

In dit proefschrift wordt “activity-based protein profiling” (ABPP) als een techniek toegepast om kleine, zeer selectieve moleculen voor diacylglycerol lipases te ontdekken. Deze techniek maakt gebruik van fluorescente stoffen, zogenaamde “activity-base probes” (ABPs), die een covalente binding vormen met het katalytische aminozuur van het eiwit. Hierdoor is deze methode zeer geschikt voor het bestuderen van de diacylglycerol lipases en alle andere de α , β -hydrolase domein bezittende eiwitten. De kracht van deze techniek is dat de ABP alleen een binding aangaat met een eiwit dat functioneel actief is. Daarnaast is deze techniek uniek, omdat het werkt in levende cellen, organen en zelfs dieren. Dit is belangrijk omdat de activiteit en lokalisatie van vele eiwitten wordt gereguleerd door posttranslationele modificaties en eiwit-eiwit interacties.

In **hoofdstuk 1** wordt de ABPP-methode beschreven en wordt uitgelegd hoe deze techniek kan worden toegepast om de interactie tussen kleine moleculen en eiwitten te bestuderen. Wanneer een verzameling van eiwitten, ook wel proteoom genoemd, eerst wordt behandeld met een remmer en daarna met een ABP kan door middel van het meten van de fluorescentie de affiniteit van het kleine molecuul voor het eiwit bepaald worden.

Hoofdstuk 2 beschrijft de fysiologische rol van 2-AG in de hersenen. Deze rol is intensief onderzocht door middel van modulatie van de activiteit van de eiwitten die verantwoordelijk zijn voor de synthese en afbraak van 2-AG. Dit endocannabinoïde activeert de cannabinoid CB₁ receptor in de hersenen en speelt een rol bij hersenontstekingen, angst en verslaving. 2-AG heeft niet alleen een belangrijke rol als signaallipide voor de CB-receptoren, maar is ook een tussenproduct voor de vorming van arachidonzuur en ontstekings-stimulerende prostaglandinen. De affiniteit van 2-AG voor GPR55, TRPV1, GABA_A and Adenosine A₃ receptoren wordt ook beschreven. Aangezien 2-AG een belangrijke rol speelt in meerdere ziekteprocessen worden de enzymen die betrokken zijn bij de vorming en afbraak van 2-AG beschouwd als interessante eiwitten voor de ontwikkeling van nieuwe geneesmiddelen.

Hoofdstuk 3 beschrijft de ontwikkeling van een ABP voor diacylglycerol lipase- α (DAGL- α). Het ontwerp van de ABP is gebaseerd op het geneesmiddel Orlistat[®] (THL) dat wordt gebruikt voor de behandeling van obesitas. Dit molecuul staat bekend als remmer van verschillende lipases in de alveesklier, maar ook als remmer van DAGL- α . Het molecuul is gesynthetiseerd met een fluorescent label voor visualisatie en een biotine voor zuivering en identificatie. Deze ABP (MB064) bood de unieke mogelijkheid om de activiteit van DAGL- α in zijn natuurlijke omgeving te meten en visualiseren. Remming van

DAGL- α is een mogelijke strategie zijn voor de behandeling van obesitas, maar ook voor ziektes waarin neuroinflammatie een rol speelt, zoals de ziekten van Alzheimer, Parkinson en Multiple Sclerosis. Met behulp van deze ABP en een biochemische assay is een kleine bibliotheek van verbindingen getest voor remming van de activiteit van DAGL- α . Dit heeft geleid tot de identificatie van een reversibele DAGL- α remmer LEI104. Deze stof was uiterst selectief voor DAGL- α . LEI104 vertoonde interactie met maar één extra eiwit, namelijk fatty acid amide hydrolase (FAAH). Dit eiwit is verantwoordelijk voor de afbraak van het andere endocannabinoïde anandamide. Om de rollen van 2-AG en anandamide te kunnen onderscheiden is het belangrijk om selectiviteit over FAAH te verkrijgen.

Hoofdstuk 4 beschrijft het verbeteren van LEI104 tot een meer selectieve remmer. Met behulp van computer simulaties werd inzicht verkregen in de manier waarop LEI104 kon worden verbeterd. Dit leidde tot ontwikkeling van een nieuwe remmer (LEI105). Deze stof was tien keer actiever op zowel DAGL- α als DAGL- β . Om de selectiviteit van deze remmer te bestuderen werd er een competitieve en vergelijkende ABPP methode opgezet, die gebruik maakt van twee ABPs. Deze methode, chemical proteomics genoemd, kan worden gebruikt om de selectiviteit van de stoffen te bepalen over een grote groep eiwitten die aanwezig zijn in de hersenen. Deze methode toonde aan dat LEI105 een zeer selectieve remmer was. Er was geen affiniteit meer voor FAAH of andere eiwitten die betrokken zijn bij de synthese of afbraak van endocannabinoiden. Vervolgens werd de activiteit van LEI105 in levende cellen en muizen hersenen getest. Hiermee werd aangetoond dat LEI105 de meest selectieve remmer voor DAGLs tot op heden is. LEI105 werd gebruikt om belangrijke vraagstukken over de functie van DAGLs te beantwoorden.

Hoofdstuk 5 is gericht op de optimalisatie van de activiteit van LEI105 en verbetering van de farmacokinetische en farmacodynamische eigenschappen van de remmer. Een serie van variaties op LEI105 is gemaakt waarbij de para-tolueen groep is vervangen door andere gesubstitueerde fenylen of heterocyclische groepen. Dit heeft geresulteerd in de identificatie van remmer **16**. Deze verbinding had een hogere activiteit tegen DAGL- α vergeleken met LEI105. Daarnaast was dit molecuul ook minder vet dan LEI105. In een DAGL- α assay die gebruik maakt van het natuurlijk substraat liet verbinding **16** een pIC_{50} van 7.6 ± 0.11 zien. Het is interessant om deze stof verder te karakteriseren met het oog op *in vivo* actieve remmers.

Hoofdstuk 6 past de competitieve en vergelijkende ABPP met twee ABPs toe op verschillende hersengebieden. Hierdoor kon de relatieve activiteit van de α,β -hydrolase domein bezittende eiwitten die een rol spelen in het endocannabinoïde metabolisme, zoals ABHD4, ABHD6, ABHD12, MAGL, FAAH en DAGL- α , bestudeerd worden in de hippocampus, striatum, cerebellum en frontale cortex. Er werd ontdekt dat de endocannabinoid hydrolase activiteit van de verschillende eiwitten niet evenredig verdeeld was over de hersengebieden. Daarnaast is de methode toegepast om te aan te tonen dat de cannabinoid CB₁ receptor geen regulerende functie heeft op de activiteit van de eiwitten die verantwoordelijk zijn voor de vorming en afbraak van endocannabinoiden.

Hoofdstuk 7 beschrijft de systematische zoektocht naar α,β -hydrolase domein bezittende eiwitten die gedetecteerd worden door de ABPs die zijn ontwikkeld in hoofdstuk 3. Met behulp van chemical proteomics is gebleken dat ongeveer 66 α,β -hydrolase eiwitten gedetecteerd kunnen worden in de milt, long, alvleesklier, hersenen, hart, testikels, nier en lever van muizen. De ABPs zijn hierdoor erg geschikt voor het ontdekken van nieuwe remmers voor eiwitten waarvan de functie nog niet bekend is. Om dit te demonstreren is een bibliotheek van 206 verschillende stoffen getest op de activiteit van ABHD2, ABHD3, ABHD4, ABHD6, ABHD11, ABHD12 en ABHD16A. Dit resulteerde in de ontdekking van α -ketoamide **60** en urea **183** als remmers voor ABHD2 en ABHD3, respectievelijk. Kort geleden is ontdekt dat ABHD2 2-AG een hydrolase is die de activatie van spermatoïden reguleert. Remming van ABHD2 activiteit zou in de toekomst mogelijk toegepast kunnen worden als mannelijk anticonceptie middel. ABHD3 hydrolyseert fosfatidylcholines met kortere vetzuurstaarten die oxidatief gemodificeerd zijn. Deze laatste groep van verbindingen is mogelijkerwijs betrokken bij de inductie van celsterfte en atherosclerose. De beschreven stoffen in dit hoofdstuk zijn nuttige gereedschappen om de exacte functies van ABHD2 en ABHD3 verder te onderzoeken.

Ten slotte, de ontwikkeling van MB064 als nieuwe activity-based probe, zoals beschreven in dit proefschrift, heeft een belangrijke rol gespeeld in het ontsluiten van het onderzoeksveld van de diacylglycerol lipases. Het eiwit kan nu beter bestudeerd worden in cellen en diermodellen en nieuwe remmers voor dit eiwit kunnen nu eenvoudiger worden ontdekt. Remmers van diacylglycerol lipases kunnen leiden tot potentieel nieuwe therapeutische behandelingen van obesitas en neuroinflammatoire ziektes, zoals de ziekte van Alzheimer, ziekte van Parkinson en Multiple Sclerosis. Daarnaast is de verwachting dat MB064 en gerelateerde activity-based probes een belangrijke rol gaan spelen in het identificeren van kleine moleculen voor andere eiwitten uit de α,β -hydrolase familie.

List of publications

Baggelaar, M. P.; Maccarrone, M.; van der Stelt, M.; 2-Arachidonoylglycerol: a Signaling Lipid. *Manuscript in preparation*.

Deng, H.; van der Wel, T.; van den Berg, R. J. B. H. N.; van den Nieuwendijk, A. M.C.H.; Janssen, F. J.; Baggelaar, M. P.; Overkleeft, H. S.; van der Stelt, M. Chiral Disubstituted Piperidiny Ureas: a Class of Dual Diacylglycerol Lipase- α and ABHD6 Inhibitors. *Manuscript submitted*.

van Esbroeck, A. C. M.; Janssen, A. P. A.; Cognetta, A. B.; Ogasawara, D.; Shpak, G.; van der Kroeg, M.; Kantae, V.; Baggelaar, M. P.; de Vrij, F. M. S.; Deng, H.; Allarà, M.; Fezza, F.; Lin, Z.; van der Wel, T.; Soethoudt, M.; Mock, E. D.; den Dulk, H.; Baak, I. L.; Florea, B. I.; Hendriks, G.; de Petrocellis, L.; Overkleeft, H. S.; Hankemeier, T.; Cravatt, B. F.; de Zeeuw, C. I.; Di Marzo, V.; Maccarrone, M.; Kushner, S. A.; van der Stelt, M. BIA 10-2474 is a non-selective FAAH inhibitor that disrupts lipid metabolism. *Manuscript submitted*.

Baggelaar, M. P.; van Esbroeck, A. C. M.; van Rooden, E.; Florea, B. I.; Overkleeft, H. S.; Marsicano, G.; Chaouloff, F.; van der stelt, M. Chemical Proteomics Maps Brain Region Specific Activity Of Endocannabinoid Hydrolases. *ACS Chem. Biol.* **2017**, DOI: 10.1021/acscchembio.6b01052.

Deng, H.; Kooijman, S.; van den Nieuwendijk, A. M. C. H.; Ogasawara, D.; van der Wel, T.; van Dalen, F.; Baggelaar, M.P.; Janssen, F.; van den Berg, R. J. B. H. N.; den Dulk, H.; Cravatt, B. F.; Overkleeft, H. S.; Rensen, P. C. N.; van der Stelt, M. Triazole Ureas act as Diacylglycerol Lipase Inhibitors and Prevent Fasting-induced Refeeding. *J. Med. Chem.* **2017**, *60*, 428-440.

Soethoudt, M.; Grether, U.; Fingerle, J.; Grim, T.; Fezza, F.; de Petrocellis, L.; Ullmer, C.; Rothenhausler, B.; Perret, C.; van Gils, N.; Finlay, D.; MacDonald, C.; Chicca, A.; Gens, M.; Stuart, J.; de Vries, H.; Mastrangelo, N.; Xia, L.; Alachouzos, G.; Baggelaar, M. P.; Martella, A.; Mock, E.; Deng, H.; Heitman, L.; Connor, M.; di Marzo, V.; Gertsch, J.; Lichtman, A.; Maccarrone, M.; Pacher, P.; Glass, M.; van der Stelt, M. Cannabinoid CB2 Receptor Ligand Profiling Reveals Biased Signaling and Off-target Activity: Implications for Drug Discovery, *Nat. Commun.* **2017**, *8*, 13958.

Ogasawara, D.; Deng, H. Viader, A.; Baggelaar, M. P.; Breman, A.; den Dulk, H.; van den Nieuwendijk, A. M.; Soethoudt, M.; van der Wel, T.; Zhou, J.; Overkleeft, H. S.; Sanchez-Alavez, M.; Mo, S.; Nguyen, W.; Conti, B.; Liu, X.; Chen, Y.; Liu, Q. S.; Cravatt, B. F.; van der Stelt, M.; Rapid and profound rewiring of brain lipid signaling networks by acute diacylglycerol lipase inhibition. *Proc. Natl. Acad. Sci. U S A*. **2016**, *113*, 26-33.

Mukhopadhyay, P.; Baggelaar, M. P.; Erdelyi, K.; Cao, Z.; Cinar, R.; Fezza, F.; Ignatowska-Janlowska, B.; Wilkerson, J.; van Gils, N.; Hansen, T.; Ruben, M.; Soethoudt, M.; Heitman, L.; Kunos, G.; Maccarrone, M.; Lichtman, A.; Pacher, P.; Van der Stelt, M.; The novel, orally available and peripherally restricted selective cannabinoid CB2 receptor agonist LEI-101 prevents cisplatin-induced nephrotoxicity. *Br. J. Pharmacol.* **2016**, *173*, 446-4458.

Janssen, F. J.; Baggelaar, M. P.; Hummel, J. J.; Overkleeft, H. S.; Cravatt, B. F.; Boger, D. L.; van der Stelt, M. Comprehensive Analysis of Structure-Activity Relationships of α -Ketoheterocycles as sn-1-Diacylglycerol Lipase α Inhibitors. *J. Med. Chem.* **2015**, *58*, 9742-9753.

Baggelaar, M. P.; Chameau, P. J.; Kantae, V.; Hummel, J.; Hsu, K. L.; Janssen, F.; van der Wel, T.; Soethoudt, M.; Deng, H.; den Dulk, H.; Allara, M.; Florea, B. I.; Di Marzo, V.; Wadman, W. J.; Kruse, C. G.; Overkleeft, H. S.; Hankemeier, T.; Werkman, T. R.; Cravatt, B. F.; van der Stelt, M. Highly Selective, Reversible Inhibitor Identified by Comparative Chemoproteomics Modulates Diacylglycerol Lipase Activity in Neurons. *J. Am. Chem. Soc.* **2015**, *137*, 8851-8857.

Ouairy, C. M.; Ferraz, M. J.; Boot, R.G.; Baggelaar, M. P.; van der Stelt, M.; Appelman, M.; van der Marel, G. A.; Florea, B. I.; Aerts, J. M.; Overkleeft, H. S.; Development of an acid ceramidase activity-based probe. *Chem. Commun.* **2015**, *51*, 6161-6163.

van der Wel, T.; Janssen, F. J.; Baggelaar, M. P.; Deng, H.; den Dulk, H.; Overkleeft, H. S.; van der Stelt, M. A natural substrate-based fluorescence assay for inhibitor screening on diacylglycerol lipase α . *J. Lipid Res.* **2015**, *56*, 927-9235.

Janssen, F. J.; Deng, H.; Baggelaar, M. P.; Allara, M.; van der Wel, T.; den Dulk, H.; Ligresti, A.; an Esbroeck, A. C.; McGuire, R.; Di Marzo, V.; Overkleeft, H. S.; van der Stelt, M. Discovery of glycine sulfonamides as dual inhibitors of sn-1-diacylglycerol lipase α and α/β -hydrolase domain 6. *J. Med. Chem.* **2014**, *57*, 6610-6622.

Baggelaar, M. P.; Janssen, F. J.; van Esbroeck, A. C. M.; den Dulk, H.; Allara, M.; Hoogendoorn, S.; McGuire, R.; Florea, B. I.; Meeuwenoord, N.; van den Elst, H.; van der Marel, G. A.; Brouwer, J.; Di Marzo, V.; Overkleeft, H. S.; van der Stelt, M. Development of an activity-based probe and in silico design reveal highly selective inhibitors for diacylglycerol lipase- α in brain. *Angew. Chem. Int. Ed.* **2013**, *52*, 12081-12085.

Baggelaar, M. P.; Huang, Y.; Feringa, B. L.; Dekker, F. J.; Minnaard, A. J.; Catalytic asymmetric total synthesis of (S)-(-)-zearalenone, a novel lipoxxygenase inhibitor. *Bioorg. Med. Chem.* **2013**, *21*, 5271-5274.

Barroso, S.; Castelli, R.; Baggelaar, M. P.; Geerdink, D.; ter Horst, B.; Casas-Arce, E.; Overkleeft, H. S.; van der Marel, G. A.; Codée, J. D.; Minnaard, A. J.; Total synthesis of the triglycosyl phenolic glycolipid PGL-tb1 from *Mycobacterium tuberculosis*. *Angew. Chem. Int. Ed.* **2012**, *51*, 11774-11777.

Book chapter

Marc P. Baggelaar & Mario van der Stelt, Competitive ABPP of Serine Hydrolases: A Case Study on DAGL-Alpha, chapter 12 in “Activity-Based Proteomics” Springer New York, (ISBN 978-1-4939-6439-0), **2016**.

Patent

Janssen, F. J.; Baggelaar, M. P.; Hummel, J. A.; van Boeckel, C. A. A.; van der Stelt, M. Pharmaceutically active compounds as DAG-lipase inhibitors, European patent Number EP15169052.6. Filing date 23 May **2016**; publication date 22 November **2016**.

Curriculum Vitae

Marc Pieter Baggelaar was born on December 29th 1984 in Harlingen, the Netherlands. He obtained his higher general secondary education diploma (Havo) at the CSG Anna Maria van Schuurman in Franeker in 2002 and his pre-university education diploma (VWO) at the RSG Simon Vestdijk in Harlingen in 2004.

He subsequently started a Bachelor Physics and Spatial Planning & Design before starting his Bachelor Chemistry, followed by a Master Organic Chemistry. He obtained his Bachelor and Master's degree in Organic Chemistry in 2011 and 2012, respectively.

As part of the Master's program he performed a research internship in the Bio-organic chemistry group at Groningen University under the supervision of prof. dr. A. J. Minnaard. The aim of the research was the development of a catalytic asymmetric synthesis of the macrolactone (S)-(-)-Zearalenone using asymmetric allylic alkylation for the introduction of the stereocenter. He was awarded the "Unilever research prize 2012" for his master thesis entitled "Catalytic asymmetric total synthesis of (S)-(-)-Zearalenone, a novel lipooxygenase inhibitor". In addition, he has performed a research internship in the Bio-organic synthesis group at Leiden University under the supervision of prof. dr. H. S. Overkleef and prof. dr. G. A. van der Marel. The aim of this internship was the total synthesis of a triglycoside that is part of a glycolipid which was isolated from the cell wall of *Mycobacterium tuberculosis*.

In July 2012 he started his doctoral studies at Leiden University in the Bio-organic synthesis group. This research was conducted under the supervision of prof. dr. H. S. Overkleef and dr. M. van der Stelt. During the final two years of his doctoral studies he transferred to the new department of Molecular Physiology led by dr. M. van der Stelt. Part of the research described in this thesis was performed at the department of chemical physiology at the Scripps research institute in La Jolla (USA) under the supervision of prof. dr. B. F. Cravatt (May-July 2014).

Posters on parts of the Ph.D. research were presented at various national and international conferences (2012-2016). Oral presentations were given at the NWO conference Molecules: Synthesis and Properties (the Netherlands, 2013), European Workshop on Cannabinoid Research (Italy, 2015), CHAINS (the Netherlands, 2015) and the 26th Annual International Cannabinoid Research Society Symposium on the Cannabinoids (Poland, 2016).

In August 2017 he will start his postdoctoral research as a Marie Curie fellow in the group of prof. dr. E. Tate at Imperial College London (United Kingdom).